Unclassified

Security Classification of this page

REPORT DOCUMENTATION PAGE

1a Report Security Classification: Unclassified	1b Restrictive Markings
2a Security Classification Authority	3 Distribution Availability of Report: Approved for public release; distribution is unlimited.
2b Declassification/Downgrading Schedule	
4 Performing Organization Report Number(s)	5 Monitoring Organization Report Number(s)
6a Name of Performing Organization: Naval Postgraduate School; 6b Office Symbol (*If Applicable*): OC	7a Name of Monitoring Organization: Naval Postgraduate School
6c Address (*city, state, and ZIP code*): Monterey, CA 93943-5000	7b Address (*city, state, and ZIP code*): Monterey, CA 93943-5000
8a Name of Funding/Sponsoring Organization; 8b Office Symbol (*If Applicable*)	9 Procurement Instrument Identification Number
8c Address (*city, state, and ZIP code*)	10 Source of Funding Numbers: Program Element Number; Project No; Task No; Work Unit Accession No

11 Title (*Include Security Classification*) ASSESSING THE ENERGETIC INTERACTIONS OF SUBTIDAL FLOW ON THE CONTINENTAL SLOPE IN AN EASTERN BOUNDARY REGION

12 Personal Author(s) Tisch, Timothy Daniel

13a Type of Report	13b Time Covered	14 Date of Report (*year, month,day*)	15 Page Count
Doctoral Thesis	From To	December 1992	222

16 Supplementary Notation The views expressed in this thesis are those of the author and do not reflect the official policy or position of the Department of Defense or the U.S. Government.

17 Cosati Codes			18 Subject Terms (*continue on reverse if necessary and identify by block number*)
Field	Group	Subgroup	California Current, California Undercurrent, eddy potential energy, energy time series, spectral analysis, energetic events

19 Abstract (*continue on reverse if necessary and identify by block number*)

Seventeen-month time series (May 1989 - October 1990) of current, temperature and conductivity were obtained from 100, 350, and 500 m depth at site P2, located on the 800 m isobath off Point Sur, and one-year time series (May 1990 - May 1991) of the same variables at similar depths were obtained from site P3, approximately 25 km farther offshore on the 1800 m isobath.

Results show that no net growth or decay of eddy potential energy (EPE) occurred at either mooring site during their respective deployment periods. At mooring P2, baroclinic instabilities within the water column were signaled by downgradient horizontal eddy heat fluxes that converted mean potential energy (MPE) to EPE at both 225 and 425 m. The dominant balance at 225 m was between mean flow advection (source) and upward eddy heat fluxes (EPE to eddy kinetic energy, EKE), with additional losses coming from downstream advection by the eddy flow. At 425 m, the dominant balance was between downgradient eddy heat fluxes (source) and downstream advection by eddy flow (sink). Unlike 225 m, vertical eddy heat fluxes at 425 m were a weak source (EKE to EPE) while mean flow advection was negligible. At P3, the net balance involved only downward eddy heat fluxes (source) and downstream advection by eddy flow (sink), as mean advection and MPE-EPE conversions were negligible.

Analysis of energetic events within the time series of terms in the EPE equation did not reveal any canonical or common pattern which would explain the temporal means described above, but suggest the flow in this region is highly variable. In fact, during most events magnitudes of terms were anywhere from 10 to 200 times that of the associated temporal mean. Events at P2 involved both horizontal and vertical processes and had longer time scales (several days to weeks) compared to those at P3, which had much shorter time scales and appeared to involve vertical processes only.

20 Distribution/Availability of Abstract	21 Abstract Security Classification
[X] unclassified/unlimited [ ] same as report [ ] DTIC users	Unclassified
22a Name of Responsible Individual: Steven R. Ramp	22b Telephone (*Include Area code*): (408) 646-3162 — 22c Office Symbol: OC/Ra

DD FORM 1473, 84 MAR 83 APR edition may be used until exhausted

All other editions are obsolete

security classification of this page: Unclassified

Approved for public release; distribution is unlimited.

Assessing the Energetic Interactions of Subtidal Flow on the Continental Slope in an Eastern Boundary Region

by

Timothy Daniel Tisch
Lieutenant, NOAA Corps
B.S., State University of New York, Maritime College, 1982
M.S., Naval Postgraduate School, 1990

Submitted in partial fulfillment of the requirements for the degree of

DOCTOR OF PHILOSOPHY IN PHYSICAL OCEANOGRAPHY

from the

NAVAL POSTGRADUATE SCHOOL
December 1992

ABSTRACT

Seventeen-month time series (May 1989 - October 1990) of current, temperature and conductivity were obtained from 100, 350, and 500 m depth at site P2, located on the 800 m isobath off Point Sur, and one-year time series (May 1990 - May 1991) of the same variables at similar depths were obtained from site P3, approximately 25 km farther offshore on the 1800 m isobath.

Results show that no net growth or decay of eddy potential energy (EPE) occurred at either mooring site during their respective deployment periods. At mooring P2, baroclinic instabilities within the water column were signaled by downgradient horizontal eddy heat fluxes that converted mean potential energy (MPE) to EPE at both 225 and 425 m. The dominant balance at 225 m was between mean flow advection (source) and upward eddy heat fluxes (EPE to eddy kinetic energy, EKE), with additional losses coming from downstream advection by the eddy flow. At 425 m, the dominant balance was between downgradient eddy heat fluxes (source) and downstream advection by eddy flow (sink). Unlike 225 m, vertical eddy heat fluxes at 425 m were a weak source (EKE to EPE) while mean flow advection was negligible. At P3, the net balance involved only downward eddy heat fluxes (source) and downstream advection by eddy flow (sink), as mean advection and MPE-EPE conversions were negligible.

Analysis of energetic events within the time series of terms in the EPE equation did not reveal any canonical or common pattern which would explain the temporal means described above, but suggest the flow in this region is highly variable. In fact, during most events magnitudes of terms were anywhere from

10 to 200 times that of the associated temporal mean. Events at P2 involved both horizontal and vertical processes and had longer time scales (several days to weeks) compared to those at P3, which had much shorter time scales and appeared to involve vertical processes only.

TABLE OF CONTENTS

LIST OF TABLES

LIST OF FIGURES

ACKNOWLEDGMENTS

As I learned during my pursuit of a Master's Degree, a scientific project is rarely the result of one individual's efforts. There are a great number of individuals who have provided moral and scientific support during my research and I would like to take this time to offer my thanks and appreciation. I would first like to thank my doctoral committee, Professors Ramp, Collins, Haney, Batteen and Gragg, for their collective wisdom and guidance and for making sure that I always kept on track. Next, I would like to thank the NOAA Corps and the Office of Ocean and Earth Sciences for allowing me this great opportunity. I would also like to thank CAPT C.K. Roberts who was the driving force behind my acceptance into the program, and to CAPT Kurt Schnebele, CDR Dan Tracy, and LCDR Bob Maxson, NOAA Corps who have been a source of encouragement over the last few years. The technical assistance from Mr. Paul Jessen, Mrs. Arlene Guest, Mr. Todd Anderson, and the rest of the Oceanography Staff has been invaluable and should not go unrecognized. For their generous assistance with data processing, primarily with gap-filling techniques, I thank Professor Peter Lewis and Bonnie Ray of the Operations Research Curriculum. Their technical and programming support saved countless hours of work.

Most importantly, I would like to thank my family, my sons Michael and Daniel, and especially my wife Kathleen, who have survived it all. I know it has been anything but fun and I thank you for your constant love and support, for without you none of this would have been possible. You guys are the greatest.

I would like to say a special thank you to my late sister, Debra, and mother-in-law, Louise, who always demonstrated a "do good" attitude in life and never seemed to quit in whatever they did. Through their actions, I learned that success comes to those who believe in their own abilities. Their wisdom has helped me through the last few years, and allowed me see this research through to completion.

I. INTRODUCTION

A. THE CALIFORNIA CURRENT SYSTEM - A GENERAL OVERVIEW

The large-scale atmospheric forcing in the eastern Pacific Ocean consists of the North Pacific (sub-tropical) high, the Aleutian low, and in summer the thermal low over the western United States. The North Pacific high is most intense during the summer months while the Aleutian low is most intense during the winter months. The high migrates annually from its maximum southern position at 28°N, 130°W in February to its maximum northern position at 38°N, 150°W in August (*Huyer*, 1983). The U.S. thermal low is centered near 35°N in summer and enhances the equatorward wind stress over the coastal waters off northern California (*Reinecker and Ehret*, 1988). A region of positive wind stress curl exists near the coast throughout the year, is best developed from May to September, and has greater spatial variability during winter (*Nelson*, 1977).

This forcing creates the anticyclonic North Pacific gyre. The northern side of the gyre is comprised of the West Wind Drift and the North Pacific Current which flows easterly then splits near 45°N in winter, 50°N in summer (*Pickard and Emery*, 1982) to form the poleward flowing Alaska Current and the equatorward flowing California Current (CC). Offshore the CC has been characterized as a surface current (0-300 m deep) carrying water equatorward throughout the year along the west coast of North America (*Lynn and Simpson*, 1987). Near 20°N it turns westward as part of the North Equatorial Current. The average speed of the CC off the coast of California is generally less than 25 cm s^{-1} (*Reid and Schwartzlose*, 1962).

Within 150 km of the coast there is a fall-winter reversal of the surface flow known as the California Countercurrent (CCC, *Simpson et al.*, 1986). This current has also been called the Inshore Countercurrent (IC, *Lynn and Simpson*, 1987) off southern California, and is generally referred to as the Davidson Current (DC) north of Point Conception. We adopt the term Davidson Current (DC) to refer to this feature off Point Sur. The reversal of winds from northwesterly in summer to southeasterly in winter, which causes downwelling at the coast, seems to be the forcing mechanism of this poleward surface current (*Huyer et al.*, 1989).

The California Undercurrent (CUC) flows poleward throughout the year. While it has been observed off northern Baja California (*Wooster and Jones*, 1970), central California (*Chelton*, 1984; *Lynn and Simpson*, 1987; *Tisch et al.*, 1992), Oregon (*Halpern et al.*, 1978), Washington (*Cannon et al.*, 1975; *Reed and Halpern*, 1976), and as far north as Vancouver Island, British Columbia (*Reed and Halpern*, 1976; *Ikeda et al.*, 1984), the spatial continuity of this current along the west coast of North America has not been observed. It has its origin in the eastern equatorial Pacific and is centered primarily over the continental slope. Based upon available observations of the winds and the CUC between San Francisco and Baja California, *Hickey* (1979) concluded that the location, strength and core depth show considerable seasonal variability and can be related to the seasonal variability in wind stress and wind stress curl. Similar results were drawn from simple correlations between the current and variability within these fields (*Lynn and Simpson*, 1987) although many of the dynamical features have not been completely justified (*Chelton*, 1984). *Tisch et al.*, (1992), using hydrographic data collected off Point Sur, California, found the location,

strength and core depth to be strongly related to specific wind events, both local and remote. While these observations have revealed that the core depth and speed can vary from location to location, little is known about what causes the observed variability and more importantly what actually drives the undercurrent (*Huyer et al.*, 1989).

B. SUBTIDAL VARIABILITY WITHIN THE CALIFORNIA CURRENT SYSTEM

Collectively the CC, DC, and CUC comprise what is known as the California Current System (CCS). Much of our present understanding of the circulation within the CCS has come from analyzing hydrographic data, moored current meter measurements, buoy drift trajectories and, more recently, satellite imagery of the sea surface, which has been collected in conjunction with observational programs conducted within the CCS. A common goal of these programs has been to study the kinematics and dynamics within the CCS and eastern boundary current regions in general, and to examine the role played by these currents in larger gyre-scale circulations.

Of particular interest in some of the more recent studies are: 1) the time variability of poleward flows and their role in gyre-scale processes; 2) the dynamical processes which govern the wind-driven circulation over the continental slope; and 3) the nature and structure of cold filaments found in eastern boundary current regions. In addition to the aforementioned observational programs, several numerical models of the CCS have been developed to further investigate possible mechanisms for producing the observed variability in eastern boundary currents. Using simple three-dimensional linear models forced by realistic winds from the region off central California, *McCreary* (1981) and *McCreary et al.*, (1987) have been successful at producing

poleward undercurrents. The poleward surface flow and undercurrents generated by these models depended upon the alongshore wind stress, and the existence of an alongshore pressure gradient. Models forced solely by curl of the wind stress did not produce poleward undercurrents, however, they did produce poleward surface currents nearshore. The primitive equation model of *Batteen et al.* (1989), forced by a band of steady alongshore wind, also generated an equatorward coastal jet and poleward undercurrent, which became unstable with time, and led to the production of eddies and jets with significant onshore and offshore directed flows. In a similar experiment, *Batteen et al.*, (1989) also found that a variation of alongshore wind stress can play a role in determining the location of eddy generation regions. These studies, however, are just part of a vast amount of literature on the subject of eastern boundary regions, and more specifically, the CCS. For the sake of brevity, the following discussion will focus on descriptions of the variability observed within the CCS during some of the large-scale systematic programs, with particular attention to the time and space scales of these motions.

Chelton (1984) and *Lynn and Simpson* (1987), using 23 years of hydrographic data collected in conjunction with the California Cooperative Fisheries Investigations (CalCOFI) program, examined the seasonal variability of alongshore geostrophic currents along the west coast of the United States. This large-scale sampling grid was initiated in 1949 and extends from Vancouver Island near the Canadian border to the southern tip of Baja California. These historical data reveal the CC within the upper 200 m flowing equatorward with its core located between 100 km and 200 km off the coast. The core location appears to be coincident with a transition zone that separates the coastal region

from the oceanic environment and is characterized by recurrent eddies and energetic meanders (*Lynn and Simpson*, 1987). There are two maxima during the year, between February and March and July through September (climatologically the time of maximum equatorward wind stress) where the velocities exceed -9.0 cm s^{-1}. The seasonal average geostrophic flow in the upper 100 m relative to 500 m off Point Sur and Point Conception is equatorward flow from February to September and poleward flow from October to January (*Chelton*, 1984). The CUC was present over the continental slope for most of the year, with the exception of early spring (March - May) and poleward flow extended to the surface in the wintertime (October - February). The surface flow throughout this region was found to lead the annual wind forcing, computed from the spatial averages of *Nelson* (1977), by about one month while the deeper poleward flow was found to lag the poleward barotropic pressure gradient by about two months (*Chelton*, 1984). These time scales are in reasonable agreement with the modeling results of *Philander and Yoon* (1982). Using 200-day periodic alongshore wind stress, they found that the alongshore surface velocity led the alongshore pressure gradient and wind stress by approximately 25 days, while the undercurrent lagged the alongshore pressure gradient by approximately 75 days.

Wickham et al. (1987) examined current meter and hydrographic data collected off Cape San Martin, California between 1978 and 1980 and found that the undercurrent had a jet-like core with maximum velocities in excess of 15 cm s^{-1}, and was confined to within 30 km of the coast in the upper 300 m. The currents exhibited a strong annual cycle, similar to the results of *Chelton* (1984). *Tisch et al.*, (1992) found that the position of the core off Point Sur, California

varied between 12 and 42 km from shore, and between depths of 70 and 460 m, with speeds ranging from less than 5 cm s^{-1} to 35 cm s^{-1}, with maximum flow occurring in winter.

While these observational studies began to identify the kinds of variability present within the CCS, and some of the basic time scales, the Coastal Ocean Dynamics Experiment (CODE) was the first study to address the issue of identifying and studying the dynamical processes of the wind-driven motion of water over the slope. This experiment was one of the first heavily instrumented programs of its kind conducted off the west coast of the United States. CODE was located off the northern California continental shelf between Point Reyes and Point Arena and occurred during the spring and summer of 1981 (CODE 1) and 1982 (CODE 2) (*Beardsley and Lentz*, 1987). Results from CODE 1 showed that the current field over the shelf was highly coherent in the vertical but exhibited significant horizontal mesoscale variability suggesting that the flow over the shelf and slope may be strongly influenced by eddy-like features, both offshore and within the coastal flow, local and remote wind forcing, and local topographic effects (*Beardsley and Lentz*, 1987). Therefore, in CODE 2, high vertical resolution was replaced with increased horizontal instrumentation to investigate this mesoscale variability.

Strub et al. (1987) investigated the annual variations in atmospheric forcing, currents, water temperature, and sea level along the west coast of the United States between 35° N and 48° N. They found that monthly mean winds in fall/winter were poleward north of 35° N to 45° N for three to six months, and were weakly equatorward or zero south of 35° N. The monthly mean alongshore currents over the mid-shelf and shelf break for depths of 35 m or

deeper were poleward, and were associated with higher coastal sea levels and relatively warmer water temperatures. In spring/summer, they found the monthly mean winds to be equatorward for three (near 48°N) to six months (near 35°N). At these times sea levels were lower and the water temperature cooler. The monthly mean currents at 35 m over the shelf were equatorward from one to six months, being both longer in the north and over the shelf break than to the south or over mid-shelf (*Strub et al.*, 1987). The seasonal cycles of all variables showed a poleward propagation, with stations in the south leading those in the north by one to two months. Annual mean currents over the shelf break at 35° and 48° N were found to oppose the annual winds, while between 35° N to 43° N, strongly fluctuating currents existed both in summer and winter regimes.

Noble et al. (1987) found subtidal current fluctuations (33 hours < period < 32 days) over the continental slope off northern California to be strongly polarized along local topography, and poleward in the mean. Alongslope currents on the upper slope were highly coherent in the vertical, with the first mode EOF (empirical orthogonal function) explaining approximately 75% of total variance. The alongslope variance was between 3 and 50 times greater than cross-slope variance. These observations also imply that the upper slope flow is mainly an extension of the poleward undercurrent observed over the California slope (*Chelton*, 1984; *Tisch et al.*, 1992), although as mentioned earlier, the continuity of the CUC has not yet been established. Mid-slope (instrument located on the 2200 m isobath) flow was generally weak, with no significant mean flow. Subtidal currents in the adjacent ocean basin were found to have no stable orientation, with a weak southerly mean flow. In this location, the easterly

variance was one to two times the northerly variance. The subtidal current fluctuations in each of these regions (upper slope, mid-slope, adjacent ocean basin) were generally incoherent with each other, and only weakly coherent with wind stress and sea level, whereas *Winant et al.* (1987) found that the subtidal currents over the shelf are, in general, coherent with sea level and wind stress. As a result, these observations indicate that shelf and slope flow may not be correlated with each other even when separated in the horizontal direction by as little as 25 km.

Currents over the central California shelf and upper slope were also studied as part of the Central California Coastal Circulation Studies (CCCCS) program, conducted between Point Conception and San Francisco from February 1984 through July 1985 (*Chelton et al.*, 1988). Consistent with the findings during CODE (*Winant et al.*, 1987), the alongshelf current fluctuations were found to be highly correlated with local winds (response within 0.5 day) and propagated poleward in rough agreement with the second-mode coastal trapped wave estimated by the model of *Chapman* (1987). In both the CCCCS and CODE regions, however, the correlation between currents and winds beyond the shelf break showed a marked decrease, and illustrate that currents separated by only 10-15 km cross shore show less correlation than shelf currents separated by as much as 220 km alongshore (*Noble et al.*, 1987; *Chelton et al.*, 1988).

During the Northern California Coastal Circulation Studies (NCCCS) program, conducted between San Francisco and the California-Oregon border from March 1988 through October 1989 (*EG&G*, 1988), the average annual flow was generally more poleward than the seasonal average flow during CODE (*Magnell*, 1991). Strong poleward flow was observed over the shelf at nearly

every instrument location during late summer and was in opposition to equatorward wind stress. Very low frequency current fluctuations, O(months), were observed at all mooring locations and found to be poorly correlated along the coast, and with the local wind stress. Currents in the 2 to 20 day band were found to be correlated best with winds to the south, suggestive of remote forcing. This is consistent with the findings of *Davis and Bogden* (1989) who, based on CODE data, discuss a length scale of 500 km associated with remote wind forcing. *Magnell* (1991) also found that alongshelf pressure gradients, forced by alongshelf variations in wind stress (τ^y), were highly correlated with the local current accelerations.

Strong poleward mean flow, in opposition to the equatorward wind stress, was observed during the CCCCS experiment and spread offshore to a distance of 300 km. Similar occurrences were observed in July 1981 (*Chelton et al.*, 1988) and in July 1989 (*Tisch et al.*, 1992), where poleward flow extended to 80 - 150 km offshore. These bursts of poleward flow were believed to have been the result of large-scale wind relaxations that occurred previously over the central and southern California regions. The coastal response to a relaxation from upwelling were examined by *Huyer and Kosro* (1987) and *Send et al.* (1987) during CODE. While the appearance of poleward surface flow and associated warm water, in response to a cessation of equatorward upwelling favorable winds, is similar to these larger poleward bursts, the poleward flow observed in the CODE region appeared to be trapped to a narrower region over the continental shelf, and had a time scale of approximately one week (compared to nearly six months in 1981 and 1984) (*Chelton et al.*, 1988).

Utilizing data from the Ocean Prediction Through Observation, Modeling, and Analysis (OPTOMA) program, *Reinecker et al.* (1988) found strong vertical coherence at all mooring locations on the continental rise in the upper 600 m of water column, with the velocity components being in phase for periods longer than about 10 days (over vertical separations of up to 500 m). Motions in the upper ocean were not highly coherent with those in the lower ocean, and band-averaged coherences of u, v, and T as a function of vertical separation showed a decrease in coherence as vertical separation increased for periods longer than 10 days. Temperature was found to be less coherent at smaller separations than u and v. At 350 m depth, the highest coherence was found between the out-of-phase v components at periods of 45-90 days. At periods of 9 - 13 days, they observed a surface and bottom intensification of the nearshore kinetic energy, which they found to be partially consistent with the presence of topographic Rossby waves.

Adding to the mesoscale variability within the CCS are filaments and jets, which extend offshore from the shelf break to several hundred kilometers (*Brink and Cowles*, 1991). Filaments are commonly observed features in satellite sea surface temperature and ocean color (CZCS) imagery of the central California coastal waters from Cape Blanco to Point Conception (*Bernstein et al.* 1977; *Breaker and Gilliland*, 1981; *Ramp et al.*, 1991a). It has been the goal of the Coastal Transition Zone Experiment (CTZ, conducted from 1986 through 1988 offshore of the CODE region), to study, among other things, the physical structure and characteristics of these cold filaments, with an emphasis on furthering the present understanding of the kinematics and dynamics involved. Several theories have been proposed for their physical cause: 1) baroclinic

instability of the flow within the CCS (*Ikeda and Emery*, 1984); 2) irregular coastline geometry (*Peffley and O'Brien*, 1976; *Crepon et al.*, 1984); 3) variable bottom topography (*Preller and O'Brien*, 1980); 4) alongshore variation of wind stress (*Batteen et al.*, 1989): and 5) interaction with an offshore eddy field (*Reinecker et al.*, 1988; *Reinecker and Mooers,* 1989). However, which cause(s) will generate these features in a particular geographical location is still an area of active research.

Analyzing buoy drifter tracks from the CTZ experiment, *Brink et al.* (1991) found that in the summer and fall, the CC may be characterized as a meandering coherent jet, which on average flows southward to at least 30° N. Between 33° N and 39° N, core velocities of 50 cm s^{-1} were typical, and current meanders had alongshore wavelengths of O(300 km) and cross-shore amplitudes of O(100-200 km). These observations are consistent with those of *Bernstein et al.* (1977), who observed the CC to be a meandering jet, with wavelengths of 300 to 500 km. *Brink et al.* (1991) also found that this meandering can lead to large eddy kinetic energies and eddy diffusivities, especially north of 36 ° N. In general, the results from the CTZ program reveal that the core of the CC in summertime is unstable, leading to the formation of a meandering jet surrounded by persistent eddies (*Brink and Cowles*, 1991). *Huyer et al.* (1991) conducted repeated mesoscale surveys throughout the CTZ region and found that a meandering baroclinic equatorward jet was common to all. The core velocity exceeded 50 - 70 cm s^{-1}, and may be coincident with the core of the CC. They also observed a poleward flowing undercurrent adjacent to the continental slope at depths of 150 - 250 m, with core velocities up to 20 cm s^{-1}.

From these studies we have begun to assimilate a vast amount of information on the kinematical and dynamical aspects of the CCS, and eastern boundary regions in general, and have demonstrated that the CCS is not a simple, but rather a complex and highly variable flow regime, consisting of eddies, filaments, and energetic baroclinic jets. In light of this it is surprising that the study of energetic processes within eastern boundary regions has not gained more attention. If the poleward undercurrent, found in eastern boundary regions, is unstable, it is likely to play an important role in the generation of these cross-shore jets and eddies (*Mooers*, 1989). Therefore, the study of energetics within eastern boundary regions is crucial to determine if this transfer mechanism is substantial, and to identify what energy conversion processes and balances actually exist.

C. ENERGETICS OF OCEANIC GYRES, INCLUDING BOUNDARY CURRENTS

The study of energetics of the world oceans has primarily focused on determining the effects of eddies and time-dependent phenomena on the mean circulation of oceanic gyres, including boundary regions. As discussed earlier, this eddy variability can act as a signal for such oceanic processes as instabilities associated with strong currents, and as a mechanism for the transport of heat and momentum. The distribution of eddy kinetic energy throughout the world ocean has also provided a means for validating numerical ocean models (*Holland and Schmitz*, 1985; *Schmitz and Holland*, 1982, 1986; *Hall*, 1991).

In recent years, a great deal of effort has been put forth in studying the interactions of eddies and western boundary currents (WBC), largely because of the role that WBCs play in determining the nature of basin-scale flow (*Dewar and Bane*, 1985), and because the strongest oceanic eddy variability is associated

with WBCs, and their extensions (*Hall*, 1991). In-depth analyses of the energetics of eddy-mean flow interactions have been made for the Florida Current (*Schmitz and Niiler*, 1969; *Brooks and Niiler*, 1977), the Gulf Stream (*Webster*, 1961, 1965; *Watts and Johns*, 1982; *Dewar and Bane*, 1985, 1989a, b; *Hall*, 1986a; *Rossby*, 1987), and the Kuroshio Extension (*Nishida and White*, 1982; *Hall*, 1991). The following discussion highlights some of the methods and key results obtained from some of these studies.

Using data from multiple current meter moorings, located within the Gulf Stream (GS), *Dewar and Bane* (1985, 1989a, b) have computed energy budgets for the mean and eddy flow fields. This was accomplished by using the ensemble averaged horizontal momentum equations, multiplied (vector multiplication) by the ensemble averaged velocity. They found that a release of mean kinetic energy by the eddies constituted the dominant form of energy conversion within the GS off Charleston, South Carolina (*Dewar and Bane*, 1985), and that eddy pressure work may be important in the fluctuating energy budget. Their calculations also revealed that the mean kinetic energy flux within the GS in the South Atlantic Bight increases downstream, and the eddies tended to decelerate the mean flow. In order to obtain a balance in the mean flow equations, they concluded that the GS in the Bight must be releasing mean potential energy by flowing down a mean pressure gradient. Similar results were obtained in the GS farther to the north (*Dewar and Bane,* 1989a), where flow below 880 m depth was down a mean pressure gradient; however, above this depth, they concluded that a conversion of mean kinetic energy to mean potential energy occurred via a flow up a mean pressure gradient.

Hall (1986a) examined the energetics of the GS at 68° W, using eddy kinetic and potential energy equations, derived from the horizontal momentum and heat equations, respectively. Results indicated a net conversion of mean to eddy kinetic and potential energies, with energy exchanges being dominated by motions in the upper 1000 m of the water column. The well-defined structure of horizontal and vertical velocity, and temperature (*Hall*, 1986b) made it possible for this study to deduce the time-averaged structure from data from a single current meter mooring (*Hall*, 1986a).

A similar study was conducted by *Hall* (1991) in the Kuroshio Extension, using data from a single current meter mooring. Once again, horizontal derivatives within the momentum equations could be estimated based upon the cross-stream structure of the Kuroshio Extension defined by *Hall* (1989a). In this study baroclinic and barotropic energy conversions within the current were examined using both geographic and "stream" coordinate systems. Cross-stream position was quantified in terms of the measured temperature at 350 dbar, and an alongstream flow direction defined by the measured current shear. Based upon this information the time series of velocity and temperature were rotated into a "stream" coordinate system, whose axes were attached to the meandering current. Using stream coordinates, *Hall* (1991) found significant conversions of mean to eddy potential energy on the anticyclonic side of the current, and smaller conversions of eddy to mean energy over the cold portion. In the geographic coordinate system, the Reynolds stresses were much stronger than for the stream coordinate system and resulted in relatively large apparent eddy to mean kinetic energy conversions.

While these and other studies have examined the nature of energetic conversions within western boundary regions from different perspectives, there is very little information about conversion processes within eastern boundary regions. As the results from the observational and modeling studies within the CCS have demonstrated, a great deal of mesoscale variability exists, and one could expect intense eddy-mean flow interactions to occur. To date no comparable studies of energetics over the continental slope within eastern boundary currents have been conducted, nor have there been any based upon direct observations within the CCS. Recently, however, a wind-driven eddy-resolving limited-area quasi-geostrophic (QG) model has been used by *Auad et al.*, (1991) to examine the circulation and energetics within the CCS. The model includes quasi-realistic bottom topography, true coastline, and is embedded within a coarser model covering most of the North Pacific Ocean. QG theory is an approximation to the primitive equations when the Rossby number is small and the scaled solution remains O(1) (*Walstad et al.*, 1991). Based upon comparisons between observations and modeling results within the Gulf Stream and Kuroshio Extension (*Schmitz and Holland,* 1982, 1986), QG models are capable of accurately reproducing the observed eddy energy fields and their associated time scales (*Auad et al.*, 1991).

The model simulated the main components of the CCS, namely the CC, CUC, DC, and a feature known as the Southern California Eddy, within the Southern California Bight. The simulated CC consisted of active eddy-mean flow interactions, and was an effective source of both first-mode baroclinic annual Rossby waves between 25° and 33° N, which propagated westward through the model domain, and long period (> 200 days) waves north of 34° N, believed to

result from baroclinic instability (BCI). This eddy-mean flow interaction is consistent with earlier observations, which have characterized the CC as a meandering feature rich in mesoscale variability (*Lynn and Simpson*, 1987; *Brink and Cowles*, 1991). Mesoscale variability within the model was characterized by periods of O(100 days), and wavelengths of O(200 km). These length scales are somewhat smaller than the observations of *Bernstein et al.*, (1977) and *Brink et al*, (1991), but are consistent with the idea that the CC can be thought of as a meandering jet surrounded by eddies.

Near-surface circulation was found to be energetically dominated by the mean flow, whereas the deeper (below ~ 3500 m) circulation was dominated by the eddy field. Energy transmitted by the wind to the mean flow in the upper 500 m was both fluxed out of the open boundaries as a result of the β effect and also transformed into available potential energy (APE). Baroclinic processes were then responsible for converting this APE into a highly energetic eddy field (*Auad et al.*, 1991). Below 500 m depth, energy appeared to be radiated vertically through action of the eddies themselves. In the core of the simulated CC, they found that downgradient eddy fluxes of temperature were of greater importance in the production of eddy kinetic energy than was the advection of available eddy PE.

Walstad et al., (1991) recently investigated the dynamics of the Coastal Transition Zone off northern California, through the use of assimilation modeling techniques. In their study, a regional baroclinic QG model was driven by initial and boundary conditions derived from objective analysis of hydrographic and acoustic Doppler current profiler (ADCP) data, collected in late May and early June 1987. During this period, the CTZ consisted of a

meandering jet in the southwest portion, inflow from a jet in the northwest portion, a cyclonic eddy in the northeast portion and a poleward current in the southeast portion. *Pierce et al.* (1991) found that local Rossby numbers calculated across this meandering jet approached a maximum value of nearly 0.2, and concluded that the QG approximation still remains valid in this region.

In their analysis, *Walstad et al.*, (1991) found that the divergence of horizontal advection of kinetic energy was a mechanism forcing the jet meander, with pressure work redistributing energy both horizontally and vertically, while the total pressure work divergence nearly balanced the total time rate of change of kinetic energy following a parcel (DKE/Dt). They also found that the initial meander pattern which developed in the jet was primarily the result of barotropic instability (BTI), while buoyancy (the PE to KE conversion term) and vertical pressure work divergence were active on wavelengths greater than 200 km. However, below the main thermocline in the vicinity of the meander, both baroclinic and barotropic mechanisms were found to be important. Based upon these results, they concluded that a large mixed instability meander was responsible for the propagation of the jet away from the coast and out of the region.

The linear stability of a CTZ jet was examined by *Pierce et al.* (1991) using a six-layer QG model with observed velocity profiles, based upon the objective analysis of *Walstad et al.* (1991), serving as the basic state for the model. Their results indicated that barotropic instability within the cross-jet component of the divergence in advection of kinetic energy led to a net transfer of mean kinetic to perturbation kinetic energy. When perturbation wavelengths were less than 90 km, the resulting instabilities were almost entirely barotropic in nature. For

wavelengths between 110 - 190 km, eddy potential energy began feeding back to the mean; however, the barotropic conversion process was still able to maintain the instability. At these wavelengths, there was also a strong transfer of eddy kinetic energy downward through the model layers. When the perturbation wavelength was equal to 260 km, both mean potential and mean kinetic energy were feeding the perturbation at all levels, signifying that both barotropic and baroclinic processes were contributing to the growth of the disturbance. The kinetic energy transformation was the dominant process in the upper 500 m depth, while below this depth the potential energy conversion exceeded the kinetic energy conversion (*Pierce et al.*, 1991). The 260 km wavelength was the fastest growing mode, with the ratio of BCI/BTI being nearly 0.9, while for wavelengths greater than 260 km, they found that the instabilities were more baroclinic in nature (*Pierce et al.*, 1991).

D. SCIENTIFIC OBJECTIVE OF THE DISSERTATION

The purpose of this dissertation will be to examine the energetics of the low frequency variability observed within the CCS using current meter data collected off Point Sur, California. To date, no detailed study of energetic interactions within eastern boundary currents, based upon direct observations, has been made over a continental slope region. A detailed study of the energetic interactions between mean and eddy fields will not only provide a means for comparison with the modeling results of *Auad et al.* (1991), *Walstad et al.* (1991), and *Pierce et al.* (1991), discussed above, but will hopefully provide us with a better understanding of the California Current System and eastern boundary currents in general.

While the energy studies of *Hall* (1986a, 1991) were based upon data from single current meter moorings, detailed descriptions of the cross-stream structure of the Gulf Stream and Kuroshio Currents provided the necessary information to evaluate several terms in the eddy kinetic energy (EKE) equation, as well as terms in the eddy potential energy (EPE) equation. The EKE equation, obtained by multiplying the u and v momentum equations by u' and v', respectively, adding them together and taking the time average, requires information on horizontal gradients of velocity. The data set used in this study does not contain enough information for the computation of these horizontal gradients. Furthermore a well-defined cross-stream structure for the CCS off Point Sur, comparable to those used by *Hall* (1986a, 1991), does not exist. Therefore, the method chosen to examine energetic conversions in this study must rely solely on the data set available, and will be limited to the use of the eddy potential energy equation.

To accomplish this task, I have chosen an approach similar to that of *Niiler and Hall* (1988) and *Hall* (1991), in which they examined low-frequency eddy variability within the eastern North Pacific Subtropical gyre, and the Kuroshio Extension, respectively, using data from a single mooring. *Niiler and Hall* (1988) examined the energy conversions between the mean flow, very low frequency motion, and eddy band through use of the eddy potential energy equations. For their data set (a three year time series) the low frequency (periods greater than 200 days) and eddy bands (periods from 40 to 200 days) were determined from the spectral characteristics of the data. All computations in these two studies were performed using data which were synthesized at mid-depth levels between the instrumented depths. In creating these mid-depth time

series, *Niiler and Hall* (1988) and *Hall* (1991) were also able to obtain time series of the horizontal gradients of temperature ($\partial T/\partial x$, $\partial T/\partial y$), which appear in the EPE equation, through the use of the thermal wind relations. Using the observed data from above and below, $\partial T/\partial x$ and $\partial T/\partial y$ were calculated at mid-depths using the velocity shear at the midpoint.

In proceeding with this method, it has been necessary to synthesize time series of all variables (u, v, w, T) and $\nabla_H T$ at the mid-depth levels between the actual instrumented depths. A complete description of the data sets and data processing methods, which includes the technique used to create each of these time series, is contained in Chapter II, with the exception of w, which is found in Chapter IV. General characteristics and details on the spectral analysis of these data sets can be found in Chapter III. The plan of the dissertation is to examine the energetic conversions through use of the eddy potential energy equation. The development of this conceptual model has been described in Chapter IV, with specific details being deferred to Appendix D. Time series of each term in the eddy potential energy equation have been computed using this model and allow for examination of energetics within individual events as well as in the mean. From this we may learn whether the mean values are the result of a few specific events or are actually representative of the mean state off Point Sur. Periods where locally intense bursts (growth/decay) occur within these terms will also be examined to determine how eddy potential energy is growing or decaying and what the dominant source and sink terms are.

II. DATA AND METHODS

A. DATA COLLECTION

1. Current Meter Data

Vector-averaged current velocities, current directions, temperature, conductivity, and pressure were collected at two mooring sites, denoted P2 and P3, off Point Sur, California (Table 1). Mooring P2, located on the 800 m isobath over the continental slope, was equipped with three Aanderaa vector averaging current meters (Model RCM8) placed nominally at 100, 350, and 500 m depths. Mooring P3, located near the 1800 m isobath, was equipped with four current meters placed nominally at 100, 350, 500, and 1000 m depths (Figure 1). Data were recorded at 30 minute intervals using solid state Data Storage Units (DSU), each of which is capable of storing 65530 10-bit words. At this interval each DSU could hold up to seven months of data, thus requiring data collection to occur over several deployments between May 1989 and May 1991 (Table 2, Figure 2).

Current velocities were measured through the use of a shrouded paddle wheel and electronic counter assembly located at the top of the recording unit. Velocity, in units of cm s^{-1}, was determined from the number of revolutions made by the paddle wheel during each sampling interval. The sensor had an accuracy of $\pm$ 1.0 cm s^{-1} over its range of 2.0 - 250 cm s^{-1}, while below a velocity threshold of 2.0 cm s^{-1} the paddle wheel would stall (*Aanderaa*, 1990). Both pressure sensors and the mooring dynamics program in use at the Naval Postgraduate School (NPS) indicated a maximum mooring tilt of 11.7°

Table 1. POINT SUR MOORING LOCATIONS

Mooring	Geographical Position	Instrumented Levels	Depth
P2	36 20.0' N 122° 10.2' W	100, 350, 500 m	800 m
P3	36 20.0' N 122° 27.6' W	100, 350, 500, 1000 m	1800 m

Table 2. CURRENT METER DEPLOYMENT DATES

Mooring	No.	Deployment	Recovery
P2	1	11 May 1989	24 August 1989
P2	2	25 August 1989	14 December 1989
P2 & P3	3	15 December 1989	12 May 1990
P2	4	14 May 1990	9 October 1990
P3	4	13 May 1990	10 October 1990
P2	5	10 October 1990	12 May 1991
P3	5	11 October 1990	12 May 1991

(*Sielbeck*, 1991), which is just below the acceptable level for proper compass operation; however, most of the time the mooring tilt was below this value.

Current direction was measured by a magnetic compass/potentiometer assembly located below the storage unit. The compass was oil damped and required an average of 3 to 5 seconds to resolve directional changes of 90° or more. It could function properly up to a maximum tilt angle of 12° from the vertical and had a resolution of 0.35°. The accuracy of the compass varied between ± 5.0° for current velocities of 5 - 100 cm s^{-1}, and ± 7.5° for velocities of 2.5 - 5 cm s^{-1} and 100 - 200 cm s^{-1}. Combined magnetic deviation and

variation for each unit was determined on a surveyed test bench at NPS prior to each deployment and was accounted for in the postprocessing software (*Sielbeck*, 1991).

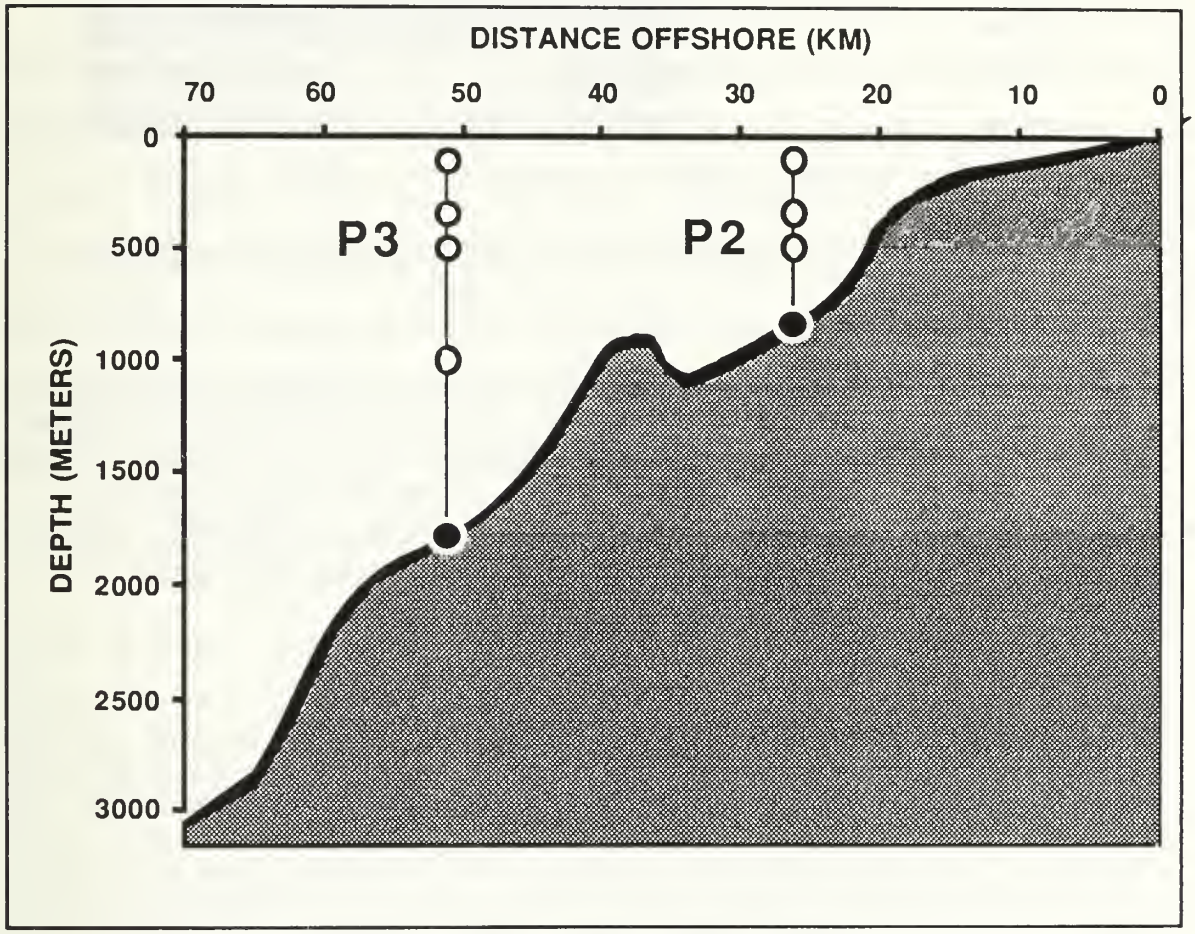

Figure 1. Current Meter Configuration at Moorings P2 and P3 (Adapted from: *Sielbeck*, 1991)

2. Hydrographic Data

During the deployments of moorings P2 and P3, oceanographic research cruises were being conducted as part of the Point Sur Transect (POST) and California Undercurrent (CUC) Programs conducted by the Department of

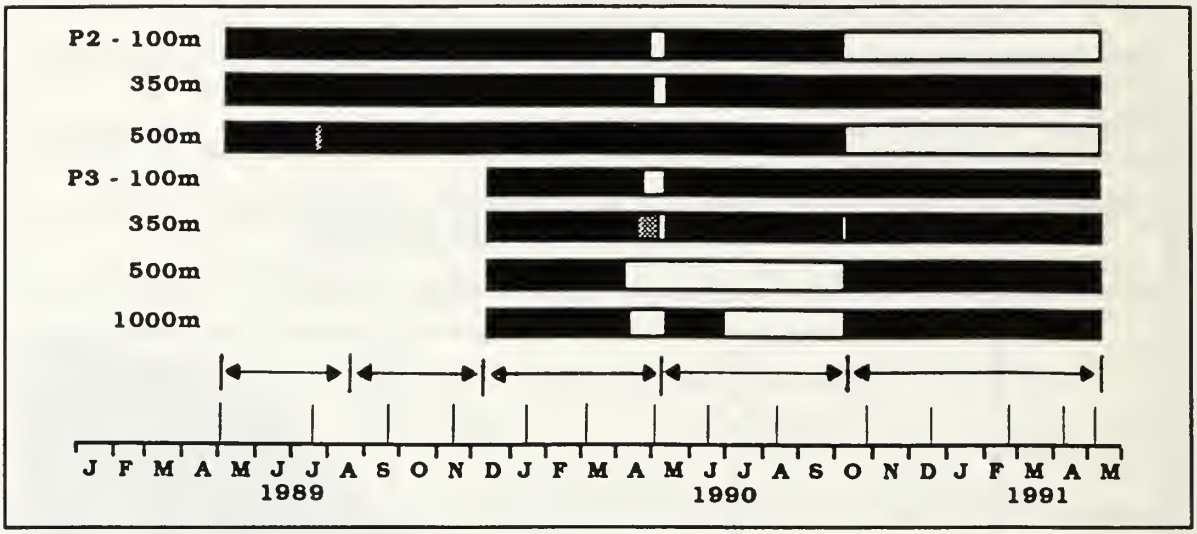

Figure 2. **Current Meter Deployments at Moorings P2 and P3:** The solid (blank) bars represent areas where good (no) data was obtained. The two shaded areas (P2-500m and P3-350m) represent areas where only u,v data was bad. Horizontal arrows denote individual deployments and the small vertical lines represent the times of hydrographic cruises listed in Table 3.

Oceanography at NPS. The POST, established in 1987, has been occupied 6-8 times yearly to examine long-term variability in the CCS off Point Sur, California. Data were collected at stations along the transect from the surface to within 50 - 150 m of the bottom using Neil Brown Instrument Systems (NBIS) Mark IIIB CTD's. For a complete description of the POST and CUC programs, along with detailed information on CTD calibrations, the reader is referred to *Tisch* (1990). Hydrographic data from stations located near moorings P2 and P3, collected during 14 cruises (Table 3), have been used to identify a relationship between temperature and pressure at each mooring and to compute density, ρ, and an equivalent compressibility coefficient, α, (*Dewar and Bane*, 1985; *Niiler and Hall*, 1988) at each instrument location. This information is

required for the calculation of terms found in the heat and energy equations and will be discussed in detail later in the chapter.

B. DATA PROCESSING

Upon recovery, raw data from the DSUs were downloaded to a computer and converted to standard scientific units using the sensor calibration equations. Data were then visually inspected for outliers or periods suspect of instrument failures or malfunctions, and were edited or deleted manually when necessary. The data were then filtered prior to further analyses using methods originally developed at Oregon State University (*Denbo et al.*, 1984). A standard right-hand coordinate system is used where x, y, and z are positive east, north, and up, respectively, and pressure, P, is positive downward.

1. Filtering

The postprocessed records were initially filtered with a Cosine-Lanczos filter utilizing a centered 25 point data window. This filter had a half power period of 2.9 hours (8.4 cpd) and completely removed signals whose periods were shorter than 2.0 hours. The 30 minute records were then interpolated to 60 minute intervals using Lagrangian polynomials, which allow for interpolation of unevenly spaced data points to specified intervals (*Gerald and Wheatley*, 1989) with each point falling on an even hour. At this stage any gaps in the hourly data sets were identified and filled using procedures described in the next section.

2. Data Gaps and Gap Filling Procedures

The presence of gaps in a time series has a negative effect on the proposed statistical analyses, especially when dealing with frequency-domain

Table 3. **HYDROGRAPHIC CRUISES OCCURRING DURING CURRENT METER DEPLOYMENTS:** Cruise designations beginning with ST were in conjunction with the POST program, while CU pertains to the CUC program. POST stations 3 - 6 and CUC stations 5, 6, 10, and 11 were used for this study.

Cruise Designation	Date of CTD casts
STMAY89	5/5/89
CUJUL89	7/29/89
CUSEP89	9/26/89
CUNOV89	11/16/89
CUJAN90	1/18/90
CUMAR90	3/2/90
STMAY90	5/2/90
CUJUN90	6/16-17/90
CUAUG90	8/13-14/90
CUOCT90	10/25-26/90
CUDEC90	12/13/90
CUFEB91	2/21-22/91
CUAPR91	4/5-6/91
STMAY91	5/8/91

calculations. Therefore to obtain the longest possible segments, thus ensuring a continuous time line, gap filling techniques were required. Care must be taken to select a procedure, though ad hoc, which will introduce a minimum amount of error into subsequent analyses. There were two kinds of gaps in the data: short

gaps, usually between deployments, which could be filled using simple techniques, and gaps greater than 1 day which required more sophisticated methods. A period of 16 to 18 hours was common between recovery and re-deployment of instrumentation (Table 4). With the exception of the pressure time series, only those gaps in the hourly data sets where the gap length/record length ratio was 0.1 or less were filled.

During the third deployment at mooring P2 (Table 2), the pressure sensor at the 350 m depth failed at deployment. To create a time series of pressure at this level, a value of 250 m, the amount of wire between instruments, was added to the pressure of the 100 m sensor. A similar procedure was used to correct for erroneous pressure values at the 500 and 1000 m instruments during the first deployment at P3. The time series at 500 m showed considerable noise, and the variance (σ^2 = 81.86 dbar^2) was an order of magnitude larger than the upper level instruments (σ^2 < 2.0 dbar^2). Such variability at depth is highly unlikely given the nature of flow throughout the region and is an indication that the sensor failed. The pressure at 1000 m showed less variability (σ^2 < 9 dbar^2) than at 500 m; however it contained a drift over time. This drift was not present in data from the three instruments lying above it in the water column, indicating that the mooring's anchor did not drag along the bottom and that this data was also in error. Here the time series from the 350 m instrument was used to create new time series at these levels by adding 150 m and 650 m, respectively, which once again was the amount of wire between instruments. This method does not account for the fact that the upper level instruments may be "blown over" more than the lower instruments, as is usually the case in stronger flow regimes such

Table 4. **TEMPORAL EXTENT OF GAPS AT MOORINGS P2 AND P3:** The asterisks indicates that only u, v data was missing from the current meter record.

Instrument	Starting Date	Ending Date	Duration
P2 - 100 m	3 Jun 89 / 1200*	4 Jun 89 / 0500*	18 hrs*
	24 Aug 89 / 1800	25 Aug 89 / 1000	17 hrs
	14 Dec 89 / 0900	15 Dec 89 / 0300	19 hrs
	28 Apr 90 / 1600	13 May 90 / 2300	~15 days
P2 - 350 m	24 Aug 89 / 1700	25 Aug 89 / 1000	18 hrs
	14 Dec 89 / 1000	15 Dec 89 / 0300	18 hrs
	1 May 90 / 1500	13 May 90 / 2300	~13 days
	9 Oct 90 / 1500	10 Oct 90 / 0800	18 hrs
P2 - 500 m	23 Jul 89 / 0600*	27 Jul 89 / 1400*	105 hrs*
	24 Aug 89 / 1800	25 Aug 89 / 1000	17 hrs
	14 Dec 89 / 1000	15 Dec 89 / 0300	18 hrs
	12 May 90 / 2100	13 May 90 / 2200	26 hrs
P3 - 100 m	24 Apr 90 / 2000	13 May 90 / 0400	~20 days
	10 Oct 90 / 0900	11 Oct 90 / 0100	17 hrs
P3 - 350 m	16 Apr 90 / 2300*	7 May 90 / 0100*	~20 days*
	7 May 90 / 0200	13 May 90 / 0400	~7 days
	8 Oct 90 / 1100	11 Oct 90 / 0100	63 hrs
P3 - 500 m	7 Apr 90 / 0900	11 Oct 90 / 0100	~188 days
P3 - 1000 m	10 Apr 90 / 1100	13 May 90 / 0400	~34 days
	1 Jul 90 / 0900	11 Oct 90 / 0100	~102 days

as the Gulf Stream and Kuroshio currents, where stronger currents (in excess of 1.0 m s^{-1}) can cause vertical excursions of several hundred meters (*Hall,* 1989b). However, the small variability shown in the time series of pressure (Table 5) show that blowover was very small (less than 2 m) and would indicate that this

procedure can be used in this region without introducing significant error into subsequent calculations.

Missing hourly data points of velocity (u, v) and temperature for the periods between deployments (gaps less than 18 hours) were interpolated by use of a cubic spline, while for pressure, which showed considerably less variability during deployments, simple linear interpolation was used. In these cases, the gap length/record length ratio was considerably smaller than 0.1, and the gap length itself was less than the half power period of the low pass filter. Since the focus of this study is on subtidal variability (periods longer than two days), it is expected that this technique will introduce minimal error into further analyses.

To make the time series from mooring P2 complete for examining spectral properties and studying energetic conversions over a 17-month period, three additional gaps, one occurring at each of the instrumented depths and all less than two weeks in duration (Table 4), had to be filled using a more rigorous technique. Briefly, this technique consists of: 1) initially filling the gaps with linearly interpolated values; 2) detrending the time series using least squares techniques; 3) estimating the sample periodogram; 4) removing any dominant cycles within the detrended data set (here being the diurnal and semi-diurnal signals): 5) fitting a first order autoregressive model, AR(1), to the detrended and deseasonalized data; 6) forecasting and backcasting from each end of the gap to interpolate the values across the gap; and 7) adding the estimated trend and cycle back to the interpolated times series. A similar procedure was also applied to the 63 hour gap in the 350 m record at mooring P3 (Table 4) so that a continuous record, one year in length, could be obtained. The specific details of

this technique, developed by P.A. Lewis and B.K. Ray of NPS, are contained in Appendix B.

The gap-filled hourly data sets were filtered using a second Cosine-Lanczos filter, having a half power period of 46.59 hours (0.515 cpd) designed to remove diurnal, inertial, and shorter period energy within the signal. The filter utilized a centered 121 point data window to produce a single filtered data point. The filtered data were then decimated to six hourly values for subsequent analyses. Plots of current velocity vectors and temperature for moorings P2 and P3 using this filter are contained in Appendix A. Basic statistics of these data sets by deployment can be found in Table 5. A comparison of basic statistics, based upon the entire 17 months of data before and after the use of the technique discussed above, shows very little change in the mean and variances of both time series (Table 6). Similarly, the autospectra based on the first year of data alone and the 17 month gap filled series, were very similar in the spectral shape with little change in the higher frequencies, and more energy contained in the lower frequencies of the latter (expected with the longer data set). Based upon these results, this technique appears to be have been successful at filling the large gaps in the P2 and P3 data sets, while at the same time introducing a minimal amount of error into these signals. However, caution must be exercised when examining energetics during this period to avoid erroneous conclusions based upon synthetic data.

Table 5. BASIC DATA STATISTICS FOR MOORINGS P2 AND P3: Statistics are based upon six-hourly low pass filtered data for actual deployment dates. Units are cm s^{-1}, °C, and dbar for velocity, temperature and, pressure, respectively. Positive (negative) values indicate northward (southward) or eastward (westward) flows.

Mooring		$\bar{u}$	σ_u	$\bar{v}$	σ_v	$\bar{T}$	σ_T	$\bar{P}$	σ_P
Deployment	*#1*								
P2	100 m	-5.43	11.41	8.89	12.58	9.07	0.37	112.14	0.77
	350 m	-3.18	6.78	7.50	12.50	7.05	0.23	364.44	0.78
	500 m	-3.00	5.44	4.09	12.46	6.13	0.20	519.06	0.42
Deployment	*#2*								
P2	100 m	-6.46	9.78	5.45	13.64	9.56	0.23	131.60	0.53
	350 m	-5.36	6.41	-3.45	11.48	7.13	0.23	385.21	1.26
	500 m	-3.3	5.97	-2.14	10.72	5.92	0.22	538.09	1.00
Deployment	*#3*								
P2	100 m	-5.05	10.9	7.97	14.28	9.61	0.36	109.26	0.87
	350 m	-1.99	6.73	5.91	9.07	7.06	0.29	359.94	1.17
	500 m	-0.43	5.99	3.20	9.13	5.96	0.18	510.00	1.18
P3	100 m	-4.65	10.00	4.00	13.34	9.75	0.35	106.60	1.08
	350 m	-3.78	6.76	2.82	10.07	6.88	0.30	363.71	1.56
	500 m	-3.36	5.57	2.52	8.46	5.79	0.22	513.64	1.70
	1000 m	-1.57	3.59	0.69	6.70	3.96	0.07	1013.56	1.69
Deployment	*#4*								
P2	100 m	-9.46	12.56	14.85	14.91	9.52	0.57	102.08	1.70
	350 m	-3.06	6.46	7.62	9.33	7.08	0.30	350.33	1.26
	500 m	-0.52	6.09	3.26	10.27	5.95	0.25	501.64	0.76
P3	100 m	-1.76	11.24	2.97	7.50	9.56	0.52	83.11	0.95
	350 m	-1.45	6.80	3.42	5.34	6.78	0.27	346.57	0.81
	1000 m	-1.71	3.71	0.97	5.12	3.94	0.55	995.97	6.38
Deployment	*#5*								
P2	350 m	-0.67	6.55	4.03	8.90	6.95	0.27	347.05	1.62
P3	100 m	-4.46	11.01	2.62	11.79	9.99	0.61	80.03	0.49
	350 m	-2.84	6.37	2.20	7.68	6.93	0.23	339.20	1.30
	500 m	-2.20	5.81	1.35	7.41	5.88	0.15	483.16	0.70
	1000 m	-1.36	4.00	0.41	6.34	3.94	0.82	999.53	1.45

Table 6. **COMPARISON OF PRE- AND POST-FILL DATA STATISTICS AT MOORINGS P2 AND P3:** Statistics are based upon six-hourly low pass filtered data from May 1989 to October 1990 for the 100 and 500 m levels and to May 1991 for the 350 m level for P2, and from May 1990 to May 1991 for P3. Units are cm s^{-1} and °C for velocity and temperature, respectively, and (cm s^{-1} , °C)^2 for variances. Positive (negative) values indicate northward (southward) or eastward (westward) flows.

Depth	$\overline{u}$	σ_u^2	$\overline{v}$	σ_v^2	$\overline{T}$	σ_T^2
Pre-Fill						
P2 -100 m	-6.79	88.18	9.68	165.61	9.46	0.19
P2 - 350 m	-2.50	22.18	4.44	75.09	7.04	0.05
P2 - 500 m	-1.61	13.53	2.18	58.00	5.99	0.04
P3 - 350 m	-2.26	29.05	2.71	25.78	6.87	0.05
Post-Fill						
P2 -100 m	-6.83	87.22	9.51	163.69	9.46	0.19
P2 - 350 m	-2.53	22.37	4.44	75.52	7.04	0.05
P2 - 500 m	-1.60	13.44	2.21	57.68	5.99	0.04
P3 - 350 m	-2.21	28.98	2.65	25.86	6.87	0.05

3. Time Series Synthesis

Before one can examine energy conversions and balances through the use of the heat equation, it is first necessary to obtain a time series for the horizontal gradient of temperature. The horizontal derivatives of temperature appear in several terms of the full heat and energy equations, the development of which appears later in this text. A time series of $\nabla_H T$ can be obtained by using

the thermal wind relations as proposed by *Niiler and Hall* (1988), along with the velocity and temperature data from two levels in the array. The resulting time series will be for the mid-depth between the two levels used. Therefore, it also becomes necessary to synthesize time series of u, v, and T for this same level before any further calculations can be made. For moorings P2 and P3 these levels will be at 225 dbar and 425 dbar, with an additional level of 750 dbar for P3 due to the instrument at 1000 m. All calculations were performed using the low pass filtered data sets, because it is within these lower frequencies where the thermal wind relation is a useful approximation.

a. Calculation of Temperatures and Velocities

There have been several different schemes (see Appendix C) used in recent years to correct a time series of temperature for vertical excursions of the mooring. In this study, the objective was not to correct the temperature time series for mooring motion ($\sigma^2 < 2$ dbar in most cases) but rather to synthesize a time series of temperature for the mid-depth between instrumented levels at moorings P2 and P3. Several methods of interpolation (linear, exponential, and polynomial functions) were investigated (Appendix C), and while the smallest errors were obtained by using a quadratic (cubic) function at P2 (P3) to model T vs. P at each site, the errors bars (95% significance level) for each method overlapped. This implies that no one method is significantly different from another, and therefore the linear approach was selected for use in these computations. The equation for linear prediction of temperature can be written as

$$T(P)_{new} = T_1 - \frac{(T_2 - T_1)(P_1 - P)}{P_2 - P_1} \qquad (1)$$

where the subscripts 1 and 2 refer to the upper and lower levels, respectively, and P is the pressure level of interest.

Linear interpolation methods have been used by several investigators (*Hall and Bryden*, 1985; *Hogg*, 1986) when correcting velocities for mooring motions in deeper water (near 400-500 m); however, they may not be suitable for shallower instruments (*Hall*, 1989b). In regions of intensified surface flow, the vertical structure of density and velocity are often modeled with an exponential dependence (*Gill et al.*, 1974; *Hall* 1989b, 1991). The velocity calculation scheme used by *Hall* (1989b, 1991) required the use of velocity and pressure records for two levels, and was either a linear or exponential interpolation depending upon the signs of velocity at each level. When the components of velocity (u_1 and u_2) at both levels were of the same sign and not equal, the mid-depth velocity was calculated assuming an exponential dependence between the two levels, whereas, when the components of velocity (u_1 and u_2) at both levels were of opposite sign or equal in value, the mid-depth velocity was calculated assuming a linear dependence between the two levels.

A problem with this particular scheme is that the results depend upon the choice of (x,y) coordinate axes, such that changing the definition of the axes changes the type of interpolation used. Additionally, by alternating velocity calculations between exponential and linear, it is possible to introduce errors into the energy calculations, through false fluctuations which may result from this scheme. Because the distances over which we are interpolating are relatively small compared to some of these other studies, and the fact that a linear approach was found to be satisfactory in the temperature calculations a linear approach

will also be used here for the sake of consistency. As with the temperature prediction, the velocity prediction equation is formulated as

$$u(P)_{new} = u_1 - \frac{(u_2 - u_1)(P_1 - P)}{P_2 - P_1} \tag{2}$$

where once again the subscripts 1 and 2 refer to the upper and lower levels, respectively, and P is the pressure level of interest. Sample time series of actual and synthesized data for mooring P3 are shown in Figures 3 through 5, and show that this method is acceptable and does not appear to have introduced any erroneous signals into the data.

b. Computation of Horizontal Temperature Gradients

To compute $\nabla_H T$, the approach of *Niiler and Hall* (1988) and *Hall* (1991), which utilize the thermal wind relations, has been used. By assuming a linearized equation of state of the form $\rho = \rho_0(1-\alpha T)$, the thermal wind relations can be solved for horizontal temperature gradients at mid-depth levels as

$$\frac{\partial T}{\partial x} = \frac{f}{g\alpha}\frac{\partial v}{\partial z} \qquad \frac{\partial T}{\partial y} = -\frac{f}{g\alpha}\frac{\partial u}{\partial z} \tag{3}$$

where f is the Coriolis parameter (8.5699×10^{-5} s^{-1} at 36° 20' N), g is the gravitational acceleration (980 cm s^{-1}), and α is an equivalent compressibility coefficient (*Dewar and Bane*, 1985). Vertical velocity shear is determined from

the upper and lower level time series. The value of α is defined as

$$\alpha = -\frac{1}{\rho_0}\frac{d\rho}{dT} = -\left(\left(\frac{1}{\rho_0}\frac{\partial\rho}{\partial T}\right) + \left(\frac{1}{\rho_0}\frac{\partial\rho}{\partial S}\right)\frac{dS}{dT} + \left(\frac{1}{\rho_0}\frac{\partial\rho}{\partial P}\right)\frac{dP}{dT}\right) \qquad (4)$$

(a) (b) (c)

where (a) is the thermal expansibility coefficient, (b) is the salinity contraction coefficient, and (c) is the isothermal compressibility coefficient. These values have been obtained from the UNESCO International Oceanographic Tables (*UNESCO*, 1987). Based upon the magnitudes of these coefficients, the isothermal compressibility term, (c), which is two orders of magnitude smaller than (a) and (b), has been neglected in these calculations. The mean value for T, S, and dS/dT, at each mooring and synthesized depth, were determined from an average T-S profile based upon the CTD data (28 stations) discussed earlier. Using this information with the interpolation procedure described in the UNESCO tables, a value of α was obtained for each synthesized depth at moorings P2 and P3 (Table 7). Once the values of α were obtained, $\nabla_H T$ could then be calculated through equation (3). The temporal variability of α is small and had little effect in the energy calculations.

The validity of the thermal wind relations in this flow regime can be determined by examining the local Rossby number in conjunction with the scales of motion expected in this region. The Rossby number, which is the ratio of the non-linear terms in the equations of motion to the Coriolis term, is defined as

$$Ro^{\#} = \frac{\frac{U^2}{L}}{f_o U} = \frac{U}{f_o L} \tag{5}$$

where U, L, and f_o represent the characteristic velocity, length scale of motion, and Coriolis parameter, respectively. Table 8 contains values of the local Rossby number based upon selected velocity - length scale combinations. Based upon the time series data from moorings P2 and P3, peak velocities in the low-pass filtered data rarely exceed 40 cm s^{-1}, and typical length scales for subtidal motions are greater than 50 km, as cited earlier. Therefore, it appears that we can expect the local Rossby number to be on the order of 0.1 or less. This is consistent with the observations of *Pierce et al.*, (1991), who found the local Rossby number to be approximately 0.2 across a CTZ jet, and concluded that the regime could still be approximated by QG dynamics.

At 425 dbar, the values of α at each mooring appear comparable to each other; however, this is not the case at the 225 dbar level, where the difference becomes larger. The reason for this may come from the fact that the value of dS/dT, based upon CTD data, is different at each mooring location. At P2 the mean values of T and S are 8.180 °C and 34.077 psu, respectively, while at P3 the values were 7.997 °C and 34.075, respectively. The local gradients of dS/dT, computed over 20 m, were -0.154 and -0.082, for P2 and P3, respectively. If we remove the contribution of these gradients from term (b) in equation 2-4 (Table 7), we obtain the nearly identical values of 7.623 x 10^{-4} and 7.622 x 10^{-4}, for P2 and P3, respectively. This indicates that the reduced local gradient within the mean T-S curve at P3 was responsible for the observed difference in the values of α.

Table 7. **NUMERICAL VALUES OF ρ and α AT MOORINGS P2 AND P3:** Computed from UNESCO International Oceanographic Tables using an average T-S profile based upon CTD data collected during the mooring deployments. Components (a) and (b) are the thermal expansibility and salinity contraction coefficients, respectively, from equation 4.

Mooring	Depth (dbar)	ρ (g cm^{-3})	(a)x 10^{-4}	(b)x 10^{-4}	α ($°C^{-1}$)x 10^{-4}
P2	225	1.026524	-1.506	-1.174	2.680
P2	425	1.026850	-1.377	-0.443	1.820
P3	225	1.026547	-1.485	-0.626	2.111
P3	425	1.026863	-1.356	-0.527	1.883
P3	750	1.027206	-1.255	-0.803	2.058

Table 8. **LOCAL ROSSBY NUMBER AS A FUNCTION OF LENGTH SCALE AND VELOCITY:** The values of the local Rossby number (Ro) have been computed in accordance with equation 5. Based upon the typical scales of motion expected off Point Sur in the CCS and the observed current velocities, the value of the local Ro should lie within the region to the right of the double line.

Velocity ($cm\ s^{-1}$)	Length Scale (km)						
	10	*20*	*30*	*40*	*50*	*100*	*200*
10	0.10	0.05	0.033	0.025	0.02	0.01	0.005
20	0.2	0.1	0.067	0.05	0.04	0.02	0.01
30	0.3	0.15	0.1	0.075	0.06	0.03	0.015
40	0.4	0.2	0.133	0.10	0.08	0.04	0.02
50	0.5	0.25	0.167	0.125	0.10	0.05	0.025

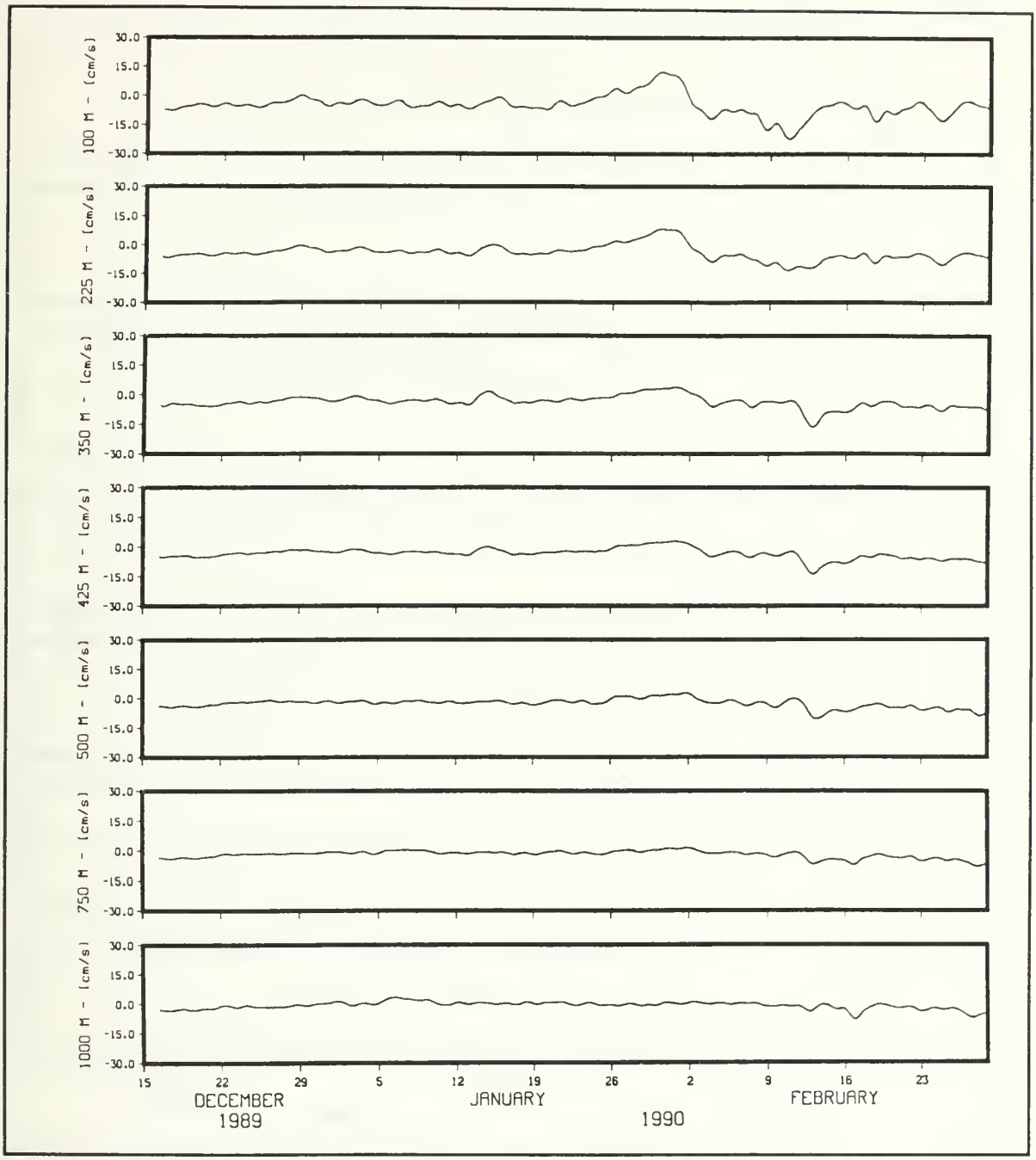

Figure 3. **U- Component of Velocity at Mooring P3:** Data has been low pass filtered and decimated to six hourly points. From top to bottom are the 100, 225, 350, 425, 500, 750, and 1000 dbar levels. Data at the 225, 425 and 750 dbar levels have been synthesized using data from bracketing levels as described in the text. Units are cm s^{-1}.

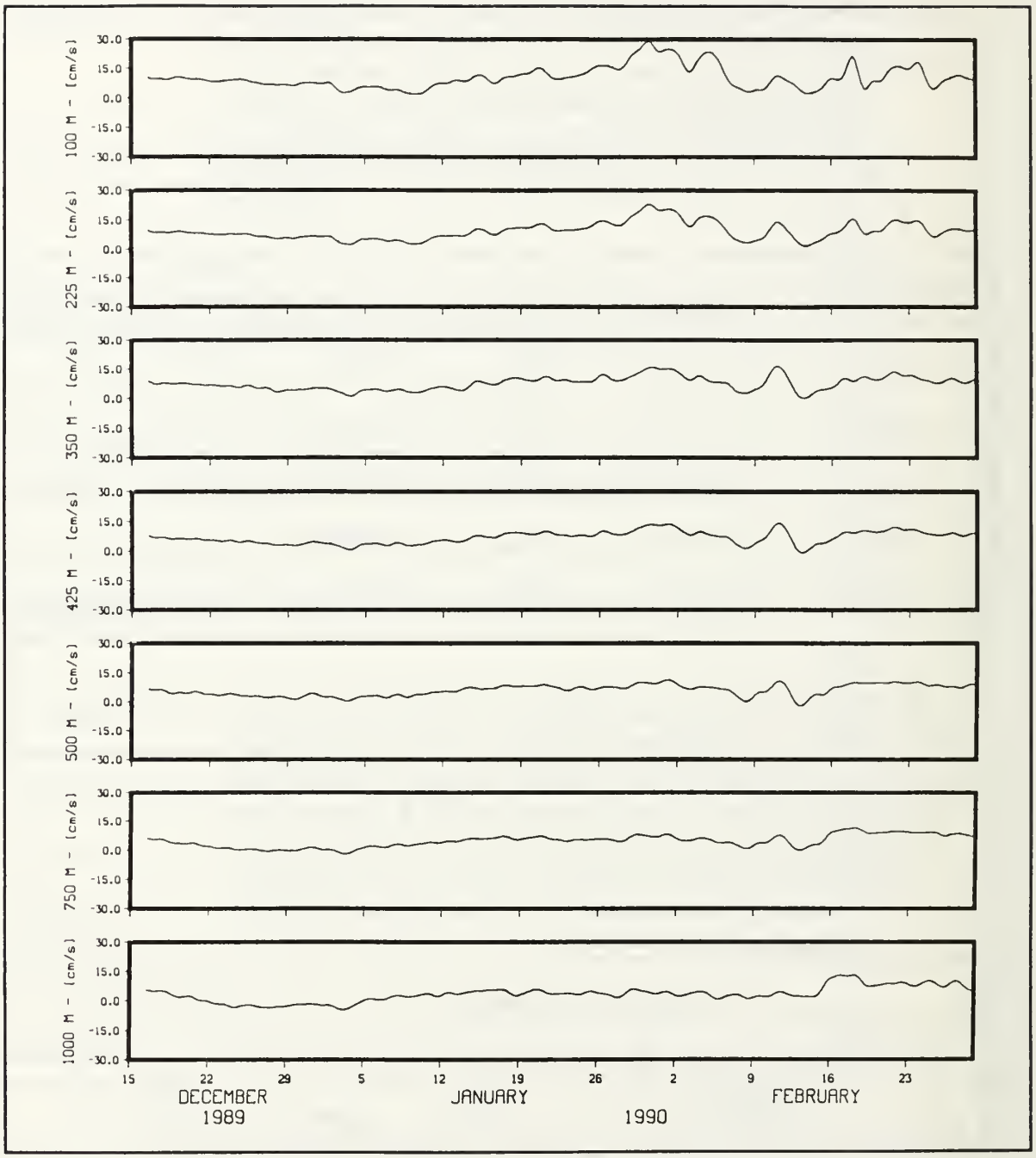

Figure 4. **V- Component of Velocity at Mooring P3:** Same as in Figure 3, but for the v-component of velocity. Units are cm s^{-1}.

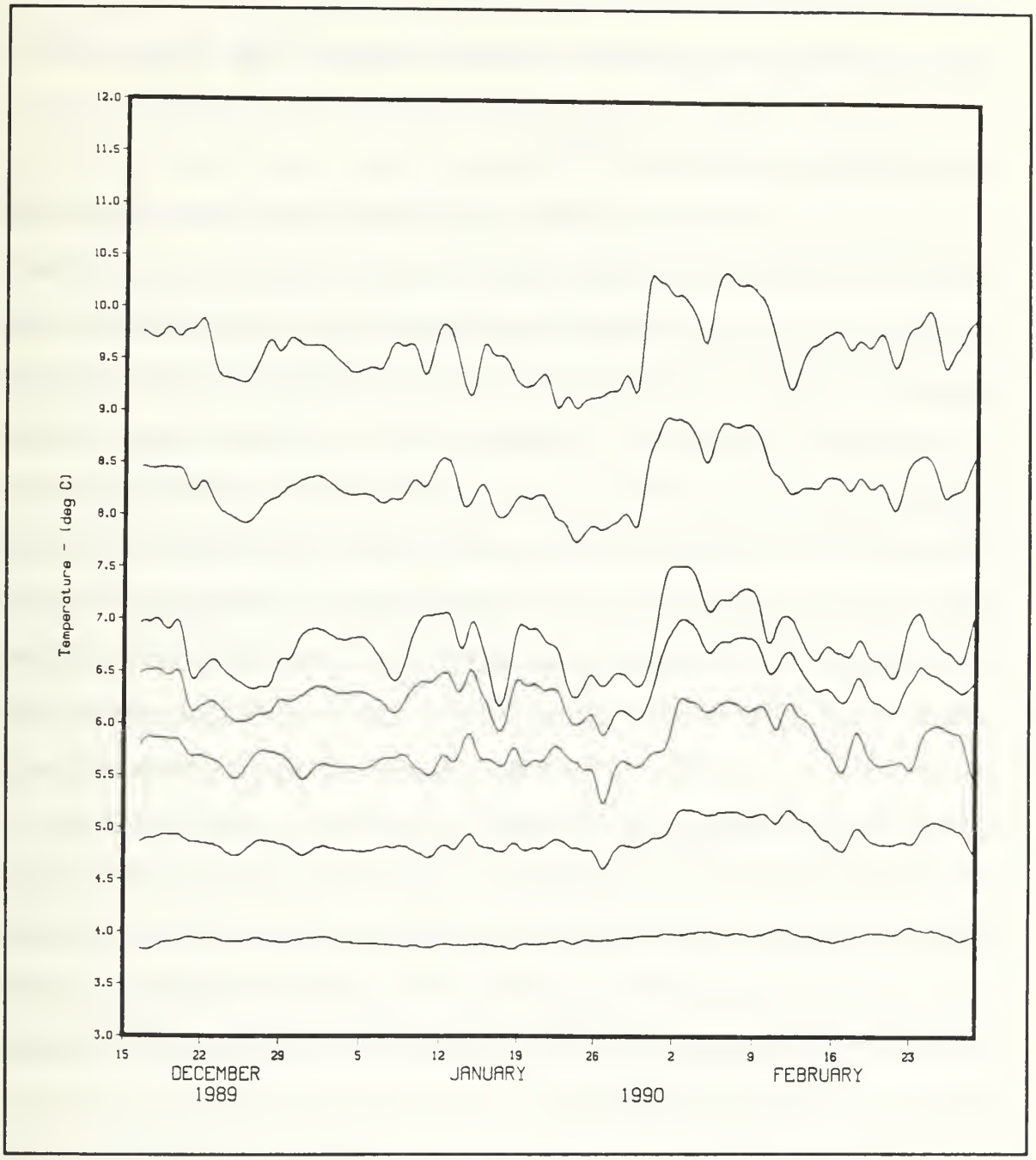

Figure 5. **Temperature at Mooring P3:** Data has been low pass filtered and decimated to six hourly points . From top to bottom are the 100, 225, 350, 425, 500, 750, and 1000 dbar levels. Data at the 225, 425 and 750 dbar levels have been synthesized using data from bracketing levels as described in the text. Units are °C.

III. CHARACTERISTICS OF THE POINT SUR DATA SETS

A. GENERAL OBSERVATIONS

At mooring P2, the low-frequency current fluctuations between 100 and 500 m exhibited strong vertical coherence and were characterized by episodes of both strong poleward and equatorward flow (Appendix A). The fluctuations were distinctly wavelike in appearance, and had typical peak amplitudes of ± 40.0 cm s^{-1}, a period of approximately 215 days, and were not phase locked with the seasons (*Ramp et al.*, 1991b). Strong poleward flow was observed between November 1989 and February 1990, and also between June and September 1990. This signal was not apparent in the local wind stress and coastal sea level (*Ramp et al.*, 1991b). Currents were, in the mean (based upon all the data), northward and westward (north-east coordinate system), and decreased in magnitude with depth (Table 6). Similar results were observed using data from individual deployments (Table 5), with the exception of the second deployment (August to December 1989), where strong shear existed between 100 and 350 m depth (Table 5, Appendix A), and the mean flow was to the south and west below 350 m. While the direction of flow was generally the same between deployments, the individual statistics did not remain constant indicating the presence of very low frequency variability at this location.

A well known property of autocorrelation functions is that any strong periodicities in a given time series will also appear in its autocorrelation function (*Bendat and Piersol*, 1986). Using this property, it is possible to determine the dominant signals within these time series by estimating them as four times the first zero crossing of the respective autocorrelation function. The

autocorrelation functions for mooring P2 (Figure 6), based upon the same time periods listed in Table 6, reveal a very low frequency signal in the alongshore currents at all depths, with a period of approximately 230 days at 100 m and 350 m, and 207 days at 500 m, which is similar to the value of 215 days cited earlier. This signal is not present in the autocorrelation functions for the cross-shore components which appear to be dominated by fluctuations shorter than 80 days. It is interesting to note that the temperature fluctuations at 100 m depth appear to be dominated by this 230 day signal, as indicated by the dotted line in Figure 6, which closely resembles the autocorrelation function for the alongshore component. However, below 100 m depth, the autocorrelation function for temperature more closely resembles the cross-shore component of flow, which is dominated by shorter period fluctuations. The presence of this very long period oscillation will influence the determination of the mean flow at this location, and may indicate that future studies will require more than 17 months of data to obtain a better estimate of the temporal mean.

Farther offshore, at mooring P3, flow was also highly coherent over the instrumented range of the 100 - 1000 m depths, but was less energetic than flow inshore at P2 by a factor of two (*Ramp et al.*, 1991b). On average, the flow was poleward with speeds of about 11 cm s^{-1} (Table 5); however, the records did contain two intense bursts of equatorward flow (velocity greater than 40 cm s^{-1}), which lasted approximately 30 to 45 days. These bursts were highly coherent in the vertical, and appeared between March and April during both years (Appendix A). Whether or not their occurrence during this particular time period has any significance or was purely coincidental lies outside the scope of

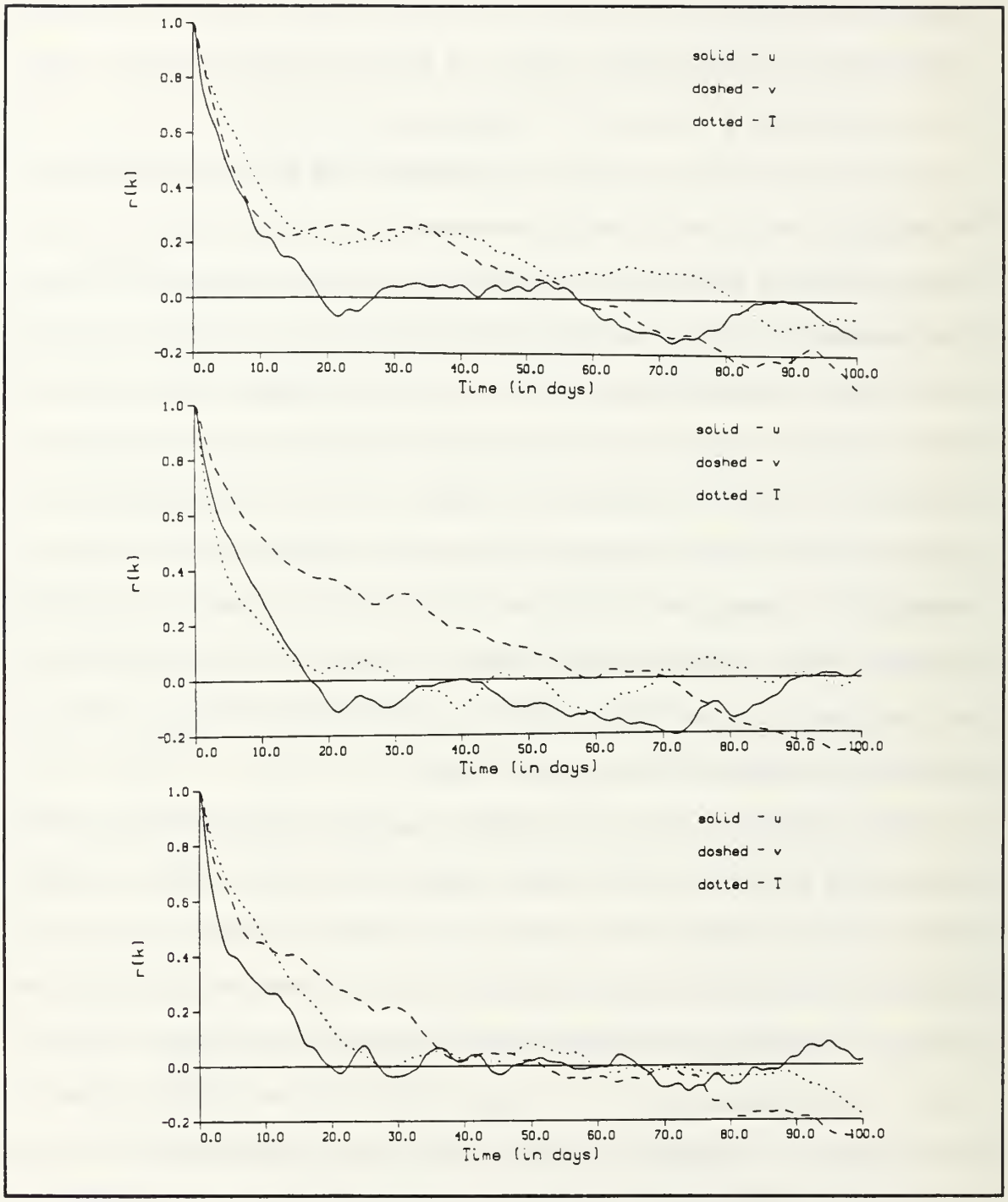

Figure 6. **Autocorrelation Functions for Mooring P2:** Top, middle and bottom panels are the 100, 350 and 500 m levels, respectively. Solid (dashed) curve represents u (v) component, while the dotted curve is for temperature.

this study and will not be addressed here. It is interesting to note that while these bursts stand out as the dominant features in the velocity records at P3, they did not occur at mooring P2, located only 25 km away.

The autocorrelation functions for the 100 and 350 m depths at P3 (Figure 7), based upon the time period listed in Table 6, reveal that while shorter periods do exist, the time series contain a dominant long period fluctuation between approximately 120 and 160 days duration. At both levels, all three autocorrelation functions appear very similar in structure.

B. SPECTRAL ENERGY ANALYSIS

To estimate the frequency distribution of energy present within these records at subtidal frequencies, variance-conserving autospectra were employed. Initially, the longest time series at each mooring location, namely P2 - 350 m depth and P3 - 100 m depth, were analyzed to identify areas of significant energy intensification. The time series at the 350 m level at P2 is the longest continuous record of this study, and runs from May 1989 through May 1991. At P3, the records were considerably shorter, with the longest being at the 100 m level between May 1990 and May 1991 (corresponding with data periods used in Table 6).

The spectra at these two locations were computed using 5 overlapping fundamental piece lengths of 243 days at P2 and 3 of 180.5 days at P3. These particular piece lengths were chosen to attain the highest possible confidence, while at the same time allowing for calculation of spectral energy out to periods of 180.5 to 243 days. The records themselves are too short to establish the secular variability off Point Sur, and the use of a longer piece length would only

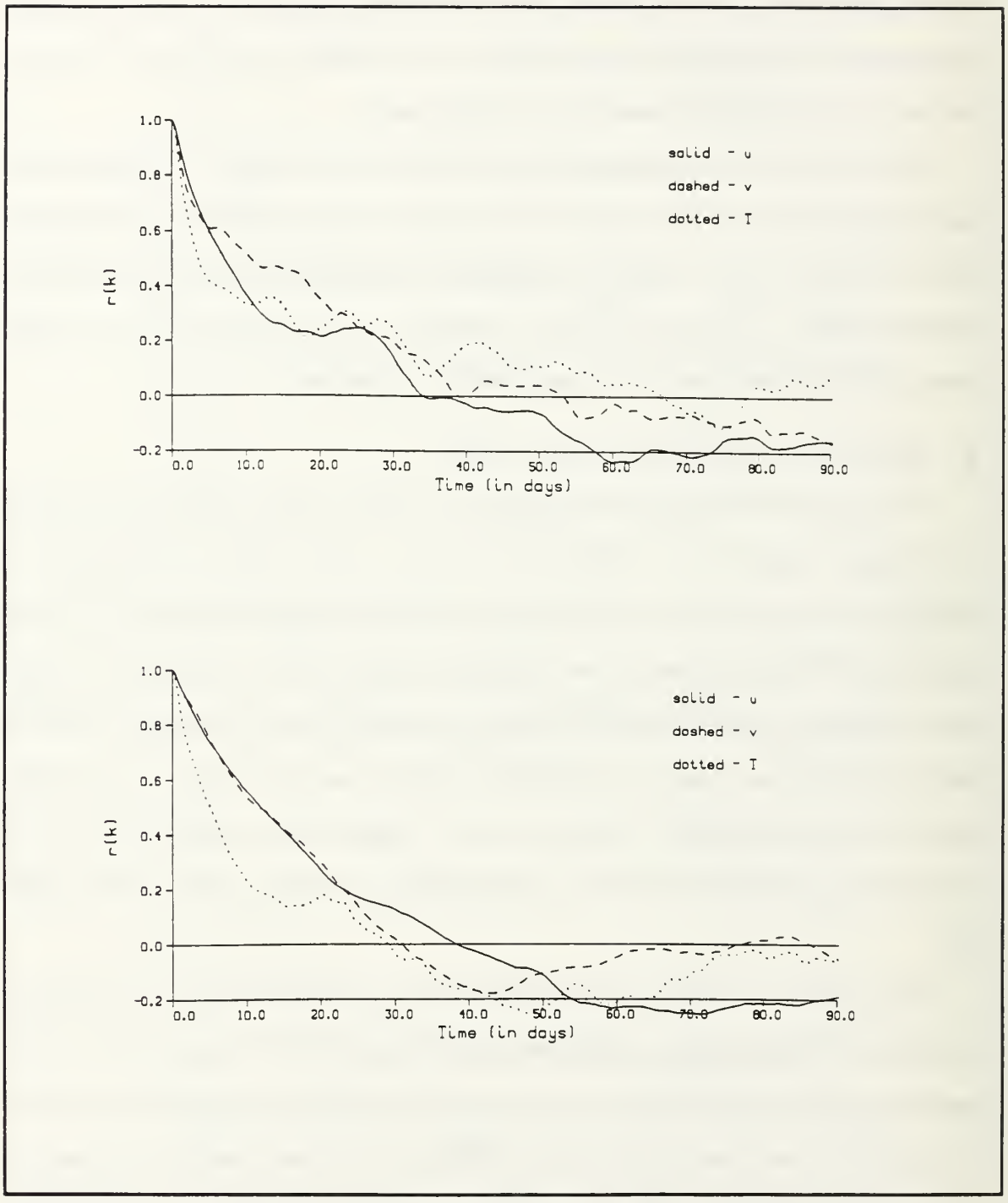

Figure 7. **Autocorrelation Functions for Mooring P3:** Upper (lower) panel is the 100 (350) m level. Solid (dashed) curve represents u (v) component, while the dotted curve is for temperature.

act to decrease the confidence in the resulting spectra below significant levels. Each data segment was demeaned and detrended, using least squares, prior to application of the Fast Fourier Transform (FFT). A Chi-square distribution was used to compute 95% confidence limits. In a variance-conserving presentation these confidence limits vary with both spectral amplitude and frequency making them difficult to display.

At mooring P2 (350 m), there is a strong peak in the energy spectrum of the u-component at the 48 day period (Figure 8), while in the more energetic v-component (Figure 9) the peak lies at a slightly shorter period (35 days). Peaks at the 27 and 48 day periods occur in the temperature spectrum (Figure 10), in general agreement with the velocity spectrum. At longer periods (longer than 80 - 120 days), the spectra of the u-component and temperature indicate a significant reduction in energy. However, the same is not true for the v-component, which contains energy from the lower frequency signal which appeared in the autocorrelation function (Figure 6).

Because of fewer data segments (only three segments in one year of data), the spectra at P3 (100 m) will have inherently less confidence associated with them; however, they do reveal that more energy is contained in the u-component (Figure 11) than in the v-component (Figure 12). Peaks in the u-component found at the 25 and 90 day periods, contain more energy than peaks in the v-component at 90 day periods, as well as at shorter periods. In both the v-component and temperature spectra (Figure 13), more energy is contained at the shorter periods (< 20 days), and may be associated with the shallower depth of this instrument.

Because of instrument failures, most records at P3 were six months or less in duration, and only the time series described above provided continuous data for at least one year. Therefore, the study of energetics off Point Sur will be limited to using the longer time series of P2, which cover a 17-month period between May 1989 and October 1990, and the 100 and 350 m records at P3 between May 1990 and May 1991.

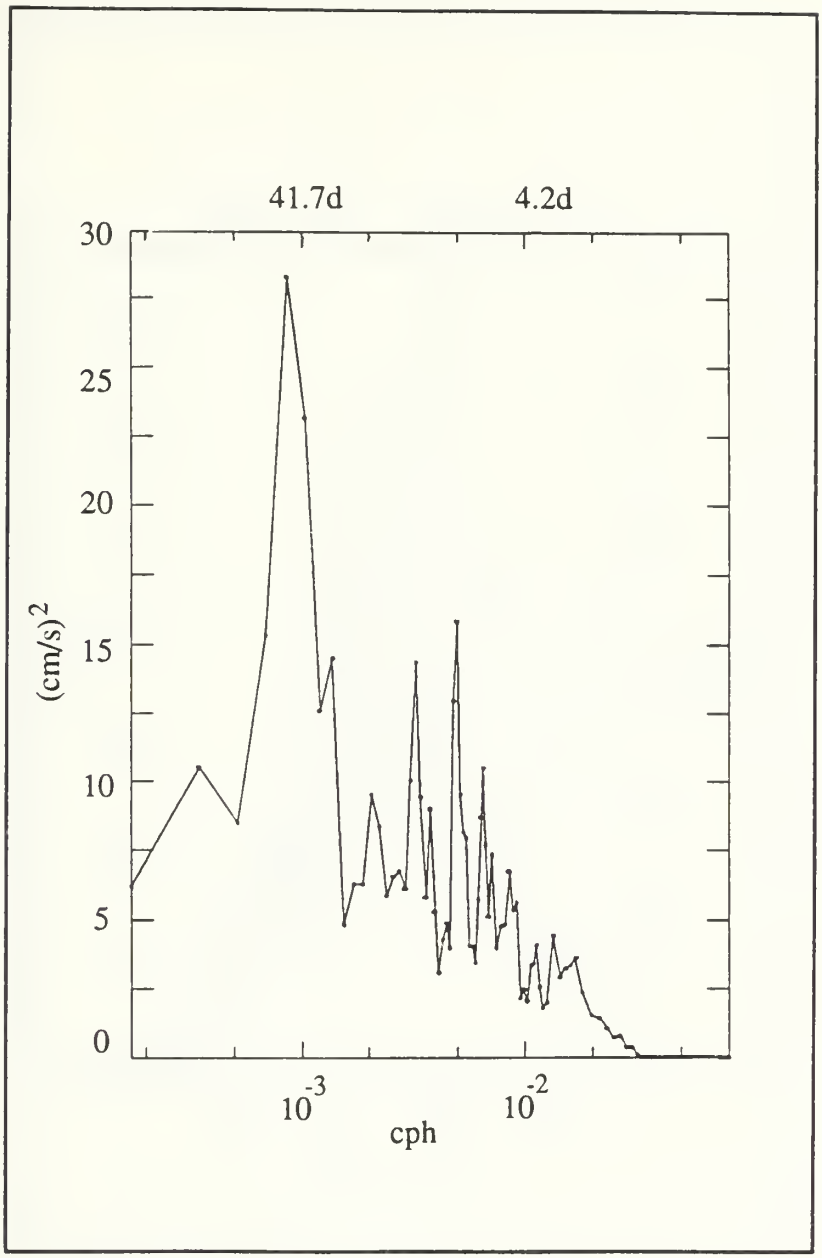

Figure 8. Spectral Energy of U-component of Velocity at 350 m at Mooring P2: Auto-spectrum of low pass filtered data. Plot is based upon two years of data, and has been computed using five overlapping pieces as described in text. The 95% confidence factors are 0.49 and 3.08, which when multiplied by spectral estimates yield the 95% confidence intervals.

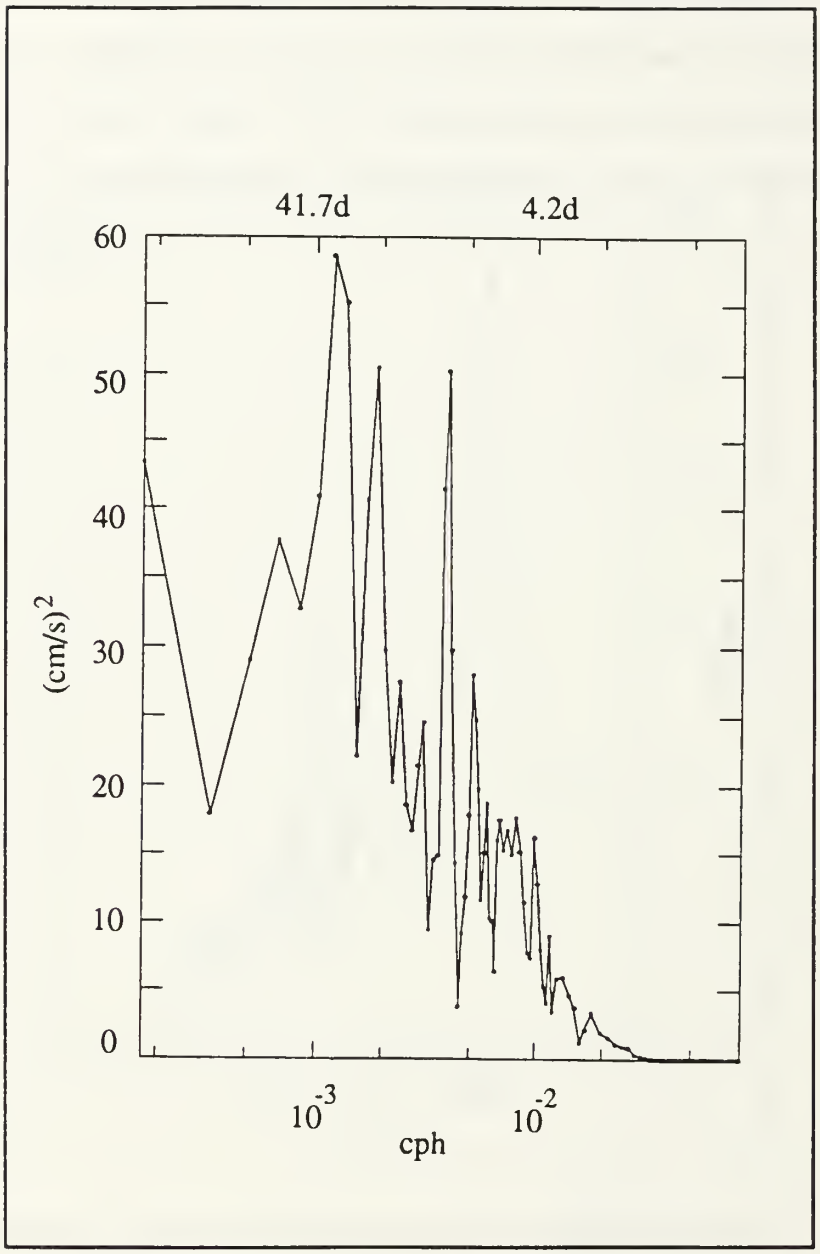

Figure 9. Spectral Energy of V-component of Velocity at 350 m at Mooring P2: Auto-spectrum of low pass filtered data. Plot is based upon two years of data, and has been computed using five overlapping pieces as described in text. The 95% confidence factors are 0.49 and 3.08, which when multiplied by spectral estimates yield the 95% confidence intervals.

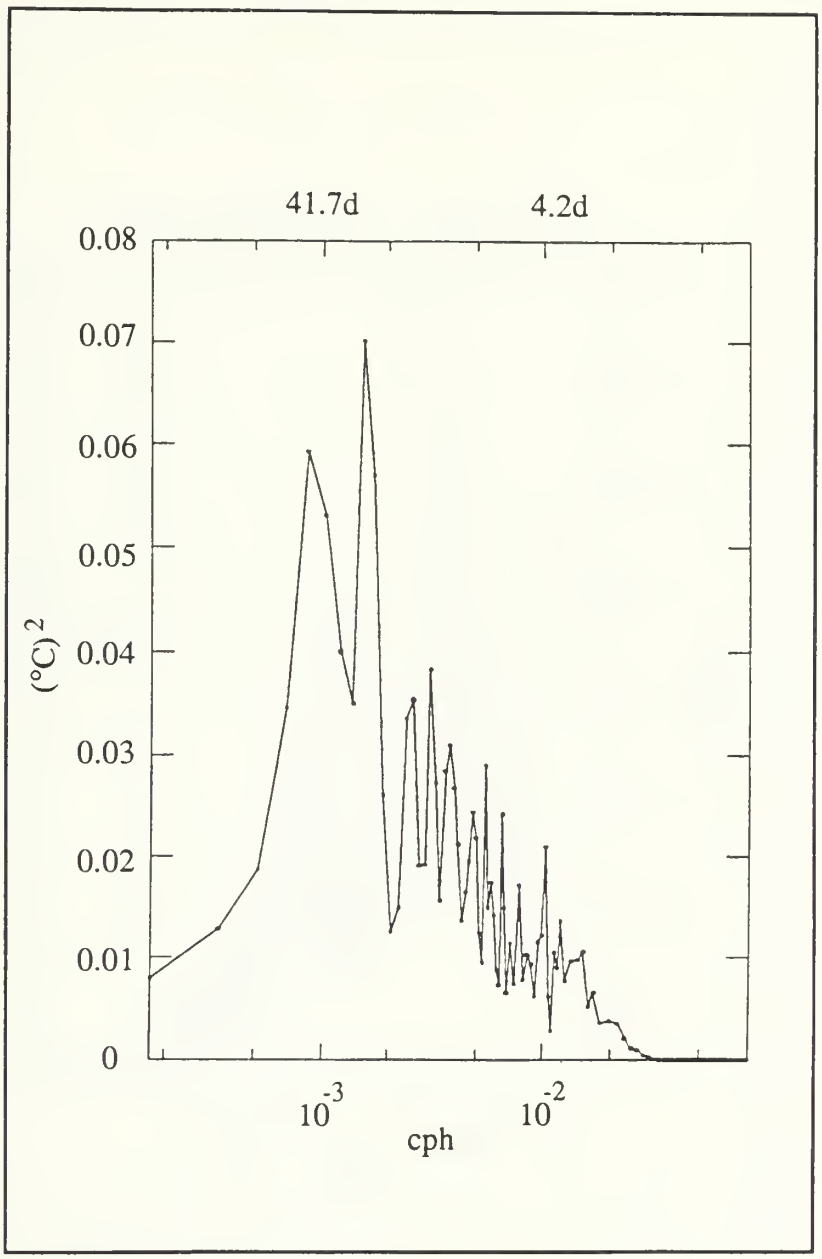

Figure 10. Spectral Energy of Temperature at 350 m at Mooring P2: Auto-spectrum of low pass filtered data. Plot is based upon two years of data, and has been computed using five overlapping pieces as described in text. The 95% confidence factors are 0.49 and 3.08, which when multiplied by spectral estimates yield the 95% confidence intervals.

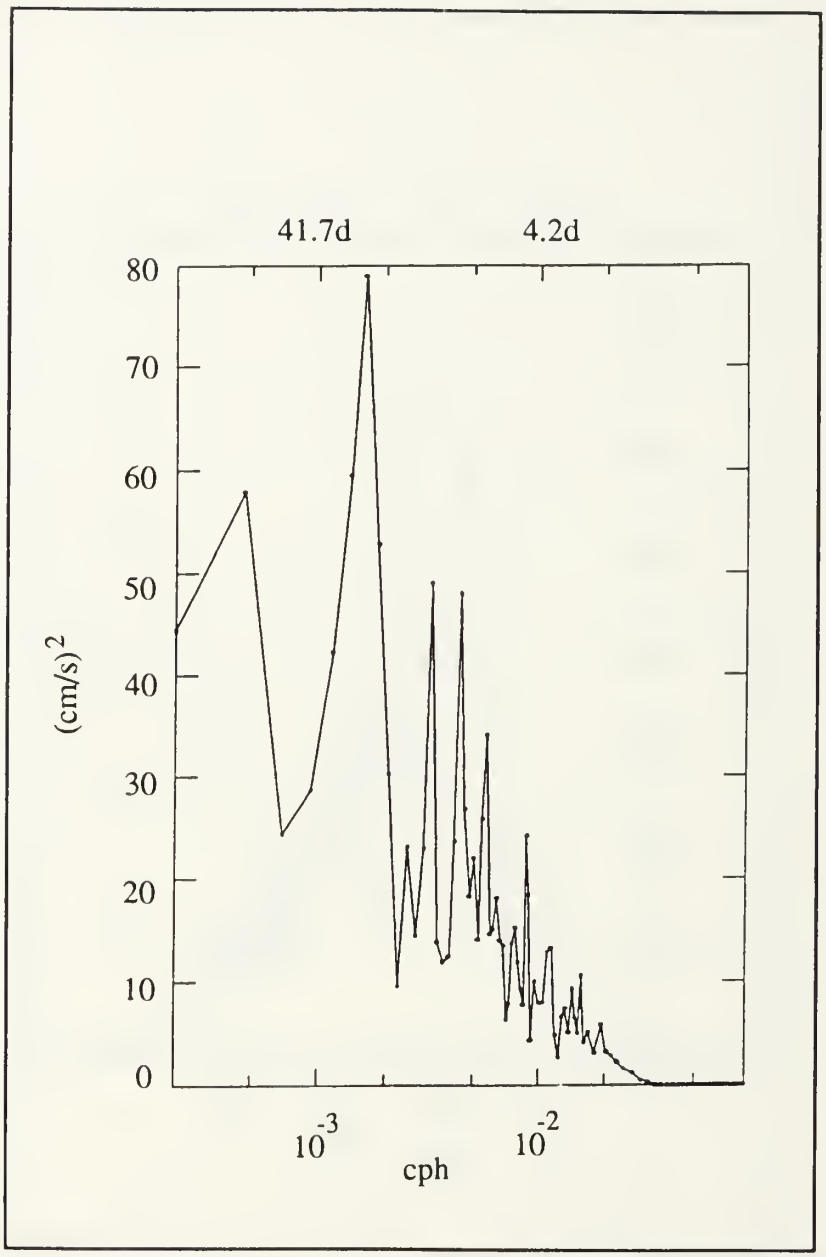

Figure 11. Spectral Energy of U-component of Velocity at 100 m at Mooring P3: Auto-spectrum of low pass filtered data. Plot is based upon one year of data, and has been computed using three overlapping pieces as described in text. The 95% confidence factors are 0.42 and 4.85, which when multiplied by spectral estimates yield the 95% confidence intervals.

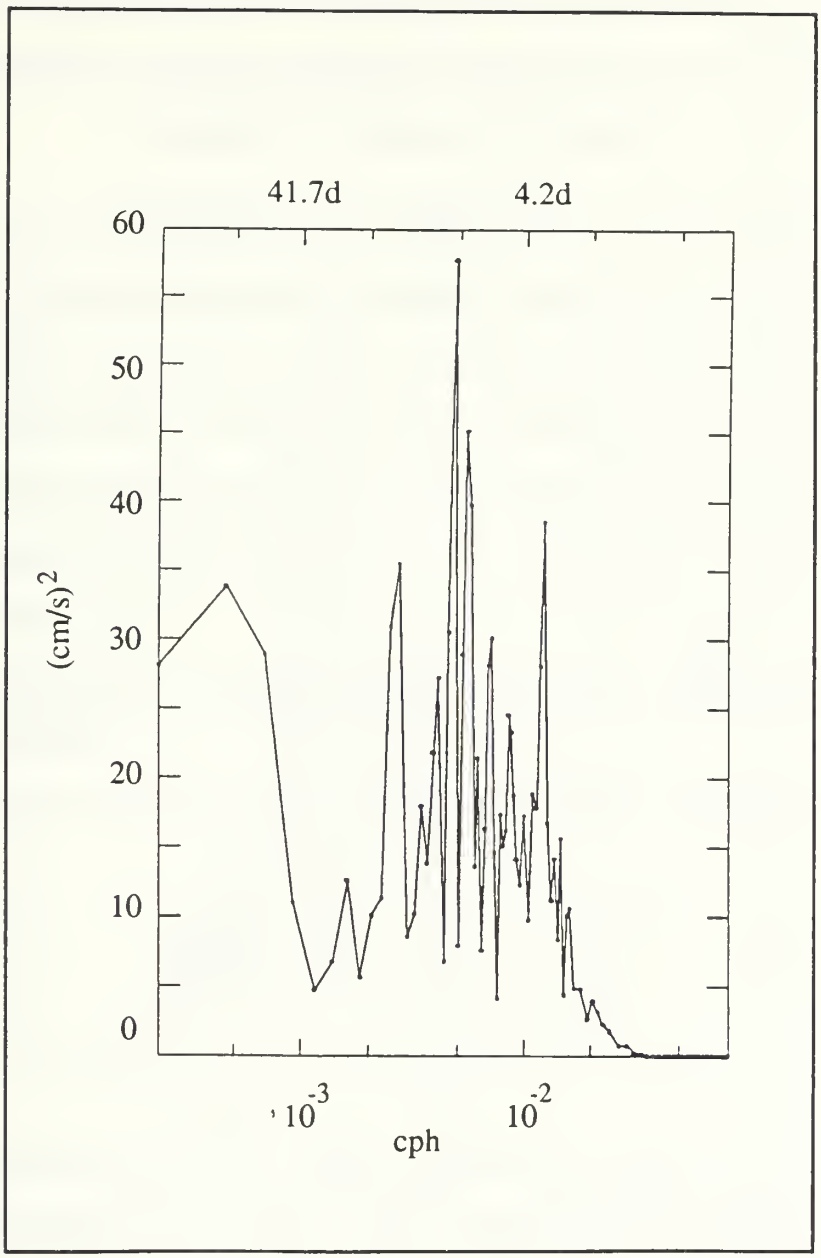

Figure 12. Spectral Energy of V-component of Velocity at 100 m at Mooring P3: Auto-spectrum of low pass filtered data. Plot is based upon one year of data, and has been computed using three overlapping pieces as described in text. The 95% confidence factors are 0.42 and 4.85, which when multiplied by spectral estimates yield the 95% confidence intervals.

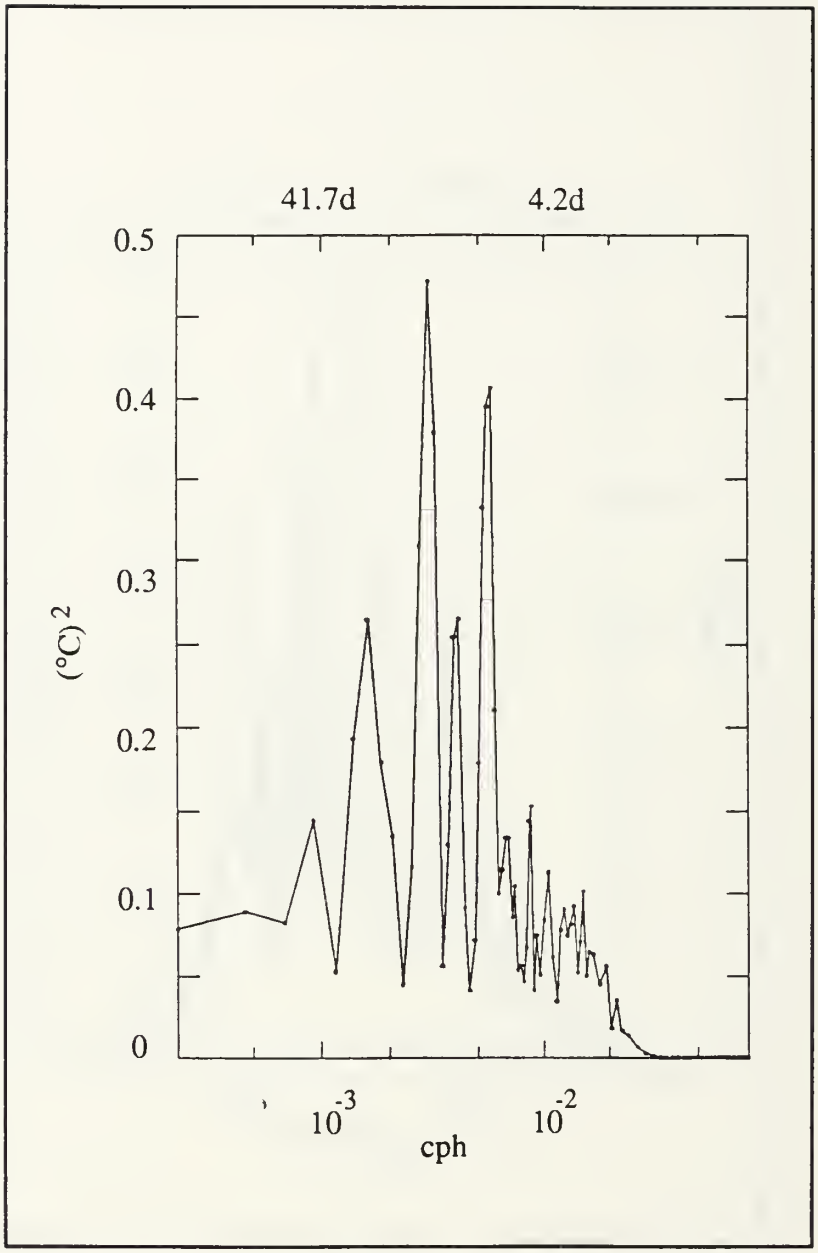

Figure 13. Spectral Energy of Temperature at 100 m at Mooring P3: Auto-spectrum of low pass filtered data. Plot is based upon one year of data, and has been computed using three overlapping pieces as described in text. The 95% confidence factors are 0.42 and 4.85, which when multiplied by spectral estimates yield the 95% confidence intervals.

IV. A CONCEPTUAL MODEL FOR INVESTIGATING ENERGETIC INTERACTIONS MEASURED AT A SINGLE CURRENT METER MOORING

In this study, a method of analysis similar to *Niiler and Hall* (1988) and *Hall* (1991) will be used to investigate the energetic interactions occurring within the flow field along the continental slope off Point Sur, California. The eddy potential energy equation is used to study these interactions. The basic equations and some discussion of their derivation are contained in the following sections; however, the complete derivations, along with fully expanded terms, have been deferred to Appendix D.

A. THE THERMAL ENERGY EQUATION AND VERTICAL VELOCITIES

To begin, we consider the basic temperature equation which can be written as

$$\frac{\partial T}{\partial t} + u\frac{\partial T}{\partial x} + v\frac{\partial T}{\partial y} + w\,\theta_z = 0 \tag{6}$$

where θ_z represents the actual potential temperature gradient at a given level (i.e., 225 or 425 dbar in this study). When considering temperature fluctuations in the vertical and their role in energy conversions, we must use potential temperature, (θ), instead of temperature to account for the effects of adiabatic compressibility. Using the rules of Reynolds averaging, an equation for the mean temperature can be obtained by taking the time average of (6):

$$\bar{u}\frac{\partial \bar{T}}{\partial x} + \overline{u'\frac{\partial T'}{\partial x}} + \bar{v}\frac{\partial \bar{T}}{\partial y} + \overline{v'\frac{\partial T'}{\partial y}} + \bar{w}\,\bar{\theta}_z + \overline{w'\theta'_z} = 0$$

- or -

$$\overline{\vec{v}_H}\cdot\nabla_H\bar{T} + \overline{\vec{v}_H'\cdot\nabla_H T'} + \bar{w}\,\bar{\theta}_z + \overline{w'\theta'_z} = 0, \qquad (7)$$

where the overbar represents the time average of a quantity, and $\partial\bar{T}/\partial t$ is zero. By definition, the time average of a product, $\overline{AB}$, is equal to $\bar{A}\,\bar{B} + \overline{a'b'}$, where $A = \bar{A} + a'$ and $B = \bar{B} + b'$. Therefore, the equation for the mean temperature includes interactions between the mean and eddy fields, where the eddy fields can encompass a wide range of frequencies. By subtracting (7) from (6), we obtain the equation for the fluctuating temperature field

$$\frac{\partial T'}{\partial t} + \vec{v}\cdot\nabla T' + \overrightarrow{v'_H}\cdot\nabla_H\bar{T} + w'\,\bar{\theta}_z - \overline{\vec{v}'\cdot\nabla T'} = 0, \qquad (8)$$

where primes denote fluctuating quantities, the subscript H refers to horizontal components and derivatives, and all vertical components associated with nonsubscripted terms involve θ' in lieu of T'. Here again the nonlinear advective portion may contain contributions from a wide range of frequencies.

As pointed out by *Niiler and Hall* (1988), the definition of mean and eddy fields in these equations must be considered carefully. The calculation of the mean is restricted to the length of the time series, which in this case is 17 months, yet as seen in the v-component of flow (Figures 6 and 9), energy does exist at very low frequencies (longer than 200 days). These very low

frequencies will affect the estimate of the mean and will require careful consideration.

The terms necessary to evaluate these equations at the 225 dbar and 425 dbar levels are u, v, w, T, $\nabla_H T$, and α. Details on the procedures used to calculate these terms were previously discussed in Chapter II, with the exception of vertical velocity, w. Vertical velocity is important in the conversion of potential energy to kinetic energy, and vice-versa, through vertical eddy heat fluxes and can be calculated at each depth from equation (6) as

$$w = -\left[\frac{\partial T}{\partial t} + u\,\frac{\partial T}{\partial x} + v\,\frac{\partial T}{\partial y}\right]\left[\theta_z\right]^{-1} \tag{9}$$

where the local time change of temperature at these depths has been computed using a centered finite-difference scheme. This method has been used by *Hall* (1991) to compute vertical velocity in the Kuroshio Extension (bottom depth in excess of 5000 m). In the present study, time series of vertical velocity were computed using both θ_z and $\overline{\theta}_z$ at each mooring (see Figures D1-D3 in Appendix D). Based upon these results, it appears that either method could be used to obtain vertical velocities at these locations; however, as discussed in the next section, terms involving vertical advection of eddy energy (which appear as a result of the time variability of θ_z) were of comparable magnitude to the horizontal advective terms. Therefore, the time series of the actual vertical temperature profile, θ_z, have been used to compute the vertical velocities used throughout this study.

B. THE EDDY POTENTIAL ENERGY EQUATION

The equation for eddy potential energy (EPE) can be found by multiplying the fluctuating heat equation (8) by $\rho_0 g\alpha T'/\bar{\theta}_z$. This multiplicative factor is the same as that used by *Hall* (1991), except that it has been multiplied by a mean density, ρ_0, in order to obtain units of ergs cm^{-3} s^{-1}. This difference comes from the fact that α in her formulation had units of gm cm^{-3} $°C^{-1}$, whereas in this study α has units of $°C^{-1}$. Values of ρ_0 (mean density) have been determined at each level based upon CTD data, whereas the value of $\bar{\theta}_z$ comes directly from the time series of θ_z (calculated directly from time series of θ above and below) at each depth. Defining eddy potential energy as EPE = $\frac{1}{2}\rho_0 g\alpha T'^2 \bar{\theta}_z^{-1}$, after *Hall* (1991), this equation can be written as

$$\underset{(1)}{\frac{\partial EPE}{\partial t}} + \underset{(2)}{\bar{\vec{v}} \cdot \nabla EPE} + \underset{(3)}{\vec{v'} \cdot \nabla EPE} +$$

$$\underset{(4)}{\overrightarrow{v'_H T'} \cdot \frac{\rho_0 g\alpha}{\bar{\theta}_z} \nabla_H \bar{T}} + \underset{(5)}{\rho_0 g\alpha \overline{w'T'}} = \underset{(6)}{\frac{\rho_0 g\alpha T'}{\bar{\theta}_z} \overline{\vec{v'} \cdot \nabla T'}} \qquad (10)$$

where once again overbars and primes denote time mean and fluctuating quantities, respectively, and the subscript H refers to horizontal components and derivatives. Briefly, the first three terms represent: (1) local growth or decay of eddy potential energy; (2) advection of eddy potential energy by the mean flow; and (3) self-advection of eddy potential energy by the fluctuating eddies.

Term (4) represents a conversion of energy between eddies and the mean baroclinic flow. *Hall* (1986a, 1991) interprets downgradient eddy heat fluxes

(term 4 above) as a signature of baroclinic instability processes, while downgradient eddy momentum fluxes (terms which appear in the kinetic energy equation) are associated with barotropic instability. Similar interpretations have been made by *Dewar and Bane* (1985, 1989b), where the eddy potential energy equation was derived from the density equation instead of the temperature equation. *Dewar and Bane* (1989b) have also interpreted these processes in terms of the direction of eddy momentum and heat fluxes relative to the mean momentum and heat gradients, and found that the release of energy to the eddy field will occur if the eddy fluxes are downgradient ($-\overrightarrow{\overline{v'_H T'}} \cdot \nabla_H \overline{T} > 0$). Term (5) appears with opposite sign in the eddy kinetic energy equation and represents exchanges between eddy potential and eddy kinetic energy. In the ocean, with z taken to be positive upwards, a downward heat flux ($-w'T' > 0$) represents a conversion of EKE to EPE. This situation occurs when either cold water is moved upward or warm water is moved downward, so that isothermal surfaces are displaced away from their mean positions. Conversely, an upward heat flux ($-w'T' < 0$) represents a conversion of EPE to EKE, and occurs when either cold water is moved downward or warm water is moved upward, so that isothermal surfaces are brought closer to their mean positions. Term (6) is a residual term based upon the mean eddy advection of the disturbance temperature, a constant, and T' (the only non-constant quantity in the term) and has no clear physical interpretation. It was found to be small in this study and has subsequently been neglected.

It should be noted that the terms involving the spatial variability of the mean potential temperature gradients, $\overline{\theta}_z$, have been omitted from equation (10). This omission is necessary since we only have data from single moorings, which do

not allow for determination of this variability. Terms involving spatial derivatives of $\overline{\theta}_z$ come from rewriting the advective term in the eddy potential energy equation as follows

$$\frac{\vec{v}}{\overline{\theta}_z} \cdot \nabla\left(\rho_0 g\alpha \frac{T'^2}{2}\right) = \vec{v} \cdot \nabla EPE - \rho_0 g\alpha \vec{v} \frac{T'^2}{2} \cdot \nabla\left(\frac{1}{\overline{\theta}_z}\right) \qquad (11)$$

(a) (b) (c)

where (a) is the direct result of multiplying equation (8) by $\rho_0 g\alpha T'/\overline{\theta}_z$, and (b) and (c) come from using the relation $\nabla\bullet(ab) = a\bullet\nabla b + b\bullet\nabla a$. As mentioned above, we do not have the data set to calculate the actual spatial variability within $\overline{\theta}_z$; however, as shown in Appendix D, it is possible to utilize data from a 6-month period common to both P2 and P3 to examine the effect of neglecting these terms. Using data during this common time period, as outlined in Appendix D, the ratio (x-component only, since P2 and P3 are east-west of each other) of term (c) to term (a) in (11) was 0.0113, which is much less than 1, indicating that term (a) can be approximated by term (b) alone without introducing any significant error into subsequent energy calculations. This result is similar to *Hall* (1991), who found these were typically an order of magnitude smaller than other terms in the energy equation, and therefore also neglected them from subsequent analyses.

While the spatial variability of the mean vertical potential temperature gradient, $\overline{\theta}_z$, has been neglected in equation (10), it is important to note that the time variability of the actual gradient (θ_z), which appears in both the mean and eddy advection terms of (10), has not. Comparison of horizontal advection of disturbance temperature to vertical advection of disturbance temperature (Figures D4-D6 in Appendix D) in all three time series used in this energy study

reveals that, in general, the horizontal component of advection is larger than the vertical component. However, there are periods where the magnitudes are quite similar, and periods do exist where the vertical advective term is the larger term (Mooring P3, Figure D6), and may contribute significantly to the energy balance of (10). Therefore, it is not appropriate to neglect the temporal variability of θ_z, a result also found by Hall (1991), who also retained these terms in her analyses.

To obtain the mean values of the terms in the eddy potential energy equation, we simply take the time average of (10), which becomes

$$\underset{(1)}{\frac{\partial \overline{EPE}}{\partial t}} + \underset{(2)}{\overline{\vec{\bar{v}} \cdot \nabla EPE}} + \underset{(3)}{\overline{\vec{v}' \cdot \nabla EPE}} +$$

$$\underset{(4)}{\overline{\vec{v}'_H T' \cdot \frac{\rho_0 g \alpha}{\bar{\theta}_z} \nabla_H \bar{T}}} + \underset{(5)}{\rho_0 g \alpha \overline{w'T'}} = 0 \qquad (12)$$

where terms 1 - 5 have the same meaning as in equation (10), except now they represent the time mean values. This is also equation (3.1) in *Hall* (1991).

V. RESULTS

Using techniques outlined in chapters II and IV, time series of u, v, w, T, $\partial T/\partial x$, $\partial T/\partial y$, and θ_z, along with time series of the 5 terms in the eddy potential energy equation (eq. 10, see Appendix E) were computed at mooring P2 for the 225 and 425 m levels (17 months of data) and at mooring P3 for the 225 m level (one year of data). The time mean values for each of the five terms in the EPE equation, computed in accordance with equation (12), are therefore restricted to these record lengths. Prior to discussing results of these calculations, it is important to mention that low frequency signals, including seasonal flow reversals which are generally observed within the CCS (*Chelton*, 1984; *Lynn and Simpson*, 1987), observed variability in the strength and location of the CUC off Point Sur (*Tisch et al.*, 1992) along with the existence of mesoscale eddies, make the determination of the temporal means difficult and can act to widen the respective error bars on terms in the energy equation. Such low frequency variability does exist in these time series as seen in Appendix A and as illustrated by the respective autocorrelation functions and autospectra of chapter II. As a result we find in some cases, the error bars for the terms in the eddy potential energy balance were quite large and did include zero, thus implying the mean values are not statistically different from zero. However, in cases where the error bars barely include zero, we may be confident that the sign of the term is correct and therefore discuss its particular role in the overall eddy potential energy balance in this region.

Error bars shown and discussed throughout this chapter refer to the standard error of the mean. While these error bars provide some measure of confidence

in the calculated means, they do not represent the 95% significance level, which would be far too restrictive in this type of study where relatively weak mean flows exist in the presence of much stronger mesoscale variability. For the three components of velocity and those energy terms which do not include a product with a mean value (i.e., all except terms 2 and 4 in (12)), the standard error of the mean was calculated in the usual way, dividing the standard deviation (σ) by the appropriate number of degrees of freedom (υ). For each time series a unique number of degrees of freedom was determined by dividing the total record length by the value of the first zero crossing of the associated autocorrelation function, after *Ramp* (1989). The standard errors of the components of velocity (u, v, and w), ∇EPE (three components), horizontal eddy heat flux (u'T' and v'T'), and mean horizontal temperature gradient ($\nabla_H T$) were computed in this way. For terms 2 and 4 in equation (12), which involve the product of two mean quantities, the error propagation technique of *Brooks and Niiler* (1977) was used. For example, the standard error of the x-components is computed as

$$\sigma_{\overline{u}\cdot\overline{\frac{\partial EPE}{\partial x}}} = \sigma_{\overline{u}}\, c\left|\overline{T'T'_x}\right| + \left|\overline{u}\right| \sigma_{c\overline{T'T'_x}} + \sigma_{\overline{u}}\, \sigma_{c\overline{T'T'_x}}$$

and

$$\sigma_{\overline{u'T'}\cdot\frac{\partial(c\overline{T})}{\partial x}} = \sigma_{\overline{u'T'}}\, c\left|\overline{T}_x\right| + \left|\overline{u'T'}\right| \sigma_{c\overline{T}_x} + \sigma_{\overline{u'T'}}\, \sigma_{c\overline{T}_x}$$

where c is a multiplicative constant equivalent to $\alpha\rho_0 g\overline{\theta}_z^{-1}$ that has a unique value for each level at each mooring, and the overbars represent a time-mean value. In other words, the standard error for each component is the sum of the standard error of one quantity multiplied by the absolute value of the mean of the other (and vice-versa) plus the product of their standard errors. By using absolute

values, we eliminate possible cancellation of terms and obtain the maximum possible error from this technique. The net standard error for these terms can then be calculated as the sum of squares of the above standard errors as

$$\sigma_{\overline{\vec{v}\cdot\nabla EPE}} = \sqrt{\sigma^2_{\overline{x\text{-comp}}} + \sigma^2_{\overline{y\text{-comp}}} + \sigma^2_{\overline{z\text{-comp}}}}$$

and

$$\sigma_{\overline{v'_H T'}\cdot\nabla_H(c\overline{T})} = \sqrt{\sigma^2_{\overline{x\text{-comp}}} + \sigma^2_{\overline{y\text{-comp}}}} \quad ,$$

where again the overbars represent the time-mean value.

A. THE TIME-MEAN EDDY POTENTIAL ENERGY BALANCE OFF POINT SUR AT MOORINGS P2 AND P3

At mooring P2, the largest source of EPE resulted from a net advection toward this location (convergence of EPE) by the mean flow (Figure 14, Table 9) balanced by a net conversion of eddy potential energy (EPE) to eddy kinetic energy (EKE) at 225 m, through vertical eddy heat fluxes (term 5 in (12)). The eddy field, unlike the mean, represented a sink through a net downstream advection (divergence of EPE) of EPE. As cited earlier, the CCS is generally considered to be baroclinically unstable due to vertical shear within the water column, which would imply that the eddy field should gain potential energy from the mean field (i.e., weaken the mean temperature gradient). This was found to be the case at 225 m depth, where a somewhat weaker source of EPE comes from horizontal eddy heat fluxes acting on the mean temperature gradients (term 4 of (12)), signaling the presence of baroclinic instabilities within the flow field. These downgradient heat fluxes produced a net conversion of potential energy from mean (MPE) to the eddies (EPE). As a result of these processes, there was

TABLE 9. **MEAN AND STANDARD ERRORS FOR SELECTED TERMS IN THE EDDY POTENTIAL ENERGY EQUATION AT MOORINGS P2 AND P3:** Values for mooring P2 are based upon the 17 month period between May 1989 and October 1990 (2055 data points), while those for P3 are based upon the one year period between May 1990 and May 1991 (1448 data points). The multiplicative constant (c) is equivalent to $\alpha\rho_0 g\bar{\theta}_z^{-1}$ and has a unique value for each level at each mooring. The sign convention for the five terms in the energy equation is the same as described in chapter IV, where the local rate of change of EPE is on the lhs of equation (12) while the others have been evaluated as if they were on the rhs of (12), such that a +/- represents a gain (source) / loss (sink).

Term	P2	225 m	P2	425 m	P3	225 m
	μ	σ_μ	μ	σ_μ	μ	σ_μ
u (cm s^{-1})	-5.18	± 1.23	-2.61	± 0.80	-2.69	± 2.29
v (cm s^{-1})	7.38	± 3.44	3.49	± 2.89	2.70	± 2.14
w (cm s^{-1})	-0.0017	± 0.0008	-0.0020	± 0.0009	0.000	± 0.0010
T (°C)	8.39	± 0.13	6.64	± 0.09	8.19	± 0.10
u'T' (°C cm s^{-1})	-0.17	± 0.32	-0.14	± 0.18	-0.77	± 0.44
v'T' (°C cm s^{-1})	-0.37	± 0.87	-0.65	± 0.70	-0.05	± 0.43
T_x (x10^{-8} °C cm^{-1})	6.39	± 4.73	7.78	± 5.25	0.239	± 3.03
T_y (x10^{-8} °C cm^{-1})	4.62	± 2.12	5.50	± 1.95	1.78	± 1.76
θ_z (x10^{-5} °C cm^{-1})	9.57	± 0.69	7.27	± 0.49	11.4	±0.88
x 10^{-3} (ergs cm^{-3} s^{-1})						
EPE_t	-0.013	± 0.055	+0.010	± 0.026	0.000	± 0.083
$\vec{\bar{v}} \cdot \nabla EPE$	+0.148	± 0.275	-0.040	± 0.112	-0.015	± 0.107
$\vec{v'} \cdot \nabla EPE$	-0.088	± 0.114	-0.104	± 0.095	-0.063	± 0.048
$\vec{v'}_H T' \cdot \nabla_H c\bar{T}$	+0.080	± 0.224	+0.118	± 0.181	+0.005	± 0.076
$\alpha\rho_0 g w'T'$	-0.153	± 0.060	+0.037	± 0.032	+0.074	± 0.067

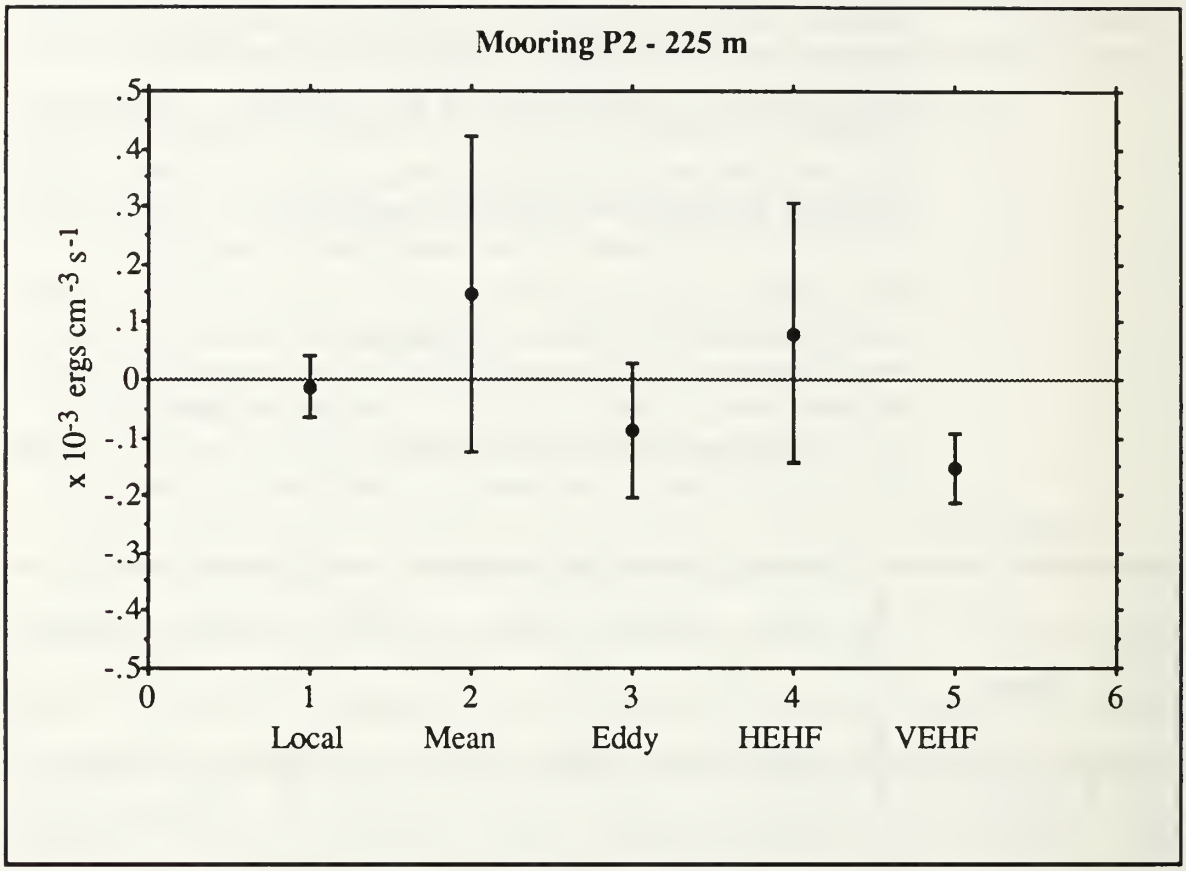

Figure 14. Eddy Potential Energy Balance at Mooring P2 - 225 m: Mean values of the five terms in the EPE equation, which have been evaluated as Local = Mean + Eddy + HEHF + VEHF, such that a +/- sign represents a gain (source)/loss (sink). Error bars represent the standard error of the mean as described in the text. Units are ergs cm^{-3} s^{-1}.

no significant growth or decay of EPE at 225 m depth (the local term is less than zero; however, not significantly nonzero). This is an encouraging result since, in the mean, it is expected that the total amount of EPE at a given location not grow or decay (*Hall*, 1991). A significantly nonzero value for this term would indicate that the sampling period was inadequate for this purpose, and calculated means are not representative of their true values.

To determine which of the individual components are primarily responsible for the sign and magnitude of the values listed in Table 9, we can examine vector diagrams of $\overrightarrow{\overline{v}_H}$ and $\overline{\nabla_H EPE}$, and $\overrightarrow{\overline{v'_H T'}}$ and $\nabla_H \overline{cT}$ (Figure 15). The upper panel of Figure 15 illustrates the mean flow advection of eddy potential energy, while the individual components and associated error bars are shown in Figure 16 for comparison. The mean flow at this depth was toward the northwest (325° T) at approximately 9.0 cm s^{-1}, while the gradient of EPE indicates that more eddy potential energy could be found inshore and slightly north of this location. From this we see that the x-component of mean flow advection (+0.213 ± 0.140 ergs cm^{-3} s^{-1}) was responsible for the energy growth observed at the mooring (Table 9 and Figure 14) while the y-component (-0.079 ± 0.224 ergs cm^{-3} s^{-1}), which is nearly orthogonal to the gradient, acted as a sink representing a downstream flux of energy. A weak contribution to the growth of energy due to mean flow advection also came from vertical advection (+0.014 ± 0.074 ergs cm^{-3} s^{-1}), due to downward vertical flow in the mean and a vertical gradient of EPE, which pointed toward the surface. For convenience, the factor of 10^{-3} has been dropped from these values and those appearing throughout the remainder of this chapter. The larger error bars associated with the y-component (Figure 16) are to be expected in light of the low frequency signals described earlier and are the primary source of uncertainty within the overall advection term. Given the existence of these very low frequency signals in the meridional component of flow and the fact that the error bars associated with the zonal component of advection do not cross zero, it is believed that the resulting sign of the mean advection term is correct and represents a source of EPE at this depth.

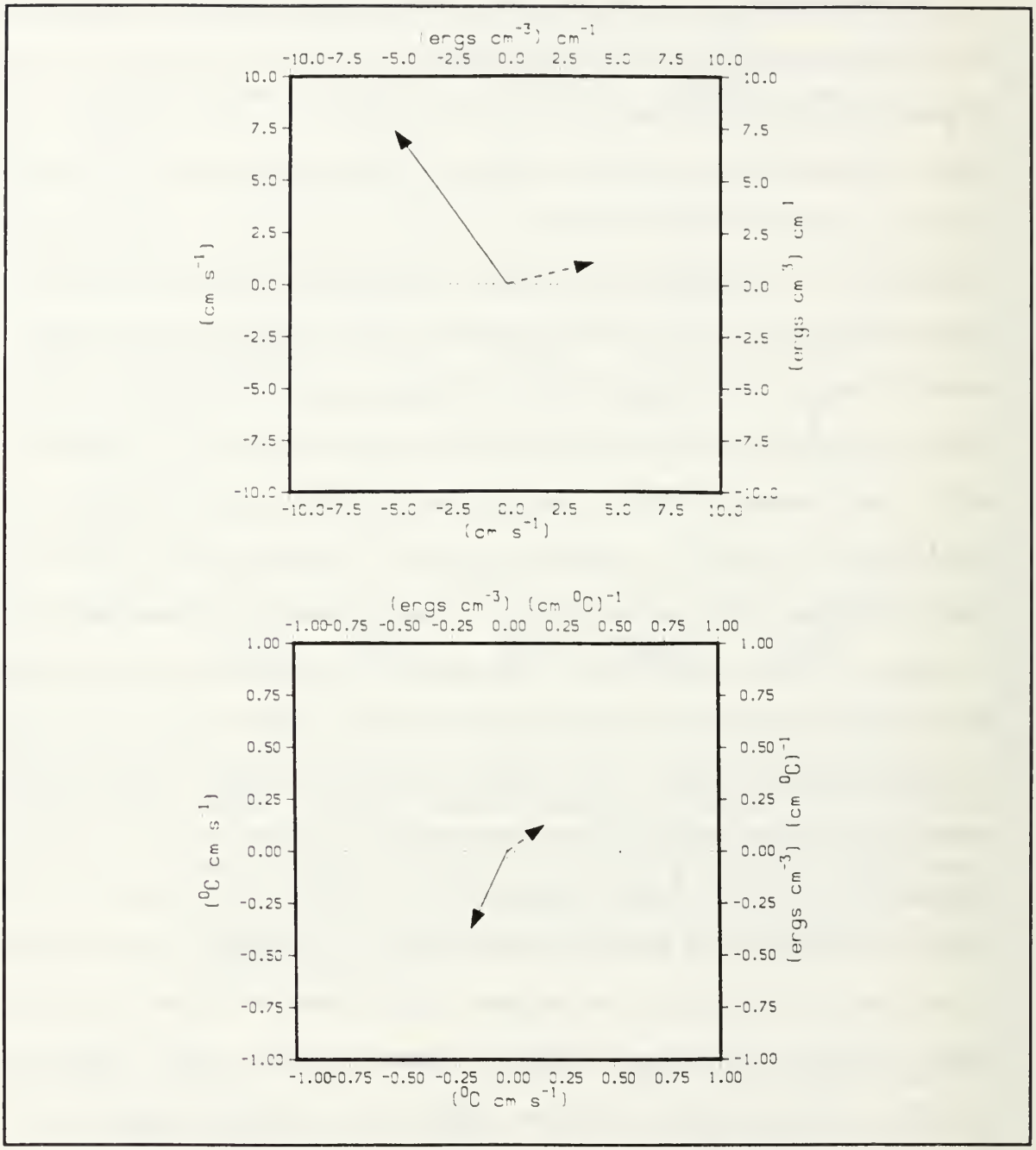

Figure 15. Vector Diagrams of $\overrightarrow{v_H}$, $\overline{\nabla_H EPE}$, $\overline{\overrightarrow{v'_H T'}}$ and $\nabla_H c\overline{T}$ at Mooring P2 - 225 m: Top panel contains $\overrightarrow{v_H}$ (solid) and $\overline{\nabla_H EPE}$ (dashed, multiplied by 10^5) with units as shown. Bottom panel contains $\overline{\overrightarrow{v'_H T'}}$ (solid) and $\nabla_H c\overline{T}$ (dashed, multiplied by 10^3) with units as shown.

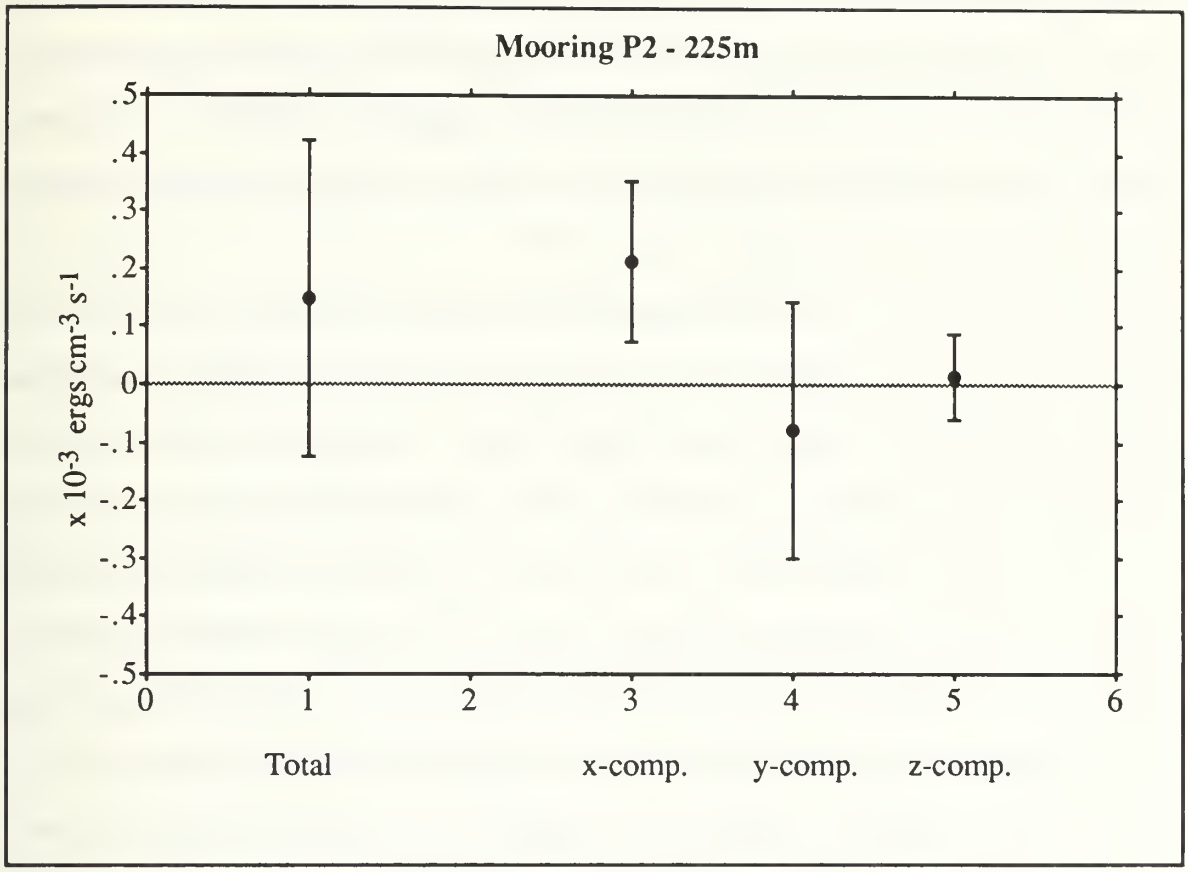

Figure 16. **Components of Mean Flow Advection of EPE at Mooring P2 - 225 m:** Mean values of the three components of the mean advection of EPE, along with the total value from Figure 14. A +/- sign represents a gain (source)/loss (sink). Error bars represent the standard error of the mean as described in the text. Units are ergs cm^{-3} s^{-1}.

The sign of individual components of eddy advection of EPE were the same as the corresponding components of mean advection; however, the relative magnitudes were not. In this case, the y-component was the dominant term having a magnitude of -0.210 ± 0.131 ergs cm^{-3} s^{-1}, a local loss of EPE which represents a downstream growth of energy, while the x- and z-components had magnitudes of $+0.115 \pm 0.123$ and $+0.006 \pm 0.032$, respectively. Similar to the advection by the mean flow, the resulting sign of the complete eddy advection

term was the same as that of its largest component, which was significantly non-zero. Therefore, we see that while the mean flow acts as a source by advecting EPE to this location, net advection in the alongshore direction by eddies produces an overall downstream growth of energy, and thus represents a sink for EPE at the 225 m level at P2.

As mentioned earlier, downgradient heat fluxes represent a conversion of energy from the mean (MPE) to the eddies (EPE) due to baroclinic instabilities resulting from a mean shear in the water column. This process can be seen in the lower panel of Figure 15, where the mean horizontal temperature gradient, and hence $\nabla_H c\overline{T}$, implies that a greater amount of mean (available) potential energy lies to the north and east of the mooring at this depth (indicating that the mean state isotherms slope downward in this direction) and the mean eddy heat flux is toward the southwest (205° T) with a magnitude of approximately 0.41 °C cm s^{-1}. Since these two vectors are in opposite quadrants, both the x- and y-components of mean eddy heat flux are downgradient and lead to conversions of MPE to EPE. The net values in these directions are of comparable magnitude, being $+0.031 \pm 0.123$ and $+0.048 \pm 0.187$ ergs cm^{-3} s^{-1}, respectively. If the net eddy heat flux vector were upgradient (in the direction of increasing MPE), the vectors would lie in the same quadrant and the eddies would then augment or feed the mean energy state (MPE) at the expense of local EPE by strengthening the mean temperature gradient (increasing isothermal slopes).

At 425 m depth, the net energy balance is somewhat different than at 225 m depth. Once again, eddy advection is represented a local sink, implying downstream growth of EPE (Table 9, Figure 17); however, it now represents the largest loss term in the balance. In fact, the sign of the x- and y- components are

the same and negative (-0.087 ± 0.075 and -0.024 ± 0.086 ergs cm^{-3} s^{-1}, respectively), so that the horizontal eddy field as a whole produces the loss. Advection of EPE by the mean flow also represents a loss, although much weaker than the eddy term (Table 9, Figure 17), and is dominated by the zonal component of flow (Figure 18). The mean flow is again towards the northwest (323° T) with a magnitude of approximately 4.4 cm s^{-1}; however, the mean gradient of EPE at this depth indicates that EPE increases to the west, and not inshore, although it is much weaker than at 225 m. From the orientation of these vectors, we can see that the meridional component of the mean flow will not contribute much to the overall term because it is nearly orthogonal to the gradient of EPE, while the zonal component, on the other hand, is almost parallel to the gradient and was, in fact, the dominant component.

The loss of EPE due to advection appears to be balanced by both horizontal and vertical eddy heat fluxes. Downgradient heat fluxes (MPE to EPE) at 425 m depth, similar to those at 225 m depth, make this term the primary balance to advective loss. The net eddy heat flux is now more southward (192° T) and stronger (0.67 °C cm s^{-1}) than at 225 m depth while the $\nabla_H c\overline{T}$ vector is in roughly the same direction (Figure 18). Once again these vectors are in opposite quadrants; however, a stronger meridional heat flux is responsible for a greater contribution to the total term (+0.090 ± 0.164 ergs cm^{-3} s^{-1}) than the zonal component (+0.027 ± 0.076 ergs cm^{-3} s^{-1}), which is nearly opposed to $\nabla_H c\overline{T}$. A weaker source of EPE comes from a net downward heat flux (EKE to EPE), implying that in the vertical, eddy motions are displacing the isotherms

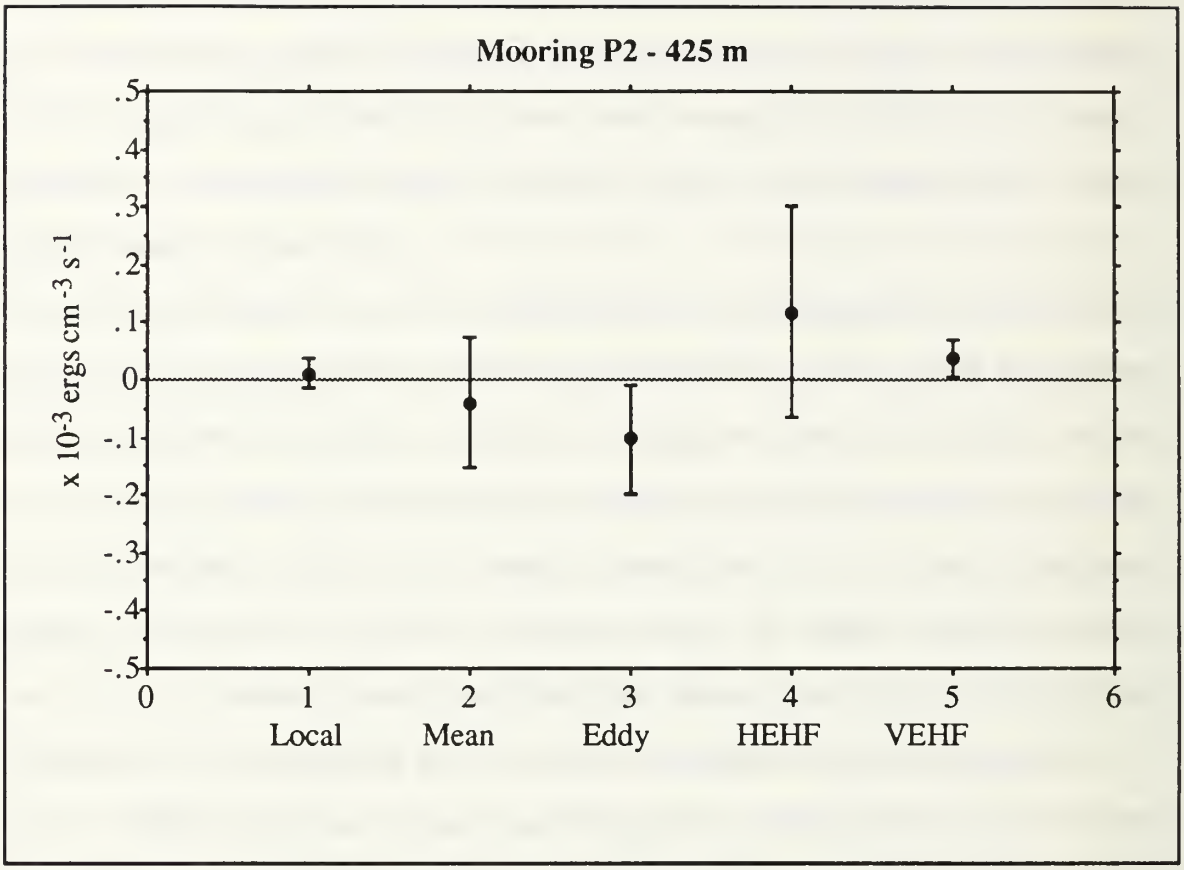

Figure 17. Eddy Potential Energy Balance at Mooring P2 - 425 m: Mean values of the five terms in the EPE equation, which have been evaluated as Local = Mean + Eddy + HEHF + VEHF, such that a +/- sign represents a gain (source)/loss (sink). Error bars represent the standard error of the mean as described in the text. Units are ergs cm^{-3} s^{-1}.

and isopycnals, thus creating more EPE at this location. This is different that at 225 m depth, where a net upward heat flux (EPE to EKE) existed and would tend to flatten out these surfaces at the expense of EPE. The slight growth of EPE ($\partial EPE/\partial t > 0$) at this depth (Table 9) is not significantly nonzero, indicating that the total EPE at the 425 m level at P2 is not growing or decaying. It is worth mentioning that the error bars for each of the five terms at 425 m are

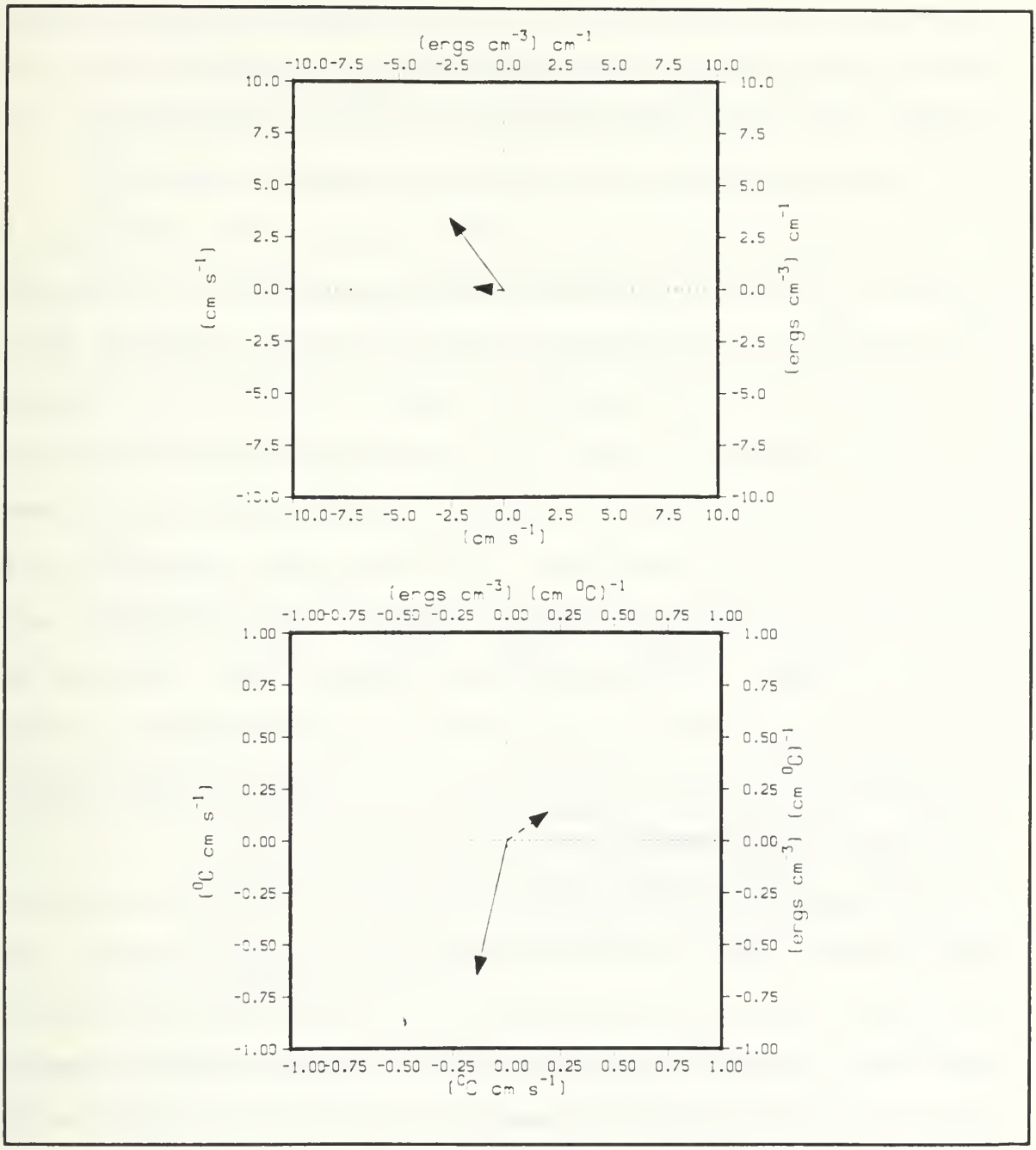

Figure 18. **Vector Diagrams of $\overrightarrow{v_H}$, $\overline{\nabla_H EPE}$, $\overrightarrow{v'_H T'}$ and $\nabla_H c\overline{T}$ at Mooring P2 - 425 m:** Top panel contains $\overrightarrow{v_H}$ (solid) and $\overline{\nabla_H EPE}$ (dashed, multiplied by 10^5) with units as shown. Bottom panel contains $\overrightarrow{v'_H T'}$ (solid) and $\nabla_H c\overline{T}$ (dashed, multiplied by 10^3) with units as shown.

smaller than corresponding terms at 225 m, presumably due to generally weaker flow and reduced variability at depth (see Appendix A). Similar to results at 225 m depth, terms involving the meridional or v-component of flow had the largest error bars, presumably due to the low frequency signals described earlier.

At mooring P3, results are based upon one year of data (unlike the 17-months at P2) and are not representative of the same time period as P2 data (with only six months of overlapping data between moorings). Therefore, caution must be exercised when comparing the results at the 225 m level for these moorings. Additionally, mooring P3 is located approximately 25 km farther offshore and, therefore, may lie in a different dynamical regime than P2, located approximately 26 km from shore. The first internal Rossby radius of deformation, $R_{d1} = \overline{N}H/\pi f$ (after *Koehler*, 1990) is a measure of the decay scale of coastal trapped waves in the offshore direction (*Allen*, 1980) and the fundamental length scale of coastal upwelling in a stratified fluid (*Huyer*, 1983). In this study, it was on the order of 8 to 14 km at P2 and 14 to 25 km at P3, in agreement with *Koehler* (1990).

Over the one-year time period at P3, there was no net growth or decay of EPE ($\partial EPE/\partial t \sim 0$). In fact, only two terms in the EPE equation were significantly nonzero and thus provided the dominant balance at P3 (Table 9, Figure 19). A net downward heat flux ($+ 0.074 \pm 0.067$ ergs cm^{-3} s^{-1}) represents a conversion of EKE to EPE, which was then advected downstream by the eddies themselves (-0.063 ± 0.048 ergs cm^{-3} s^{-1}) and to a lesser degree by the mean flow (-0.015 ± 0.107 ergs cm^{-3} s^{-1}). All three components of eddy advection were negative (losses), with the x- and y-components being of nearly equal value (-0.027 ± 0.040 and -0.031 ± 0.026 ergs cm^{-3} s^{-1}, respectively). Net mean flow

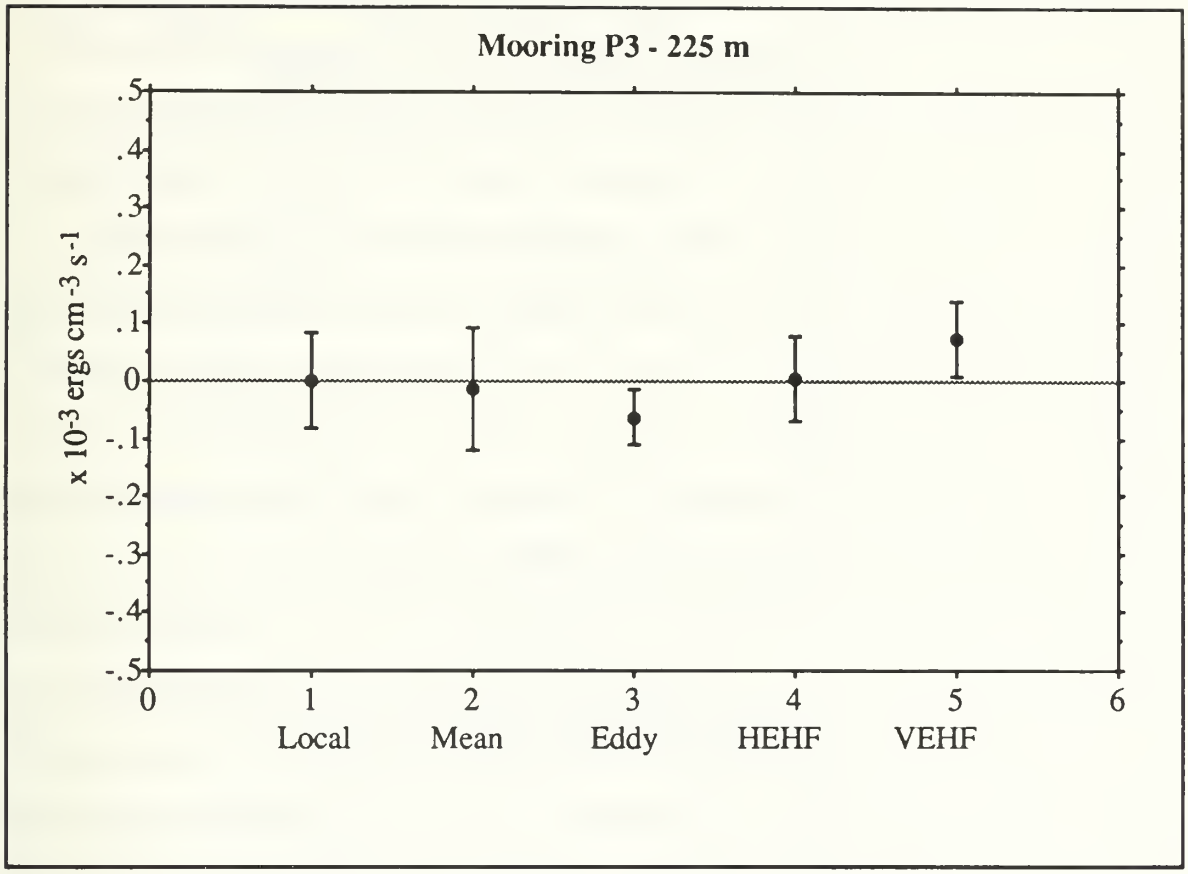

Figure 19. Eddy Potential Energy Balance at Mooring P3 - 225 m: Mean values of the five terms in the EPE equation, which have been evaluated as Local = Mean + Eddy + HEHF + VEHF, such that a +/- sign represents a gain (source)/loss (sink). Error bars represent the standard error of the mean as described in the text. Units are ergs cm^{-3} s^{-1}.

advection of EPE was much smaller than at P2 due to a generally weaker mean flow (3.81 cm s^{-1} towards the northwest (315.1° T)) which was nearly orthogonal to a weaker gradient of EPE (Figure 20). The direction of this gradient is similar to that of the 225 m level at P2, which also indicated more EPE to the north and east of the mooring. The zonal component of the mean advection was a source of EPE (+0.027 ± 0.074 ergs cm^{-3} s^{-1}), being in

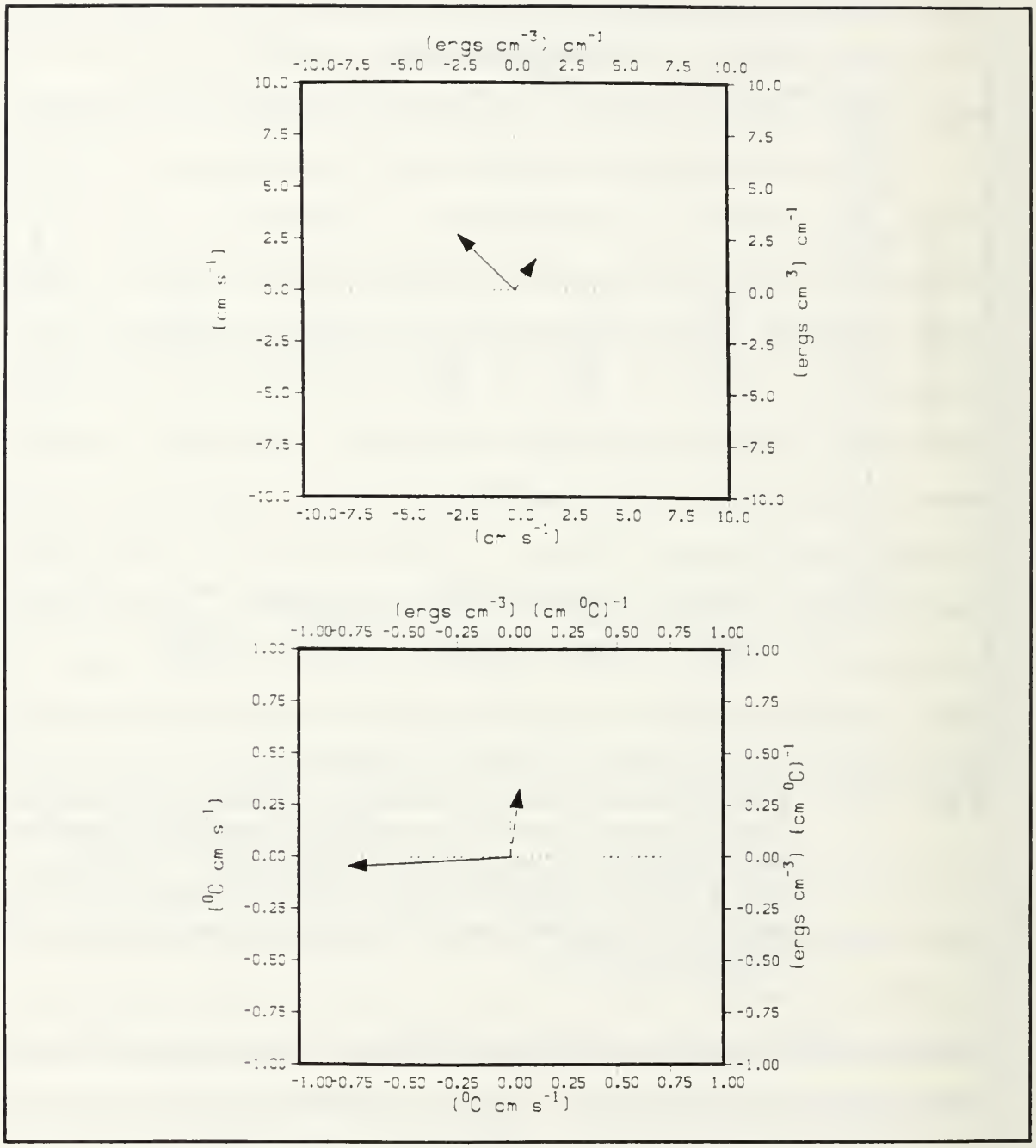

Figure 20. **Vector Diagrams of $\overrightarrow{v_H}$, $\overline{\nabla_H EPE}$, $\overline{\overrightarrow{v'_H T'}}$ and $\nabla_H c\overline{T}$ at Mooring P3 - 225 m:** Top panel contains $\overrightarrow{v_H}$ (solid) and $\overline{\nabla_H EPE}$ (dashed, multiplied by 10^5) with units as shown. Bottom panel contains $\overline{\overrightarrow{v'_H T'}}$ (solid) and $\nabla_H c\overline{T}$ (dashed, multiplied by 10^4) with units as shown.

opposition to the gradient of EPE; however, it is the meridional component (-0.042 ± 0.076 ergs cm^{-3} s^{-1}), which lies in the same direction as this gradient, that was responsible for the overall loss from mean advection. Mean advection in the vertical was nonexistent due to the lack of a mean vertical velocity.

Unlike mooring P2, where the mean horizontal eddy heat flux was toward the southwest at both depths, the net heat flux was nearly due west at mooring P3 (Figure 20), with a magnitude of -0.77 °C cm s^{-1}. However, while this appears to be a much stronger flux of heat, relative to mooring P2, the fact that it is nearly orthogonal to a much weaker $\nabla_H c\overline{T}$, produces very little conversion (if any) of energy between MPE and EPE. While the mean value for this term was weakly positive, it is not significantly non-zero, indicating the MPE-EPE conversion is almost non-existent and this conversion may not be as important at P3 as it was at P2. However, once again it should be emphasized that since we are dealing with only with one year of data from a different time period, such a conclusion must be treated with caution. It is quite possible that different results may be obtained if a longer time series and/or different time period were available.

B. GENERAL CHARACTERISTICS OF THE EPE TIME SERIES

To summarize the results of the previous section, we found that above 350 m depth at mooring P2, there was a net conversion of EPE to EKE through vertical eddy heat fluxes and downstream advection by the eddy field in the alongslope direction. These losses of EPE appear to be balanced by advection from the mean flow, which carries EPE offshore toward the mooring, and through a conversion of MPE to EPE resulting from downgradient heat fluxes. Below 350 m depth, conversions of MPE and EKE to EPE through horizontal and vertical

eddy heat fluxes provided the source of EPE while advection from both the mean and eddy fields advect EPE downstream away from the mooring. At mooring P3, EKE was converted to EPE through downward eddy heat fluxes, and was then advected downstream by the eddy flow, and to a lesser degree, by the weak mean flow. Little or no conversion of MPE to EPE occurred as a result of a reduced mean vertical shear (hence weaker mean temperature gradient, especially in the cross shore direction), which was nearly orthogonal to mean horizontal eddy heat fluxes.

In the atmosphere, disturbances within baroclinically unstable mid-latitude jet currents can lead to the formation of Rossby waves, with cyclonic and anticyclonic eddies appearing in the crests and troughs of these waves. Within these baroclinic eddies MPE is converted to EPE (*Holton*, 1979; *Kamenkovich, et al.*, 1986). These upper atmospheric eddy features in turn lead to the formation of lower level features, where the EPE is converted to EKE through the vertical motions of these eddies, and baroclinic instabilities within lower level fronts. Finally, energy is dissipated through friction within the eddy and mean flows, while the mean zonal kinetic energy (MKE) is maintained through the conversion of EKE to MKE. This latter conversion results from Reynolds stresses, u'v', and occurs when lower level cyclones occlude in a process known as barotropization (*Holton*, 1979; *Kamenkovich, et al.*, 1986). These barotropized cyclones feed energy from the eddies to the mean through a process which can be thought of as negative viscosity (*Kamenkovich, et al.*, 1986). Observations from the POLYMODE study indicate that upper ocean eddies drive lower level eddies via a barotropic cascade (*Kamenkovich, et al.*, 1986), and has been confirmed in regional numerical models (*Holland and Rhines*, 1980).

While this study deals with an oceanic eastern boundary current regime instead of a mid-latitude atmospheric jet or a large-scale ocean gyre, and the space and time scales involved are completely different, it was originally thought that representative or so-called canonical events could be identified within the time series of the five terms in the EPE equation (Appendix E) that would be of the same sign and magnitude as the mean and thus help explain the observed balance. However, a careful examination of the energetic events which do exist within these time series does not reveal any recurring events which replicate the mean. In fact, just the opposite appears to be true. Energetic bursts appear to occur under a variety of flow conditions, with each resulting in a different balance between the five terms in the EPE equation (Figures 21 and 22). In addition, these events are at times as much as 10 to 20 and up to 200 times the magnitude of the time mean values. Visual inspection of the time series of local growth/decay (Local) and vertical eddy heat fluxes (VEHF) (Figure 22 and Appendix E) suggests that these terms are dominated by higher frequency motions, compared to the remaining terms, and should be highly correlated. This strong correlation between the Local and VEHF terms is reflected in the correlation coefficients (Table 10) and in the respective autospectra (Figures 23 through 25), where the greatest correlation at each mooring was between the local growth/decay term and the vertical eddy heat fluxes, and occurred primarily at higher frequencies (periods between 2 and 20 days).

The autospectra shown in Figures 23 through 25, unlike those of Chapter III, were computed using MATLAB software for the sole purpose of providing an estimate of the basic spectral shape and are not in the so-called variance conserving form. Each was computed using a single-piece length at each

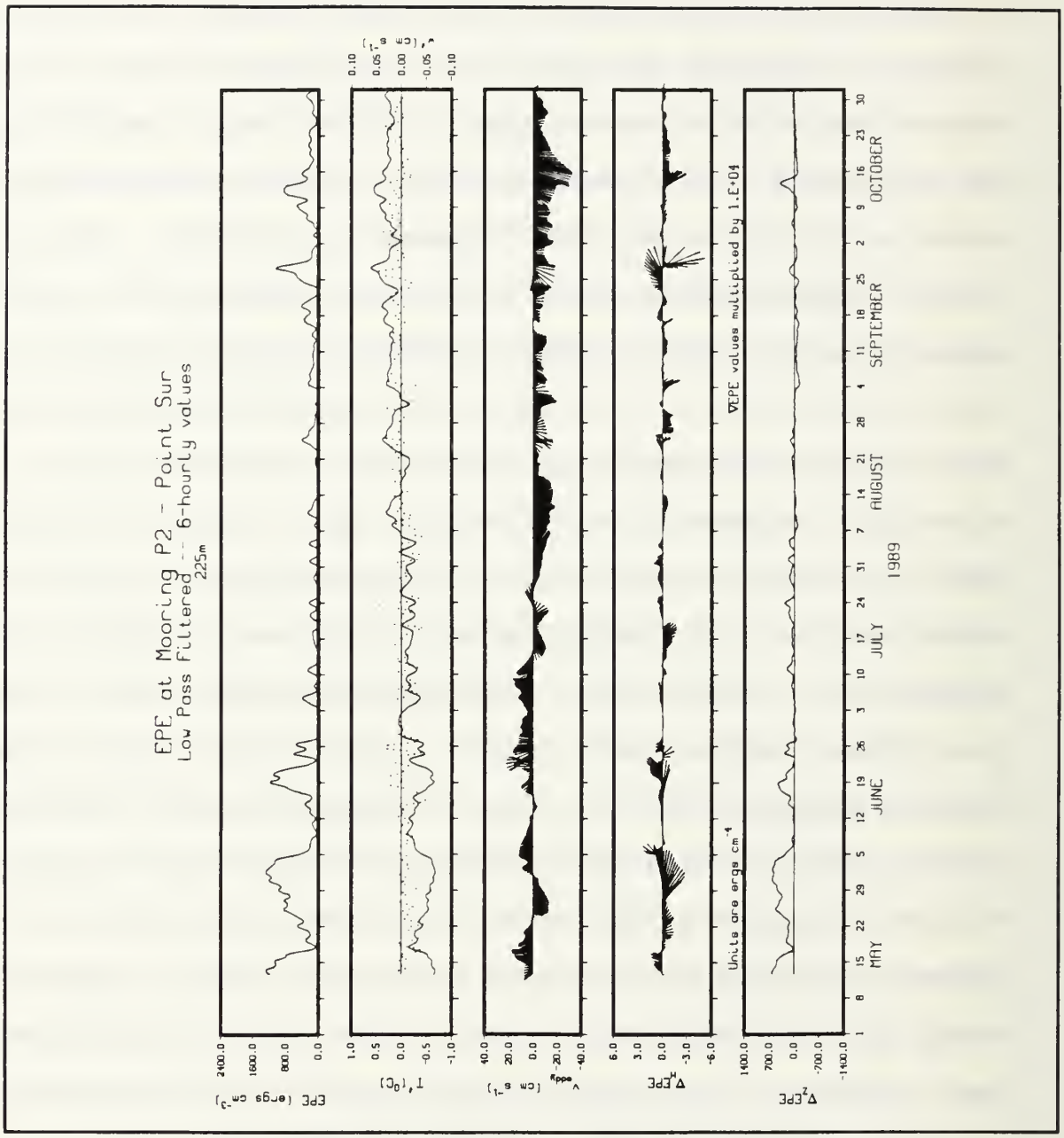

Figure 21. **Time Series of EPE, w', T', $\overrightarrow{v'_H}$, and ∇_{EPE} at Mooring P2 - 225m for the period 1 May to 31 October 1989:** Panels from top to bottom are: EPE in ergs cm^{-3}; T' (solid curve) in °C, and w' (dashed curve) in cm s^{-1}; horizontal eddy velocity in cm s^{-1}; and the horizontal and vertical gradients of EPE in (ergs cm^{-3}) cm^{-1}, where gradient values have been multiplied by 10^{+4}. (*from Appendix E*)

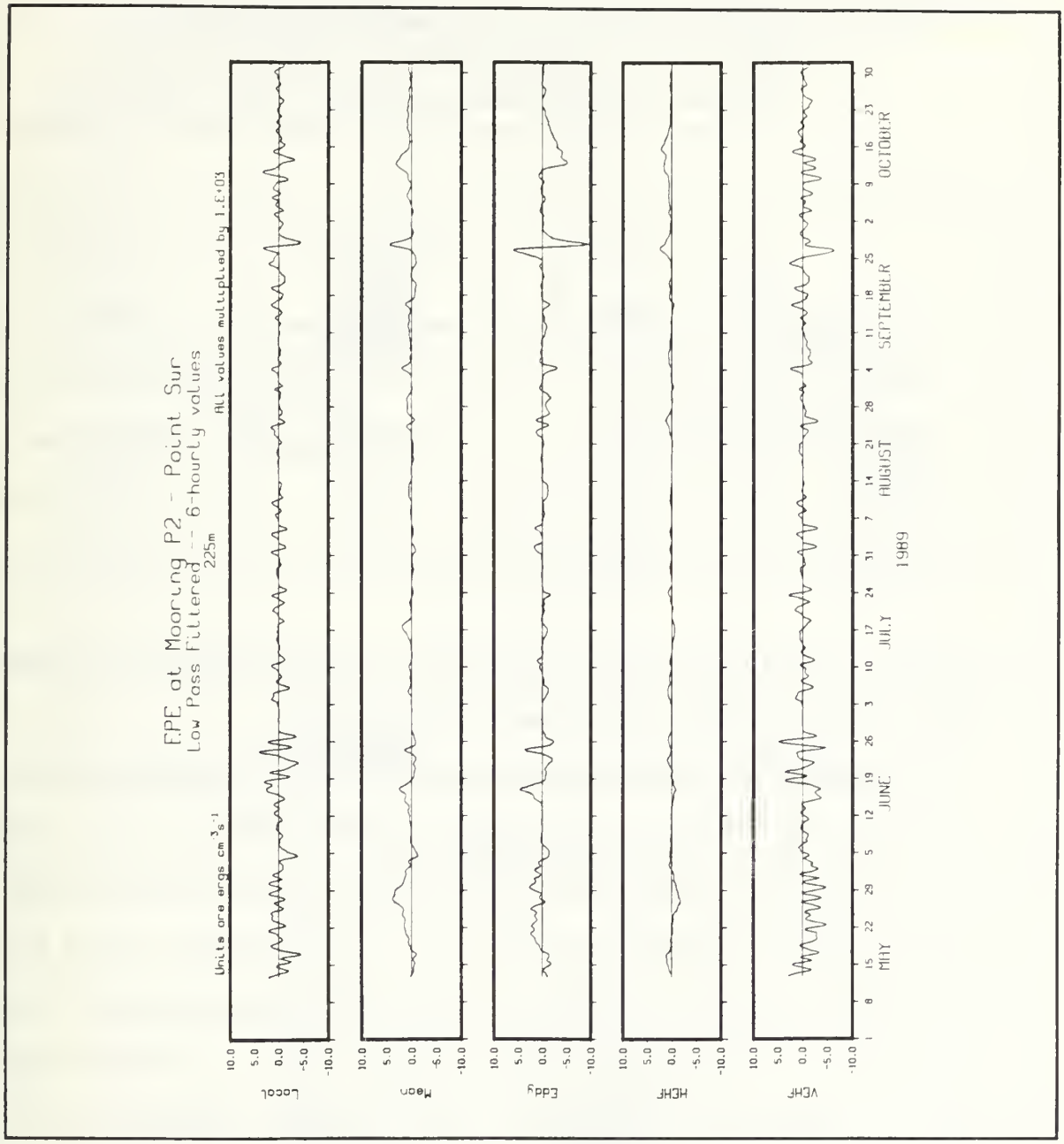

Figure 22. Time Series of the Five Terms in EPE Equation at Mooring P2 - 225m for the period 1 May to 31 October 1989: Panels from top to bottom are: local growth/decay of EPE; mean advection of EPE; eddy advection of EPE; horizontal eddy heat flux conversion term (MPE - EPE); and vertical eddy heat flux conversion term (EKE - EPE). Units are ergs cm^{-3} s^{-1} and all values have been multiplied by 10^{+3}. A positive (negative) value represents a gain/source (loss/sink). (*from Appendix E*).

Table 10. **CORRELATION COEFFICIENTS FOR SELECTED TERMS IN THE EDDY POTENTIAL ENERGY EQUATION AT MOORINGS P2 AND P3:** These correlation coefficients are based upon the time series of the five terms in the EPE equation (10) as described in Chapter IV.

	P2 - 225 m Local	P2 - 425 m Local	P3 - 225 m Local
Mean	+ 0.194	- 0.004	- 0.006
Eddy	+ 0.300	+ 0.105	+ 0.360
HEHF	- 0.193	- 0.051	- 0.009
VEHF	+ 0.633	+ 0.738	+ 0.931

mooring (512 days and 256 days at moorings P2 and P3, respectively), thereby trading spectral confidence for increased resolution.

As mentioned above, the energy spectra for moorings P2 and P3 reveal that local growth/decay of EPE and EKE-EPE conversions occur primarily between periods of 2 to 20 days. The spectra at P2 for mean advection and the MPE-EPE conversion suggest that these processes play a more important role at lower frequencies. Advection of EPE by the eddy field contains energy in both spectral regions. In general, the spectral shapes at P2 225 m and 425 m depths (Figures 23 and 24) are quite similar, where the greater variability known to exist at the 225 m level is reflected in the greater magnitudes of spectral density. At mooring P3, the primary balance in the time mean was between eddy advection and EKE-EPE conversions. These same terms were also responsible

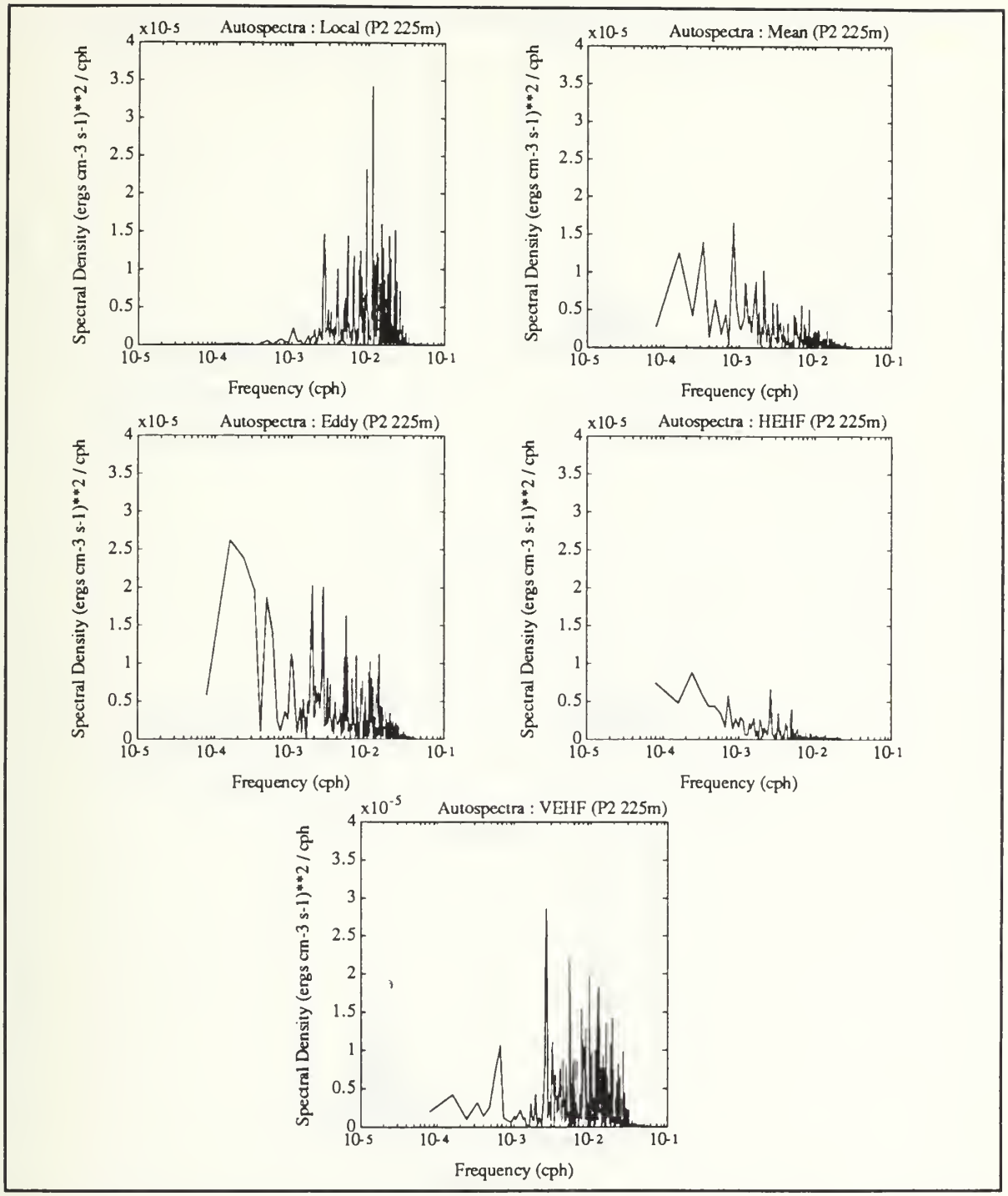

Figure 23. Spectral Energy of Terms in the EPE Equation at Mooring P2 - 225 m: Auto-spectrum of each of the five terms in the EPE equation. Plots are based upon 512 days of data using a single piece as described in text.

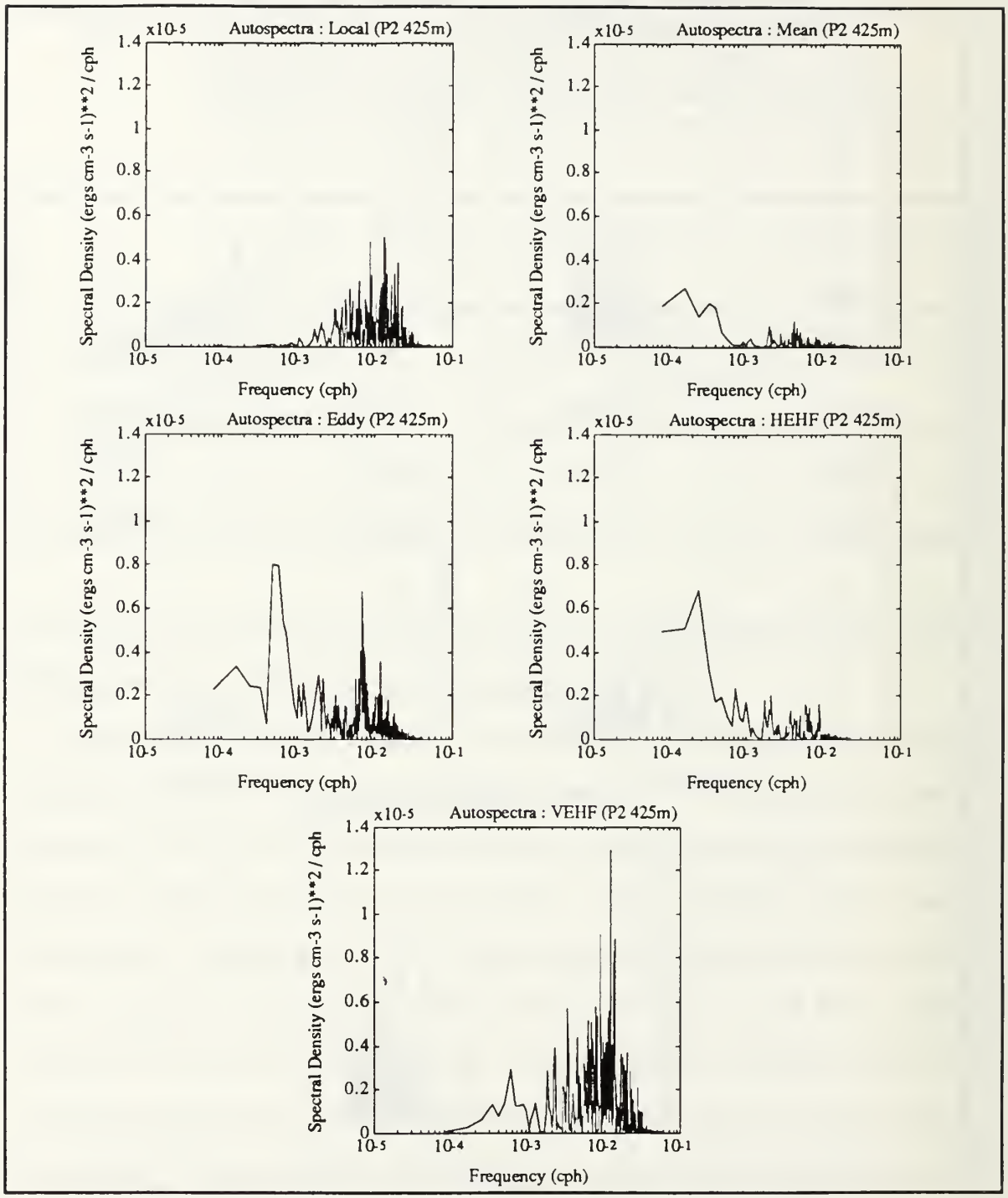

Figure 24. Spectral Energy of Terms in the EPE Equation at Mooring P2 - 425 m: Auto-spectrum of each of the five terms in the EPE equation. Plots are based upon 512 days of data using a single piece as described in text.

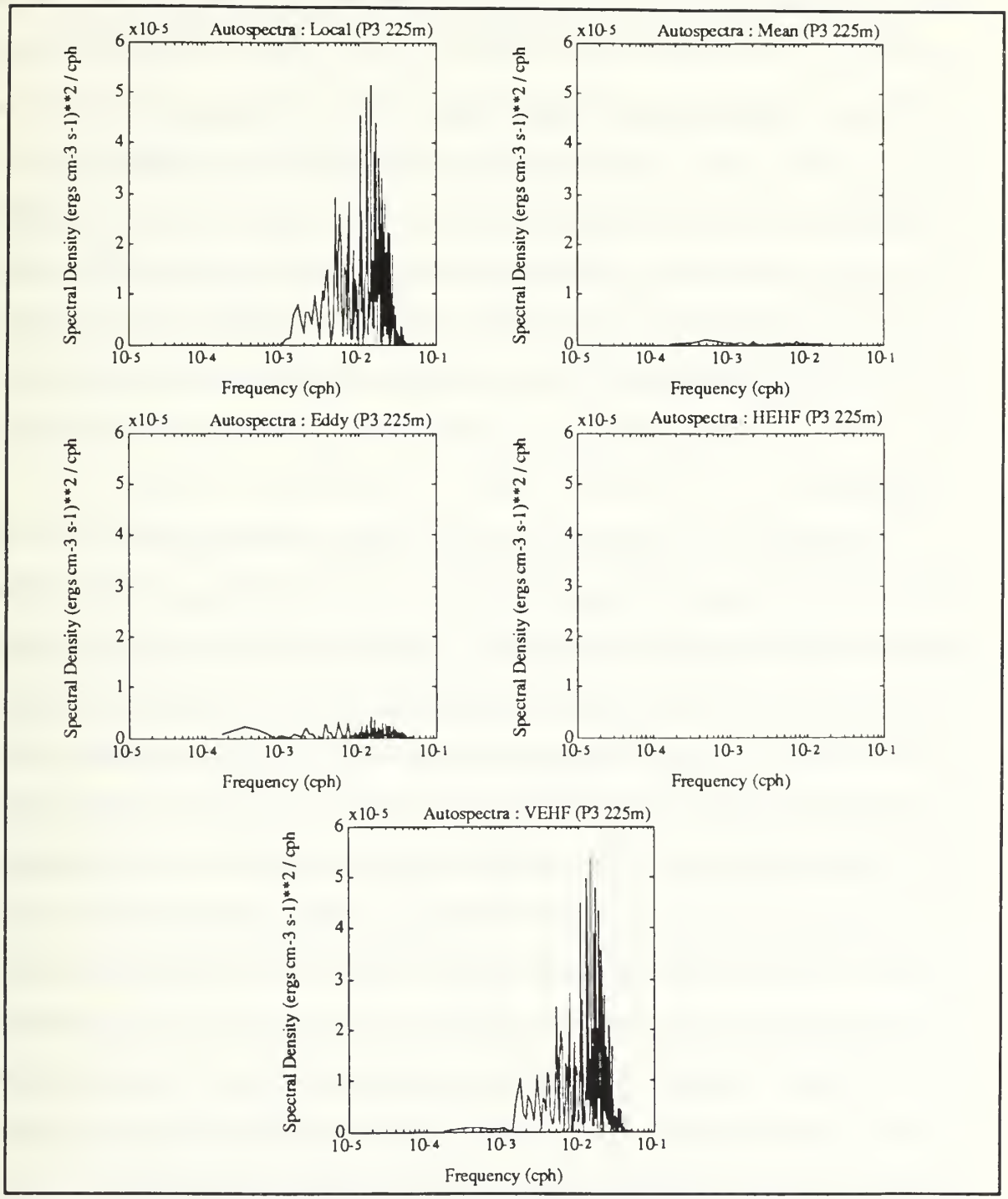

Figure 25. Spectral Energy of Terms in the EPE Equation at Mooring P3 - 225 m: Auto-spectrum of each of the five terms in the EPE equation. Plots are based upon 256 days of data using a single piece as described in text.

for the fluctuations observed in the local growth/decay of EPE as seen in Appendix E. These features are characterized quite well in both the correlation coefficients (Table 10) and spectra (Figure 25), which show that almost no energy exists in the mean advection and MPE-EPE conversion terms, in agreement with the results shown in Table 9 and Figure 19, where both terms were, in fact, quite small. The spectra for eddy advection of EPE (Figure 25) reveals that some energy exists over the same higher frequency range as for the Local and VEHF terms, as well as over the lower frequency range observed in the spectra for mean advection, although both are weak and may not be significant.

To summarize, it appears that no single energetic event exists to describe the time mean results at moorings P2 and P3. As expected from the larger mean currents and fluctuations at P2, greater variability existed in the time series of EPE at mooring P2 as compared to mooring P3. This is presumably due in part to the fact that P2 is located closer to shore, and under a greater influence of the undercurrent, which has been found to exist within 12 to 42 km of the coast in this region (*Tisch et al.*, 1992). Another source of variability may come from cyclonic and anticyclonic eddies which have been observed in this region (*Breaker and Broenkow*, 1989; *Tracy*, 1990; *Tisch et al.*, 1992), and can be seen in the time series of the currents (Appendix A). At mooring P3, the dominant form of energy growth/decay appeared to come in the form of vertical processes such as vertical eddy heat fluxes and the vertical component of eddy advection, although horizontal components of eddy advection were also important, and just as at P2, the balances during events were not consistent.

C. ANALYSIS OF ENERGETIC EVENTS OBSERVED WITHIN THE TIME SERIES OF EPE OFF POINT SUR AT MOORINGS P2 AND P3

Since this region exhibits a great amount of variability and the resulting energetic bursts (with magnitudes much greater than that of the time-mean) appear to have no common pattern, the following sections have been devoted to an in-depth description of four such events (three from P2 and one from P3) that occurred during the time of this study. When possible, supporting data, such as quantities derived from CTD data and AVHRR satellite imagery, have been included to aid in the interpretation of these energetic events.

1. Event #1 - Mooring P2 - 225 m: 18 May to 3 June 1989

Compared to the majority of energetic bursts found throughout these time series, which are of generally shorter duration, this event spans a two and a half week period from 18 May through 3 June 1989 (Figures 26 and 27), and is believed to result from the southern edge of an anticyclonic feature passing near the mooring. During the entire time segment shown in Figure 26, the disturbance temperature, T', was less than zero, and starting near the 18th, a gradual cooling trend becomes apparent, producing the corresponding rise in the level of EPE (which is proportional to T'^2) at the mooring. The beginning of this cooling trend has been chosen to signal the beginning of this event. Initially, the horizontal gradient of EPE (∇_HEPE) was nearly due south and very weak, but by the 22nd it had increased in magnitude and was directed southeastward indicating that warmer/cooler water (anomaly) lay to the northwest/southeast. The vertical gradient of disturbance temperature, θ'_z (not shown), was negative, indicating that the cool anomaly was more pronounced near the surface than at

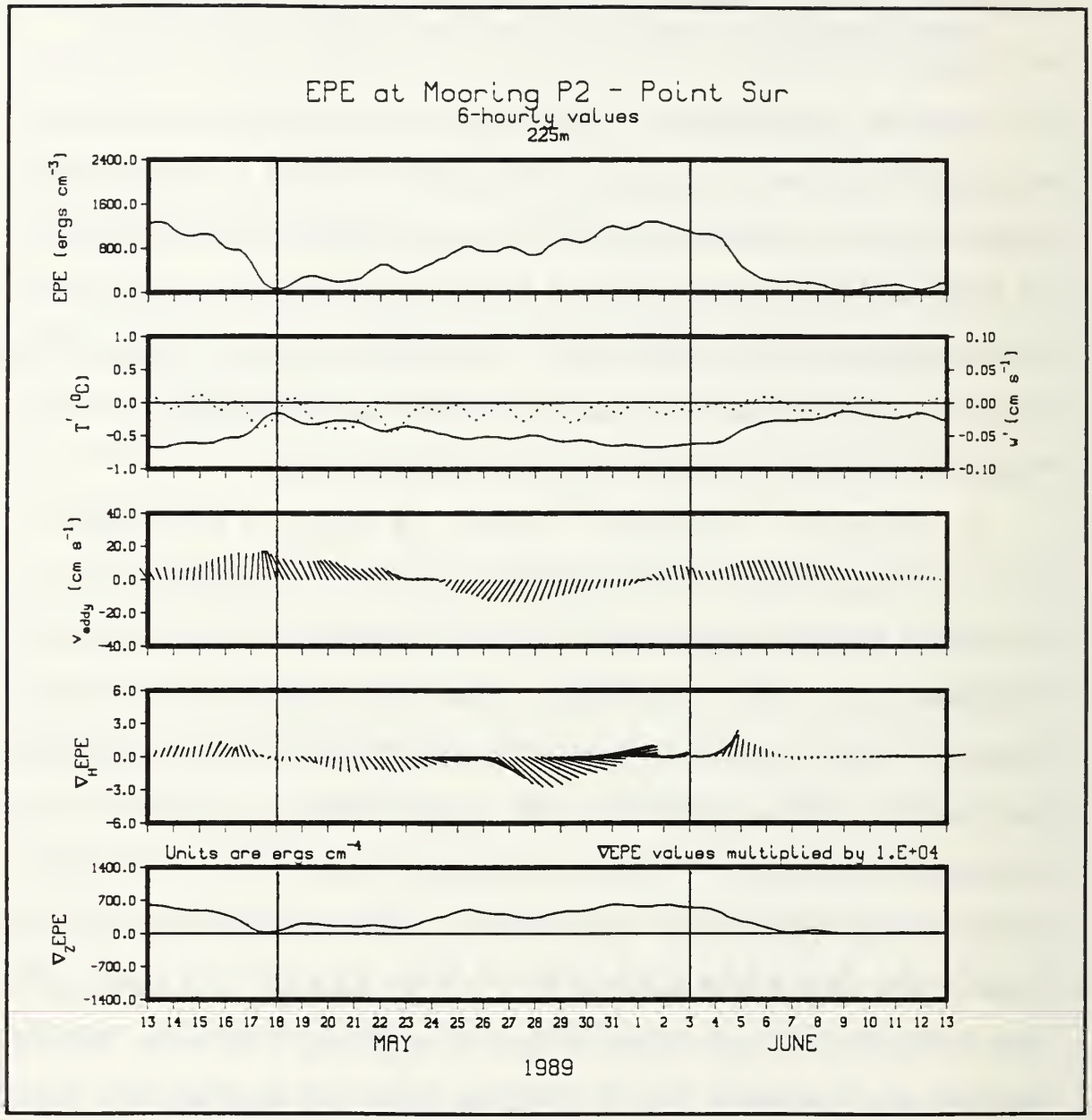

Figure 26. **Time Series of EPE, w', T', $\overrightarrow{v'_H}$, and ∇_{EPE} at Mooring P2 - 225m for the period 13 May to 13 June 1989:** Panels from top to bottom are: EPE in ergs cm^{-3}; T' (solid curve) in °C, and w' (dashed curve) in cm s^{-1}; horizontal eddy velocity in cm s^{-1}; and the horizontal and vertical gradients of EPE in (ergs cm^{-3}) cm^{-1}, where gradient values have been multiplied by 10^{+4}. Event described in text is enclosed between the vertical lines.

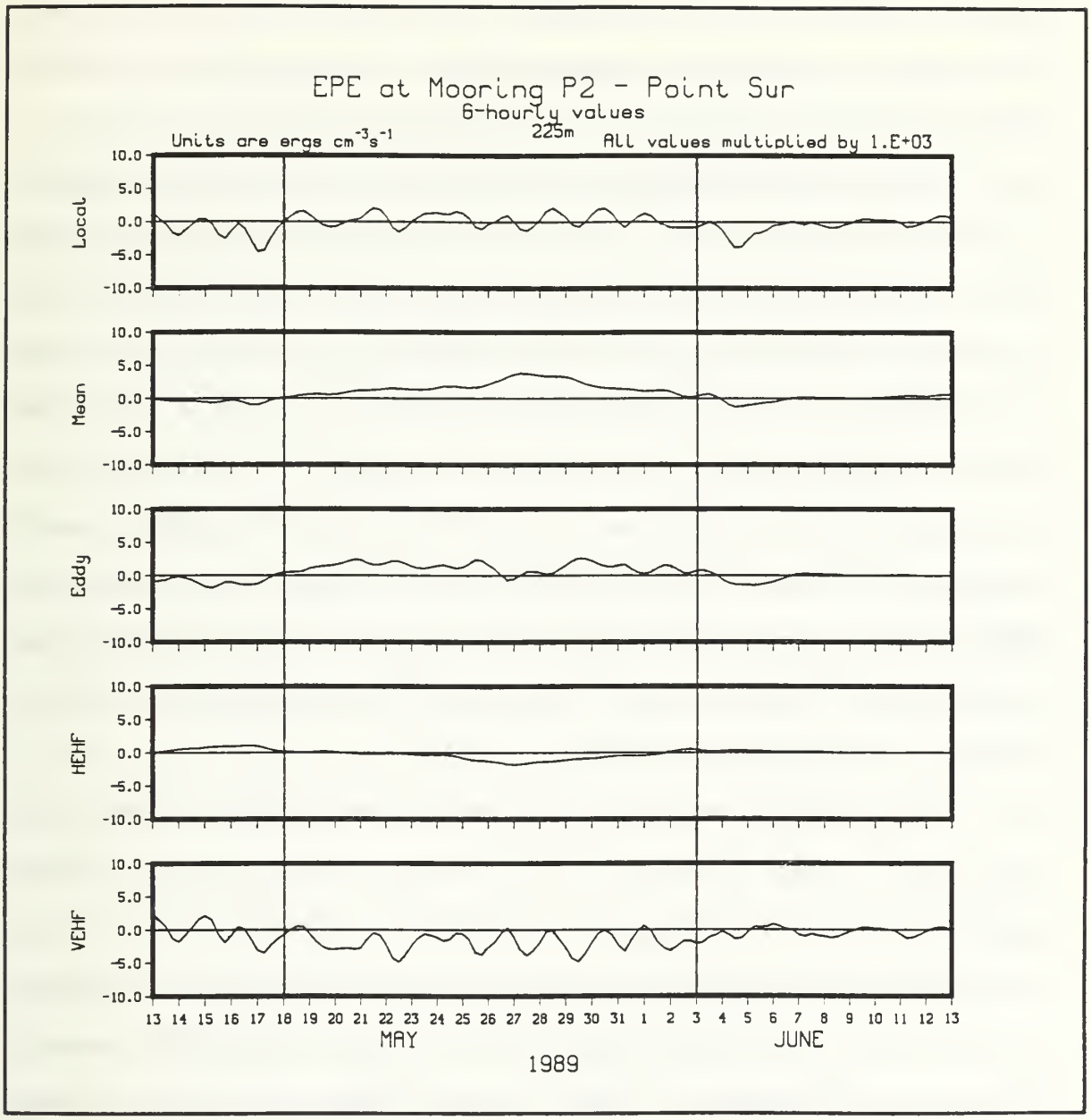

Figure 27. Time Series of the Five Terms in EPE Equation at Mooring P2 - 225m for the period 13 May to 13 June 1989: Panels from top to bottom are: local growth/decay of EPE; mean advection of EPE; eddy advection of EPE; horizontal eddy heat flux conversion term (MPE - EPE); and vertical eddy heat flux conversion term (EKE - EPE). Units are ergs cm^{-3} s^{-1} and all values have been multiplied by 10^{+3}. A positive (negative) value represents a gain/source (loss/sink). Event described in text is enclosed between the vertical lines.

depth (as seen in the 100 m temperature record for mooring P2 during May 1989, shown in Appendix A). Therefore, the vertical gradient of EPE was directed toward the surface.

As mentioned earlier, the mean flow at this level was approximately 9.0 cm s^{-1} to the northwest (325°T). Between the 18th and 22nd of May, the eddy flow was also towards the northwest (Figure 26) at about 15 cm s^{-1}. With cooler water to the southeast of the mooring, the tendency would be for both the mean and eddy flow to advect in these cooler temperatures, and hence, EPE. This advection of EPE to the mooring can be seen in Figure 27 where, in general, advection by mean and eddy flows provide the source of EPE during the entire event period. As this energy is advected in to the mooring, it is converted to EKE through vertical eddy heat fluxes, which carry the cooler water downward. No MPE-EPE conversions occur at this time since the horizontal eddy heat fluxes are nearly orthogonal to the mean temperature gradient.

Beginning on the 22nd, a counterclockwise rotation develops in the eddy velocity vectors, which shift from northwest to southwest, and appears to signal the presence of an anticyclonic feature to the northwest of the mooring. The presence of this feature on the oceanic side of Monterey Bay in late May 1989 has been documented by *Tracy* (1990) in a sequence of AVHRR satellite images from 23 May through 26 May. While AVHRR imagery only provides the temperature information of the sea surface (SST) (and not at subsurface instrumentation), the patterns observed within SST make it possible to infer the direction of surface (and sometimes subsurface) flow and, in this case, the sense of eddy rotation. The AVHRR satellite image for 25 May (Figure 28) depicts the presence of the anticyclonic feature to the northwest of the mooring and suggests

southwestward flow at the mooring, in agreement with flow conditions shown in Figure 26 and Appendix A. Similar mesoscale features have been observed off Point Sur in satellite and hydrographic data (*Tisch et al.* 1992) as well as in the time series of the currents (Appendix A). Particularly deep signatures of larger mesoscale features were observed at mooring P3 in the early spring of 1990 and 1991, penetrating to 1000 m depth on both occasions (Appendix A). The counterclockwise rotation associated with the present feature was observed in the time series of velocity at all three instrumented depths (Appendix A); however, it was more prominent in the 100 m depth record, consistent with the results of *Tracy* (1990), who found this feature to be most prominent within the upper 300 m. This also agrees with the vertical gradient of EPE which indicated that the larger temperature anomaly was near the surface. As mentioned earlier, ∇_HEPE indicates that a cooler anomaly lies inshore and to the south while warmer temperatures lie to the northwest (Figure 26). This is precisely the location of the warm core anticyclonic feature as inferred from satellite imagery (Figure 28).

Tracy (1990) found this time period to be one of active upwelling, which would produce cooler near-surface temperatures observed at the Año Nuevo and Point Sur upwelling centers (Figure 28). Because T' was negative and the temperatures were gradually cooling during this entire event, it is believed that the mooring was near the southeastern portion of the warm eddy, as suggested in the satellite image. In this case, the mean flow would then be advecting in cooler temperatures from the southeast which might have originated near the Point Sur upwelling center, while the eddy flow would be advecting in

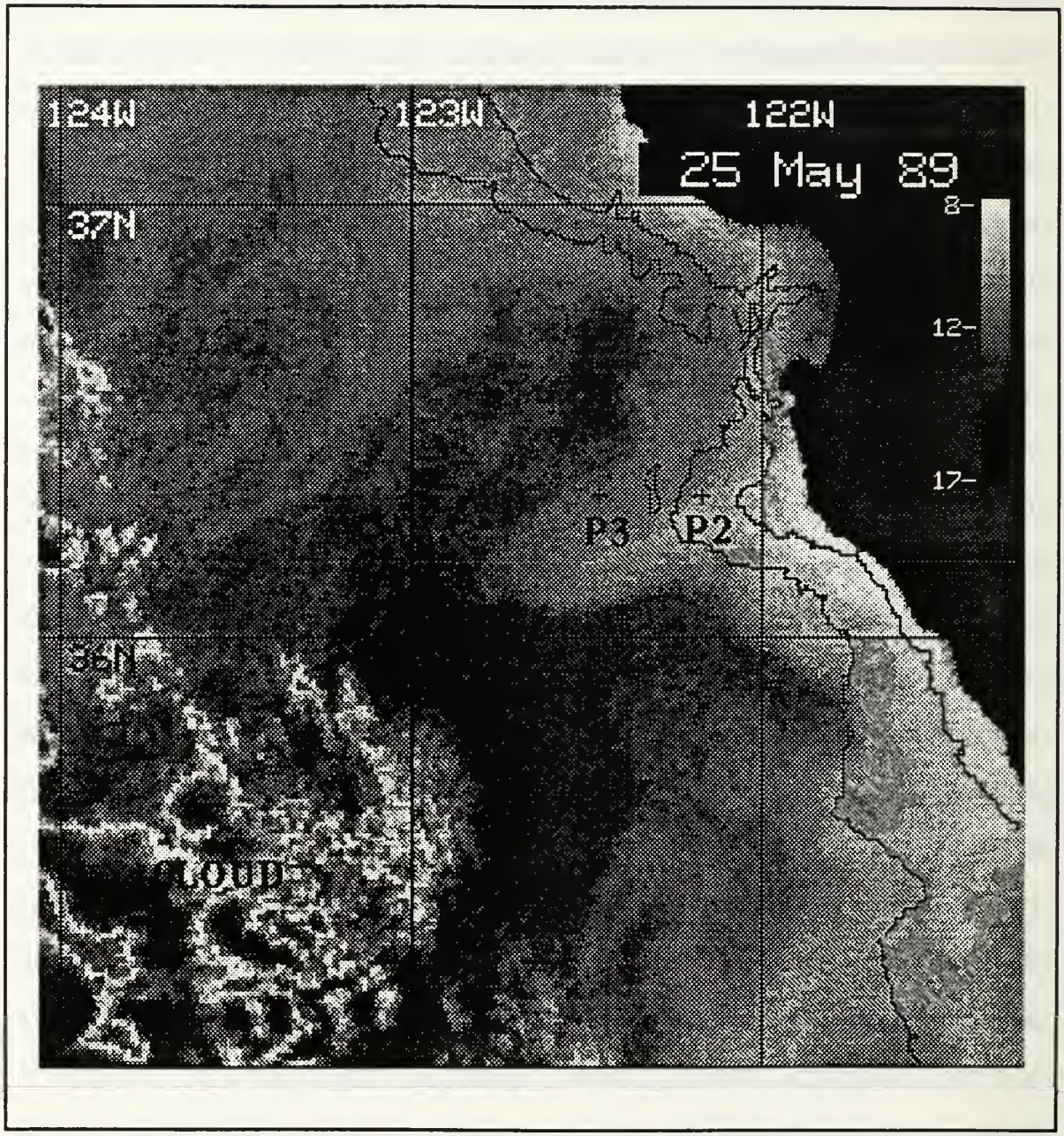

Figure 28. **NOAA AVHRR Satellite Imagery from 25 May 1989:** Lighter shades represent cooler water, while the darker shades represent warmer waters. Note the presence of warmer water to the northwest of mooring P2 and the cooler water inshore from Monterey Bay to Point Sur. An anticyclonic sense of rotation may be inferred with the surface water flowing to the southwest at the mooring.

cooler temperatures from the northeast, possibly from the Año Nuevo upwelling center, as suggested by *Tracy* (1990).

During this event the local growth/decay of EPE fluctuated about zero, while both the mean and eddy flow were advecting in EPE (Figure 27). Most of the fluctuation is seen to be due to the vertical eddy conversion (EPE to EKE) term (VEHF). The maximum advection by the mean flow occurred near 27 May, when the mean flow and ∇_HEPE were nearly opposed to one another. At the same time, the eddy flow was nearly orthogonal to this gradient (Figure 26), which means that it is neither contributing to a gain or to a loss of EPE (eddy advection near zero). The horizontal eddy heat fluxes are carrying heat towards the northeast, in the direction of the mean temperature gradient, and are thus responsible for a conversion of EPE to MPE. The maximum gradient of EPE occurred between 27 May and 1 June, during which time it rotated counterclockwise from southeast to northeast and then weakened. With T' less than zero, this implies that the warmer water moved offshore, as was observed by *Tracy* (1990), so that it was nearly due west or alternately that the cooler water was now inshore of the mooring.

In summary, we found that the source of EPE during this event was advection by both mean and eddy flows while losses occurred as a result of upgradient heat fluxes converting EPE to MPE and upward heat fluxes converting EPE to EKE. The latter conversion means that vertical motions in the water column were tending to flatten out the isothermal slopes by returning the cooler water to depth thus forcing T' towards zero. The overall result was that there was no net gain or loss of EPE, as indicated by the local term (Figure 27) which fluctuated about zero. As seen in the spectral analysis (Figure 23), the

vertical eddy heat fluxes fluctuated (as w') at a higher frequency along with the local growth/decay term, while the horizontal heat flux conversion and advective terms varied over longer periods and in this case are believed to be the result of the anticyclonic feature to the northwest. After 1 June, the eddy flow once again became poleward and the gradient of EPE diminished as the eddy moved offshore and conditions returned to normal.

2. Event #2 - Mooring P2 - 225 m: 27 September to 3 October 1990

Before proceeding to the discussion of the event at the 425 m depth level, it is worth discussing another very energetic event in the 225 m depth time series at P2 that also involves an anticyclonic feature. This particular event occurs near the end of the record between 27 September and 3 October 1990 (Figures 29 and 30). Prior to this time period, the disturbance temperatures were approximately 0.4°C above the mean and the eddy flow was poleward between 10 and 15 cm s^{-1}. By the 27th the eddy flow had begun to rotate in a counterclockwise direction while at the same time the temperature began to rise (Figure 29). This rise in temperature corresponds to the rise in the level of EPE during this time period. On the 28th, temperature reached a local maximum and the eddy flow was now southwestward, although very weak. ∇_HEPE was directed towards the northeast during this time period and developed a counterclockwise rotation as time progressed. As a result the eddy flow was advecting in the warmer temperatures (hence EPE), while the mean flow tended to carry the warm anomaly downstream, thus representing a loss of EPE (Figure 30).

Once again the horizontal gradient of EPE indicated that the warmer water (anomaly) was north of the mooring; however, in this case, the sense of

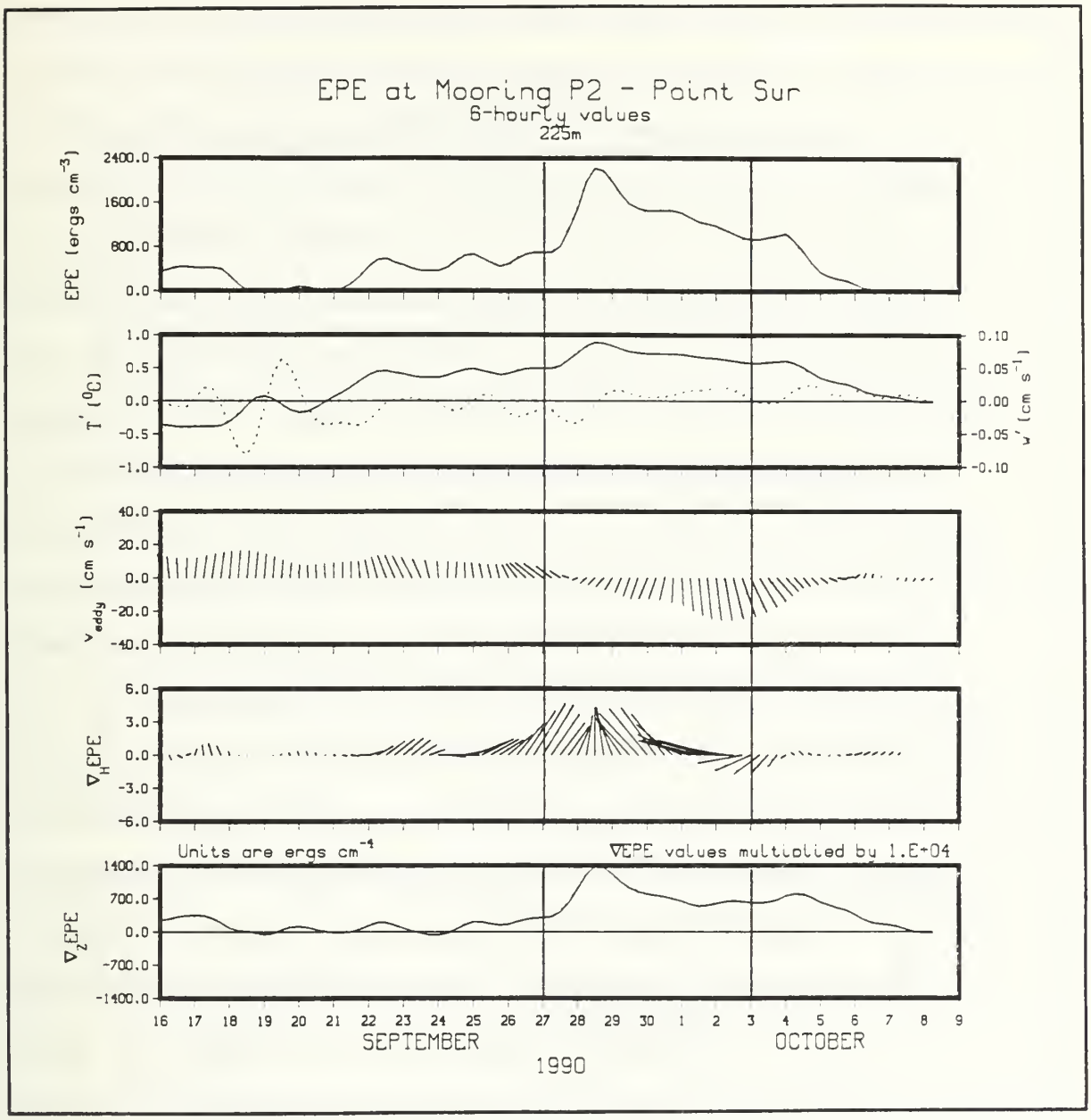

Figure 29. **Time Series of EPE, w', T', $\overrightarrow{v'_H}$, and ∇_{EPE} at Mooring P2 - 225m the period 16 September to 9 October 1990:** Panels from top to bottom and units are the same as in Figure 26. Event described in text is enclosed between the vertical lines.

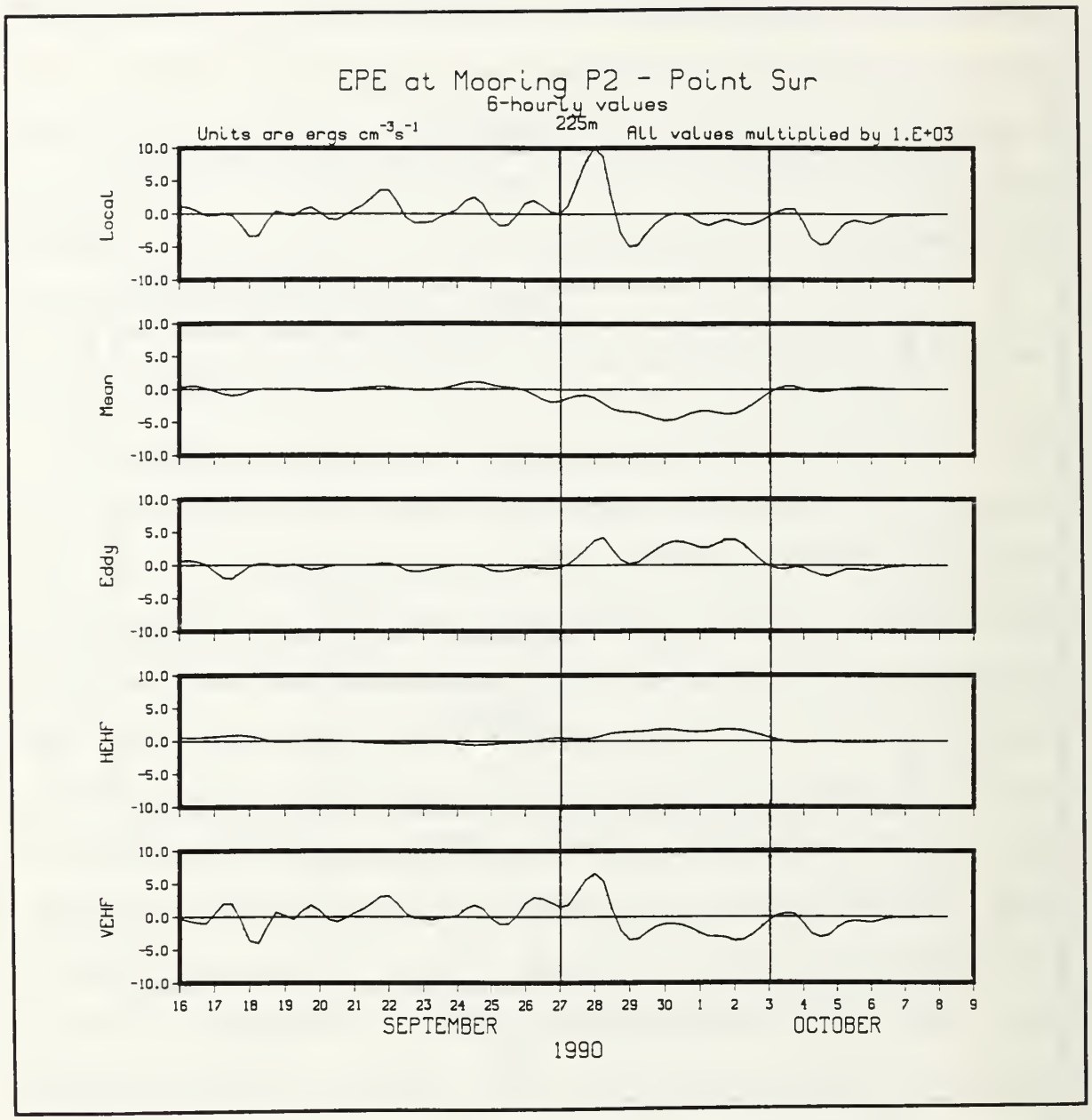

Figure 30. Time Series of the Five Terms in EPE Equation at mooring P2 - 225m for the period 16 September to 9 October 1990: Panels from top to bottom and units are the same as in Figure 27. A positive (negative) value represents a gain/source (loss/sink). Event described in text is enclosed between the vertical lines.

rotation of ∇_HEPE was the same as the eddy velocity and implied that an anticyclonic mesoscale feature had moved from northeast to southwest on the offshore side of the mooring. The southwestward eddy flow is taken to be associated with the southeast sector of the eddy, while the southeastward flow corresponds to the northeast sector. The direction of ∇_HEPE supports this idea in that when the flow was southwestward (29 September to 1 October), ∇_HEPE was directed towards the northwest, or where the center of the feature would be expected to lie. Similarly, when the flow was southeastward (1 to 3 October), ∇_HEPE was directed to the southwest, or where the center would be as it moved equatorward on the offshore side of the mooring. After 3 October, the mesoscale feature had moved farther offshore and conditions near the mooring began to return to normal.

Between the 27th and 29th of September, vertical eddy heat fluxes were converting EKE to EPE by carrying the warmer water downward ($w' < 0$) away from the surface, while after the 29th, the conversion was in the opposite direction, EPE to EKE (Figure 30), as now the vertical velocities were upward, tending to carry the warmer water back towards the surface. After an initial growth/decay of EPE (Figure 30), which was primarily the result of vertical eddy heat fluxes and horizontal eddy advection, no net growth or decay occurred. This resulted from the fact that an approximate balance was attained between eddy advection and downgradient heat fluxes (MPE to EPE) which were the suppliers of EPE and mean flow advection and vertical eddy heat fluxes which then removed this energy.

Similar to the anticyclonic feature observed in May 1989, this feature was also a near-surface phenomenon, as illustrated in the current and

temperature time series in Appendix A, and the vertical gradient of EPE which implies that the warmer anomaly is in the upper water column above 225 m. However, unlike the earlier event, the local temperatures were much higher (T' near 1.0 °C) suggesting that the semi-permanent eddy feature may have been displaced farther south during this time period, as previously observed by *Tisch et al.*, (1992). It is also worth mentioning that while the time series at moorings P2 and P3 were of different lengths and spanned different time periods, a local maximum in temperature also occurred at mooring P3 on 2 October, where the eddy flow was the eastward and southeastward, but very weak. During this same time frame, the disturbance temperatures at P3 were also positive and the gradient of EPE rotated clockwise from northeast to southeast suggesting a warm anomaly (the same feature ?) passed near the array at mooring P3, possibly between moorings P2 and P3. Unfortunately, the P2 data set ended shortly after the this event occurred, thus making any comparisons between moorings impossible, and therefore leaving this hypothesis unsubstantiated.

3. Event #3 - Mooring P2 - 425 m: October 7 to October 20 1989

This particular event occurred during the most energetic segment of the 425 m record (see Appendix E), and was characterized by a sharp drop in the disturbance temperature preceded and followed by temperatures which are nearly 0.4°C above the mean (Figures 31 and 32). A local rise in temperature beginning on 6 October can be interpreted from equation (9) as being the result of a weak downward vertical velocity. Shortly afterward, the horizontal eddy flow began to rotate slowly from southwest to southeast, and the vertical velocity changed sign (now weakly upward). At this time the gradient of EPE was directed upward and to the northwest, in opposition to the eddy flow, meaning

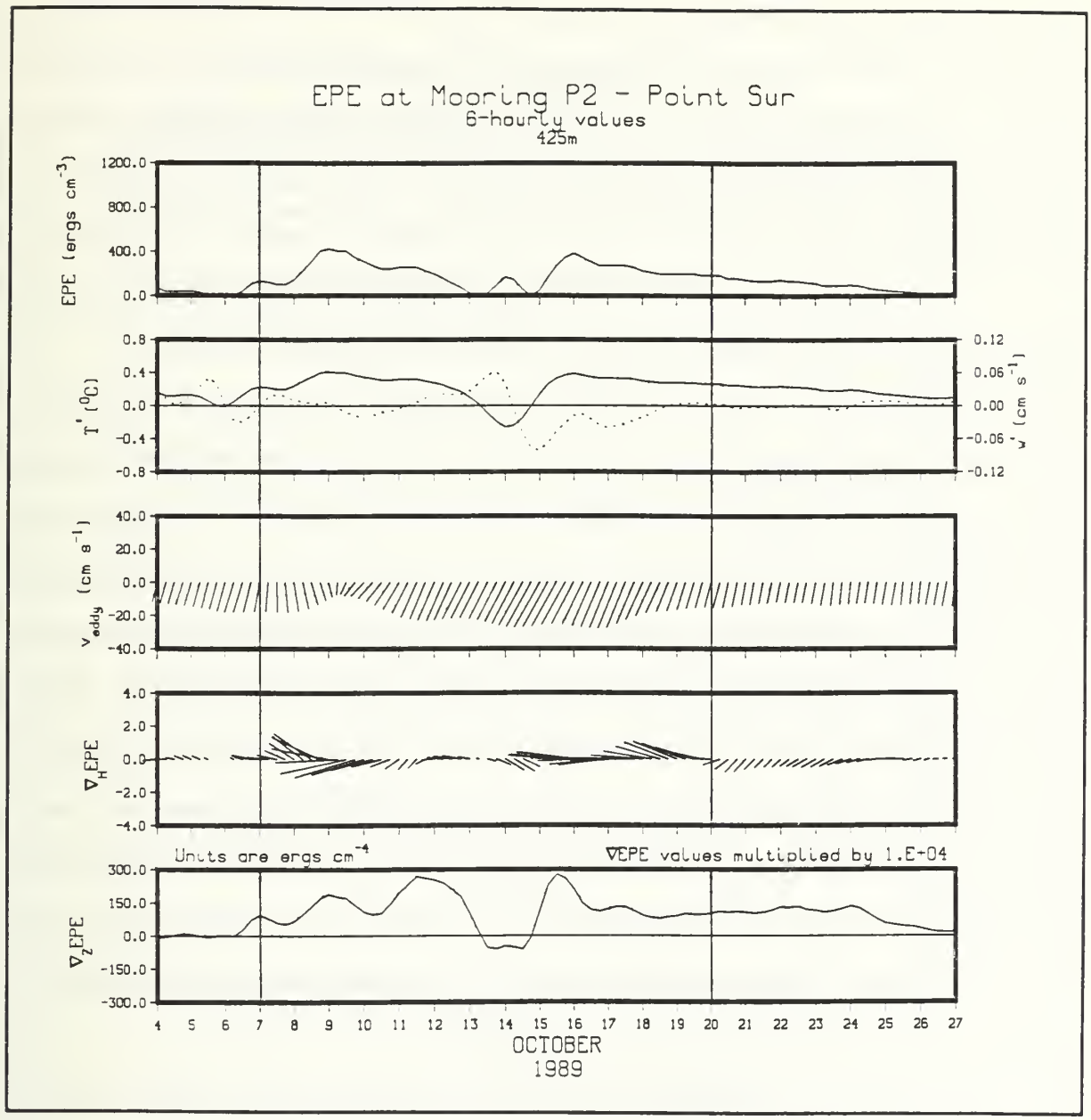

Figure 31. **Time Series of EPE, w', T', $\overrightarrow{v'_H}$, and ∇_{EPE} at Mooring P2 - 425m for the period 4 October to 27 October 1989:** Panels from top to bottom are: EPE in ergs cm^{-3}; T' (solid curve) in °C, and w' (dashed curve) in cm s^{-1}; horizontal eddy velocity in cm s^{-1}; and the horizontal and vertical gradients of EPE in (ergs cm^{-3}) cm^{-1}, where gradient values have been multiplied by 10^{+4}. Event described in text is enclosed between the vertical lines.

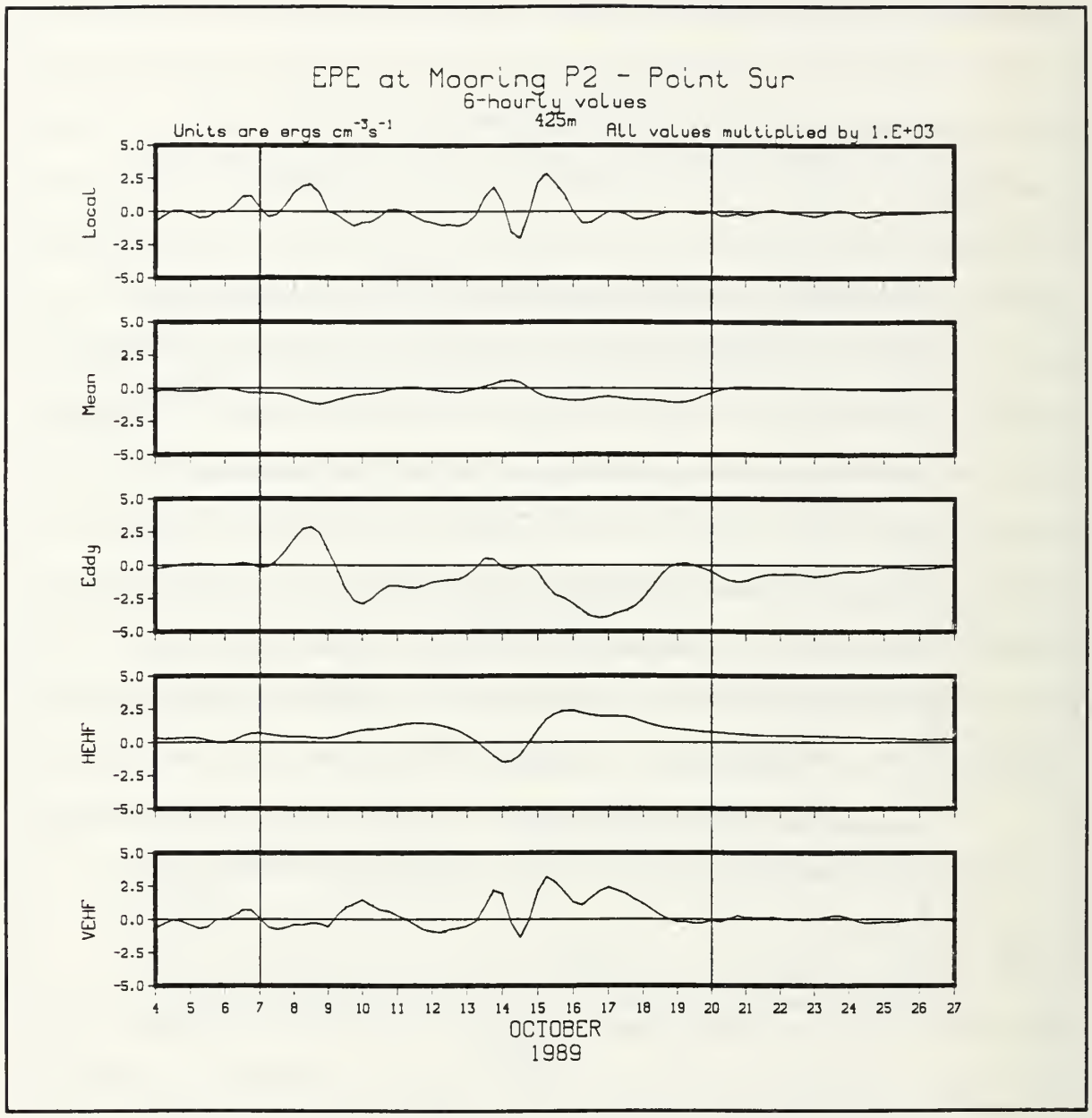

Figure 32. Time Series of the Five Terms in EPE Equation at Mooring P2 - 425m for the period 4 October to 27 October 1989: Panels from top to bottom are: local growth/decay of EPE; mean advection of EPE; eddy advection of EPE; horizontal eddy heat flux conversion term (MPE - EPE); and vertical eddy heat flux conversion term (EKE - EPE). Units are ergs cm^{-3} s^{-1} and all values have been multiplied by 10^{+3}. A positive (negative) value represents a gain/source (loss/sink). Event described in text is enclosed between the vertical lines.

that the eddy flow was advecting in warmer temperatures. The local growth of EPE near 8 October (Figure 32) was primarily the result of eddy advection, which reached a local maximum at 1200 on the 8th, along with a weaker contribution coming from a southward (downgradient) heat flux, converting MPE to EPE. Mean flow advection (4.4 cm s^{-1} , 323°T) and weak upward heat fluxes were energy sinks during this period.

Between the 8th and 10th, the eddy flow rotated back to the southwest and began to increase in magnitude. ∇_HEPE was now to the southwest and T' passed through a local maximum and began to drop (Figure 31). The eddy advective term now represented a loss of EPE, as the warmer water was carried downstream (Figure 32), and was nearly in balance with eddy heat fluxes (both horizontal and vertical) which now represented conversions of MPE and EKE to EPE. Between the 9th to the 13th, eddy velocity increased in magnitude while ∇_HEPE continued to weaken. Eddy advection was still the dominant loss term and was now being fed primarily by the conversion of MPE to EPE through downgradient heat fluxes. The vertical eddy heat flux term changed sign during this time, from source to sink, and mean flow advection was negligible since ∇_HEPE was very weak and nearly orthogonal to the mean flow.

On October 12th, the disturbance temperature began to drop rapidly from a value of approximately 0.3 - 0.4 °C to a minimum of approximately - 0.3 °C by the 14th, after which it rose just as rapidly to a value of 0.4 °C by the 16th (Figure 31). During this temperature fluctuation, ∇_HEPE was very weak but did change direction from northwest to southeast and then back to northwest. The vertical component was initially directed towards the surface, but became downward by when the temperature reached a minimum, indicating that this

small feature was a lower layer (θ' cooler at 500 m than at 350 m) disturbance. This sharp drop is clearly seen in the time series of temperature at both the 350 m and 500 m depth levels, where the drop is of longer duration at the 500 m depth level (Appendix A). The local growth of EPE seen late on the 13th (Figure 32) was primarily the result of an upward vertical velocity (Figure 31) associated with to a downward eddy heat flux. Some of this EPE is converted to MPE through a zonal eddy heat flux which was upgradient at this time. By midday on the 14th, vertical velocity was once again downward and responsible for a loss of EPE. The cooler temperatures were carried downward and were replaced by warmer waters from above. It should be mentioned that during this small event, the horizontal eddy flow remained approximately constant in both magnitude and direction suggesting that the drop and subsequent rise in temperature were the result of vertical rather than horizontal processes. Or in other words, the eddy that produced $\vec{v}'$ must be of a sufficiently large scale that the divergent part of $\vec{v}'$ is small (i.e. undetectable in Figure 31).

The local growth of EPE observed on the 15th was now the result of both horizontal and vertical eddy heat fluxes which carried warmer temperatures offshore (down the mean temperature gradient) and downward. Between the 15th and 17th, while eddy flow remained strong toward the southwest, the horizontal gradient of EPE intensified and was now nearly due west. As a result, the horizontal eddy flow was now advecting these warmer temperatures (EPE) downstream, thus representing a loss of EPE at the mooring. The zonal component of the mean flow was also responsible for a net downstream advection of EPE. These net advective losses were balanced by conversions of MPE and EKE to EPE, as illustrated by the local growth/decay term which was

nearly zero (Figure 32). After the 17th, the horizontal and vertical eddy flow began to weaken, although the directional component remained fairly constant. By the 20th, the horizontal component of velocity had diminished to half its earlier magnitude, the vertical component vanished, and temperatures continued to cool. The balance after the 20th was a conversion of MPE to EPE, which was then advected downstream by the eddy flow field. It is interesting to note that the latter portion of this event (between the 15th and 20th) was one of the only periods in these records where the sign of all energy terms were the same as the temporal means (although the magnitudes were still 10 to 40 times greater), thus illustrating the high degree of variability observed within the energy time series (Appendix E).

4. Event #4 - Mooring P3 - 225 m: 18 August to 21 August 1990

Unlike most energetic events at mooring P2, which involved more horizontal processes, events at P3 appeared to result almost entirely from vertical processes. This can be seen in the time series of terms in the EPE equation (Appendix E) as well as in the autospectra shown earlier in this chapter (Figure 25). This particular event occurs over a relatively short period of time (3 days) in contrast to those at P2 which occurred over longer periods of time. To reemphasize the point that it is only the vertical component of terms which are important and the time scales involved are much shorter, the entire month of August has been shown in Figures 33 and 34. Both the horizontal component of eddy velocity, with magnitudes generally less than 5.0 to 10.0 cm s^{-1}, and $\nabla_H EPE$ were very weak during the entire month (Figure 33). The mean flow at this level was towards the northwest and very weak (3.8 cm s^{-1}). These weaker flows and the very small horizontal gradient of EPE resulted in almost no

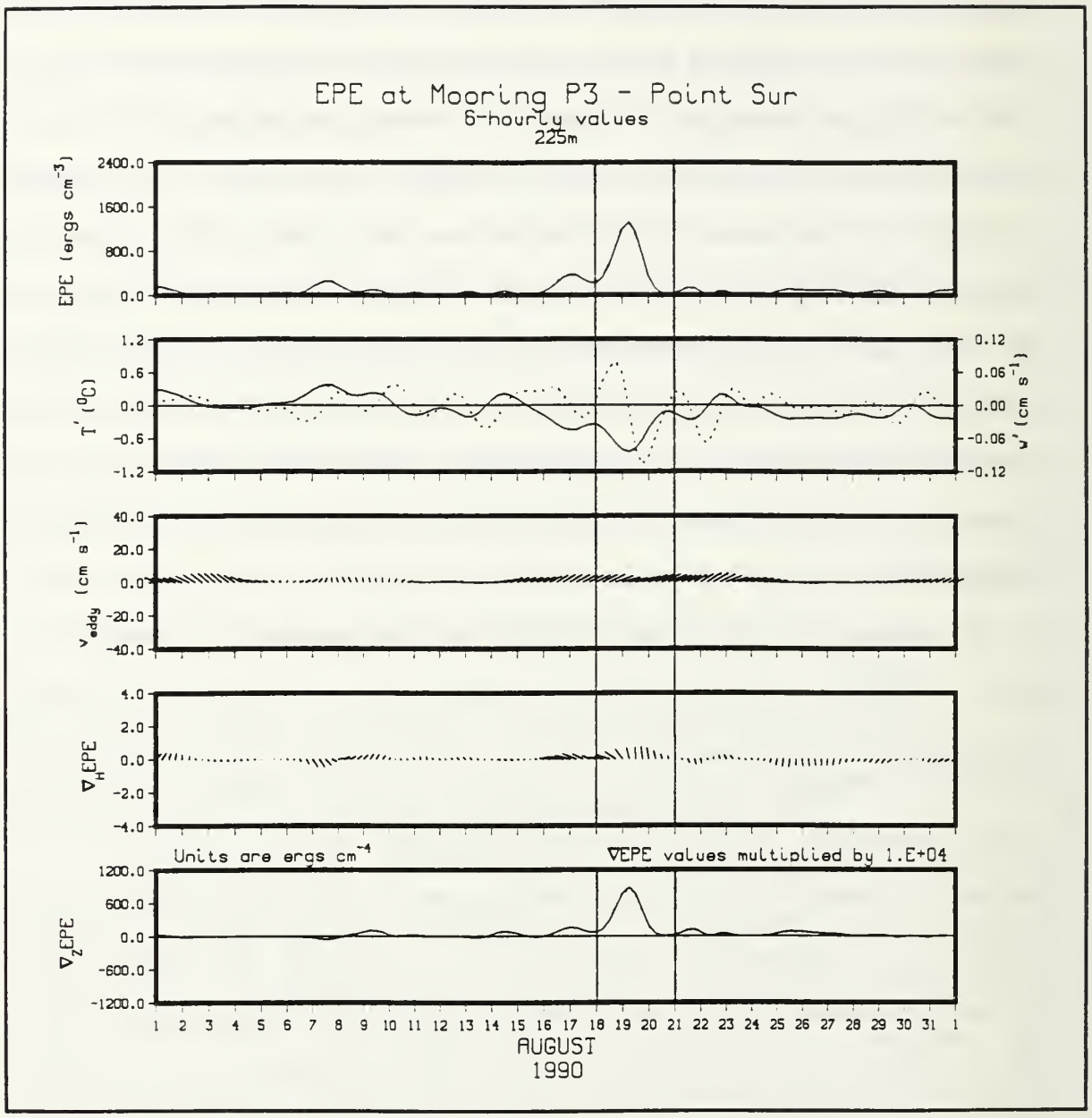

Figure 33. **Time Series of EPE, w', T', $\overrightarrow{v'_H}$, and ∇_{EPE} at Mooring P3 - 225m for the period 1 August to 1 September 1990:** Panels from top to bottom are: EPE in ergs cm^{-3}; T' (solid curve) in °C, and w' (dashed curve) in cm s^{-1}; horizontal eddy velocity in cm s^{-1}; and the horizontal and vertical gradients of EPE in (ergs cm^{-3}) cm^{-1}, where gradient values have been multiplied by 10^{+4}. Event described in text is enclosed between the vertical lines.

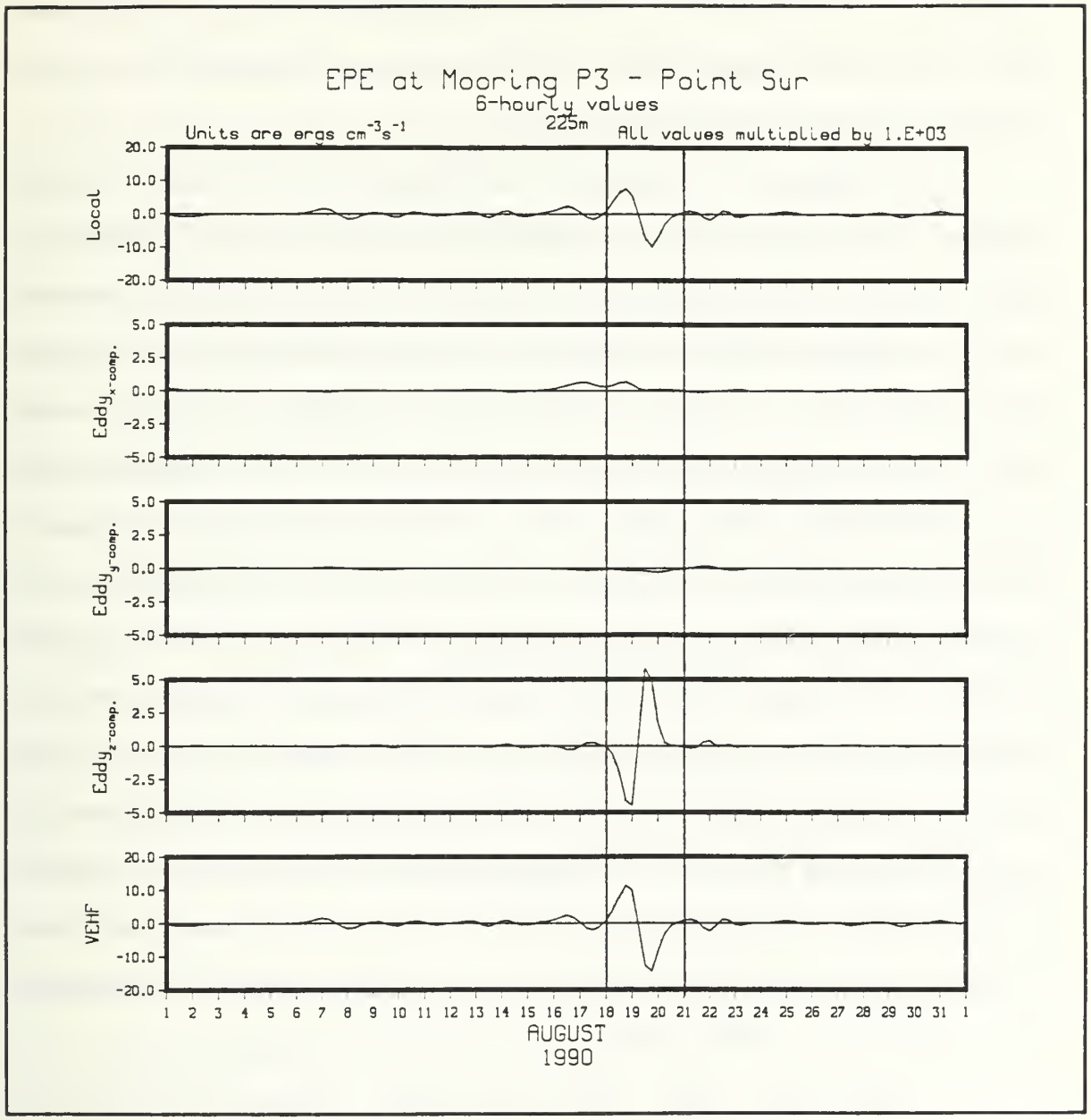

Figure 34. Time Series of Three Terms in EPE Equation at Mooring P3 - 225m for the period 1 August to 1 September 1990: Panels from top to bottom are: local growth/decay of EPE; x, y, and z-components of eddy advection of EPE; and vertical eddy heat flux conversion term (EKE - EPE). Units are ergs cm^{-3} s^{-1} and all values have been multiplied by 10^{+3}. A positive (negative) value represents a gain/source (loss/sink). Event described in text is enclosed between the vertical lines. *Note the scale change for the advective terms.*

advection in the horizontal. Therefore, the mean advective and HEHF terms have been omitted from Figure 34 and the three components of the eddy advection have been shown in their place.

Beginning on 15 August, the local temperature begins to drop; however, as mentioned above, the eddy flow is very weak and at this time is northeasterly at less that 10 cm s^{-1} (Figure 33). From equation (9), vertical velocity is dependent upon the time rate of change and advection of temperature. Because the flow is very weak and the gradients of temperature are very small, this drop in temperature can be interpreted as being the result of vertical motion in the upper water column. Prior to the 18th, we see that the fluctuations in local growth/decay term are identical to those in the vertical eddy heat flux term, meaning that these fluctuations are purely the result of conversions between EKE and EPE. On August 18th, there is a much more rapid drop in temperature, assumed to be the result of much stronger vertical velocities, bringing cooler water towards the surface. While this drop in temperatures is barely discernible near 350 m depth, it is a very prominent feature at the 100 m level (Appendix A), and occurs over a 24 hour time period. By the 19th, temperatures have begun to warm as a downward eddy velocity carries the cool water back to depth and by midday on the 20th conditions had returned to normal.

During this entire event, the vertical gradient of disturbance temperature, θ'_z, was negative indicating that the cool anomaly (θ' more negative) was above this level (as was the case, see the 100 m temperature record for mooring P3 in August 1990, shown in Appendix A). Since θ' was also less than zero, the vertical gradient of EPE implied that more EPE was in the water column above this level than below. Under these conditions, an upward vertical

velocity would tend to advect EPE away from the 225 m depth level, while at the same time this upward velocity leads to a downward heat flux by carrying cooler water towards the surface, thus providing a net source of EPE (bottom two panels in Figure 34). Conversely, when the velocity is downward, EPE will be advected in, while a net upward heat flux will convert EPE to EKE. Therefore, we see that in this particular event the two processes act in opposition to one another, with vertical eddy heat fluxes being the dominant term (just over twice the magnitude) responsible for the observed growth and decay (Figure 34). There are other events within the record at P3 where these two terms were observed to augment each other in producing large local growths and decays; however, the vertical eddy heat flux term was always much larger. The magnitude of the Local and VEHF terms during this event (and others observed in the time series in Appendix E) were larger than any event at P2, and involved only vertical components. This fact, combined with the shorter period of time over which the burst occurred, suggest that it was indeed caused by a vertical internal disturbance. Here again, fluctuations in $\vec{v}'$, which would be related to w' through the continuity equation, are small. This indicates that $\vec{v}'$ is largely rotational in character and the associated eddies therefore must be large in scale (i.e. quasi-geostrophic).

VI. DISCUSSION AND RECOMMENDATIONS

When considering eddy energetics within boundary regions of large-scale oceanic gyres, much of the attention has been focused on the western boundary currents. Western boundary currents (WBC) such as the Gulf Stream and the Kuroshio currents are intense (velocities in excess of 1-2 m s^{-1} or more) and relatively narrow features (100 - 150 km), which can extend to depths of 4000 m (*Knauss*, 1978). By comparison, eastern boundary currents (EBC) such as the California and Peru currents are much broader (several hundred km), shallower and weaker; however, the presence of filaments, mesoscale eddies and undercurrents within 100 to 200 km of the continental boundary tend to make the inshore side of these boundary currents more complex than their western boundary counterparts. It is this kind of variability that make the determination of the mean flow difficult in these regions compared to western boundary regions and may produce greater ranges of uncertainty for the temporal means of terms in the eddy potential energy equation.

A. COMPARISON WITH STUDIES OF EDDY ENERGETICS WITHIN WESTERN BOUNDARY CURRENTS

There have been numerous studies of eddy-mean flow interactions conducted within the Gulf Stream (*Webster*, 1961, 1965; *Watts and Johns*, 1982, *Dewar and Bane*, 1985, 1989a, b; *Hall*, 1986a; and *Rossby*, 1987) and the Kuroshio Extension (*Nishida and White*, 1982; *Hall*, 1991). The type and extent of data sets used and the different methodologies employed make quantitative comparison with most of these studies impossible. Therefore, discussion has

been limited to those studies where similar terms in the eddy potential energy equation have been evaluated.

Baroclinic instability resulting from vertical shear between the equatorward surface current and poleward undercurrent exists within the CCS and contributes to the growth of current meanders commonly observed in satellite imagery and hydrographic surveys (*Ikeda and Emery*, 1984; *Ikeda et al.*, 1984; *Thomson*, 1984; *Pierce et al.*, 1991). As previously mentioned, term (4) in equation (12), $\overrightarrow{v'_H T'} \cdot \nabla_H c\bar{T}$, has been interpreted as a baroclinic conversion term representing an exchange between mean and eddy potential energies (*Dewar and Bane*, 1985, 1989b; *Hall*, 1986a, 1991). When this term is negative, baroclinic instability processes convert mean to eddy potential energy through downgradient eddy heat fluxes, whereas a positive value represents a conversion of eddy to mean potential energy through upgradient eddy heat fluxes. While the temporal means for this term at mooring P2 (Table 9, Figures 14 and 17) are not significantly non-zero, their signs imply that the water column is baroclinically unstable ($-\overrightarrow{v'_H T'} \cdot \nabla_H c\bar{T} > 0$), consistent with these earlier results. At mooring P3, the mean value was very nearly zero and non-significant (Table 9).

Several values of the baroclinic conversion (BC) term from studies in the Gulf Stream (*Dewar and Bane,* 1985; *Hall,* 1986a; *Dewar and Bane,* 1989b), Kuroshio Extension (*Hall,* 1991) and our study region are presented for comparison in Table 11. These studies are hereafter referred to as DB85, H86, DB89, and H91, respectively. The two sets of values shown for H91 result from integration across the current (see H91 for details) in both stream (shown by the asterisk in Table 11) and geographic coordinate systems. The basic difference between these two systems is that a geographic coordinate system allows for the

study of the energetics of a fixed region (containing a current), whereas a rotating or stream coordinate system provides more information on the energetics and internal dynamics of a current's own coherent velocity and temperature fields (*Rossby*, 1987; *Hall*, 1991). Some obvious differences between these studies (besides geographic location) are readily apparent in both record length (205 days to 514 days) and depth of results (219 m to 650 m depth), which prevent direct comparison at common depths. For this reason, only the sign and the order of magnitude have been considered. In general, the observed variance in WBCs is less than the mean, while in EBCs it exceeds the mean. Because of the greater variance and weaker mean flows a longer record length at mooring P2 was required to gain more confidence in the temporal means of terms in the EPE equation.

Comparing values within the upper 500 m of the water column, we see that the magnitude of the BC term off Point Sur is at least three times smaller than those in the WBCs, with the exception of DB89, which is comparable in magnitude but of opposite sign. Below 500 m depth, we see that the magnitude of H86 in the Gulf Stream is nearly 5 times that of our values; however, those near 625 m depth in the Kuroshio (H91), where similar velocities (magnitudes) might be encountered, are comparable in magnitude. It is interesting to note the BC sign change in H91 when going from one coordinate system to another. In stream coordinates, the flow of energy appears to be from MPE to EPE through active baroclinic instability, consistent with earlier observations that suggested 152° E is a location of stable or growing eddy energy (*Hall*, 1991). In geographic coordinates, the flow of energy was from EPE to MPE and

TABLE 11. COMPARISON OF BAROCLINIC CONVERSION TERMS BETWEEN 36° N, 122° W AND SELECTED WESTERN BOUNDARY REGIONS: The sign convention for the baroclinic conversion term is such that a +/- sign represents a source (MPE to EPE) / sink (EPE to MPE). The asterisk by *Hall* (1991) indicates energy estimates computed in stream coordinates (see *Hall* (1991) for details). Units are 10^{-4} ergs cm^{-3} s^{-1}.

Study (Location)	Lat.	Long.	Depth (m)	Record length (days)	BC Term
Mooring P2	36.3° N	122.2° W	225	~514	+0.80
(CC)			425		+1.20
Mooring P3	36.3° N	122.3° W	225	~362	+0.05
(CC)					
Dewar & Bane '85	31.3° N	79.6° W	219	~205	+ 12.00
(GS)	32.4° N	78.1° W	219	~205	+ 78.00
Hall '86a	37.6° N	68.0° W	575	~365	+ 5.15
(GS)					
Dewar & Bane '89b	36.0° N	73.0° W	380	~380	- 0.81
(GS)					
Hall '91 *	35.0° N	152.0° E	350	~392	+3.50
(KS)			625		+0.89
Hall '91	35.0° N	152.0° E	350	~392	-10.40
(KS)			625		-0.70

was nearly three times as strong. In general, the sign of these terms indicate that all three regions have active baroclinic instabilities occurring within them; however, the dynamical processes occurring at these locations can be quite different. The BC conversion has also been found to be considerably smaller than the barotropic (BT) conversion term (*Hall*, 1986a; *Dewar and Bane*, 1985; *Dewar and Bane*, 1989b; *Hall*, 1991) and could possibly take on either sign (*Dewar and Bane*, 1989b). It is unfortunate that the present data set did not allow for the computation of the BT term.

Using direct velocity and temperature measurements from PEGASUS stations across the Gulf Stream, *Rossby* (1987) was able to evaluate the cross-stream component of the BC term. The region of maximum MPE to EPE conversion was nearly coincident with the sloping thermocline (see his figures 4 and 7). While *Rossby* (1987) cautions that the along-stream component may be quite large, the analyses of H86 and DB89 also find the cross-stream component to provide the dominant contribution to the total term. In contrast, *Brooks and Niiler* (1977) found that the alongshore component dominated farther upstream in the Florida Current. In the Kuroshio, H91 found the net BC term to be dominated by the cross-stream component. Off Point Sur, where a strictly east-north coordinate system was employed, the along-slope component provided the dominant contribution to the total term (Figure 18) at the 425 m depth at mooring P2. At the 225 m depth, the along-slope component was not significantly different from the cross-slope component as the mean eddy heat flux vector and the mean temperature gradient are very nearly orthogonal (Figure 15). Even though a stronger mean eddy heat flux occurred at mooring

P3, the fact that it was nearly across the mean temperature gradient produced little or no BC conversion.

Since the basic conceptual model of this study is the same as *Hall* (1991), it is possible to compare and contrast all five terms in the EPE equation between the Point Sur and Kuroshio study regions (Table 12). Earlier studies in WBCs (*Webster*, 1961; *Schmitz and Niiler*, 1969; *Brooks and Niiler*, 1977) have suggested that different energetic regimes may exist in the cyclonic and anticyclonic sides of these currents (*Hall*, 1991). For this reason, H91 presents an in-depth analysis of the energetics on both the anticyclonic and cyclonic sides of current separately, as well as for the current as a whole, using both coordinate systems. Because no anticyclonic-cyclonic distinction has been made in our study, only those values computed by integration across the current have been included in subsequent discussion. The geographic coordinate system of H91 is oriented in the direction of the average flow of the KS (*Schmitz*, 1984), such that the x-axis is rotated 35° south of east. As mentioned earlier, an east-north coordinate system has been employed in our study since the principle axes of the current were not well-defined. Therefore, while both estimates (geographic and stream coordinate systems) of H91 are shown in Table 12 and discussed in the following paragraphs, direct comparisons should be made between geographic coordinate systems.

Comparing the energy conversion estimates at mooring P2 (both depths) to those at 350 m depth in the Kuroshio (both coordinate systems), we see that the estimates in the Kuroshio are from 3 to 35 times larger than those of our study region, which is expected given the higher mean and eddy velocities of the

TABLE 12. COMPARISON OF TERMS IN THE EDDY POTENTIAL ENERGY EQUATION BETWEEN 36° N, 122° W AND 35° N, 152° E: Estimates of the five terms in equation (12) are shown for the present study and that of *Hall* (1991). Terms have been evaluated as Local = Mean + Eddy + HEHF + VEHF, such that a +/- sign represents a gain (source) / loss (sink). The (s) and (g) refer to stream and geographic coordinate systems, respectively. Values that were not significantly non-zero are shown in italics and asterisked. The range of uncertainty is shown in parentheses below each estimate. Units are 10^{-4} ergs cm^{-3} s^{-1}.

Mooring/ Depth	Local	Mean	Eddy	HEHF (MPE-EPE)	VEHF (EPE-EKE)
		36° N	**122° W**		
P2 - 225 m	*-0.13** (-0.68, 0.42)	*+1.48** (-1.27, 4.23)	*-0.88** (-2.02, 0.26)	*+0.80** (-1.44, 3.04)	-1.53 (-2.13, -0.93)
P2 - 425 m	*+0.10** (-0.16, 0.36)	*-0.40** (-1.52, 0.72)	-1.04 (-1.99, -0.09)	*+1.18** (-0.63, 2.99)	+0.37 (0.05, 0.69)
P3 - 225 m	*0.00** (-0.83, 0.83)	*-0.15** (-1.22, 0.92)	-0.63 (-1.11, -0.15)	*+0.05** (-0.71, 0.81)	+0.74 (0.07, 1.41)
		35° N	**152° E**		
350 m (g)	*-3.38** (-7.82, 1.06)	*+10.08** (-2.31, 24.34)	*-3.39** (-18.28, 11.50)	*-10.43** (-23.37, 0.88)	*+0.36** (-3.95, 4.68)
625 m (g)	-3.94 (-5.92, -1.96)	*+2.47** (-0.50, 5.98)	-3.43 (--6.77, -0.09)	*-0.70** (-3.64, 2.11)	-2.28 (0.52, 4.18)
350 m (s)	*(-3.49)* (-8.04, 1.06)	*(-5.13)* (-12.09, 1.71)	*(-2.38)* (-5.97, 1.21)	*(+3.50)* (-0.71, 8.40)	*(+0.51)* (-3.88, 4.93)
625 m (s)	-3.88 (-5.90, -1.86)	*(+1.17)* (-0.79, 3.23)	*(-3.81)* (-5.33, -2.29)	*(+0.89)* (-0.34, 2.08)	-2.13 (-4.03, -0.34)

Kuroshio Current. The only term which is of comparable magnitude to our estimates are the vertical eddy heat flues, which are very nearly zero. The reason for this is that on the anticyclonic side of the current vertical eddy heat fluxes represent a significant loss of EPE (VEHF < 0), while on the cyclonic side this term is a source of EPE (VEHF > 0) (*Hall*, 1991, her figures 5 and 6). Therefore, when integrated across the current the net EPE-EKE conversion becomes very small and insignificant. The BC term in stream coordinates is nearly 3.5 times greater than our estimates; however, both indicate active baroclinic instability processes are occurring (HEHF > 0), which represents a net conversion of MPE to EPE. In geographic coordinates, the BC term is three times stronger and changes sign (HEHF < 0) suggesting the flow of energy is from EPE to MPE.

In general, the energy estimates at 625 m depth are smaller than those at 350 m depth and are more comparable in magnitude (only 1.5 to 3 times larger) to those derived from the Point Sur data sets (Table 12). The estimate of the BC conversion term in stream coordinates is nearly identical in sign and magnitude to those at mooring P2 again suggesting a net conversion of MPE to EPE (HEHF > 0). In geographic coordinates, the large error bars associated with the BC estimate indicate either sign is possible, even though the mean value was negative. Unlike the estimates of VEHF at 350 m depth, a significant conversion of EPE to EKE occurs at 625 m depth which appears quite similar in both sign and magnitude to the estimates at 225 m depth at mooring P2.

While these two regions may be quite different from a dynamical standpoint, it is interesting to note that of all five terms in the EPE equation, only eddy advection term has the same sign (less than zero) at all depths in both regions

(Table 12), suggesting that eddy flow is responsible for a loss of energy through downstream advection of EPE. It is also interesting to note that the estimates of the local rate of change of EPE for the Kuroshio are negative at both depths (Table 12), with significantly non-zero values found at 625 m. The negative value would seem to suggest that eddy energy is actually decaying at this site; however, as pointed out by H91, a non-zero value may also result from an inadequate sample period. For a true ensemble average, the local term should be zero since the total amount of energy at a given location does not grow or decay (*Hall*, 1991). Off Point Sur, the estimates of this term are near zero indicating that no net growth or decay of energy has occurred over the sample period.

B. COMPARISON WITH STUDIES OF EDDY ENERGETICS WITHIN EASTERN BOUNDARY CURRENTS

Unlike the energy studies within western boundary regions that were described in the previous section, no long term studies of eddy energetics based upon direct observations of current and temperature have been conducted over the continental slope within an eastern boundary region. More recently, however, there have been a few modeling studies that specifically address eddy energetics within the CCS. Unfortunately, they are either too large-scale (*Auad et al.* 1991), encompassing the entire CCS, or relate to specific mesoscale events within the current (*Walstad et al.* 1991; *Pierce et al.* 1991), which makes term by term comparisons difficult. In addition, the complex nature of mesoscale variability in both space and time found along eastern continental boundaries, as described in Chapter I, can lead to different energy balances in coastal and offshore regimes. This has been observed in the time series of terms in the EPE equation (Appendix E) during the present study, as discussed in Chapter V, where no consistent pattern in the flow of energy could be identified between

individual energetic events. Comparing results from a primitive equation model and data from the Geosat satellite, *Parres-Sierra et al.* (1990) found that coastal regions possessed the highest concentration of eddy potential energy, resulting from the strong direct wind forcing along the coast and the poleward propagation of Kelvin waves. Because of the spatial and temporal differences that exist between the aforementioned modeling studies and the present study (single-mooring), discussion has been limited to the basic processes involved in the energy transformations.

Auad et al. (1991) have recently used the eight-layer QG model of *Holland and Vallis* (1990) to study the circulation and energetics of the CCS, while *Walstad et al.* (1991) and *Pierce et al.* (1991), have employed data assimilation in a QG model and linear stability analyses, respectively, to examine the energetics of a meandering jet within the CTZ region (north of our study region). These studies are hereafter referred to as A91, W91, and P91, respectively. To analyze the flow of energy through this system, A91 divided the central region of their model area into four separate domains, based upon mean flow direction and intensity, bottom topography, the eddy kinetic energy field, and the turbulent diffusion field (see their figure 10). Their region I, located between 33° N and 38° N and seaward of the 3650 m isobath westward to 130° W, lies closest to our study region and has been chosen for further discussion. Specific details about these models, along with some of the more general results, were described earlier in Chapter I and will not be repeated here.

Based upon two years (1979-1980) of model data, A91 were able to derive a quantitative description of the flow of energy within the CCS. Mean winds produce an increase in the mean flow kinetic energy (MKE), which is either

fluxed out the open boundary because of the beta effect and/or converted to MPE. Baroclinic instabilities within the current then produce the following transformation: MPE $\rightarrow$ EPE $\rightarrow$ EKE. A91 also mention that the direction of these fluxes represent an average process and periods may exist where fluxes are in the opposite direction. For example, Ekman transport will result in a conversion of MKE to MPE, while geostrophic currents result in a conversion of MPE to MKE.

The upper panel of Figure 35 describes the placement of energy terms within the A91 QG model using a simple two-layer model. Model layers (subscripts 1 and 2) and the interfacial boundary (denoted as $^3/_2$) are represented by boxes, while flux vectors are represented by arrows and illustrate the flow of energy through the model. $\overline{F}$ and F' represent external forcing to the uppermost layer, while $\overline{K}_{1,2}$ and $K'_{1,2}$ represent the mean and eddy kinetic energies of the upper two layers. $\overline{P}_{3/2}$ and $P'_{3/2}$ represent the mean and eddy potential energy at the interface between model layers 1 and 2. Of the remaining terms shown in this diagram, only those which involve transfers between MPE, EPE and EKE ($\overline{P} \leftrightarrow P'$, $P' \leftrightarrow K'$) and advection or divergence of EPE ($\overline{\mu}P'$ and $\mu'P'$) can be estimated in our study and will be included in subsequent discussion. For a complete description of all terms shown in Figure 35, the reader is referred to *Auad et al.* (1991) (see their Table 1).

The energy flux diagram for the upper 500 m of A91s region I is shown in the bottom panel of Figure 35 and illustrates the general flow of energy described above. It is encouraging to see that both A91 and the present study indicate that active baroclinic conversions (MPE to EPE and in some cases EPE to EKE) are occurring. The model results of A91 indicate the MPE to EPE

conversion is greater near 250 m. Even though the value of the BC estimate at P2 was slightly greater at 425 m than at 225 m depth, the range of uncertainty associated with these estimates and the lack of resolution in our data set prevent any definitive conclusion about the depth where maximum BC conversion occurs. At mooring P2, 225 m depth, the greatest loss term was through the conversion of EPE to EKE, while at 425 m and at mooring P2 (225 m depth), the conversion was of opposite sign (source) but much weaker.

As previously mentioned, it is also possible to compare terms that can be interpreted as the advection of EPE by both the mean and eddy flows. In *Auad et al.* (1991), these terms are the divergence of the mean and eddy flux of EPE, represented as $P' \rightarrow \overline{\mu}\, P'$ and $P' \rightarrow \mu' P'$ in Figure 35, where $\overline{\mu}$ and μ' refer to the mean and eddy flow, respectively, and P' represents EPE. In the upper 500 m, their model indicates that the mean flow is responsible for a net convergence of EPE, while the eddy flow produces a net divergence of EPE (Figure 35), consistent with the results obtained in this study. At the 225 m depth (P2), mean flow advection of EPE was the largest source term and eddy advection was a sink term. Maximum model estimates for each term occurred at 100 m and, in general, decreased with depth. In contrast, the magnitude of eddy advection at P2 increased slightly between 225 m and 425 m depth, where it was the largest loss term in the balance. Mean flow advection changed sign at 425 m depth, representing a loss of EPE; however, its magnitude is much smaller than at 225 m and the larger range of uncertainty imply it could take on either sign. It is interesting to notice that in the model the divergence of the eddy flux of EPE ($P' \rightarrow \mu' P'$) is negative (loss) eddy flow throughout the entire water column

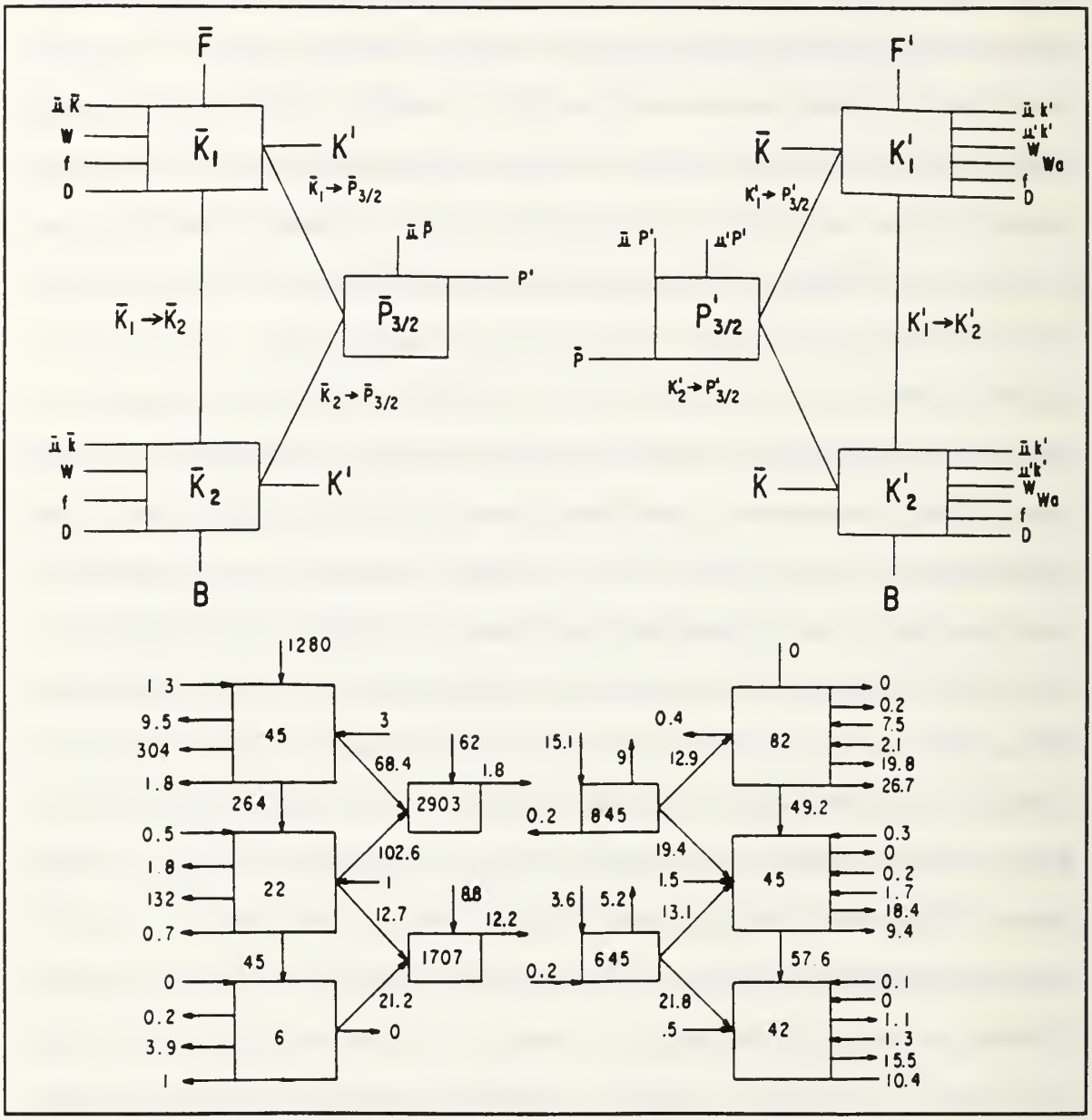

Figure 35. Energy Flux Diagram for the CCS between 33° N and 38° N: Energy flux estimates for the upper 500 m of the water column, reproduced from *Auad et al.* (1991). The upper panel describes the placement of energy terms within the layers and at interfacial boundaries (see *Auad et al.* (1991) for specific details). The lower panel is the energy flux diagram for the upper three layers (0-100 m, 100-250 m, and 250-500 m). Units are 10^2 erg cm^{-2} day^{-1} for energy fluxes (arrows) and 10^3 erg cm^{-2} for the boxes.

(Figure 35). This same result was observed in the integrated estimates of *Hall* (1991) in the Kuroshio Current and in our estimates off Point Sur, where eddy advection represented a loss at all depths. Whether or not this similarity is representative of eddy advective processes in the ocean or merely coincidence is a question that will require a great deal more data to answer.

Active baroclinic processes were also found to exist within the CTZ jet; however, they were much weaker than barotropic processes for disturbance wavelengths less than 200 km (*Walstad et al.* 1991; *Pierce et al.* 1991). The overall importance of baroclinic versus barotropic instability processes within this jet was examined by P91 using the ratio {AP}/{KP}, where AP is the volume-integrated MPE to EPE (BC) conversion and KP is the volume-integrated MKE to EKE (BT) conversion. For a disturbance wavelength of 130 km, barotropic instabilities dominated and the flow of potential energy was from the disturbance to the mean (MKE → EKE and EKE → EPE → MPE), whereas for wavelengths greater than 200 km, both processes contributed to the growth of the disturbance (MPE → EPE → EKE and MKE → EKE) (P91, see their figure 10).

C. SUMMARY

1. Sub-Tidal Variability Observed at Moorings P2 and P3

Off Point Sur, the location of the undercurrent core has been observed to vary from 12 to 42 km from shore and between 70 to 460 m depth (*Tisch et al.* 1992). Similar results were obtained earlier off Cape San Martin, approximately 70 km south of Point Sur (*Wickham et al.* 1987). The observed currents in the present study indicate that stronger poleward flow exists at P2 than at P3, which is consistent with these earlier findings, suggesting that the

core of the CUC lies closer to P2 than P3 (see records from May 1990 to October 1990 in Appendix A). Additionally, mesoscale current shear (both horizontal and vertical) has been observed throughout the water column above 1000 m and within 50 to 100 km of the coast with flow reversals occurring over distances of 25 km or less (*Tisch et al.* 1992). Geostrophic velocities (alongshore component) from hydrographic data collected in September 1989 (Figure 36) confirm the presence of strong shear above 1000 m and within 60 km of the coast, and indicate equatorward subsurface flow at mooring P2 (located between stations 5 and 6). At this time, the v-component of current velocity at P2 was equatorward at all three instrumented levels (see P2 current vectors near September 26 1989 in Appendix A), and increased in magnitude below 350 m depth, in agreement with the observed baroclinic shear (Figure 36). The magnitude of the v-component of current and alongshore geostrophic velocity agreed to within 5 cm s^{-1}. Considerable cross-slope shear is also indicated by the geostrophic velocities in Figure 36, with several sign changes occurring over approximately 30 km. Unfortunately, mooring P3 (located between stations 10 and 11) was not deployed at this time so there are no direct observations to confirm this shear; however, the earlier observations of strong cross-slope shear off Point Sur (*Wickham*, 1975; *Tisch et al.* 1992) and the good agreement between observed and geostrophic currents at mooring P2, discussed above, suggest that cross-slope shear does exist and can occur over short distances as shown in Figure 36. This cross-slope shear suggests that the barotropic conversion term (related to lateral shear) may be important off Point Sur, and should be investigated in future studies in this area.

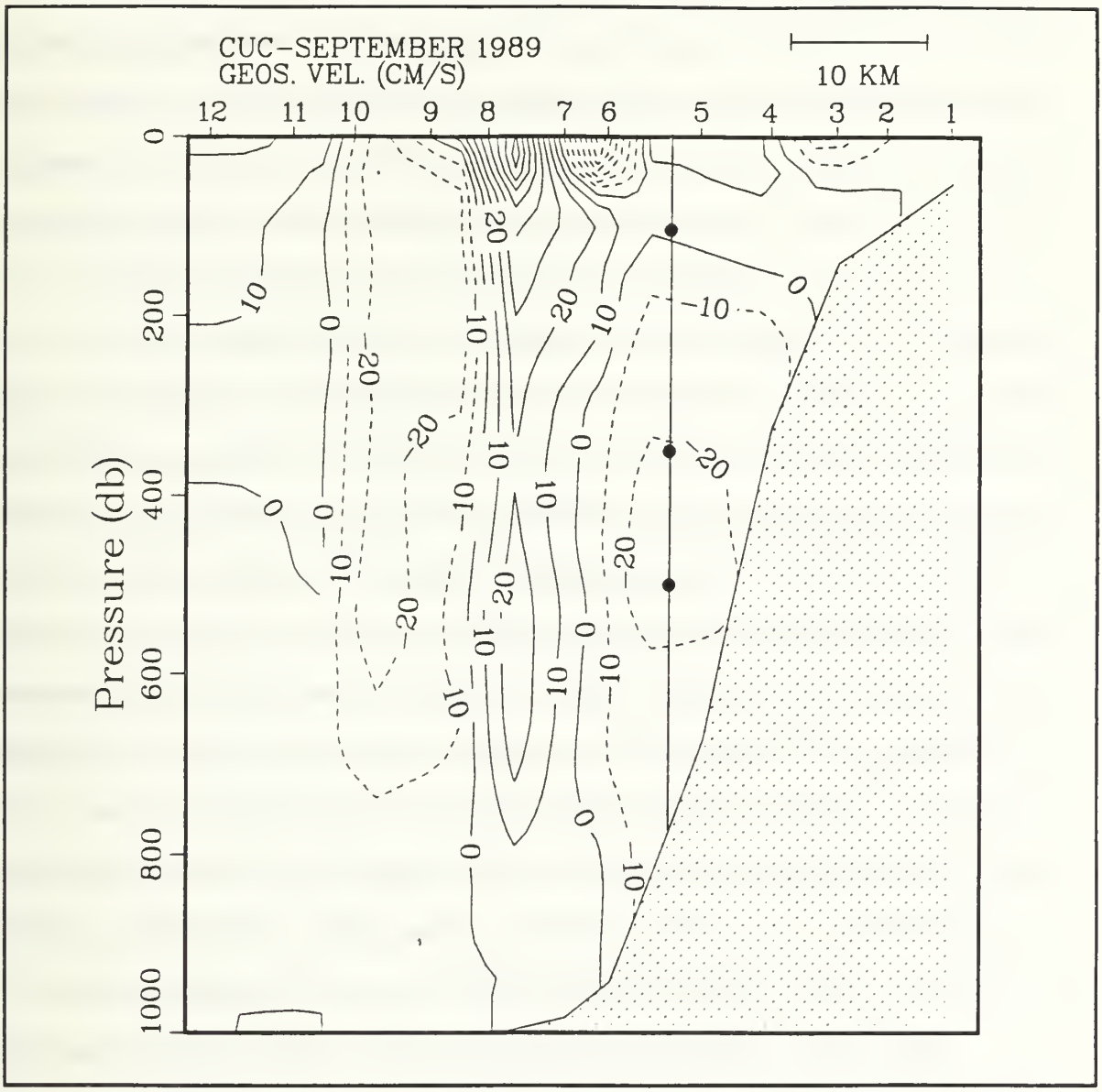

Figure 36. Vertical Section (0-1000 dbar) of Alongshore Geostrophic velocity for Cruise CUC-September 1989: The contour interval is 10.0 cm s^{-1}. Dashed lines are equatorward and solid lines are poleward. The approximate location of mooring P2 is shown by the solid vertical line.

The presence of a semi-permanent anticyclonic feature on the oceanic side of the Monterey Bay has been previously documented by several investigators (*Breaker and Broenkow*, 1989; *Tracy*, 1990; *Tisch et al.* 1992). *Tisch et al.* (1992) have also observed the southern portion of this feature as far south as Point Sur, where it influenced the flow through the Point Sur Transect. The observed currents and temperatures during this study (Appendix A) suggest that this anticyclonic feature had moved onshore and south of its usual position on several occasions thus influencing the flow at the Point Sur moorings. The large growths in EPE at the 225 m depth at mooring P2 during events 1 and 2 described in Chapter V appear to have resulted from just such a southward displacement. The counterclockwise rotation of current vectors associated with this feature during both events was observed at all three levels (100, 350 and 500 m depths), although it was more prominent in the time series at 100 m depth. While the anticyclonic features during these particular events were relatively shallow, deeper signatures of larger mesoscale features have been observed farther offshore at mooring P3. In early spring of 1990 and 1991, large mesoscale features penetrated to at least 1000 m depth (see current vectors at all four instrumented depths at mooring P3 in Appendix A), consistent with the findings of *Tisch et al.* (1992), who observed an anticyclonic mesoscale feature penetrating to 800 m depth along the Point Sur Transect in November 1988.

Baroclinic instability, resulting from current shear between an equatorward surface current and the poleward undercurrent, has been found to play an important role in the formation and growth of current meanders and eddies (*Ikeda and Emery,* 1984). Our energy analyses indicate active baroclinic instability processes in the flow off Point Sur (HEHF > 0), which might suggest

that this process is involved in the generation and maintenance of the semi-permanent anticyclonic feature described above. Another possibility is that this feature may be the inshore portion of a larger meander of the CCS which then enhances the southward flow across Monterey Bay and westward flow off Point Sur (*Tracy*, 1990; *Hicks*, 1992). Unfortunately, the exact mechanism behind the formation, maintenance and southeastward movement from its usual position is not known and is still the subject of active research.

2. Eddy Energetics at Moorings P2 and P3

Based upon 17-months of data at mooring P2, and one-year at mooring P3, we found that EPE along the continental slope off Point Sur was neither growing nor decaying ($\partial EPE/\partial t \sim 0$). This is an encouraging result since the long term total potential energy at a given location should neither grow nor decay (*Hall*, 1991). Above 350 m depth at P2, the sources of EPE were advection from the mean flow and downgradient eddy heat fluxes, which signal active baroclinic instability processes (MPE $\rightarrow$ EPE) within the water column. This apparent growth was balanced by downstream advection by the eddy flow and the conversion of EPE to EKE by upward eddy heat fluxes. Below 350 m depth, horizontal and vertical eddy heat fluxes were the sources of EPE (MPE $\rightarrow$ EPE, EKE $\rightarrow$ EPE) while both mean and eddy flow advection resulted in a downstream growth (local loss) of EPE. At mooring P3, 225 m depth, the net flow of energy was EKE $\rightarrow$ EPE $\rightarrow$ eddy advection, and to a lesser degree, mean advection, which lead to a downstream growth of EPE. The baroclinic conversion term was negligible since the net horizontal heat fluxes were nearly orthogonal to the mean temperature gradient (Figure 20).

The magnitudes of terms in the EPE equation during individual energetic events at both moorings were typically 10 to 20 times larger than the corresponding temporal means; however, no consistent balance was observed between the five terms in the equation that would account for the mean balance. Energetic bursts appear to occur under a variety of flow conditions as seen in the time series of energy terms in Appendix E and events discussed earlier in Chapter V. Events at P2 involved both horizontal and vertical terms with similar magnitudes, whereas those at P3 involved only the vertical components. In particular, the time series of local growth and vertical eddy heat fluxes (terms 1 and 5 in equation (10)) at P3 are nearly identical, implying that the growth and decay of energy at P3 is entirely due to vertical motions. This is an interesting result as the moorings are only separated by 25 km. As discussed earlier, the first baroclinic Rossby radius, calculated as $R_{d1} = \overline{N}H / \pi f$, was approximately 8 to 14 km at P2 and 14 to 25 km at P3. This value is consistent with other estimates of R_{d1} along the continental slope of California (*Huyer*, 1983; *Walstad et al.* 1991; *Pierce et al.* 1991), where R_{d1} was computed as $\overline{N}H / f$, and values of 20 to 40 km were obtained. The highly variable nature of the energetic events at moorings P2 and P3 and the fact that the moorings are separated by more than one Rossby radius suggest that the moorings lie in regions governed by different dynamical processes. Mooring P2 (P3) is less (greater) than one Rossby radius from the shelf break, indicating that trapped waves are more important features at P2 than at P3. Most of the energy bursts at P3 were caused by sharp, rapid temperature fluctuations that were present in the 100 m depth record (Figures 33 and 34, and Appendix E), suggesting they were the result of internal disturbances within the main thermocline. Vertical transfers of EPE also occurred at P2;

however, the stronger flow of the undercurrent at P2 and the presence of the mesoscale features, such as the eddy described earlier, appear to result in much stronger transfers of energy in the horizontal. At both moorings, the vertical transfers occurred over periods of 2 to 20 days (primarily between 2 and 5 days), whereas the advective and BC terms were active at periods greater than 20 days as well (Figures 23 through 25).

D. RECOMMENDATIONS FOR FUTURE WORK

While this study has provided useful information about eddy energetics along the continental slope off Point Sur, including initial estimates of the terms in the eddy potential energy equation, it has only considered half of the total energy equation. The use of current and temperature data from a single moored array provides information about vertical gradients of velocity and temperature but not for the horizontal gradients, which as we have found, can be significant off Point Sur. Using the thermal wind relation, it is possible to infer horizontal gradients of temperature, but this only allows for evaluation of the eddy potential energy equation. To examine the eddy kinetic energy equation, we require information on the horizontal gradients of velocity as well. Once these gradients have been determined, it is then possible to estimate the barotropic conversion term as well as terms involving the advection of eddy kinetic energy.

As discussed earlier, modeling studies conducted within the CCS indicate that barotropic conversions are important and can be the dominant process at the shorter disturbance wavelengths (*Walstad et al.* 1991; *Pierce et al.* 1991). The strong horizontal shear observed off Point Sur suggests that the barotropic conversion term may be important in this region as well and should be evaluated. While *Hall* (1986a, 1991) also used data from a single current meter mooring,

the well-defined structure of horizontal and vertical velocity and temperature in the Gulf Stream and Kuroshio Current allowed her to estimate the cross-stream gradient of velocity. At the present time, a well-defined cross-stream structure for the CCS off Point Sur does not exist, and in light of the variability observed in this study, the determination of such a structure will be difficult. Therefore, a much more complete study of the eddy energetics is required.

To accomplish this task, a long-term multi-array field program, with high vertical resolution, should be conducted off Point Sur in the same area as our study. The presence of very low-frequency signals (~ 215 days) in our data sets require that the proposed study be for at least three years. While this will not resolve motions that occur over several years, it will allow for better estimates of the mean fields and motions that occur at intermediate periods of 40 to 90 days out to the 215-day period. This increased resolution at lower frequencies would allow for an analyses similar to that of *Niiler and Hall* (1988) to be performed whereby the energetics within specific frequency bands could be examined. This study would also provide a check on the energy estimates obtained during our study, thus determining whether or not they are representative of the temporal mean off Point Sur.

The individual moorings should not be separated by more than 15 to 20 km in the horizontal, which is approximately the first baroclinic Rossby radius of deformation, and should be deployed in a pattern that will measure the cross-slope and alongslope parameters, similar to what was done in the Coastal Ocean Dynamics Experiment. As discussed earlier, the first baroclinic Rossby radius is a measure of the decay scale of coastal trapped waves in the offshore direction (*Allen*, 1980) and the fundamental length scale of coastal upwelling in a stratified

fluid (*Huyer*, 1983), as well as being the natural scale for the mesoscale eddy observed in this study region, which is of interest from a dynamical standpoint. The increased horizontal resolution will allow for closer study of mesoscale features, such as the anticyclonic eddy, that have be observed in the region, as well as providing estimates of mass transport and heat flux. Vertical instrumentation should extend throughout the entire water column, from the thermocline to just above the bottom, with tighter spacing near the main thermocline than at depth. This will allow for a more rigorous study of the dynamics of the system in addition to providing a more complete picture of the energy transfers throughout the water column.

A study, similar to that described above, is presently being conducted off northern California, in the vicinity of the CODE region, as part of an Office of Naval Research (ONR) Accelerated Research Initiative. The purpose of the ARI study is to describe the circulation and mesoscale variability within that particular portion of the CCS with emphasis on determining the flow of eddy energy through the system. By measuring current, temperature and pressure in both the horizontal and vertical directions for a two-year period, it is hoped that a more complete picture of the flow of eddy kinetic and potential energies will be obtained. It will be very interesting to see how the results of the ARI study compare to ours off Point Sur when it has been completed and the data analyzed.

APPENDIX A - TIME SERIES PLOTS

The data shown in this appendix have been low pass filtered using the filter described in Chapter II and decimated to six hourly values. Smaller gaps (less than 18 hours) have been filled using the techniques described in Chapter II; however, larger gaps, which were filled for purposes of spectral analysis, have been left untouched within the respective records. The orientation of the vectors are such that north is in the direction of the positive y-axis. The nominal depths for temperature time series are 100, 350 and 500 m for P2 and 100, 350, 500 and 1000 m for P3.

CURRENT VECTORS - MOORING P2

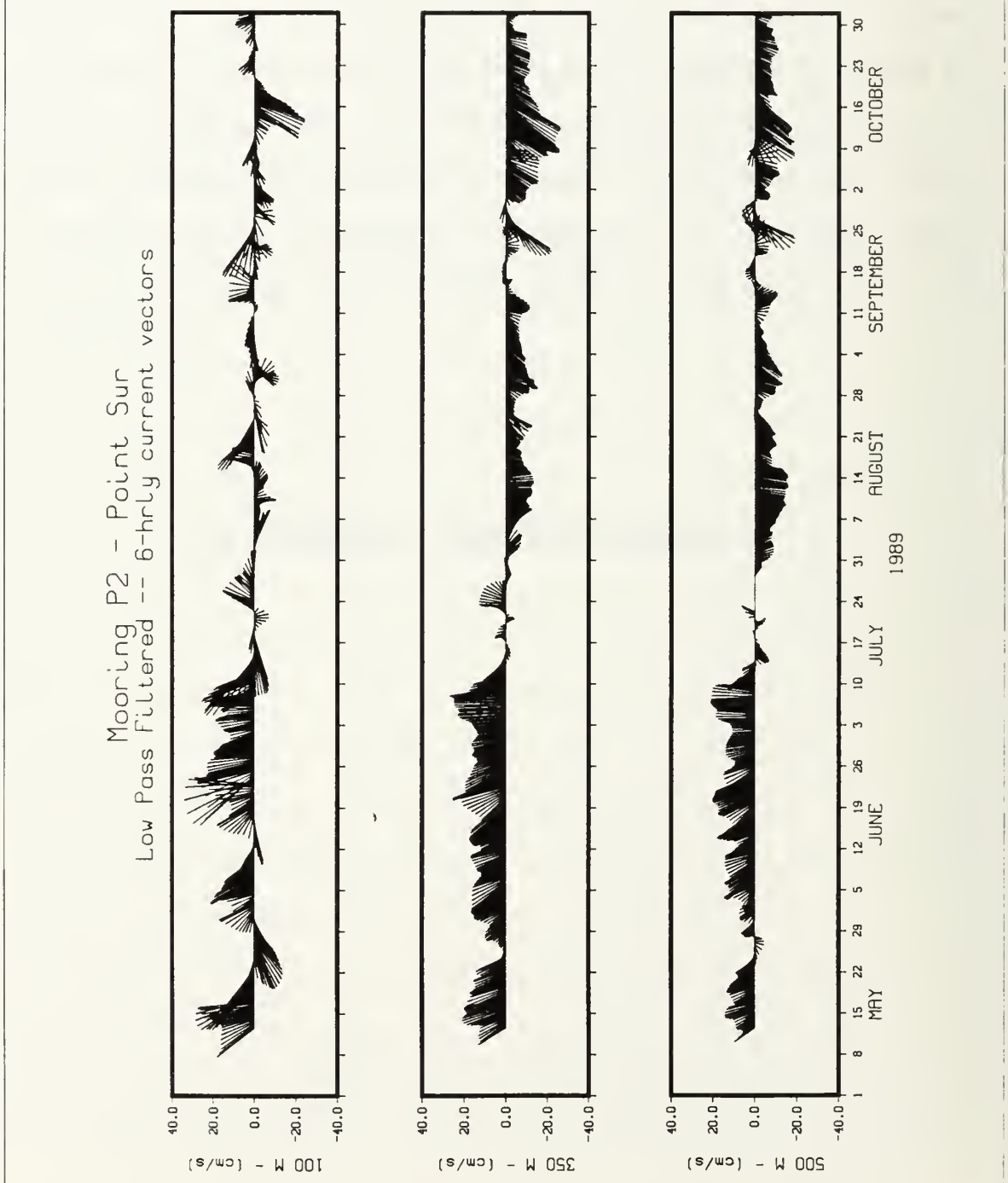
Mooring P2 - Point Sur
Low Pass Filtered -- 6-hrly current vectors
100 M - (cm/s)
350 M - (cm/s)
500 M - (cm/s)
40.0
20.0
0.0
-20.0
-40.0
1 8 15 22 29 5 12 19 26 3 10 17 24 31 7 14 21 28 4 11 18 25 2 9 16 23 30
MAY
JUNE
JULY
AUGUST
SEPTEMBER
OCTOBER
1989

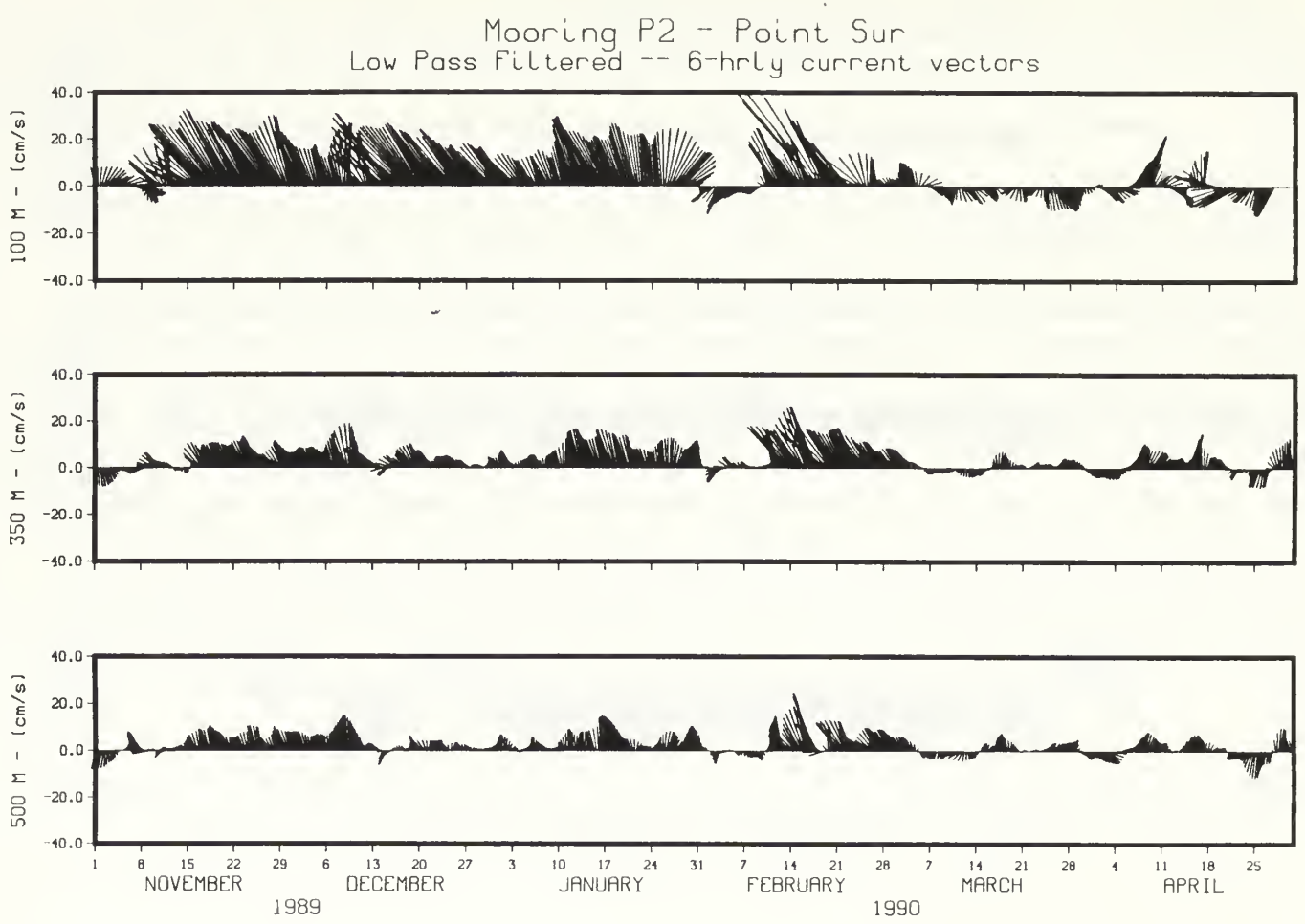
Mooring P2 - Point Sur
Low Pass Filtered -- 6-hrly current vectors
100 M - (cm/s)
350 M - (cm/s)
500 M - (cm/s)
40.0
20.0
0.0
-20.0
-40.0
1 8 15 22 29 6 13 20 27 3 10 17 24 31 7 14 21 28 7 14 21 28 4 11 18 25
NOVEMBER
DECEMBER
JANUARY
FEBRUARY
MARCH
APRIL
1989
1990

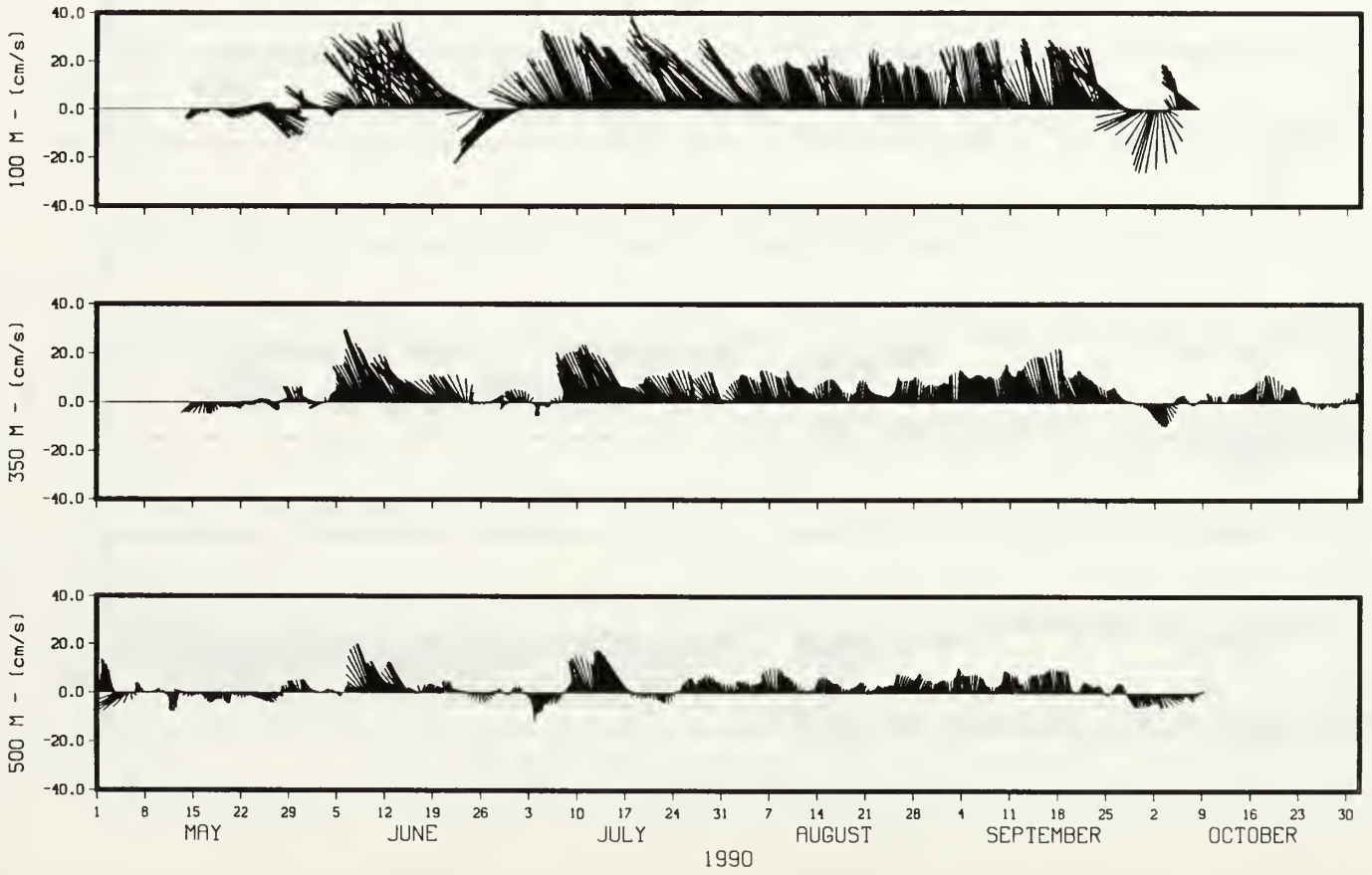
Mooring P2 - Point Sur
Low Pass Filtered -- 6-hrly current vectors
100 M - (cm/s)
350 M - (cm/s)
500 M - (cm/s)
40.0
20.0
0.0
-20.0
-40.0
1 8 15 22 29 5 12 19 26 3 10 17 24 31 7 14 21 28 4 11 18 25 2 9 16 23 30
MAY
JUNE
JULY
AUGUST
SEPTEMBER
OCTOBER
1990

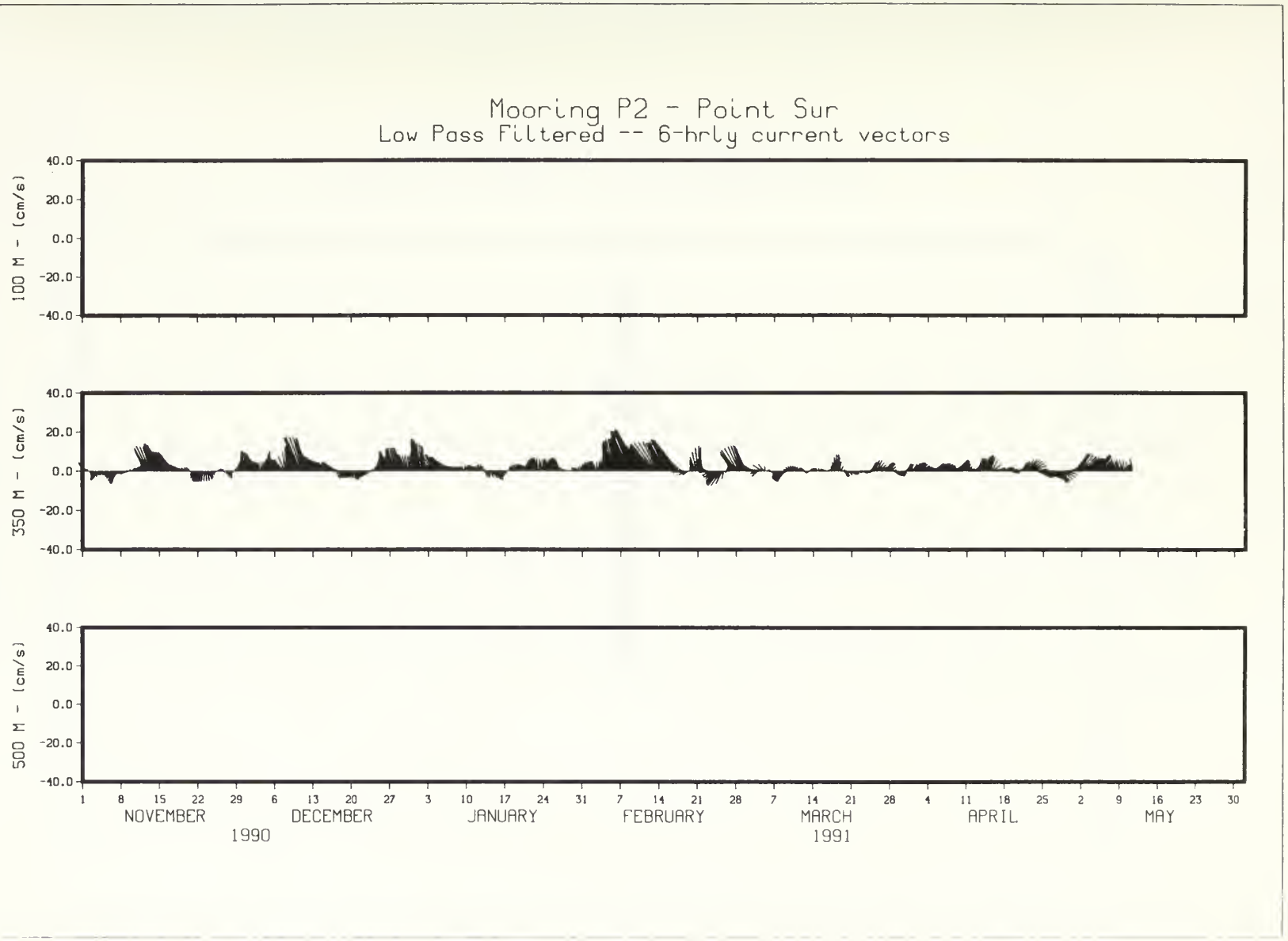
Mooring P2 - Point Sur
Low Pass Filtered -- 6-hrly current vectors
100 M - (cm/s)
350 M - (cm/s)
500 M - (cm/s)
40.0
20.0
0.0
-20.0
-40.0
1 8 15 22 29 6 13 20 27 3 10 17 24 31 7 14 21 28 7 14 21 28 4 11 18 25 2 9 16 23 30
NOVEMBER
DECEMBER
JANUARY
FEBRUARY
MARCH
APRIL
MAY
1990
1991

TEMPERATURES - MOORING P2

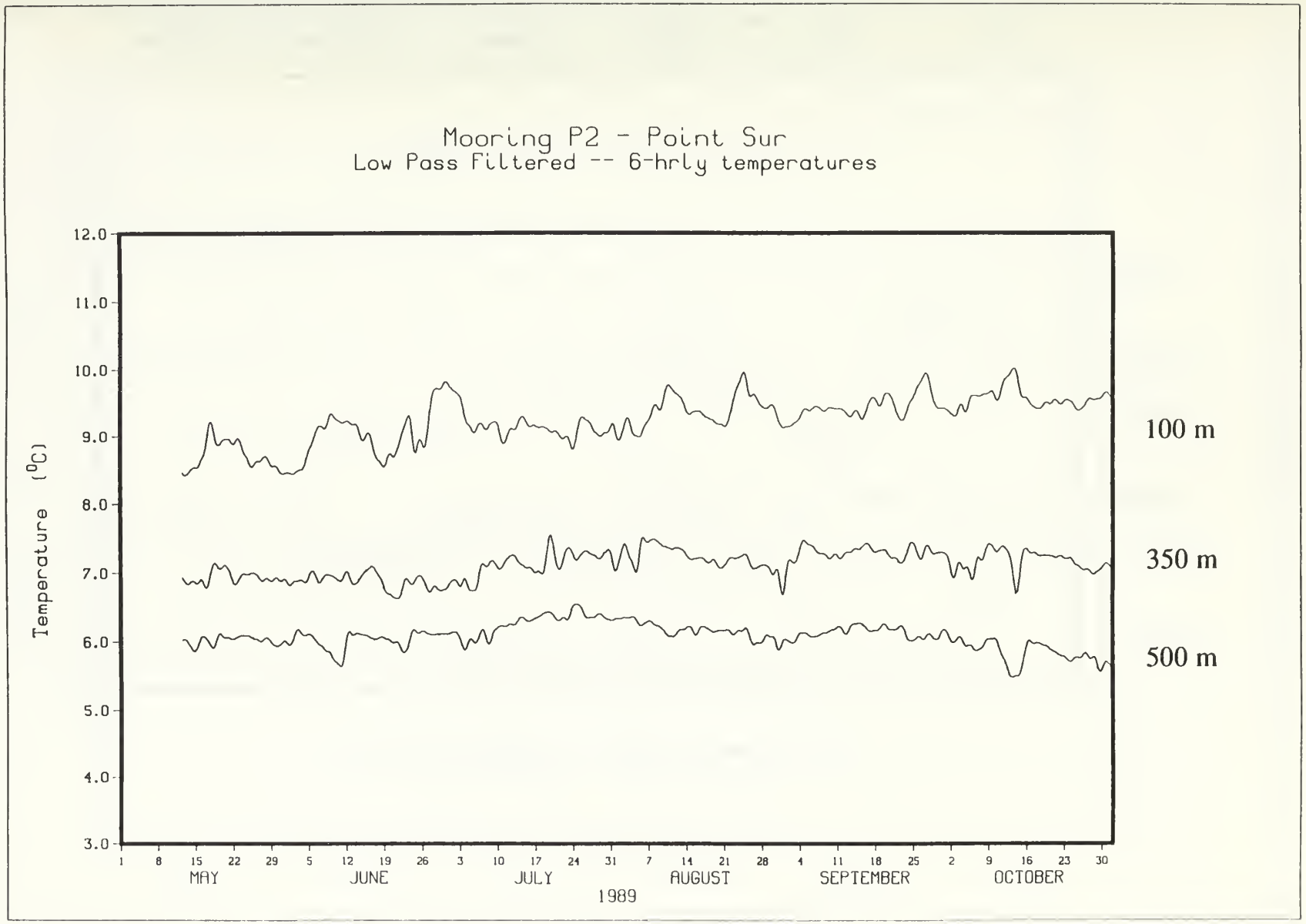
Mooring P2 - Point Sur
Low Pass Filtered -- 6-hrly temperatures
Temperature (°C)
12.0
11.0
10.0
9.0
8.0
7.0
6.0
5.0
4.0
3.0
100 m
350 m
500 m
1 8 15 22 29 5 12 19 26 3 10 17 24 31 7 14 21 28 4 11 18 25 2 9 16 23 30
MAY
JUNE
JULY
AUGUST
SEPTEMBER
OCTOBER
1989

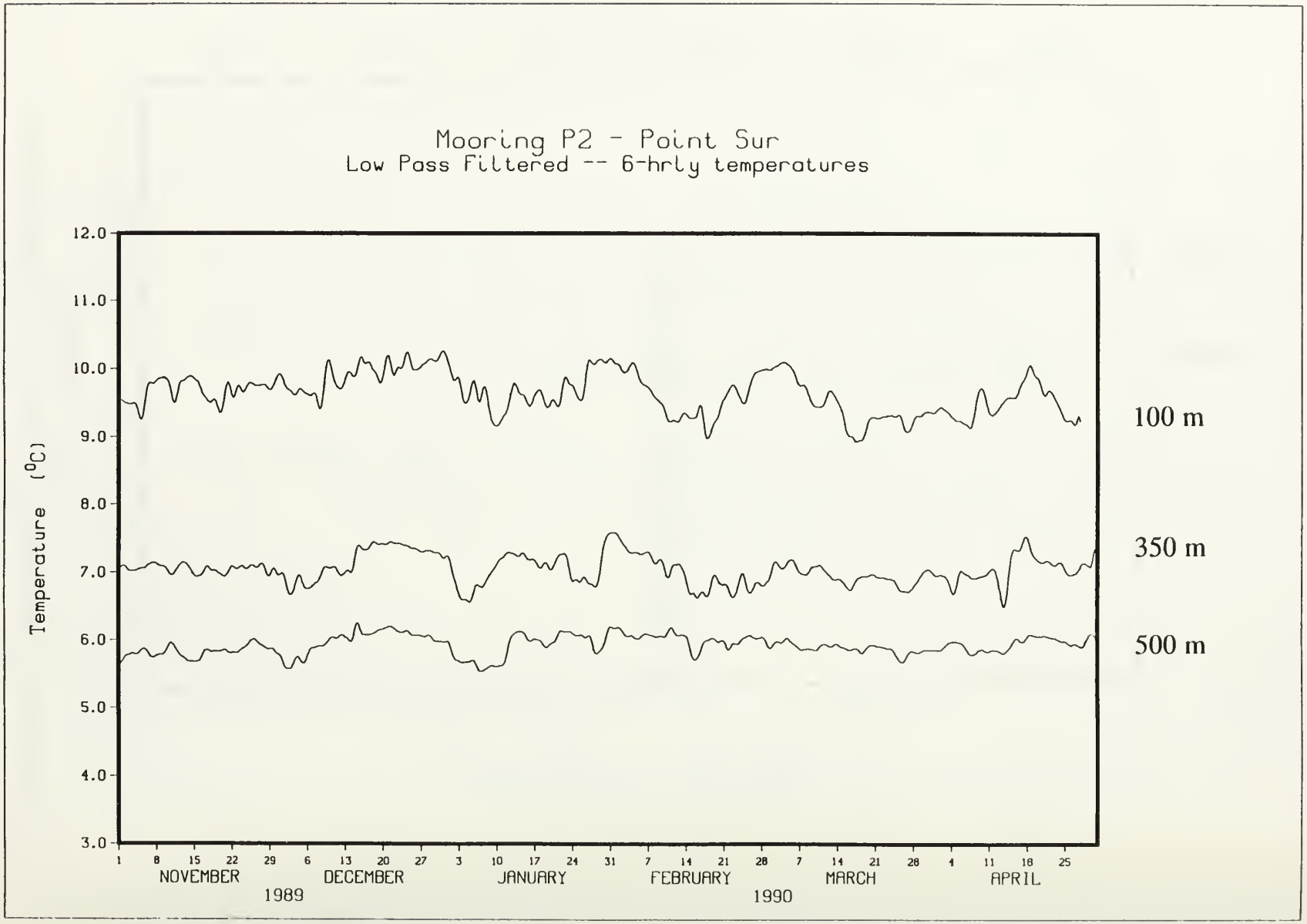
Mooring P2 - Point Sur
Low Pass Filtered -- 6-hrly temperatures
Temperature (°C)
12.0
11.0
10.0
9.0
8.0
7.0
6.0
5.0
4.0
3.0
1 8 15 22 29 6 13 20 27 3 10 17 24 31 7 14 21 28 7 14 21 28 4 11 18 25
NOVEMBER
DECEMBER
JANUARY
FEBRUARY
MARCH
APRIL
1989
1990
100 m
350 m
500 m

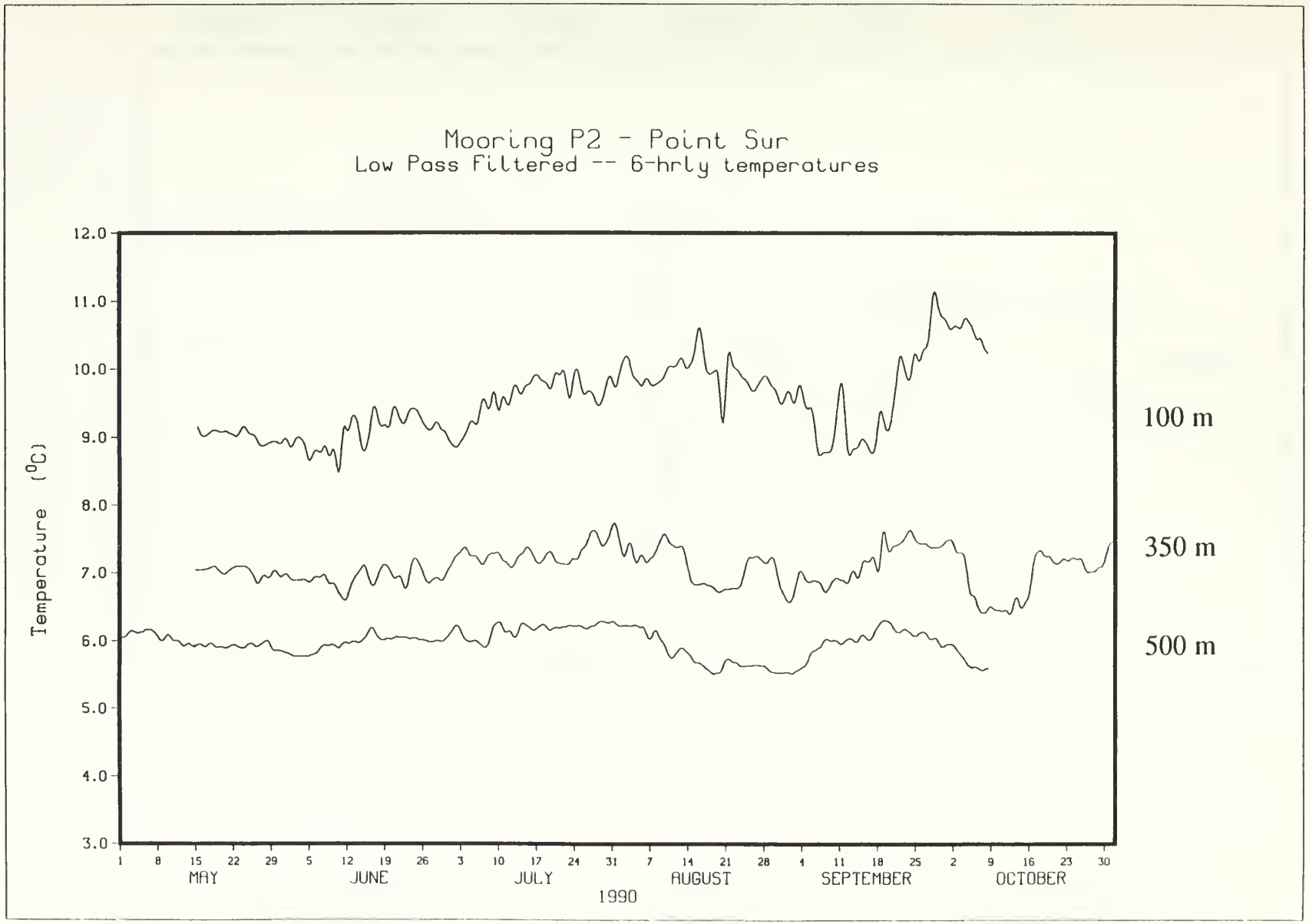
Mooring P2 - Point Sur
Low Pass Filtered -- 6-hrly temperatures
Temperature (°C)
12.0
11.0
10.0
9.0
8.0
7.0
6.0
5.0
4.0
3.0
100 m
350 m
500 m
1 8 15 22 29 5 12 19 26 3 10 17 24 31 7 14 21 28 4 11 18 25 2 9 16 23 30
MAY
JUNE
JULY
AUGUST
SEPTEMBER
OCTOBER
1990

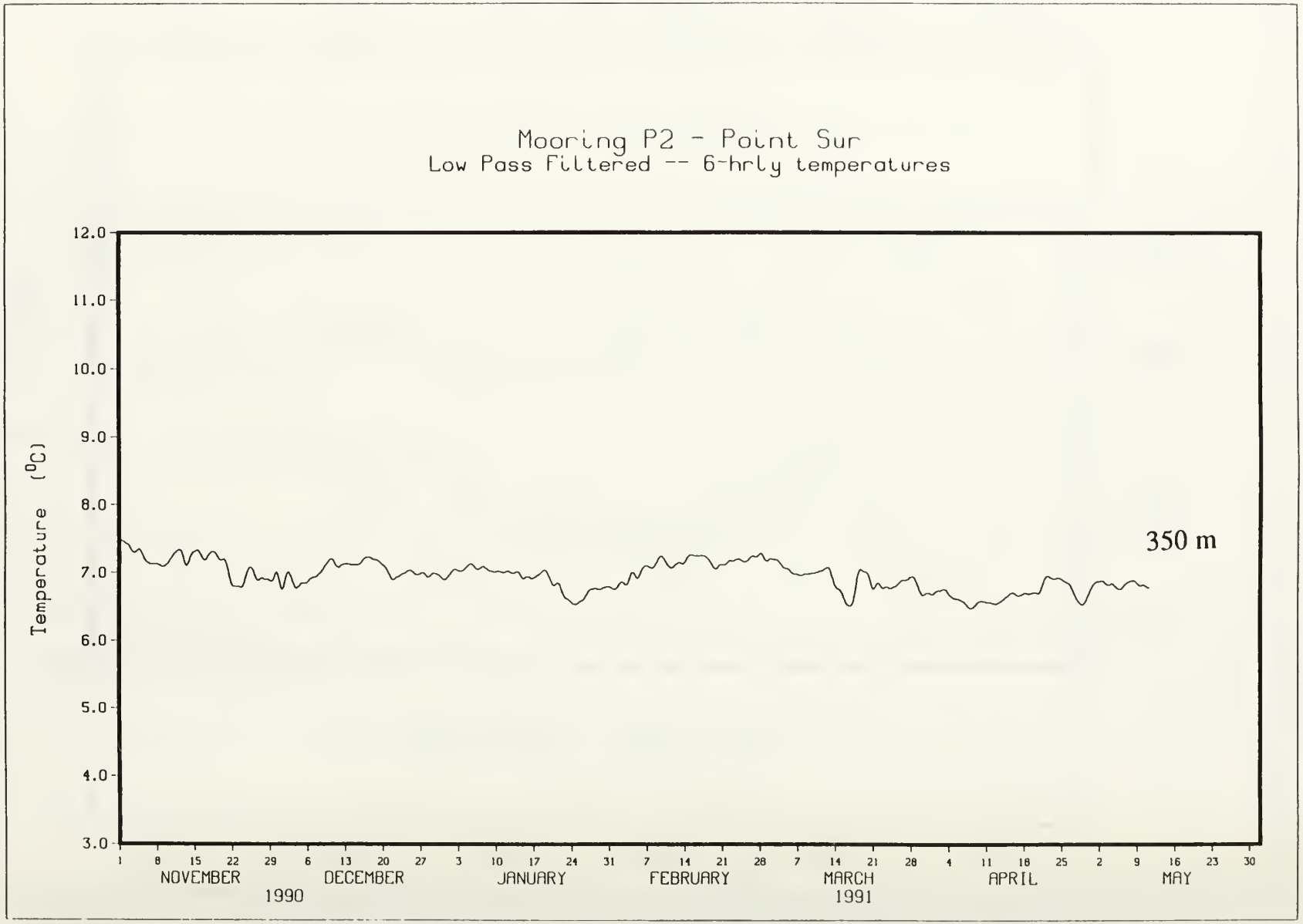
Mooring P2 - Point Sur
Low Pass Filtered -- 6-hrly temperatures
Temperature (°C)
12.0
11.0
10.0
9.0
8.0
7.0
6.0
5.0
4.0
3.0
350 m
1 8 15 22 29 6 13 20 27 3 10 17 24 31 7 14 21 28 7 14 21 28 4 11 18 25 2 9 16 23 30
NOVEMBER
1990
DECEMBER
JANUARY
FEBRUARY
MARCH
1991
APRIL
MAY

CURRENT VECTORS - MOORING P3

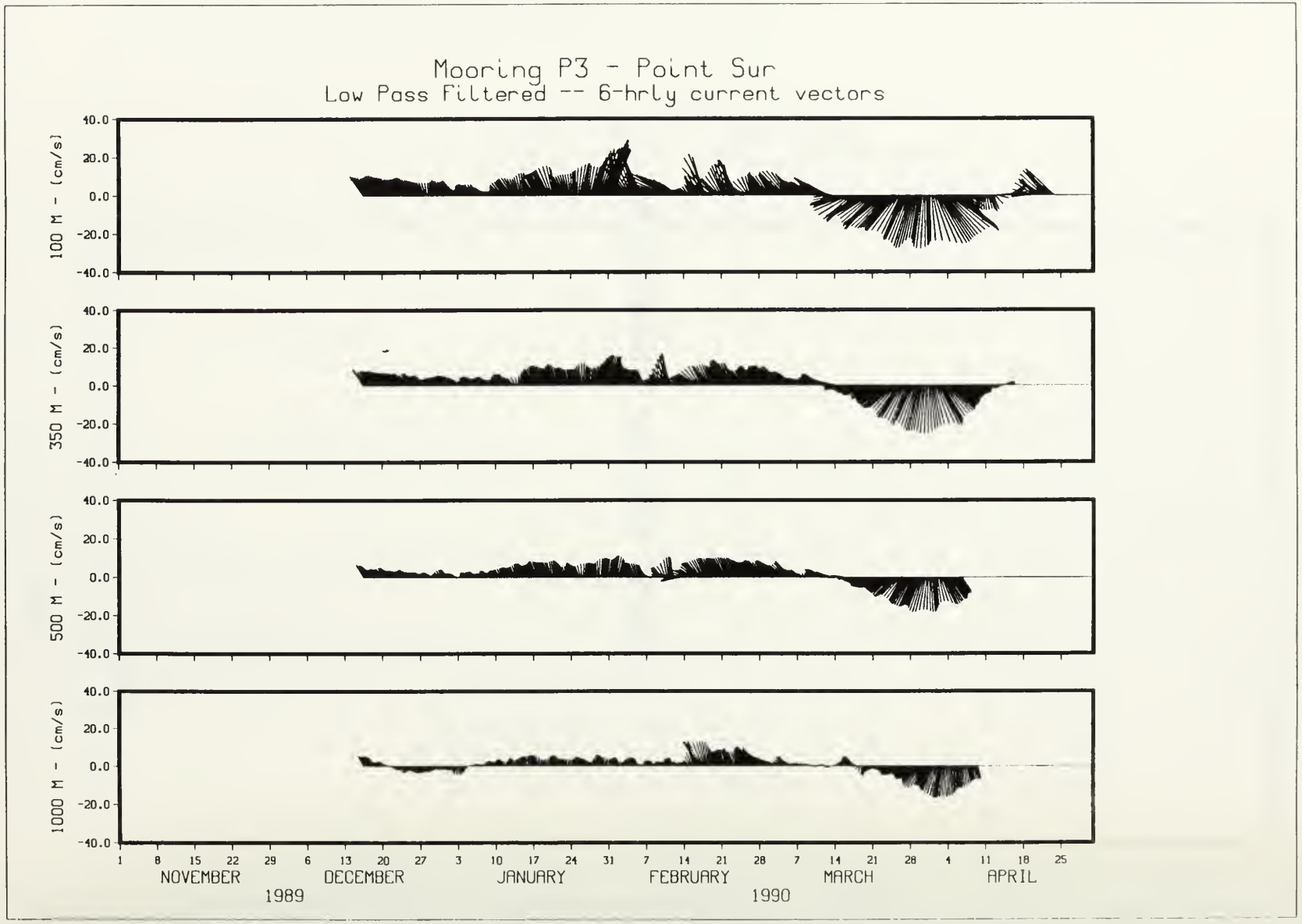
Mooring P3 - Point Sur
Low Pass Filtered -- 6-hrly current vectors
100 M - (cm/s)
350 M - (cm/s)
500 M - (cm/s)
1000 M - (cm/s)
40.0
20.0
0.0
-20.0
-40.0
1 8 15 22 29 6 13 20 27 3 10 17 24 31 7 14 21 28 7 14 21 28 4 11 18 25
NOVEMBER
DECEMBER
JANUARY
FEBRUARY
MARCH
APRIL
1989
1990

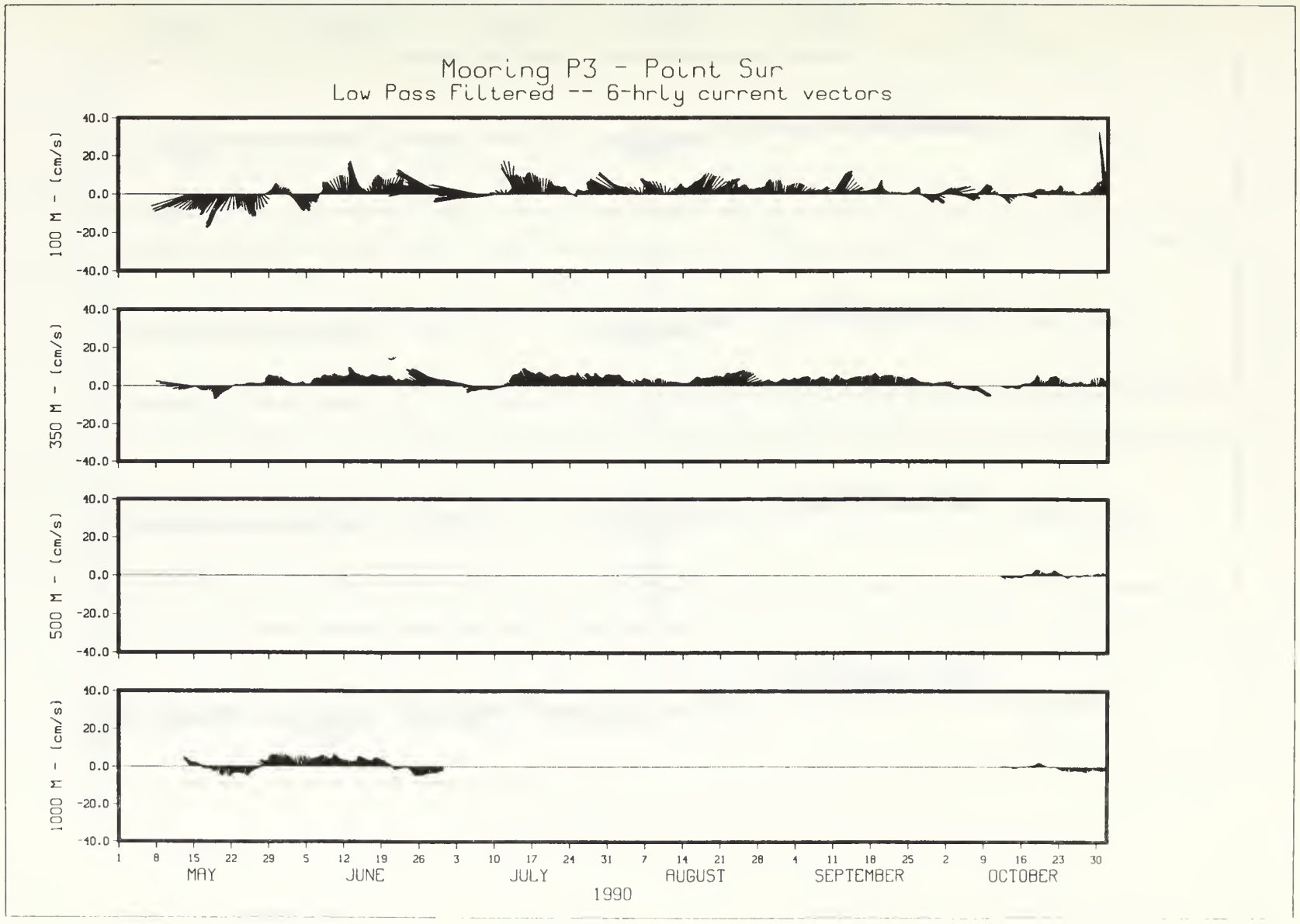
Mooring P3 - Point Sur
Low Pass Filtered -- 6-hrly current vectors
100 M - (cm/s)
350 M - (cm/s)
500 M - (cm/s)
1000 M - (cm/s)
40.0
20.0
0.0
-20.0
-40.0
1 8 15 22 29 5 12 19 26 3 10 17 24 31 7 14 21 28 4 11 18 25 2 9 16 23 30
MAY
JUNE
JULY
AUGUST
SEPTEMBER
OCTOBER
1990

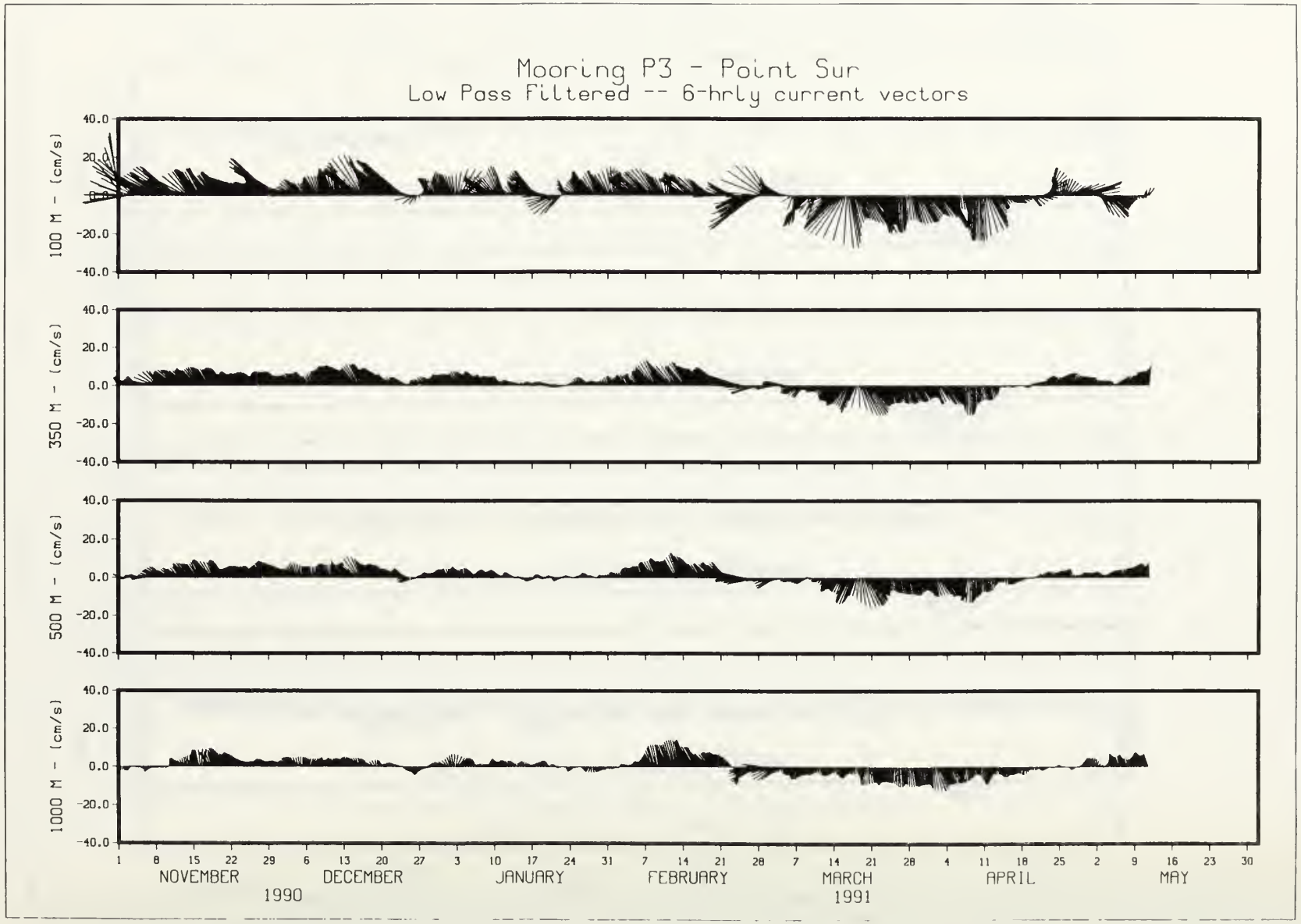
Mooring P3 - Point Sur
Low Pass Filtered -- 6-hrly current vectors
100 M - (cm/s)
350 M - (cm/s)
500 M - (cm/s)
1000 M - (cm/s)
40.0
20.0
0.0
-20.0
-40.0
1 8 15 22 29 6 13 20 27 3 10 17 24 31 7 14 21 28 7 14 21 28 4 11 18 25 2 9 16 23 30
NOVEMBER
DECEMBER
JANUARY
FEBRUARY
MARCH
APRIL
MAY
1990
1991

TEMPERATURES - MOORING P3

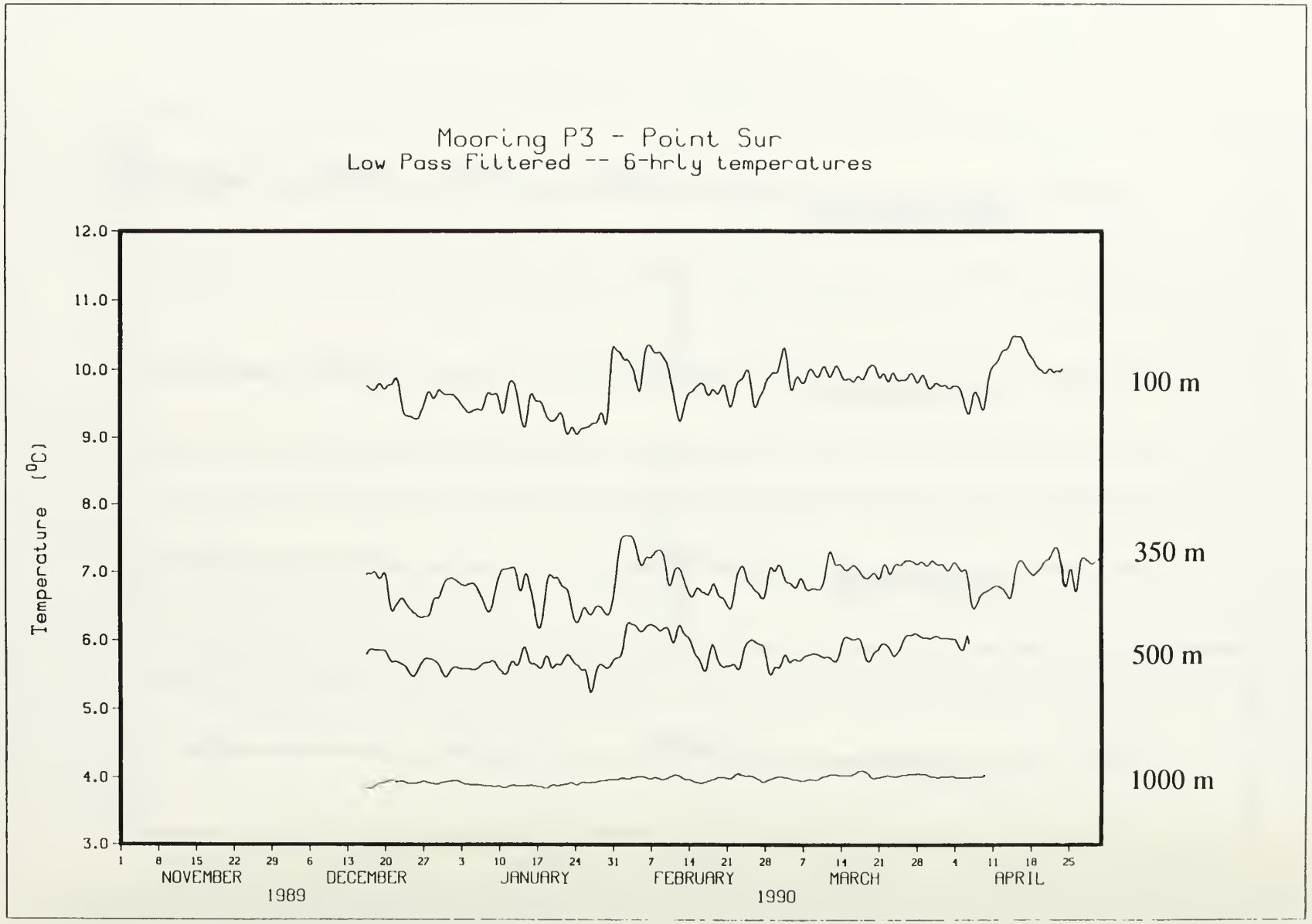
Mooring P3 - Point Sur
Low Pass Filtered -- 6-hrly temperatures
Temperature (°C)
12.0
11.0
10.0
9.0
8.0
7.0
6.0
5.0
4.0
3.0
100 m
350 m
500 m
1000 m
1 8 15 22 29 6 13 20 27 3 10 17 24 31 7 14 21 28 7 14 21 28 4 11 18 25
NOVEMBER
DECEMBER
JANUARY
FEBRUARY
MARCH
APRIL
1989
1990

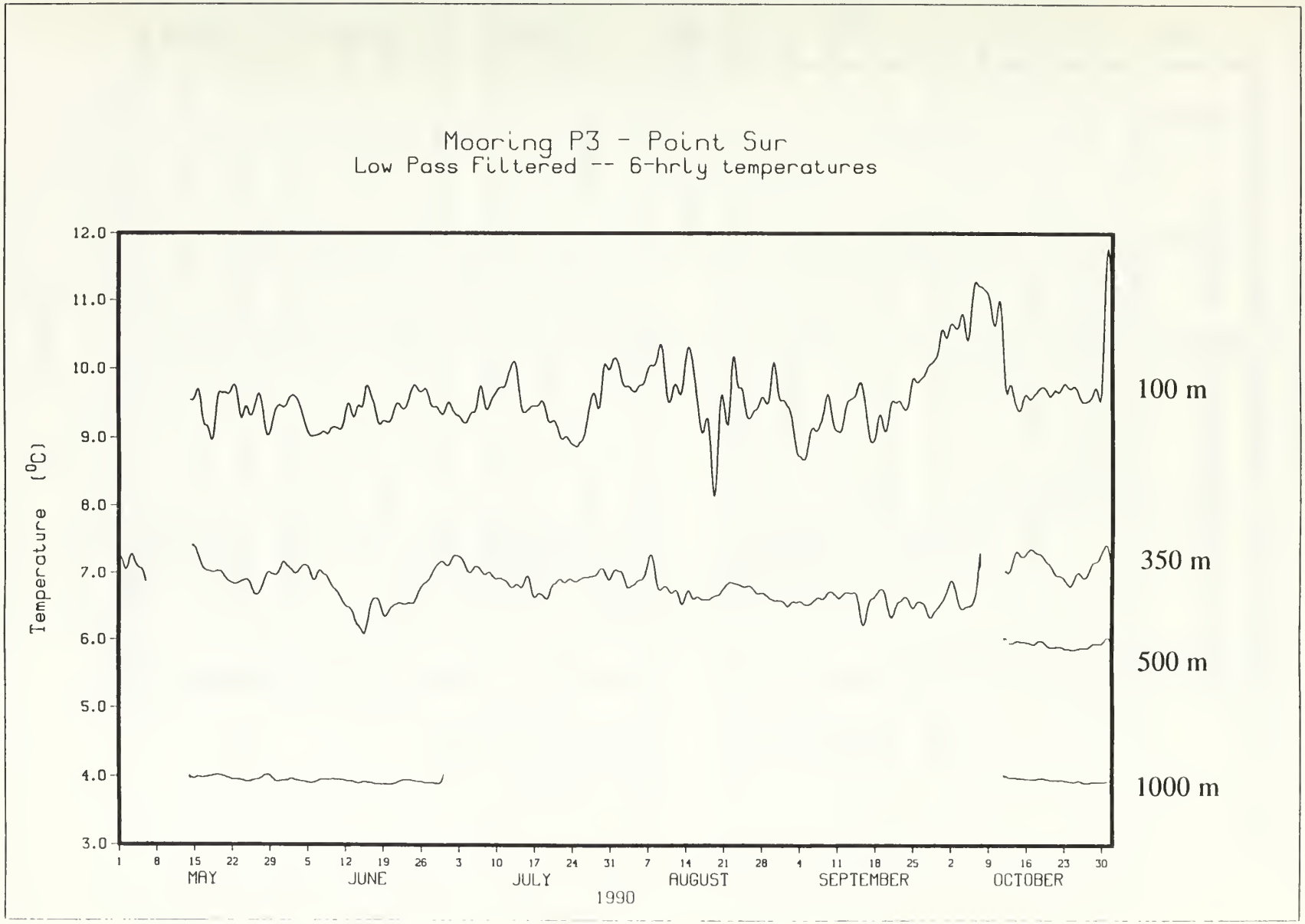
Mooring P3 - Point Sur
Low Pass Filtered -- 6-hrly temperatures
Temperature (°C)
12.0
11.0
10.0
9.0
8.0
7.0
6.0
5.0
4.0
3.0
100 m
350 m
500 m
1000 m
1 8 15 22 29 5 12 19 26 3 10 17 24 31 7 14 21 28 4 11 18 25 2 9 16 23 30
MAY
JUNE
JULY
AUGUST
SEPTEMBER
OCTOBER
1990

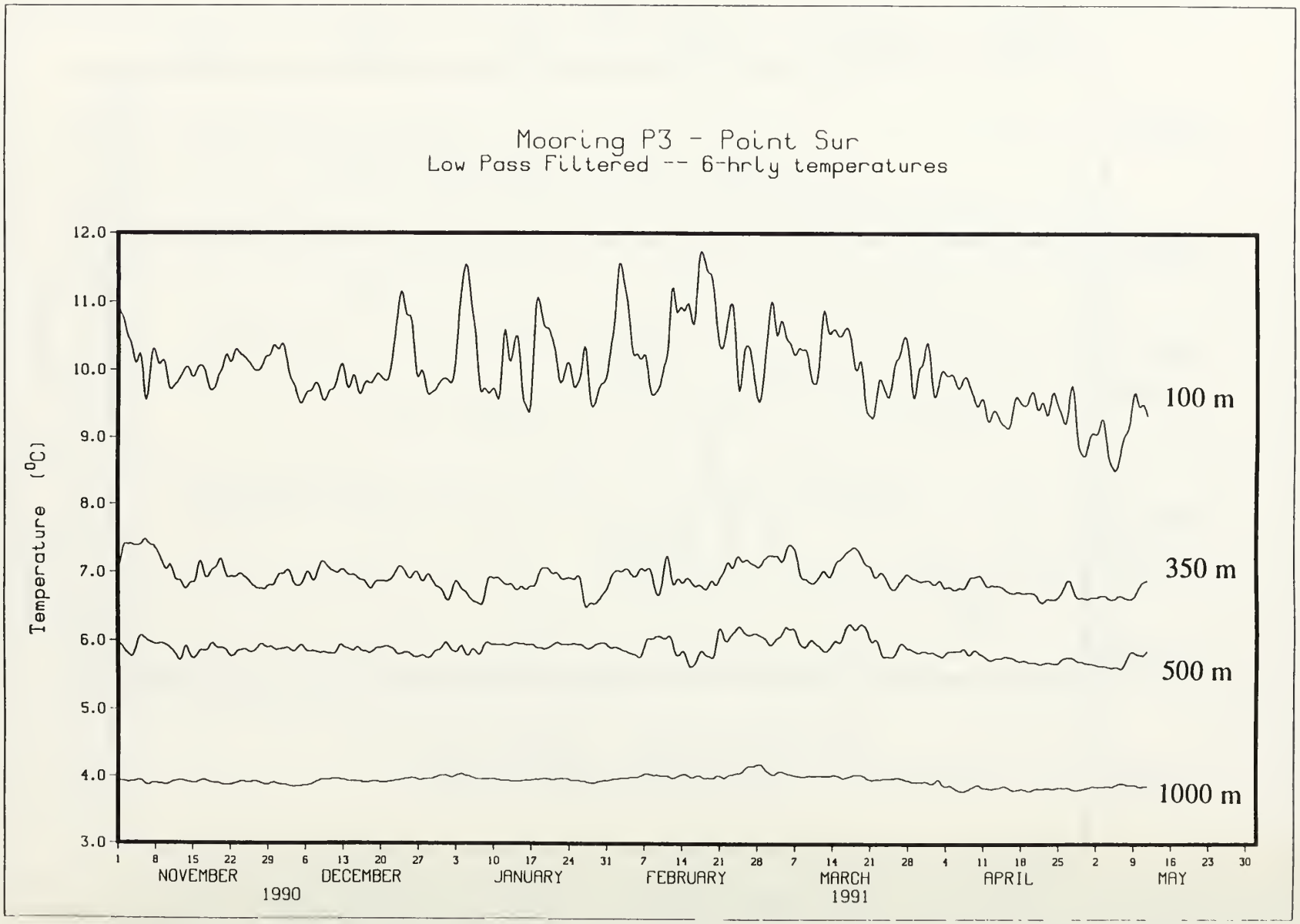
Mooring P3 - Point Sur
Low Pass Filtered -- 6-hrly temperatures
Temperature (°C)
12.0
11.0
10.0
9.0
8.0
7.0
6.0
5.0
4.0
3.0
100 m
350 m
500 m
1000 m
1 8 15 22 29 6 13 20 27 3 10 17 24 31 7 14 21 28 7 14 21 28 4 11 18 25 2 9 16 23 30
NOVEMBER
1990
DECEMBER
JANUARY
FEBRUARY
MARCH
1991
APRIL
MAY

APPENDIX B. AN INTERPOLATION ALGORITHM FOR GAPPY OCEANOGRAPHIC DATA

Any observed stationary time series may contain missing values, and these missing values must be estimated in such a way as to be characteristic of the rest of the data in order to properly calculate and analyze the spectral density. If the number of missing values constitutes a very small percentage of the data set, any logical method of handling missing values is likely to produce satisfactory results (*Jones*, 1971). In such cases, one could simply subtract the mean from the data set, insert zeros for the missing values, and then proceed to estimate the spectral density. However, when the number of missing values becomes somewhat larger, as in the case of the Point Sur current meter data, a more sophisticated approach is required.

There are numerous sources on the subject of handling times series which contain missing values (*Jenkins and Watts*, 1968; *Box and Jenkins*, 1976; *Shumway*, 1988; and *Harvey*, 1981, 1989; to name a few). These techniques are based upon autoregressive methods, state-space theory, and Kalman filters, to forecast the missing values based upon the statistics of the data set. *Sturges* (1991) used a somewhat different approach for recovering a continuous spectrum from a gappy data set, and found he was able to recover the low frequency part of the spectrum to arbitrarily high accuracy. His method involved creating a synthetic data set with the expected spectral shape of the real data, smoothing, and estimating the effective Nyquist frequency for the entire procedure. He then filtered this data set to remove frequencies above the

effective Nyquist and then solved for the sine and cosine coefficients (using least squares) that would be present in the Fourier transfom.

The following algorithm, developed by Peter A.W. Lewis and Bonnie K. Ray at the Naval Postgraduate School, Monterey, California, is similar to these techniques and has been used to fill in gaps present in the current meter data collected off Point Sur. This method allows for trends and cycles present within a time series x(t), and for the joint interpolation of two correlated times series x(t) and y(t), by incorporating an estimate of the correlation into the interpolated values.

The algorithm proceeds as follows:

1. Locate and fill in the gaps in the time series, x(t), by linearly interpolating between the two points on either side of the gap. If there are two time series which are correlated in some way (i.e., u and v velocity components), locate and fill gaps in the second series, y(t), in the same manner. The linearly interpolated time series are then referred to as $x_1(t)$ and $y_1(t)$, respectively.

   NOTE: For the sake of brevity, the procedure described from this point forward will pertain to a single times series, $x_1(t)$; however, whenever there are two series, this procedure is applied to each in exactly the same manner.

2. Remove the linear trend from the times series, $x_1(t)$, where this trend has been estimated using the least squares principle. The resulting time series becomes

$$x_2(t) = x_1(t) - \hat{a} - \hat{b}t \qquad \text{B1}$$

where $\hat{a}$ is the estimated mean and $\hat{b}$ is the estimated slope.

3. Estimate and examine the sample periodogram for the interpolated and detrended data, $x_2(t)$.

4. Calculate the probability of obtaining the computed values for the 20 largest values of the normalized periodogram under the assumption that $x_2(t)$ is a white noise process. A small probability indicates that a cycle may be present in the data.

5. Using the information obtained in step 4, along with any a priori knowledge of the series behavior (i.e., semi-diurnal, diurnal, and inertial frequencies), estimate and remove cycles from the interpolated and detrended data, if desired. Cycles are assumed to have the form

$$s_t = \sum_{j=1}^{J} \{\gamma_j \cos(\omega_j t) + \beta_j \sin(\omega_j t)\} \qquad \text{B2}$$

where ω_j ($= 2\pi f$) are frequencies you wish to remove and J is the number of cycles. The coefficients γ_j and β_j are estimated using least squares, and the resulting times series is denoted as $x_3(t) = x_2(t) - \hat{s}_t$.

6. Next, fit a first order autoregressive AR(1) model to the detrended and deseasonalized times series, $x_3(t)$. An AR(1) model has the form

$$x_3(t) = \phi x_3(t-1) + a_x(t), \qquad t = 2,3, \ldots, n \quad . \qquad \text{B3}$$

It is assumed that $a_x(t)$ is a normally distributed process having a mean of zero and variance equal to $\sigma^2_{a,x}$., i.e., $N(0,\hat{\sigma}^2_{a,x})$. ϕ is estimated using least squares, and the residual time series is computed as

$$\hat{a}_x(t) = x_3(t) - \hat{\phi} x_3(t-1), \qquad t = 2,3, \ldots, n \quad . \qquad \text{B4}$$

7. Calculate the variance of $\hat{a}_x(t)$ and generate a time series of length n having the distribution $N(0,\hat{\sigma}^2_{a,x})$. This series is denoted as $a'_x(t)$.

8. By letting l represent the length of a particular gap in the time series, x_3, and $x_3(t)$ and $x_3(t+l+1)$ the points on either side of this gap, the program then forecasts and backcasts from each end of the gap using the following recursive equations

$$\hat{x}_3(t + j) = \hat{\phi}\hat{x}_3(t + j - 1) + a'_x(t + j) \qquad \text{B5}$$

$$\hat{x}_3(t + l + 1 - j) = \hat{\phi}\hat{x}_3(t + l + 2 - j) + a'_x(t + l + 1 - j), \quad j = 1, 2, \ldots, l \quad . \qquad \text{B6}$$

The interpolated value then becomes

$$\tilde{x}_3(t + j) = w_{1,j}\,\hat{x}_3(t + j) + w_{2,j}\,\hat{x}_3(t + l + 1 - j), \quad j = 1, 2, \ldots, l \qquad \text{B7}$$

where $w_{1,j} = 1 - (j / l+1)$ and $w_{2,j} = 1 - w_{1,j}$.

9. When interpolating values for two correlated times series (such u and v components of velocity), calculate the standard deviation of the residual series $\hat{a}_x(t)$ and $\hat{a}_y(t)$ determined from equation B4. Compute the sample cross correlation, *c*, at zero lag between the two residual series. Generate a series, $a'_y(t)$, of length *n* having the distribution $N(0,\hat{\sigma}^2_{a,y})$. Generate a second series, $a''_y(t)$, also of length *n* using the following relation

$$a''_y(t) = c\left(\hat{\sigma}_{\hat{a}_y(t)} / \hat{\sigma}_{\hat{a}_x(t)}\right) a'_x(t) + \sqrt{1 - c^2}\, a'_y(t) \qquad \text{B8}$$

10. Interpolate the values for the time series $y_3(t)$ using equation B5 and B6, where $a'_x(t+j)$ is replaced by $a''_y(t+j)$.

11. Finally, add the estimated trend and cycles back into the interpolated time series, with original data unaltered and gaps filled.

The algorithm described above has been written in APL computer language and is available in the GRAFSTAT library at NPS from the authors listed above.

APPENDIX C - TEMPERATURE PREDICTION METHODS AND ERROR ANALYSIS

A. METHODS FOR SYNTHESIZING TEMPERATURES

There have been several different schemes used in recent years to correct a temperature time series for vertical excursions of the mooring in the presence of strong currents. Because background density fields can vary dramatically from one geographic location to another, there is no one temperature correction scheme applicable throughout the world's oceans (*Hall*, 1989b). *Hall and Bryden* (1985) used several CTD stations located near their mooring to parameterize $\partial T/\partial P$ as a linear function of pressure, with coefficients dependent upon the temperature at a specified level as well as the pressure range associated with each standard depth. *Hogg* (1986) developed a correction scheme which was independent of CTD data. In this method he assumed that $\partial T/\partial P$ was a quadratic function of the local temperature at each mooring site. The coefficients of the quadratic were determined from a regression analysis on estimates of $\partial T/\partial P$ based upon daily time differences, δT and δP, measured at a given instrument (*Hall*, 1989b). Both of these methods were used for correcting data collected within the Gulf Stream. To correct temperatures in the Kuroshio current to standard depths, *Hall* (1989b,1991) defined an analytic form for the basic structure of temperature between 200 and 900 dbar, based upon CTD data, and dependent upon the measured value of temperature at 350 dbar.

In this study, the objective was not to correct the temperature time series for mooring motion but rather to synthesize a time series of temperature for the mid-depth between instrumented levels at moorings P2 and P3. Four different

methods of determining T_{new} were examined, each utilizing the observed temperature information from the two time series bracketing the desired level. They were: 1) a simple linear dependence; 2) an exponential dependence (similar to velocity calculations); and a predictor-corrector scheme which utilized either 3) a quadratic or 4) a cubic function, derived from CTD collected during the current meter deployments (Table 3).

The equation for linear prediction of temperature can be written as follows

$$T(P)_{new} = T_1 - \frac{(T_2 - T_1)(P_1 - P)}{P_2 - P_1} , \qquad C1$$

where the subscripts 1 and 2 refer to the upper and lower levels, respectively, and P is the pressure level of interest. When using an exponential dependence, the equation becomes

$$T(P)_{new} = T_1 \exp\left(- \frac{\ln\left(\frac{T_2}{T_1}\right)}{(P_1 - P_2)} (P - P_1) \right) . \qquad C2$$

The predictor-corrector method used a general least-squares fit of the form

$$T(P) = a_0 + a_1 \times P + a_2 \times P^2 + a_3 \times P^3 \qquad C3$$

to model T vs P with either a quadratic function (terms a_0, a_1, and a_2) or a cubic function (terms a_0, a_1, a_2, and a_3), based upon data from 28 CTD stations (two

from each of the 14 cruises). Since T-S curves for this area usually reveal a gradual change of T with P, especially below the thermocline, it was decided to use only those values at 10 dbar increments beginning at 50 dbar and extending to either 550 dbar for P2 or 1050 dbar for P3. The 28 temperatures at each of these levels were then averaged and regressed against pressure to determine the coefficients for both the quadratic and cubic models at each mooring site (Table C1). This average T vs. P profile, in a crude sense, includes some of the seasonal variability of temperatures off Point Sur.

Table C1. LEAST-SQUARES COEFFICIENTS FOR AVERAGE TEMPERATURE PROFILE OFF POINT SUR: The coefficients for both the quadratic and cubic fits of equation (C3) are listed.

Mooring	(a_0)	(a_1) P	(a_2) P^2	(a_3) P^3
P2 - O(2)	10.995	-0.015	9.756×10^{-6}	--------
O(3)	11.457	-0.022	3.692×10^{-5}	-3.018×10^{-8}
P3 - O(2)	10.650	-0.012	5.807×10^{-6}	---------
O(3)	11.156	-0.017	1.596×10^{-5}	-6.153×10^{-9}

Once the coefficients were evaluated, a time series of temperature at the desired mid-depth level was computed as follows: 1) predict the temperatures at levels 1, 2, and the desired level using both the quadratic and cubic function defined by (C3). Input pressure came from the observed records at levels 1 and 2 or the fixed pressure value at the new level; 2) calculate the difference between the actual temperature (AT) and the predicted temperature (PT) at levels 1 and 2 as $\Delta T_{1,2} = AT_{1,2} - PT_{1,2}$; 3) predict a ΔT at the new level by

assuming a linear dependence of the temperature difference between levels 1 and 2 as

$$\Delta T_{new} = \Delta T_1 - \frac{(\Delta T_2 - \Delta T_1)(P_1 - P)}{P_2 - P_1} \qquad C4$$

and; 4) determine the new temperature at the desired level by adding in the correction factor, $T_{new} = PT_{new} + \Delta T_{new}$. This method retains the basic shape of the T vs. P profile by simply forcing it to pass through the observed temperatures at levels 1 and 2. The curve can be skewed to some degree depending upon the differences between actual and predicted temperatures at each level; however, only very large and unrealistic temperature differences could cause this method to predict completely erroneous values. Because of the availability of the CTD data collected during the deployment periods, it was possible to perform a detailed error analysis for temperature prediction.

B. ANALYSIS OF ERRORS IN PREDICTED TEMPERATURES

To determine which of the methods described earlier was the most appropriate for use in this study, each was used to predict the temperature at the 225, 425, 750 dbar levels for each of the 28 CTD casts used in determining the mean T vs P profile. Because the actual temperatures at these depths were available, an estimation of the error for each method could be calculated. The resulting relative errors for each method have been summarized in Tables C2 and C3, with 95 % error bars shown in Figure C1. At mooring P2, comparable errors were obtained for the exponential and quadratic predictions, with a mean relative error near 1-2%. Using a linear fit produced only a slightly larger mean error of 2.3%, and as shown in Figure C1, the error bars for each method

overlap, suggesting that no one method is statistically better than the others. The same is true at mooring P3, where the cubic dependence at P3 yielded the best results at all levels, with a mean relative error of less than 3%, while the linear fit had a mean error or 3%. Since the error bars in both cases overlap, it was decided to use the simple linear approach in lieu of the more complicated schemes. Maximum errors of 9.3 % at P2 and 9.8 % at P3 were encountered using a linear fit, and it is expected that the relative error using this technique will be less 10 %, and more likely less than 5%. Inspection of observed and synthesized times series (Figure 5) also appears to indicate that this procedure was successful.

Table C2. RELATIVE ERROR STATISTICS FOR TEMPERATURE PREDICTION AT MOORING P2: Section (a) includes data from both levels, while (b) and (c) are for single levels only, which allows for comparison of methods at each depth.

Method	mean	Std. Dev.	Std. Error of mean
(a) Both levels	*56 points*		
Linear	0.0213	± 0.0212	± 0.0028
Exponential	0.0175	± 0.0170	± 0.0023
Quadratic	0.0175	± 0.0158	± 0.0021
Cubic	0.0200	± 0.0156	± 0.0021
(b) 225 dbar only	*28 points*		
Linear	0.0300	± 0.0262	± 0.0049
Exponential	0.0233	± 0.0214	± 0.0040
Quadratic	0.0233	± 0.0190	± 0.0036
Cubic	0.0271	± 0.0176	± 0.0033
(c) 425 dbar only	*28 points*		
Linear	0.0125	± 0.0086	± 0.0016
Exponential	0.0117	± 0.0080	± 0.0015
Quadratic	0.0117	± 0.0090	± 0.0017
Cubic	0.0129	± 0.0090	± 0.0017

Table C3. RELATIVE ERROR STATISTICS FOR TEMPERATURE PREDICTION AT MOORING P3: Section (a) includes data from both levels, while (b), (c) and (d) are for single levels only, which allows for comparison of methods at each depth.

Method	mean	Std. Dev.	Std. Error of mean
(a) All levels	*84 points*		
Linear	0.0303	± 0.0254	± 0.0028
Exponential	0.0219	± 0.0195	± 0.0021
Quadratic	0.0250	± 0.0209	± 0.0023
Cubic	0.0209	± 0.0182	± 0.0020
(b) 225 dbar only	*28 points*		
Linear	0.0230	± 0.0195	± 0.0034
Exponential	0.0179	± 0.0140	± 0.0026
Quadratic	0.0183	± 0.0143	± 0.0027
Cubic	0.0171	± 0.0118	± 0.0022
(c) 425 dbar only	*28 points*		
Linear	0.0225	± 0.0242	± 0.0046
Exponential	0.0219	± 0.0232	± 0.0044
Quadratic	0.0215	± 0.0223	± 0.0042
Cubic	0.0213	± 0.0216	± 0.0041
(d) 750 dbar only	*28 points*		
Linear	0.0455	± 0.0256	± 0.0048
Exponential	0.0259	± 0.0200	± 0.0038
Quadratic	0.0354	± 0.0215	± 0.0041
Cubic	0.0244	± 0.0196	± 0.0037

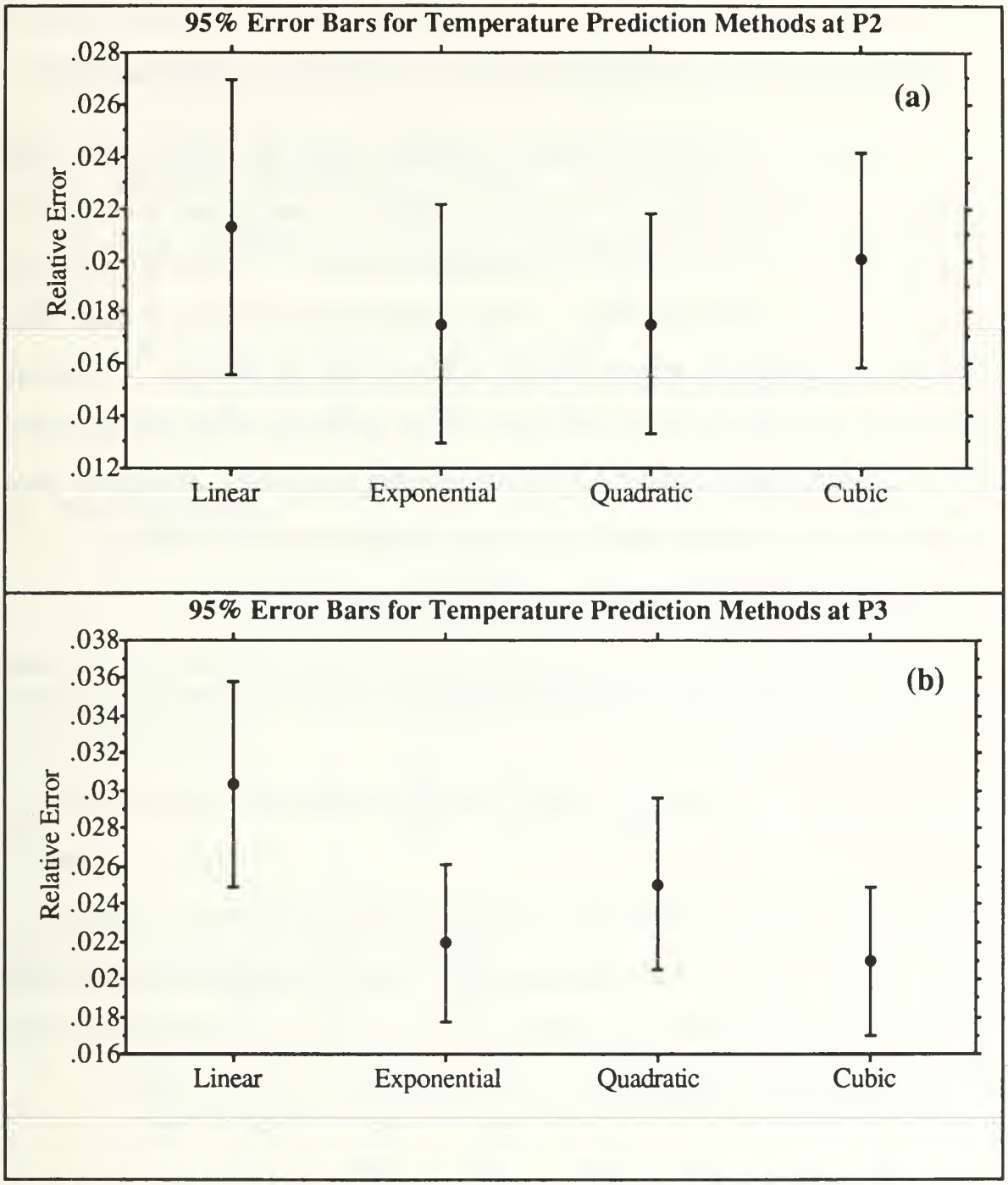

Figure C1. 95% Error Bars for Temperature Prediction Methods: Errors bars are computed at the 95% significance level using from levels (a) P2 - 225 and 425 dbar, and (b) P3 - 225,m 425, and 750 dbar. Multiplying relative error by 100 yields the percentage error for each method.

APPENDIX D - DERIVATION OF ENERGY EQUATIONS

To examine energetic interactions occurring within the subtidal flow field along the continental slope off Point Sur, California, using data from a single current meter mooring, I have used an approach similar to the methods of *Niiler and Hall* (1988) and *Hall* (1991). These methods make use of the basic heat equation from which potential energy equations can be derived. Complete derivations of equations found in Chapter IV are presented within this appendix. For an excellent description of Reynolds averaging procedures, which have been used throughout these derivations, the reader is referred to *Stull* (1988).

A. MEAN AND FLUCTUATING HEAT EQUATIONS

As mentioned earlier, the fundamental equation used in this study is the basic heat (temperature) equation, which is written as

$$\frac{\partial T}{\partial t} + u\frac{\partial T}{\partial x} + v\frac{\partial T}{\partial y} + w\theta_z = 0 \qquad \text{D1}$$

where θ_z represents the actual time-varying potential temperature gradient at a given level. All variables are functions of space and time and can be partitioned into a mean and fluctuating quantity (i.e., $u = \bar{u} + u'$). By expanding each variable, equation D1 becomes

$$\frac{\partial \overline{T}}{\partial t} + \frac{\partial T'}{\partial t} + \bar{u}\frac{\partial \overline{T}}{\partial x} + \bar{u}\frac{\partial T'}{\partial x} + u'\frac{\partial \overline{T}}{\partial x} + u'\frac{\partial T'}{\partial x}$$

$$+ \bar{v}\frac{\partial \overline{T}}{\partial y} + \bar{v}\frac{\partial T'}{\partial y} + v'\frac{\partial \overline{T}}{\partial y} + v'\frac{\partial T'}{\partial y} + \overline{w}\,\bar{\theta}_z + w'\bar{\theta}_z + \overline{w}\,\theta'_z + w'\theta'_z = 0$$

where $\partial\overline{T}/\partial t$ is zero over the record length. To obtain an equation for the mean temperature field, we must take the time average of equation D1, requiring the use of Reynolds averaging procedures. By definition, the time average (denoted by an overbar) of a product, $\overline{AB}$, is equal to $\overline{A}\,\overline{B} + \overline{a'b'}$, where $A = \overline{A} + a'$, $B = \overline{B} + b'$, $\overline{\overline{A}} = \overline{A}$ and $\overline{a'} = 0$. Using the expanded form of D1, this equation becomes

$$\overline{u}\frac{\partial\overline{T}}{\partial x} + \overline{u'\frac{\partial T'}{\partial x}} + \overline{v}\frac{\partial\overline{T}}{\partial y} + \overline{v'\frac{\partial T'}{\partial y}} + \overline{w}\,\overline{\theta}_z + \overline{w'\theta'_z} = 0$$

or in vector notation,

$$\overline{\vec{v}_H}\cdot\nabla_H\overline{T} + \overline{\vec{v}_H'\cdot\nabla_H T'} + \overline{w}\,\overline{\theta}_z + \overline{w'\theta'_z} = 0 \qquad \text{D2}$$

where the subscript H denotes horizontal components and derivatives (equation (7) in Chapter IV).

Subtracting D2 from D1 yields the following equation for the fluctuating temperature field:

$$\frac{\partial T'}{\partial t} + \overline{u}\frac{\partial\overline{T}}{\partial x} + \overline{u}\frac{\partial T'}{\partial x} + u'\frac{\partial\overline{T}}{\partial x} + u'\frac{\partial T'}{\partial x}$$

$$+ \overline{v}\frac{\partial\overline{T}}{\partial y} + \overline{v}\frac{\partial T'}{\partial y} + v'\frac{\partial\overline{T}}{\partial y} + v'\frac{\partial T'}{\partial y} + \overline{w}\,\overline{\theta}_z + \overline{w}\,\theta'_z + w'\overline{\theta}_z + w'\theta'_z$$

$$- \overline{u}\frac{\partial\overline{T}}{\partial x} - \overline{u'\frac{\partial T'}{\partial x}} - \overline{v}\frac{\partial\overline{T}}{\partial y} - \overline{v'\frac{\partial T'}{\partial y}} - \overline{w}\,\overline{\theta}_z - \overline{w'\theta'_z} = 0$$

or in vector notation

$$\frac{\partial T'}{\partial t} + \vec{v} \cdot \nabla T' + \overrightarrow{v'_H} \cdot \nabla_H \overline{T} + w' \overline{\theta}_z - \overline{\vec{v'} \cdot \nabla T'} = 0 \qquad \text{D3}$$

where some cancellations have been made, and once again the subscript H denotes horizontal components. For those terms where no subscripts exist, all three components are included, however, the vertical components involve θ' in lieu of T'. This is equation (8) in Chapter IV.

B. MEAN AND EDDY POTENTIAL ENERGY EQUATIONS

The equation for mean potential energy can be obtained by multiplying D2 by $\rho_0 g \alpha \overline{T}/\overline{\theta}_z$, as follows

$$\rho_0 g \alpha \overline{T}/\overline{\theta}_z \left[\overline{u} \frac{\partial \overline{T}}{\partial x} + \overline{u' \frac{\partial T'}{\partial x}} + \overline{v} \frac{\partial \overline{T}}{\partial y} + \overline{v' \frac{\partial T'}{\partial y}} + \overline{w}\, \overline{\theta}_z \right] = 0$$

which becomes

$$\rho_0 g \alpha / \overline{\theta}_z \left[\frac{\overline{u}}{2} \frac{\partial \overline{T}^2}{\partial x} + \overline{T}\, \overline{u' \frac{\partial T'}{\partial x}} + \frac{\overline{v}}{2} \frac{\partial \overline{T}^2}{\partial y} + \overline{T}\, \overline{v' \frac{\partial T'}{\partial y}} \right] + \rho_0 g \alpha \overline{wT} = 0$$

- or -

$$\rho_0 g \alpha / \overline{\theta}_z \left[\overline{\vec{v}_H} \cdot \nabla_H \tfrac{1}{2} \overline{T}^2 + \overline{T}\, \overline{\vec{v'}_H \cdot \nabla_H T'} \right] + \rho_0 g \alpha\, \overline{wT} = 0 \qquad \text{D4}$$

This multiplicative factor is necessary to produce the proper units since energy, in CGS units, is measured in ergs (1 erg = 1 gm cm^{-2} s^{-2}), and we are ultimately interested in the rate of change of energy per unit volume (ergs cm^{-3} s^{-1}).

The mean potential energy equation has been shown for derivational purposes, but will not be examined in this study as the focus is on the energetics associated with eddy variability.

To obtain the equation for eddy potential energy we first multiply D3 by $\rho_0 g\alpha T'/\bar{\theta}_z$ as follows

$$\rho_0 g\alpha T'/\bar{\theta}_z \left[\frac{\partial T'}{\partial t} + \bar{u}\frac{\partial T'}{\partial x} + u'\frac{\partial \bar{T}}{\partial x} + u'\frac{\partial T'}{\partial x} + \bar{v}\frac{\partial T'}{\partial y} + v'\frac{\partial \bar{T}}{\partial y} + v'\frac{\partial T'}{\partial y} \right]$$

$$+ \rho_0 g\alpha T'/\bar{\theta}_z \left[\bar{w}\,\theta'_z + w'\,\bar{\theta}_z + w'\,\theta'_z - \overline{u'\frac{\partial T'}{\partial x}} - \overline{v'\frac{\partial T'}{\partial y}} - \overline{w'\theta'_z} \right] = 0 \quad , \text{ D5}$$

which can be rewritten as

$$\frac{\rho_0 g\alpha}{\bar{\theta}_z}\frac{\partial}{\partial t}\left(\frac{1}{2}T'^2\right) + \frac{\rho_0 g\alpha}{\bar{\theta}_z}\bar{u}\frac{\partial}{\partial x}\left(\frac{1}{2}T'^2\right) + \frac{\rho_0 g\alpha}{\bar{\theta}_z}u'\frac{\partial}{\partial x}\left(\frac{1}{2}T'^2\right) + \frac{\rho_0 g\alpha}{\bar{\theta}_z}u'T'\frac{\partial \bar{T}}{\partial x}$$

$$+ \frac{\rho_0 g\alpha}{\bar{\theta}_z}\bar{v}\frac{\partial}{\partial y}\left(\frac{1}{2}T'^2\right) + \frac{\rho_0 g\alpha}{\bar{\theta}_z}v'\frac{\partial}{\partial y}\left(\frac{1}{2}T'^2\right) + \frac{\rho_0 g\alpha}{\bar{\theta}_z}v'T'\frac{\partial \bar{T}}{\partial y}$$

$$+ \frac{\rho_0 g\alpha}{\bar{\theta}_z}\bar{w}\left(\frac{1}{2}\theta'^2\right)_z + \frac{\rho_0 g\alpha}{\bar{\theta}_z}w'\left(\frac{1}{2}\theta'^2\right)_z + \rho_0 g\alpha\, w'T'$$

$$= \frac{\rho_0 g\alpha}{\bar{\theta}_z}T'\,\overline{u'\frac{\partial T'}{\partial x}} + \frac{\rho_0 g\alpha}{\bar{\theta}_z}T'\,\overline{v'\frac{\partial T'}{\partial y}} + \frac{\rho_0 g\alpha}{\bar{\theta}_z}T'\,\overline{w'\theta'_z} \quad .$$

If we define eddy potential energy (EPE) as $\rho_0 g\alpha T'^2/2\bar{\theta}_z$, we can rewrite equation D5 in vector notation as follows

$$\frac{\partial EPE}{\partial t} + \vec{\bar{v}} \cdot \nabla EPE + \vec{v'} \cdot \nabla EPE + \overrightarrow{v'_H T'} \cdot \frac{\rho_0 g \alpha}{\bar{\theta}_z} \nabla_H \bar{T}$$

$$- \rho_0 g \alpha \left[\frac{\overrightarrow{v' T'^2}}{2} \cdot \nabla \left(\frac{1}{\bar{\theta}_z} \right) + \overrightarrow{v'_H T'} \bar{T} \cdot \nabla \left(\frac{1}{\bar{\theta}_z} \right) \right] + \rho_0 g \alpha \overrightarrow{w'T'} = \frac{\rho_0 g \alpha T'}{\bar{\theta}_z} \overrightarrow{\overrightarrow{v'} \cdot \nabla T'} \quad , D6$$

where again subscripts and superscripts have the same meaning. Notice that to obtain terms which represent the advection of potential energy, we must bring $\bar{\theta}_z^{-1}$ inside the ∇ operator. Using the relation. $\nabla \bullet (ab) = a \bullet \nabla b + b \bullet \nabla a$, the following terms in equation D6 were obtained

$$\frac{\vec{\bar{v}}}{\bar{\theta}_z} \cdot \nabla \left(\rho_0 g \alpha \frac{T'^2}{2} \right) = \vec{\bar{v}} \cdot \nabla EPE - \rho_0 g \alpha \vec{\bar{v}} \frac{\overrightarrow{T'^2}}{2} \cdot \nabla \left(\frac{1}{\bar{\theta}_z} \right)$$

$$\frac{\overrightarrow{v'_H T'}}{\bar{\theta}_z} \cdot \nabla_H \left(\rho_0 g \alpha \bar{T} \right) = \overrightarrow{v'_H T'} \cdot \nabla_H \left(\frac{\rho_0 g \alpha \bar{T}}{\bar{\theta}_z} \right) - \rho_0 g \alpha \overrightarrow{v'_H T'} \bar{T} \cdot \nabla_H \left(\frac{1}{\bar{\theta}_z} \right)$$

While use of this relation has produced terms which represent the advection of eddy potential energy and also a term which involves eddy heat fluxes (a measure of baroclinic instability), we see it has also produced terms which involve knowledge of the spatial variability of $\bar{\theta}_z$. Since we only have data at single moorings, it is necessary to neglect these terms (similar to *Hall* (1991)), which is consistent with quasi-geostrophic theory in which it is assumed that this basic profile is constant in space.

While these terms have been neglected, it is possible to analyze the effect of this omission by utilizing a short overlapping data segment between P2 and P3.

This may be accomplished by examining the following ratio

$$\frac{\rho_0 g\alpha \vec{v}\frac{T'^2}{2}\cdot \nabla\left(\frac{1}{\bar{\theta}_z}\right)}{\rho_0 g\alpha \frac{\vec{v}}{\bar{\theta}_z}T'\cdot\nabla(T')} \rightarrow \frac{\frac{T'}{2}\cdot\nabla\left(\frac{1}{\bar{\theta}_z}\right)}{\frac{1}{\bar{\theta}_z}\cdot\nabla(T')}$$

Considering just the x-component, this ratio can be written as

$$\frac{\rho_0 g\alpha u\frac{T'^2}{2}\cdot\frac{\partial}{\partial x}\left(\frac{1}{\bar{\theta}_z}\right)}{\rho_0 g\alpha\frac{u}{\bar{\theta}_z}T'\cdot\frac{\partial T'}{\partial x}} \rightarrow \frac{\frac{T'}{2}\cdot\frac{\partial}{\partial x}\left(\frac{1}{\bar{\theta}_z}\right)}{\frac{1}{\bar{\theta}_z}\cdot\frac{\partial T'}{\partial x}} \rightarrow \frac{T'\,\delta\bar{\theta}}{2\,\bar{\theta}\,\delta T'}$$

where the ∂z portion of $\bar{\theta}_z$ in both the numerator and denominator of this ratio cancel each other. In general, if the ratio shown above is much less than 1, the x,y dependence of $\bar{\theta}_z$ may be neglected; however, since we must omit these terms due to lack of data, this ratio will provide us with an estimate of the error associated with our treating $\bar{\theta}_z$ as a constant in the x,y plane.

Using the 6-months of data common to P2 and P3 at 225 m, we can evaluate the terms in this ratio using the following relations

$$\delta\bar{\theta} \approx \delta\bar{T} \approx \bar{T}_{P_2} - \bar{T}_{P_3} \qquad \bar{\theta} \approx \bar{T} \approx \frac{1}{2}\left(\bar{T}_{P_2} + \bar{T}_{P_3}\right)$$

and

$$\delta T' \approx \text{rms}\left(T'_{P_2} - T'_{P_3}\right) \qquad T' \approx \text{rms}\left(\frac{1}{2}\left(T'_{P_2} + T'_{P_3}\right)\right)$$

Based upon this data, the ratio has a value of 0.0113, which is much less than 1, indicating that neglecting the spatial variability of $\bar{\theta}_z$ in the x, y plane is a valid assumption in this region.

Even though we are using a specific value of $\bar{\theta}_z$ at each level, we can also examine the vertical variability of this quantity in a manner similar to that shown above. In this formulation the ratio becomes

$$\frac{\theta' \, \delta\bar{\theta}}{2 \, \bar{\theta} \, \delta\theta'} \quad ,$$

where, using the complete data sets at each level for both moorings, we can evaluate the following terms in the above ratio as

$$\delta\bar{\theta} \approx \bar{\theta}_{100} - \bar{\theta}_{350} \qquad \bar{\theta} \approx \frac{1}{2}\left(\bar{\theta}_{100} + \bar{\theta}_{350}\right)$$

$$\delta\theta' \approx \text{rms}\left(\theta'_{100} - \theta'_{350}\right) \qquad \theta' \approx \text{rms}\left(\frac{1}{2}\left(\theta'_{100} + \theta'_{350}\right)\right) \quad .$$

Based upon the full data sets, the value of this ratio was 0.0913, 0.0710, and 0.1086, for P2 225 m, 425 m, and P3 225 m, respectively. At all three levels this value is much less than 1, indicating that the vertical variability of $\bar{\theta}_z$ is also very small.

After neglecting terms which involve the spatial variability of $\bar{\theta}_z$, equation D6 becomes

$$\frac{\partial EPE}{\partial t} + \bar{\vec{v}} \cdot \nabla EPE + \vec{v'} \cdot \nabla EPE +$$

$$\overrightarrow{v'_H T'} \cdot \frac{\rho_0 g \alpha}{\bar{\theta}_z} \nabla_H \bar{T} + \rho_0 g \alpha w' T' = \frac{\rho_0 g \alpha T'}{\bar{\theta}_z} \overrightarrow{v' \cdot \nabla T'} \quad . \qquad D7$$

Interpretations of terms on the left hand side of this equation can be found in Chapter IV, while the term on the right hand side of D7 has no clear interpretation other than the mean value of eddy advection of disturbance temperature, multiplied by the fluctuating temperature (T') and a constant. As a result, the five terms on the left hand side of D7, when computed at every time step, will not sum exactly to zero, but rather to this residual term on the right hand side. In each of the three time series examined, this term was found to be at least an order of magnitude smaller than the primary balance terms in D7, and in general, the smallest of the six terms. Only when all other terms were near zero themselves did this term reach comparable magnitude. Therefore, since this term appears to provide little or no contribution to the eddy potential energy balance it may be ignored in subsequent analyses, and the reader need only be aware of its existence.

At this point we may consider whether of not the time dependence of θ_z is important or can be neglected as well. If the time dependence of θ_z is negligible, all terms involving vertical advection of disturbance temperature will be eliminated from D7. It should be noted that while it makes little difference whether the θ_z or $\bar{\theta}_z$ is used in computing vertical velocities from equation D1(Figures D1-D3), it may be very important in the calculation of the advective terms in the energy equation. Therefore, to examine the importance of vertical advection in relation to horizontal advection, we must consider the following ratio

$$\frac{w \frac{\partial}{\partial z}\left(\frac{\rho_0 g \alpha \theta'^2}{2\,\bar{\theta}_z}\right)}{\vec{v}_H \cdot \nabla_H \left(\frac{\rho_0 g \alpha T'^2}{2\,\bar{\theta}_z}\right)} \quad \rightarrow \quad \frac{w \frac{\partial \theta'}{\partial z}}{\vec{v}_H \cdot \nabla_H T'} \; .$$

Time series of both the horizontal and vertical components of advection of disturbance temperature (Figures D4-D6), computed at each mooring, indicate that the time variability of θ_z is important and should not be neglected from equation D7. To obtain the mean values of the terms in the eddy potential energy equation, we simply take the time average of D7, which becomes

$$\frac{\partial \overline{EPE}}{\partial t} + \overline{\vec{\vec{v}} \cdot \nabla EPE} + \overline{\vec{v}' \cdot \nabla EPE}$$

$$\overline{\vec{v}'_H T'} \cdot \frac{\rho_0 g \alpha}{\bar{\theta}_z} \nabla_H \bar{T} + \rho_0 g \alpha \overline{w'T'} = 0 \quad , \qquad \text{D8}$$

which is equation (12) in Chapter IV, and equation 3.1 in *Hall* (1991).

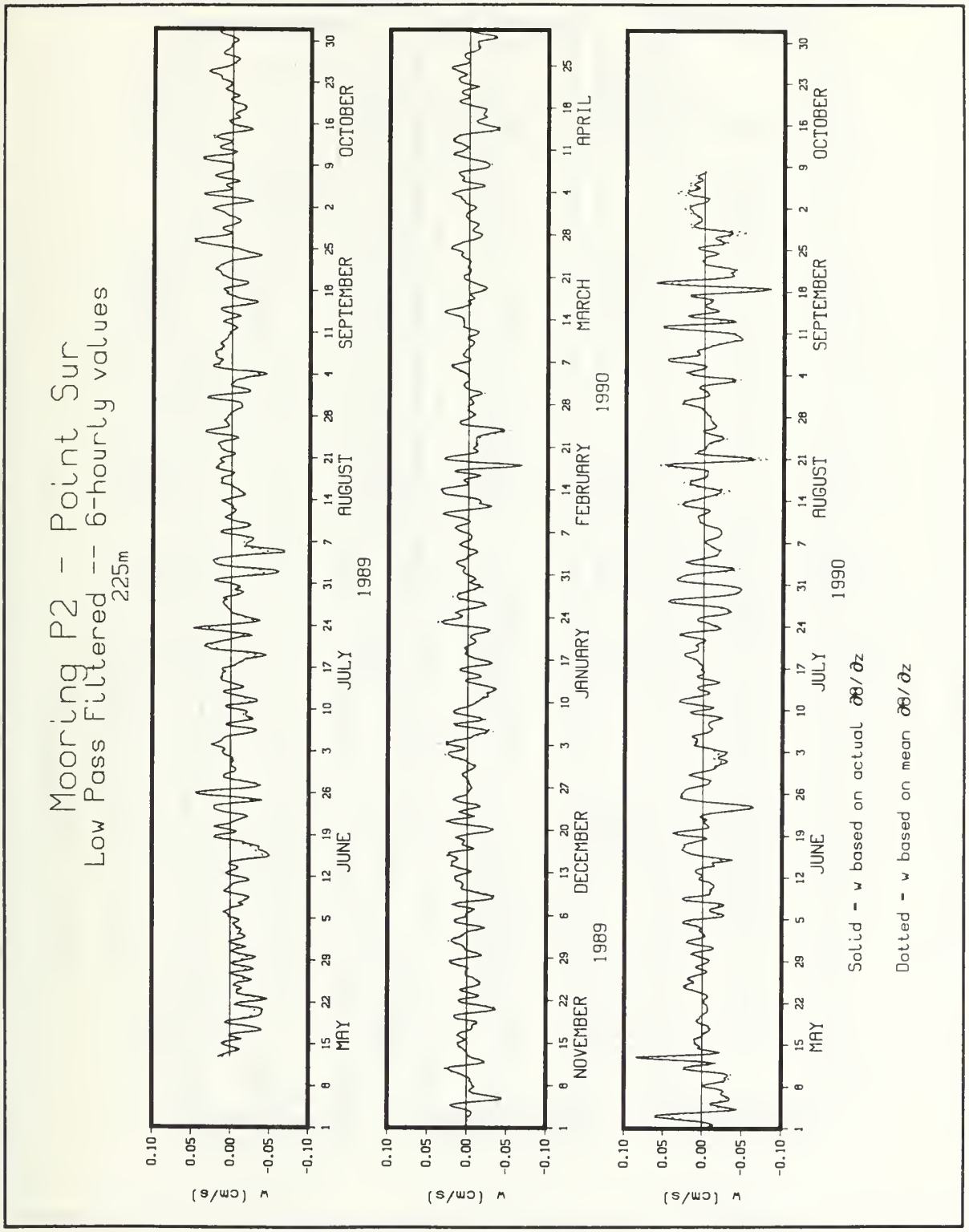

Figure D1. Vertical Velocities at Mooring P2 - 225 m: Solid (dotted) curve is based upon θ_z ($\overline{\theta_z}$). Units are cm s^{-1}.

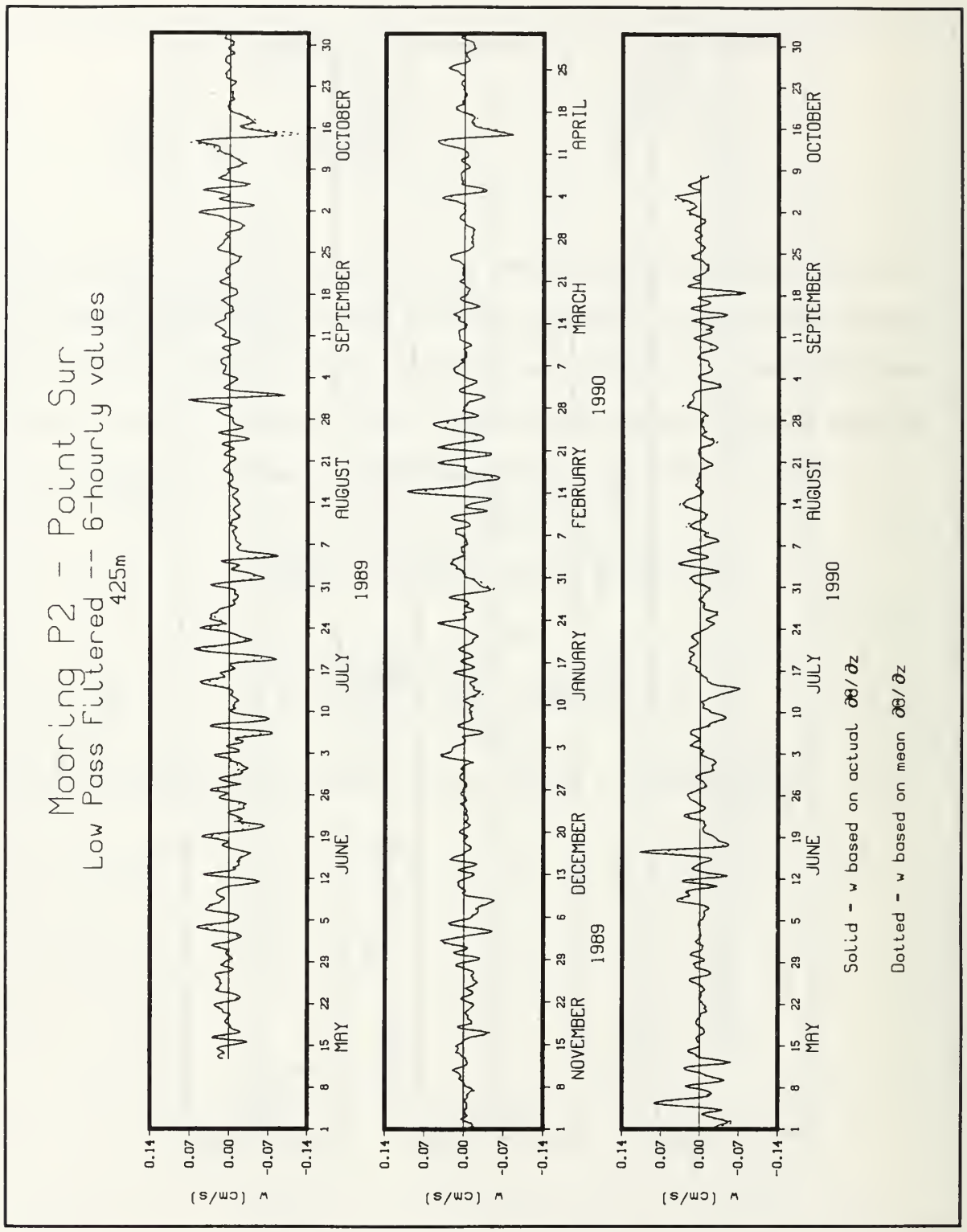

Figure D2. Vertical Velocities at Mooring P2 - 425 m: Solid (dotted) curve is based upon θ_z $(\bar{\theta}_z)$. Units are cm s^{-1}.

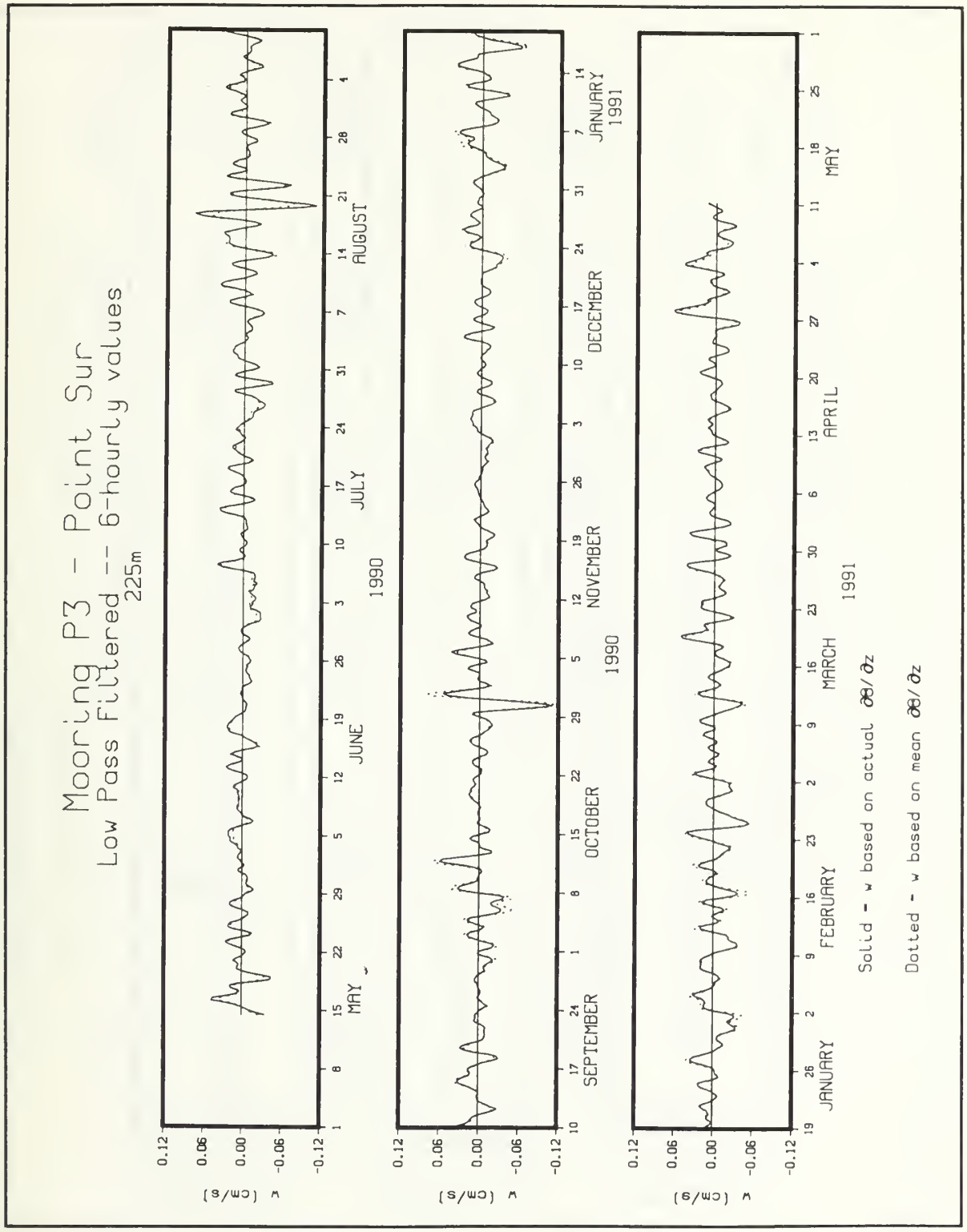

Figure D3. Vertical Velocities at Mooring P3 - 225 m: Solid (dotted) curve is based upon $\theta_z (\overline{\theta_z})$. Units are cm s^{-1}.

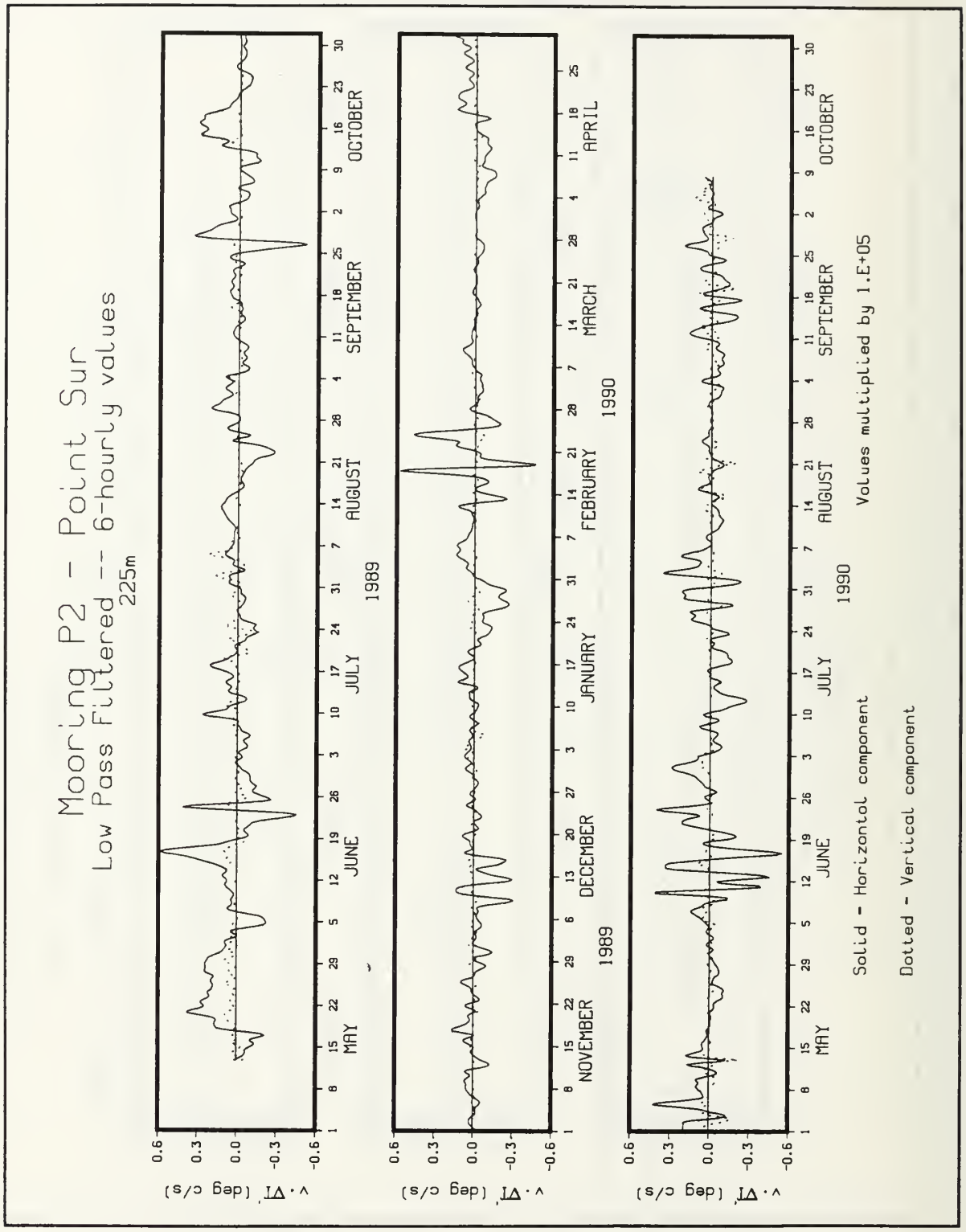

Figure D4. Advection of T' at Mooring P2 - 225 m: Solid (dotted) curve is horizontal (vertical) component. Units are °C s^{-1}.

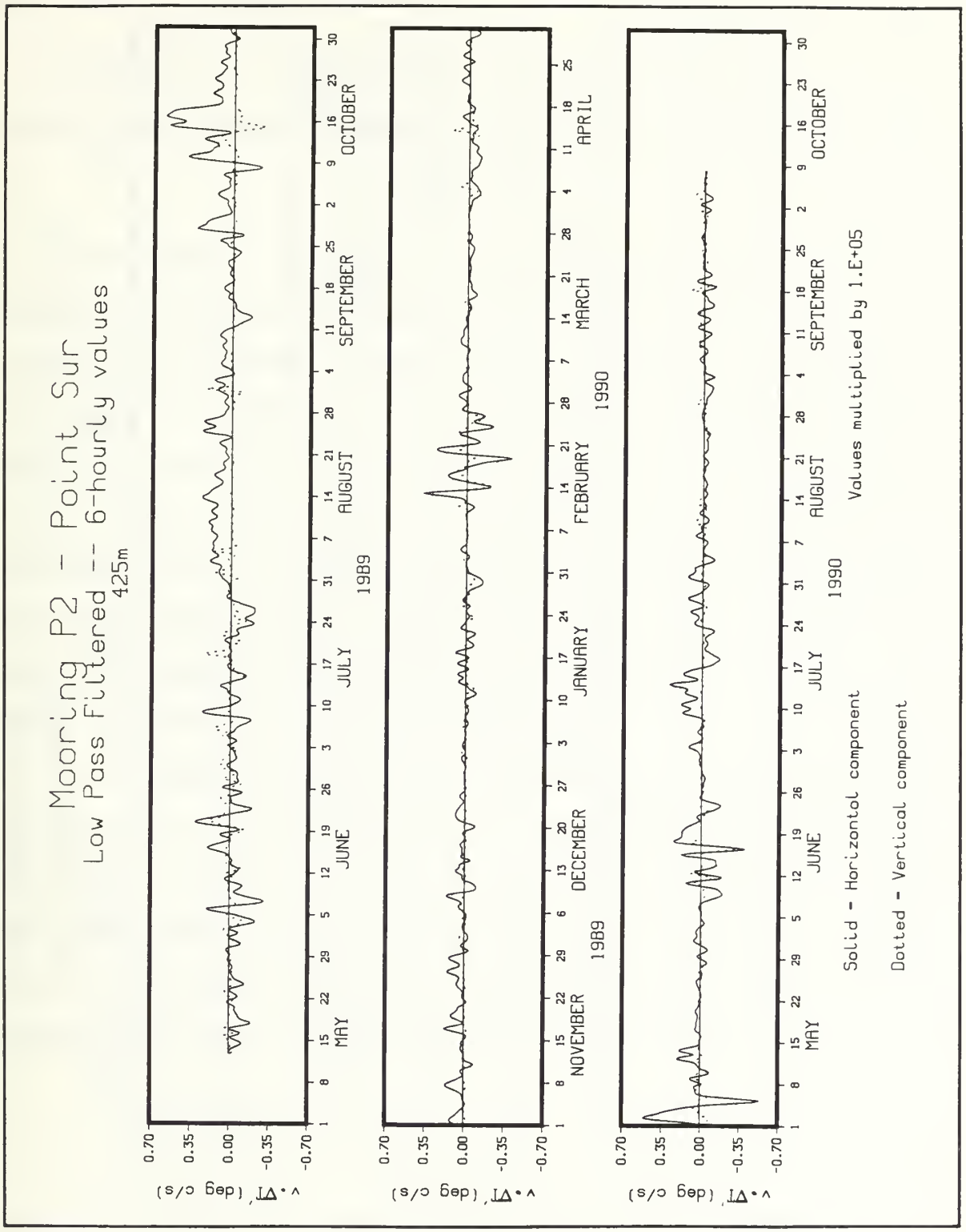

Figure D5. Advection of T' at Mooring P2 - 425 m: Solid (dotted) curve is horizontal (vertical) component. Units are °C s^{-1}.

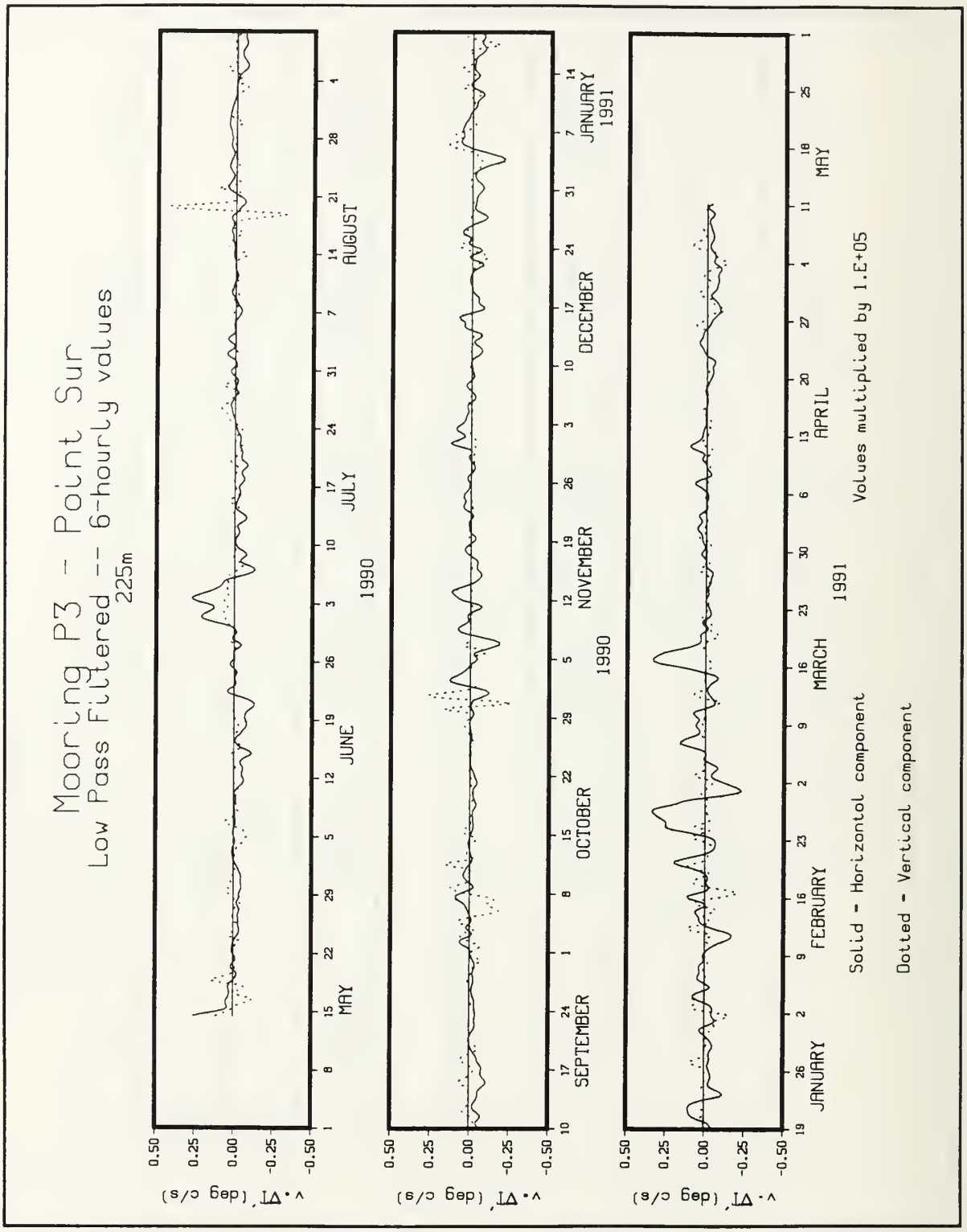

Figure D6. Advection of T' at Mooring P3 - 225 m: Solid (dotted) curve is horizontal (vertical) component. Units are °C s^{-1}.

APPENDIX E - TIME SERIES PLOTS OF TERMS IN THE EDDY POTENTIAL ENERGY EQUATION AT MOORINGS P2 AND P3

The data shown in this appendix have been computed using equation 10 in Chapter IV and represent six hourly values. There are two kinds of plots contained in this Appendix: 1) Time series plots of the five terms in equation 10 (see Chapter IV for definitions), where all values have been multiplied by 10^3; and 2) Time series plots of EPE, w', T', $\vec{v}'_H$, ∇_HEPE, and ∇_zEPE, where the latter two have been multiplied by 10^4. As expected, the values of ∇_zEPE are much larger than ∇_HEPE, since the vertical gradients of temperature are much greater than the horizontal gradients. However, when multiplied by w', which is much smaller in magnitude, the resulting advective components are of similar or smaller magnitude than the horizontal components.

For consistency and ease in analysis, these plots will be shown back to back in consecutive order. As in Appendix A, the orientation of all vectors are such that north is in the direction of the positive y-axis. Please notice that there are scale changes between levels and moorings, especially for mooring P3, where the size of the Local and VEHF terms required a much larger range than the remaining three terms. Units are as indicated on respective plots.

EDDY POTENTIAL ENERGY AT MOORING P2 - 225 M

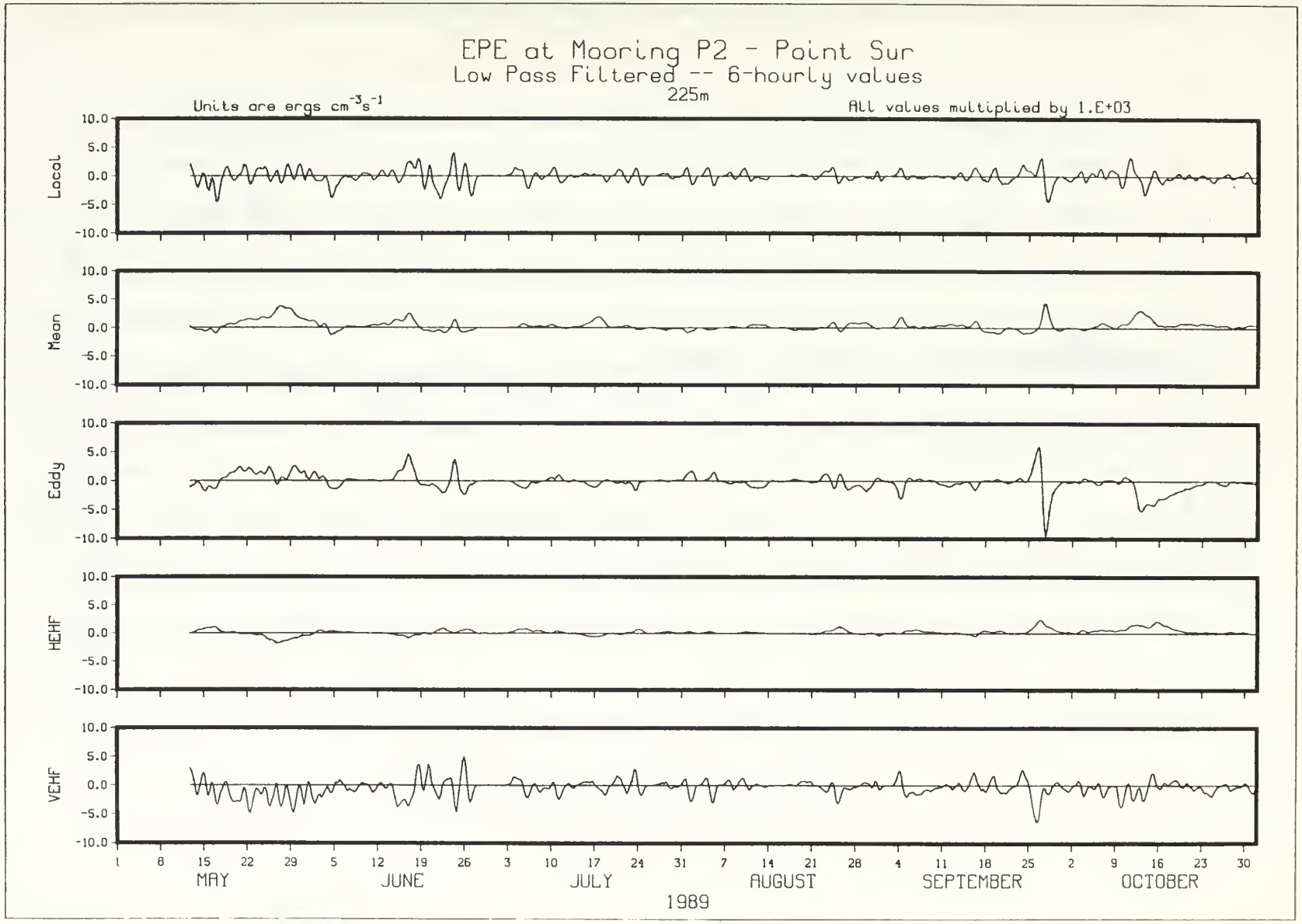
EPE at Mooring P2 - Point Sur
Low Pass Filtered -- 6-hourly values
225m
Units are ergs cm^{-3}s^{-1}
All values multiplied by 1.E+03
Local
Mean
Eddy
HEHF
VEHF
10.0
5.0
0.0
-5.0
-10.0
1 8 15 22 29 5 12 19 26 3 10 17 24 31 7 14 21 28 4 11 18 25 2 9 16 23 30
MAY
JUNE
JULY
AUGUST
SEPTEMBER
OCTOBER
1989

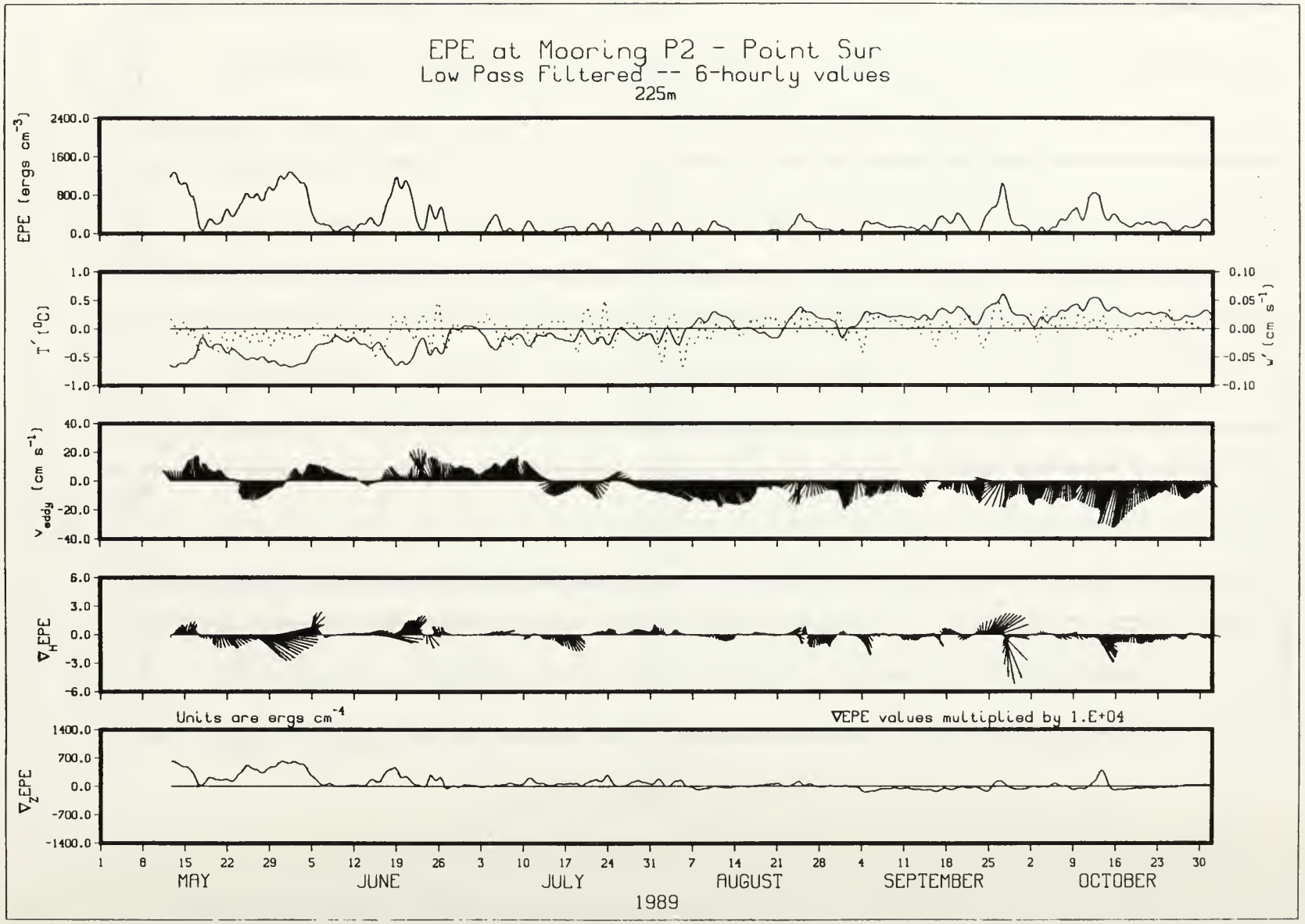
EPE at Mooring P2 - Point Sur
Low Pass Filtered -- 6-hourly values
225m
EPE (ergs cm-3)
2400.0
1600.0
800.0
0.0
T' (°C)
1.0
0.5
0.0
-0.5
-1.0
w' (cm s-1)
0.10
0.05
0.00
-0.05
-0.10
veddy (cm s-1)
40.0
20.0
0.0
-20.0
-40.0
∇HEPE
6.0
3.0
0.0
-3.0
-6.0
Units are ergs cm-4
∇EPE values multiplied by 1.E+04
∇zEPE
1400.0
700.0
0.0
-700.0
-1400.0
1 8 15 22 29 5 12 19 26 3 10 17 24 31 7 14 21 28 4 11 18 25 2 9 16 23 30
MAY
JUNE
JULY
AUGUST
SEPTEMBER
OCTOBER
1989

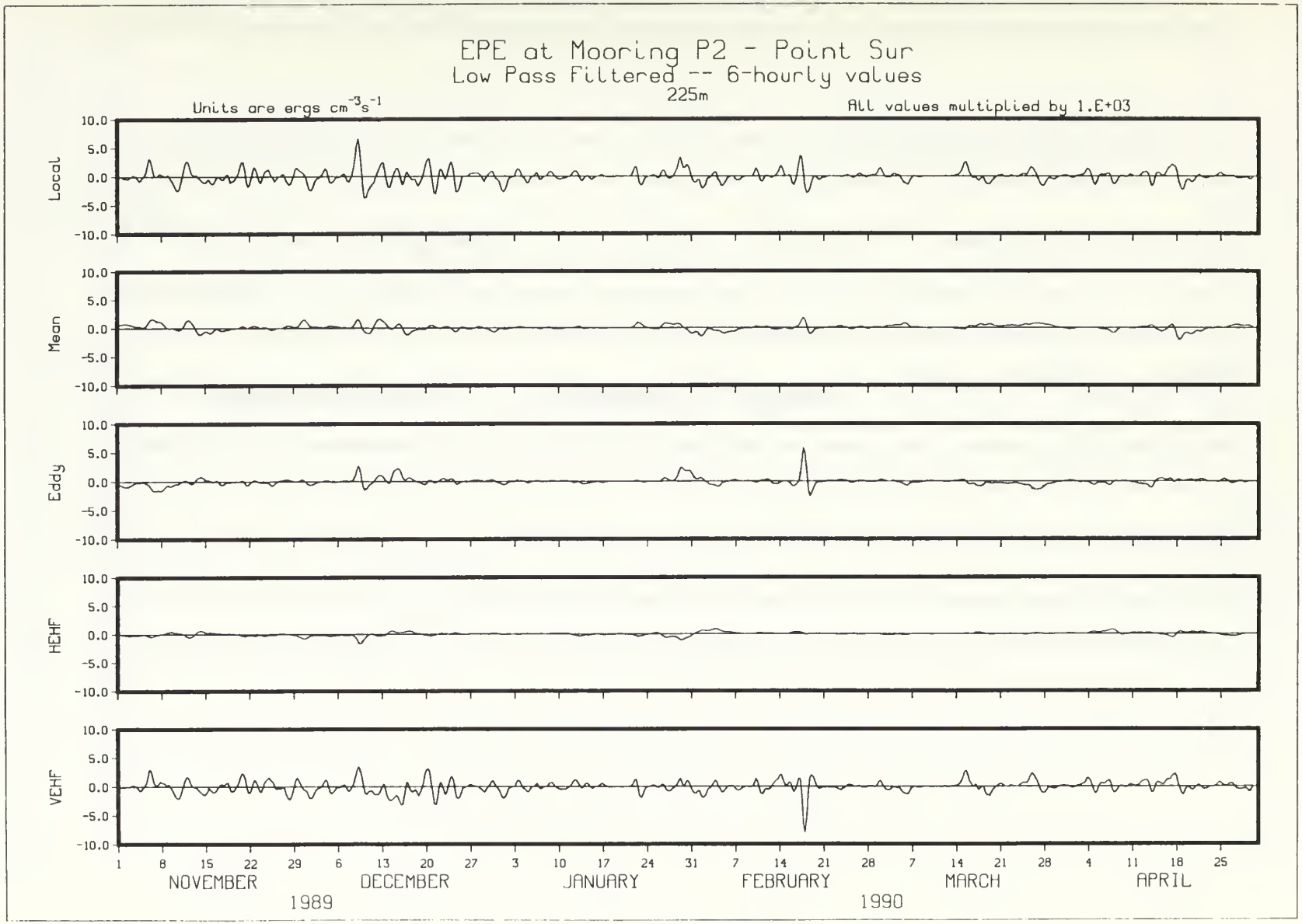
EPE at Mooring P2 - Point Sur
Low Pass Filtered -- 6-hourly values
225m
Units are ergs cm-3s-1
All values multiplied by 1.E+03
Local
Mean
Eddy
HEHF
VEHF
10.0
5.0
0.0
-5.0
-10.0
1 8 15 22 29 6 13 20 27 3 10 17 24 31 7 14 21 28 7 14 21 28 4 11 18 25
NOVEMBER
DECEMBER
JANUARY
FEBRUARY
MARCH
APRIL
1989
1990

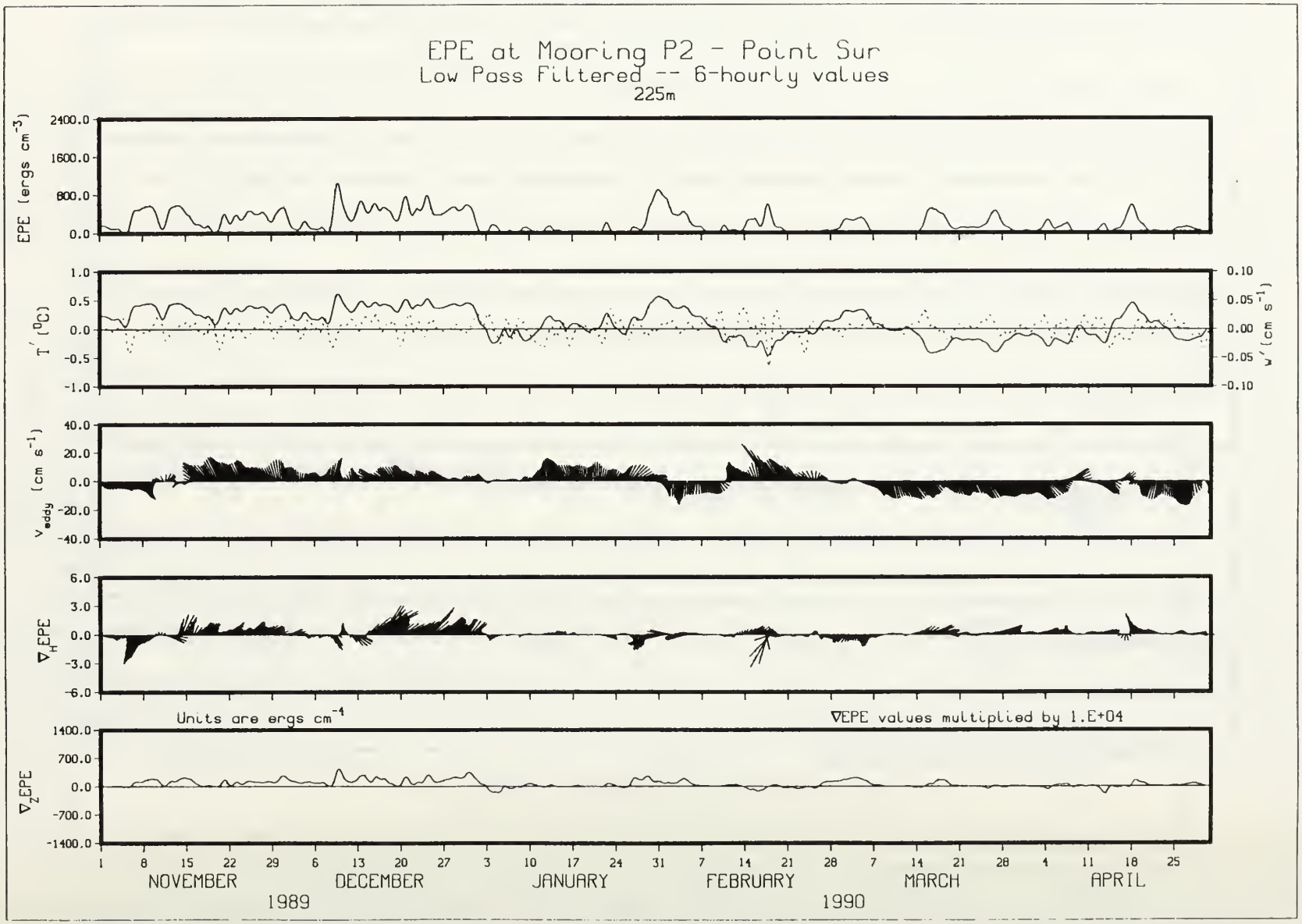
EPE at Mooring P2 - Point Sur
Low Pass Filtered -- 6-hourly values
225m
EPE (ergs cm-3)
2400.0
1600.0
800.0
0.0
T' (°C)
1.0
0.5
0.0
-0.5
-1.0
w' (cm s-1)
0.10
0.05
0.00
-0.05
-0.10
v eddy (cm s-1)
40.0
20.0
0.0
-20.0
-40.0
∇HEPE
6.0
3.0
0.0
-3.0
-6.0
Units are ergs cm-1
∇EPE values multiplied by 1.E+04
∇ZEPE
1400.0
700.0
0.0
-700.0
-1400.0
1 8 15 22 29 6 13 20 27 3 10 17 24 31 7 14 21 28 7 14 21 28 4 11 18 25
NOVEMBER
DECEMBER
JANUARY
FEBRUARY
MARCH
APRIL
1989
1990

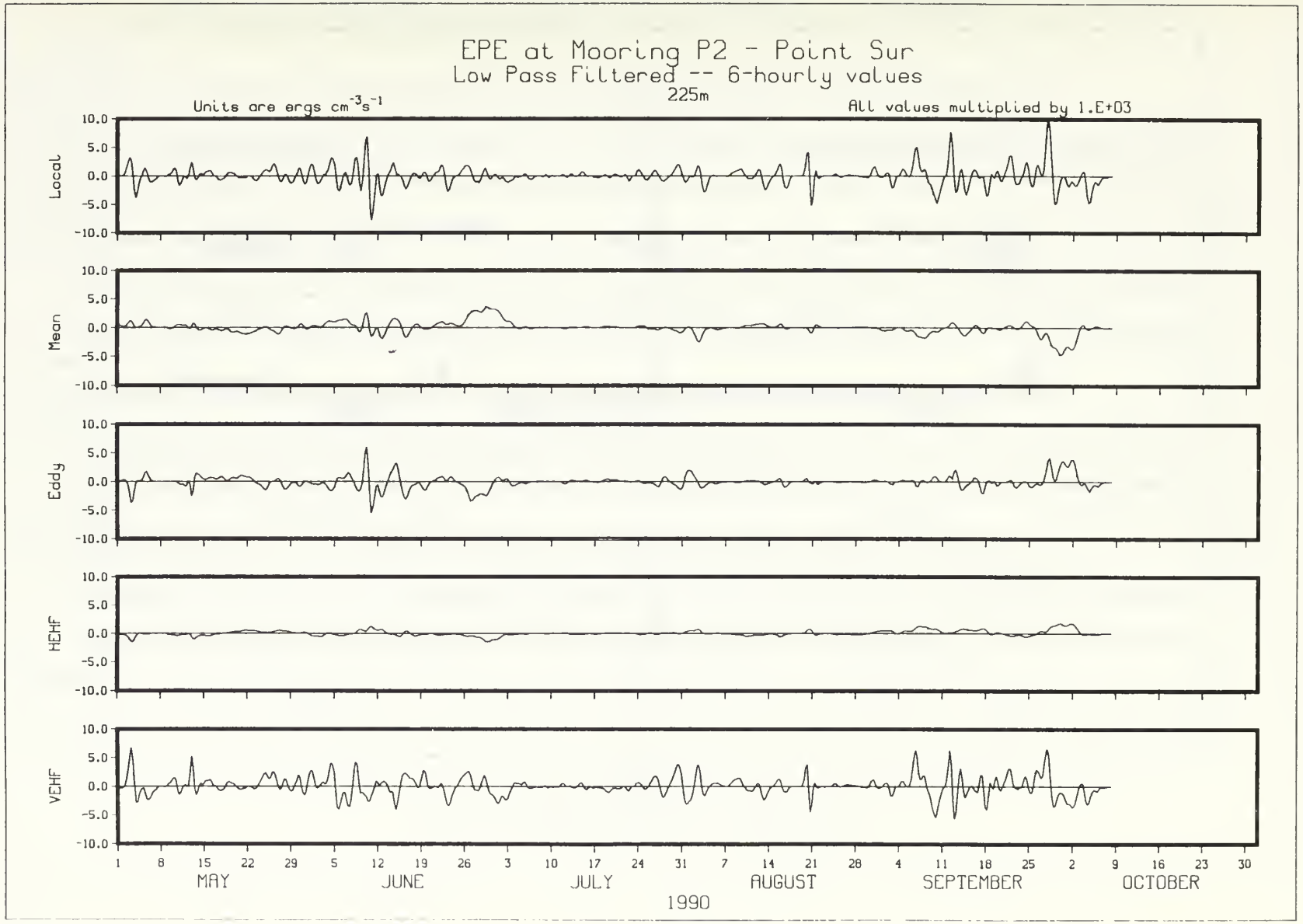
EPE at Mooring P2 - Point Sur
Low Pass Filtered -- 6-hourly values
225m
Units are ergs cm-3s-1
All values multiplied by 1.E+03
Local
Mean
Eddy
HEHF
VEHF
10.0
5.0
0.0
-5.0
-10.0
1 8 15 22 29 5 12 19 26 3 10 17 24 31 7 14 21 28 4 11 18 25 2 9 16 23 30
MAY
JUNE
JULY
AUGUST
SEPTEMBER
OCTOBER
1990

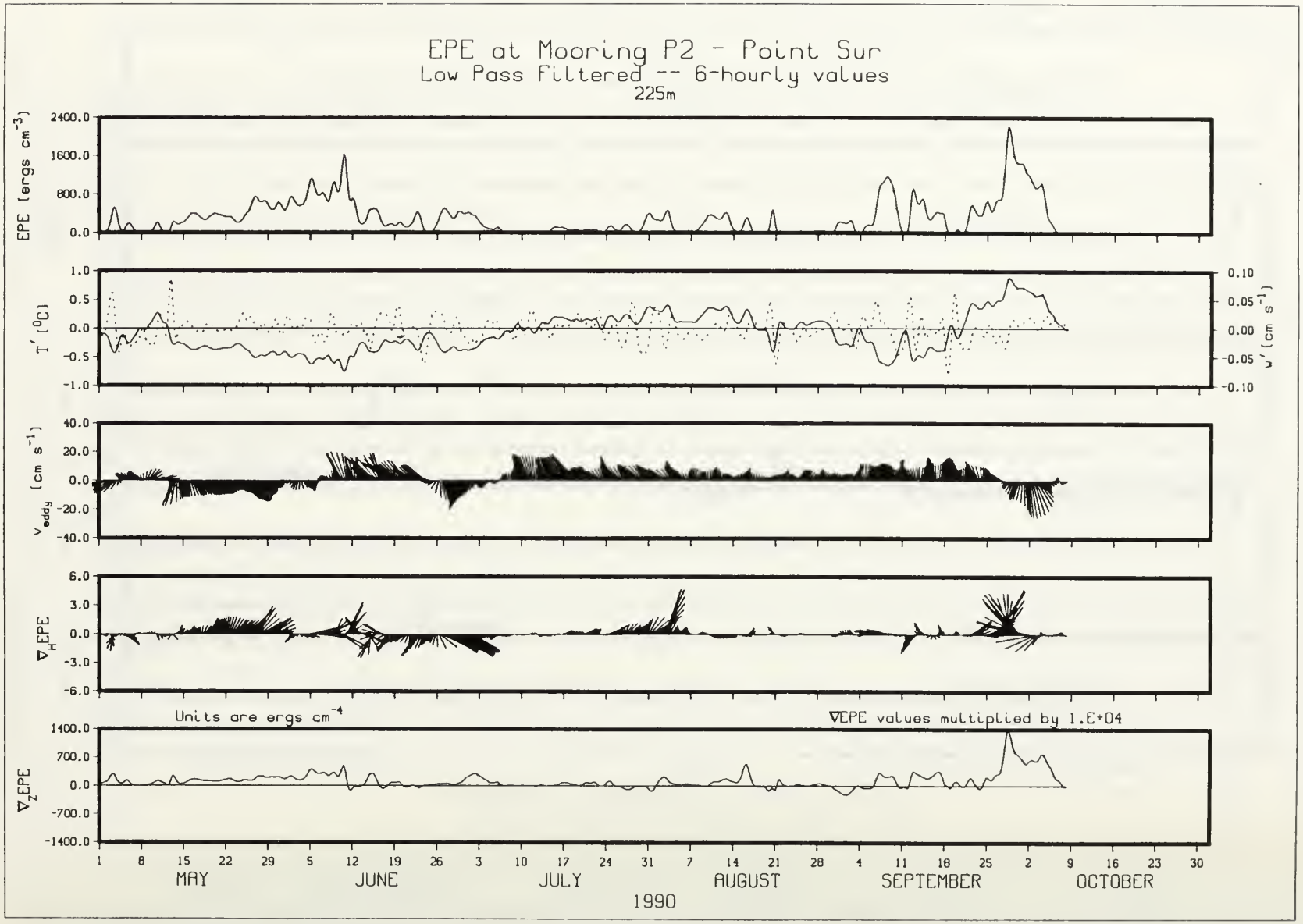
EPE at Mooring P2 - Point Sur
Low Pass Filtered -- 6-hourly values
225m
EPE (ergs cm^{-3})
2400.0
1600.0
800.0
0.0
T' (^{0}C)
1.0
0.5
0.0
-0.5
-1.0
w' (cm s^{-1})
0.10
0.05
0.00
-0.05
-0.10
v_{eddy} (cm s^{-1})
40.0
20.0
0.0
-20.0
-40.0
∇_HEPE
6.0
3.0
0.0
-3.0
-6.0
Units are ergs cm^{-4}
∇EPE values multiplied by 1.E+04
∇_zEPE
1400.0
700.0
0.0
-700.0
-1400.0
1 8 15 22 29 5 12 19 26 3 10 17 24 31 7 14 21 28 4 11 18 25 2 9 16 23 30
MAY
JUNE
JULY
AUGUST
SEPTEMBER
OCTOBER
1990

EDDY POTENTIAL ENERGY AT MOORING P2 - 425 M

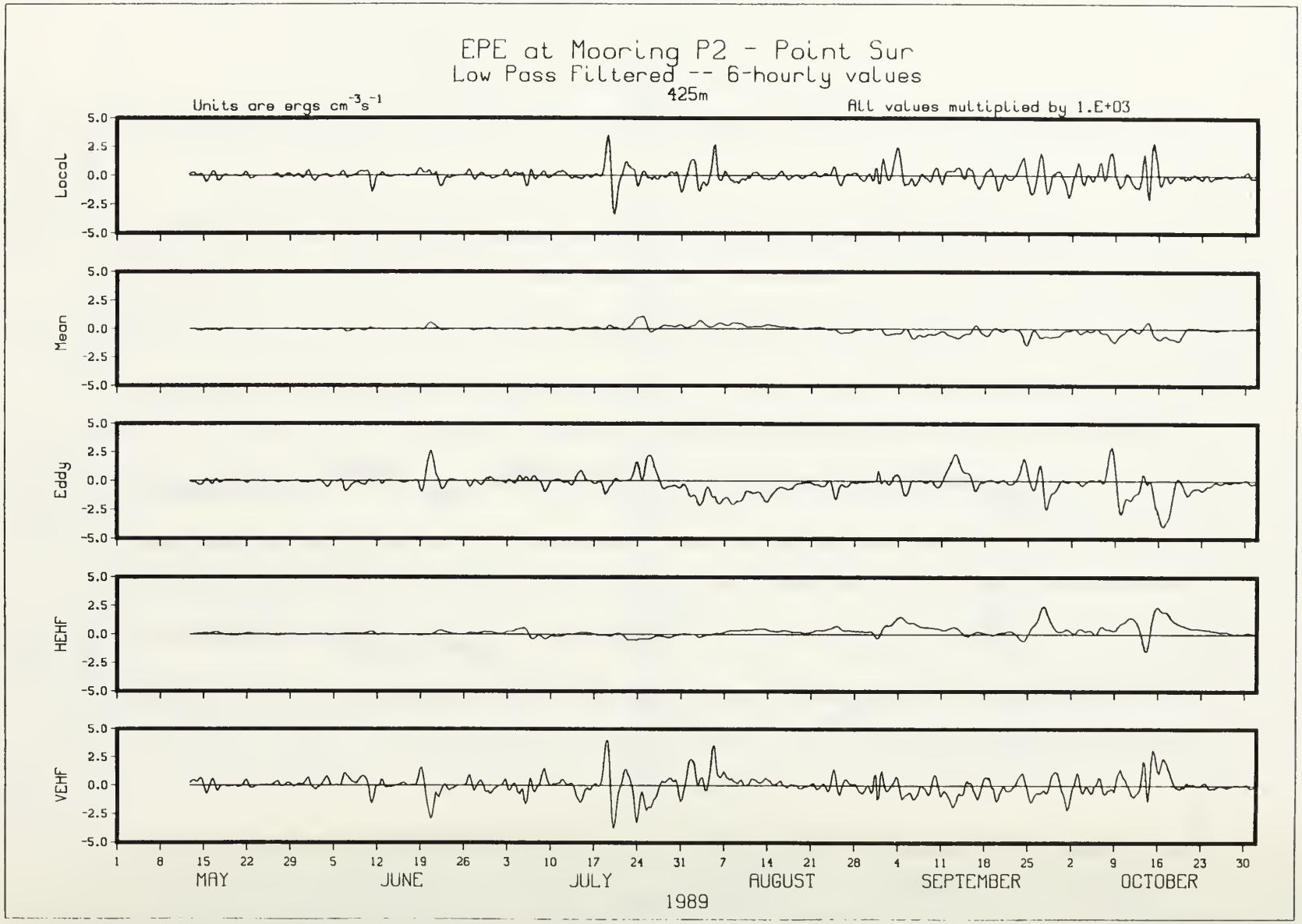
EPE at Mooring P2 - Point Sur
Low Pass Filtered -- 6-hourly values
425m
Units are ergs cm-3s-1
All values multiplied by 1.E+03
Local
Mean
Eddy
HEHF
VEHF
5.0
2.5
0.0
-2.5
-5.0
1 8 15 22 29 5 12 19 26 3 10 17 24 31 7 14 21 28 4 11 18 25 2 9 16 23 30
MAY
JUNE
JULY
AUGUST
SEPTEMBER
OCTOBER
1989

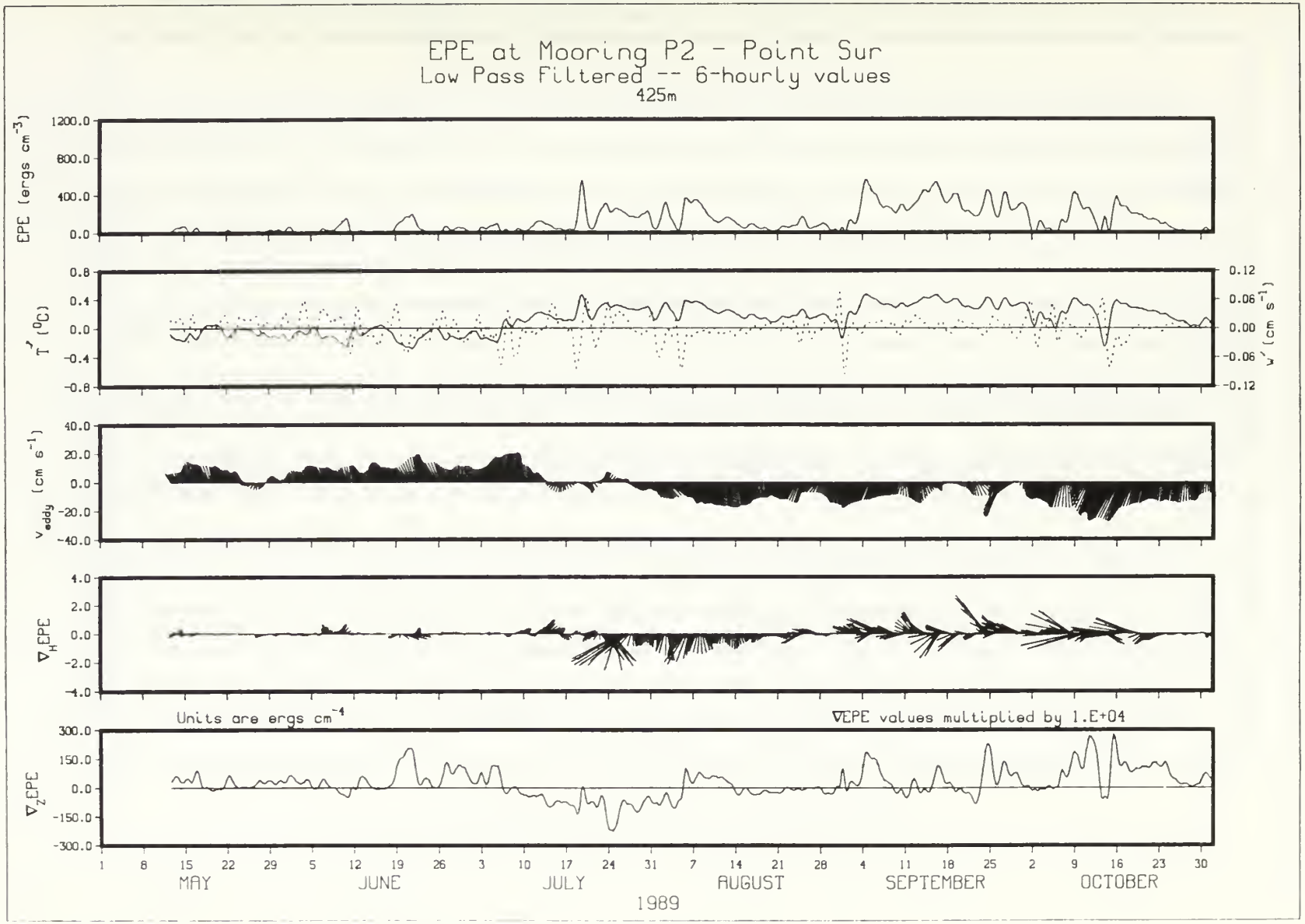
EPE at Mooring P2 - Point Sur
Low Pass Filtered -- 6-hourly values
425m
EPE (ergs cm-3)
1200.0
800.0
400.0
0.0
T' (°C)
0.8
0.4
0.0
-0.4
-0.8
w' (cm s-1)
0.12
0.06
0.00
-0.06
-0.12
veddy (cm s-1)
40.0
20.0
0.0
-20.0
-40.0
∇HEPE
4.0
2.0
0.0
-2.0
-4.0
Units are ergs cm-4
∇EPE values multiplied by 1.E+04
∇ZEPE
300.0
150.0
0.0
-150.0
-300.0
1 8 15 22 29 5 12 19 26 3 10 17 24 31 7 14 21 28 4 11 18 25 2 9 16 23 30
MAY JUNE JULY AUGUST SEPTEMBER OCTOBER
1989

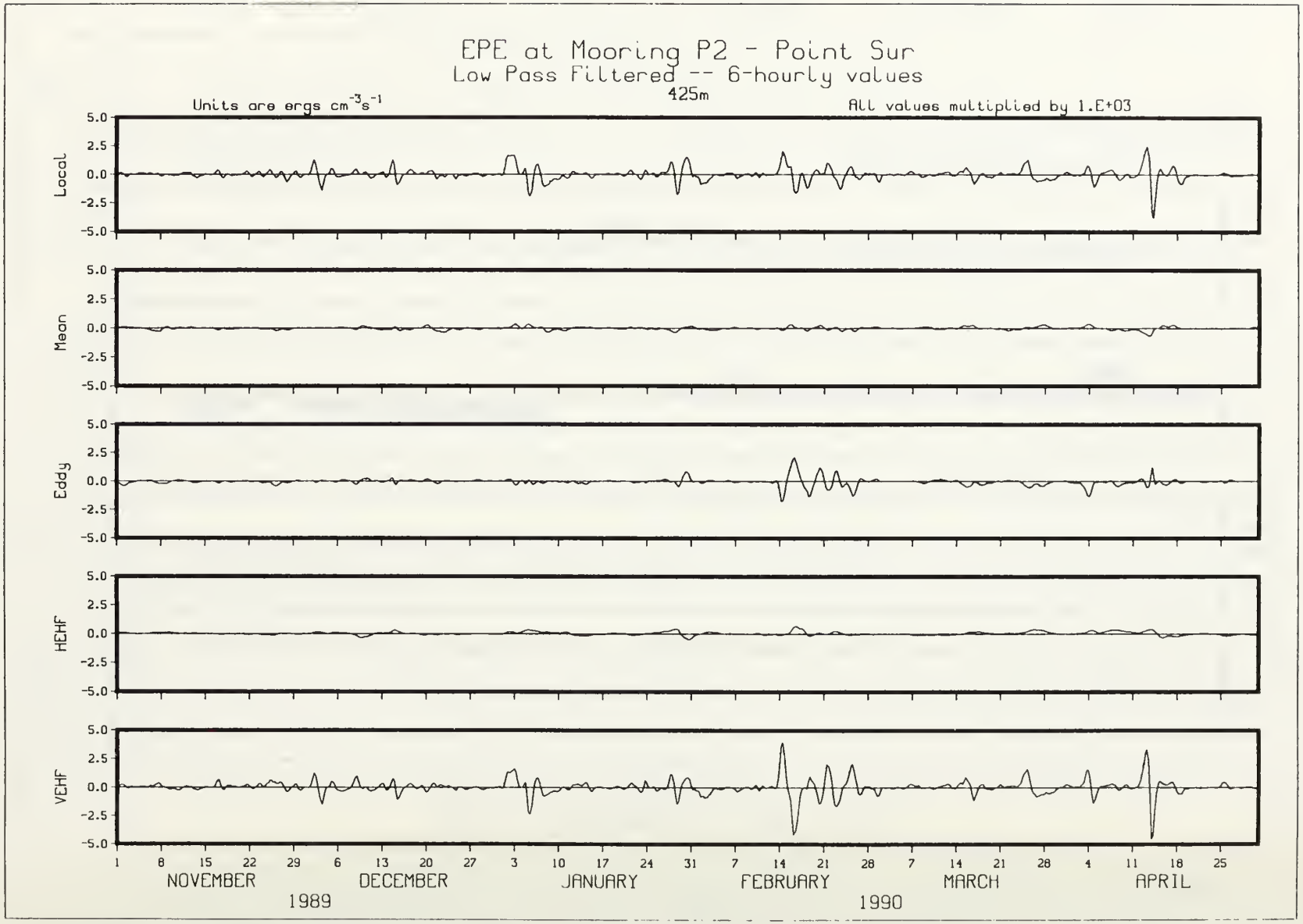
EPE at Mooring P2 - Point Sur
Low Pass Filtered -- 6-hourly values
425m
Units are ergs cm-3s-1
All values multiplied by 1.E+03
Local
Mean
Eddy
HEHF
VEHF
5.0
2.5
0.0
-2.5
-5.0
1 8 15 22 29 6 13 20 27 3 10 17 24 31 7 14 21 28 7 14 21 28 4 11 18 25
NOVEMBER
DECEMBER
JANUARY
FEBRUARY
MARCH
APRIL
1989
1990

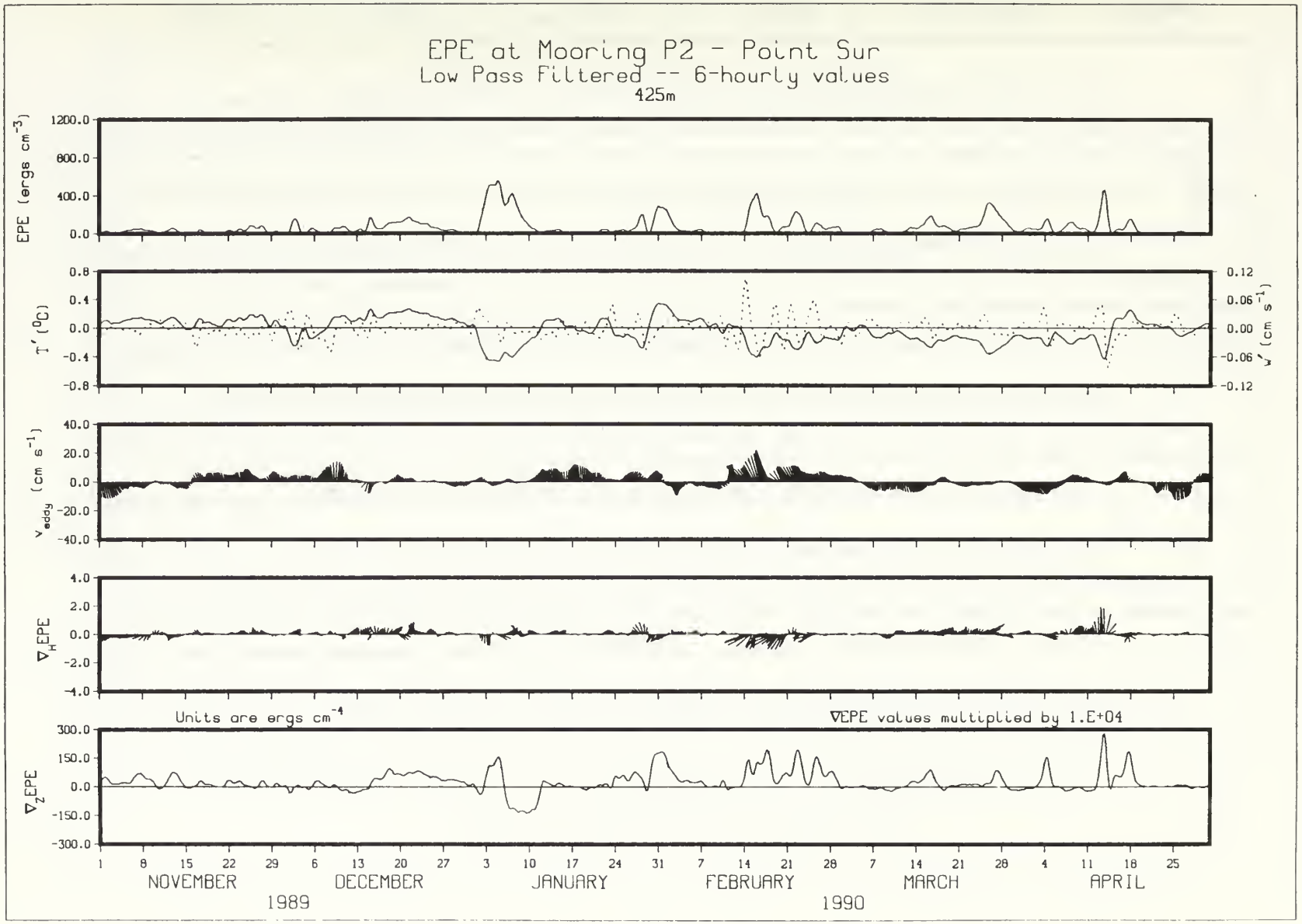
EPE at Mooring P2 - Point Sur
Low Pass Filtered -- 6-hourly values
425m
EPE (ergs cm^{-3})
1200.0
800.0
400.0
0.0
T' (^{0}C)
0.8
0.4
0.0
-0.4
-0.8
w' (cm s^{-1})
0.12
0.06
0.00
-0.06
-0.12
v$_{eddy}$ (cm s^{-1})
40.0
20.0
0.0
-20.0
-40.0
∇_HEPE
4.0
2.0
0.0
-2.0
-4.0
Units are ergs cm^{-4}
∇EPE values multiplied by 1.E+04
∇_zEPE
300.0
150.0
0.0
-150.0
-300.0
1 8 15 22 29 6 13 20 27 3 10 17 24 31 7 14 21 28 7 14 21 28 4 11 18 25
NOVEMBER
DECEMBER
JANUARY
FEBRUARY
MARCH
APRIL
1989
1990

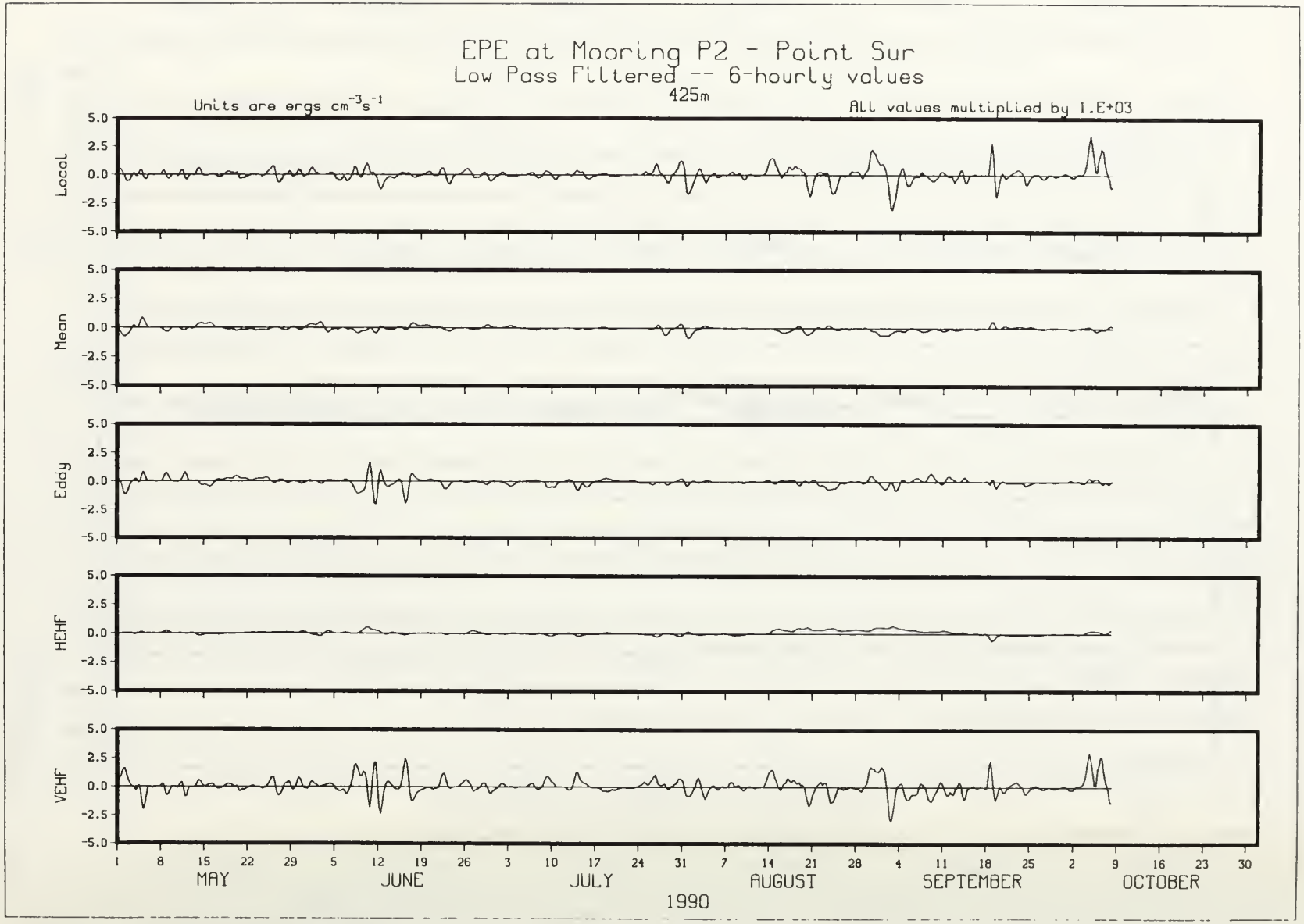
EPE at Mooring P2 - Point Sur
Low Pass Filtered -- 6-hourly values
425m
Units are ergs cm^{-3}s^{-1}
All values multiplied by 1.E+03
Local
Mean
Eddy
HEHF
VEHF
5.0
2.5
0.0
-2.5
-5.0
1 8 15 22 29 5 12 19 26 3 10 17 24 31 7 14 21 28 4 11 18 25 2 9 16 23 30
MAY
JUNE
JULY
AUGUST
SEPTEMBER
OCTOBER
1990

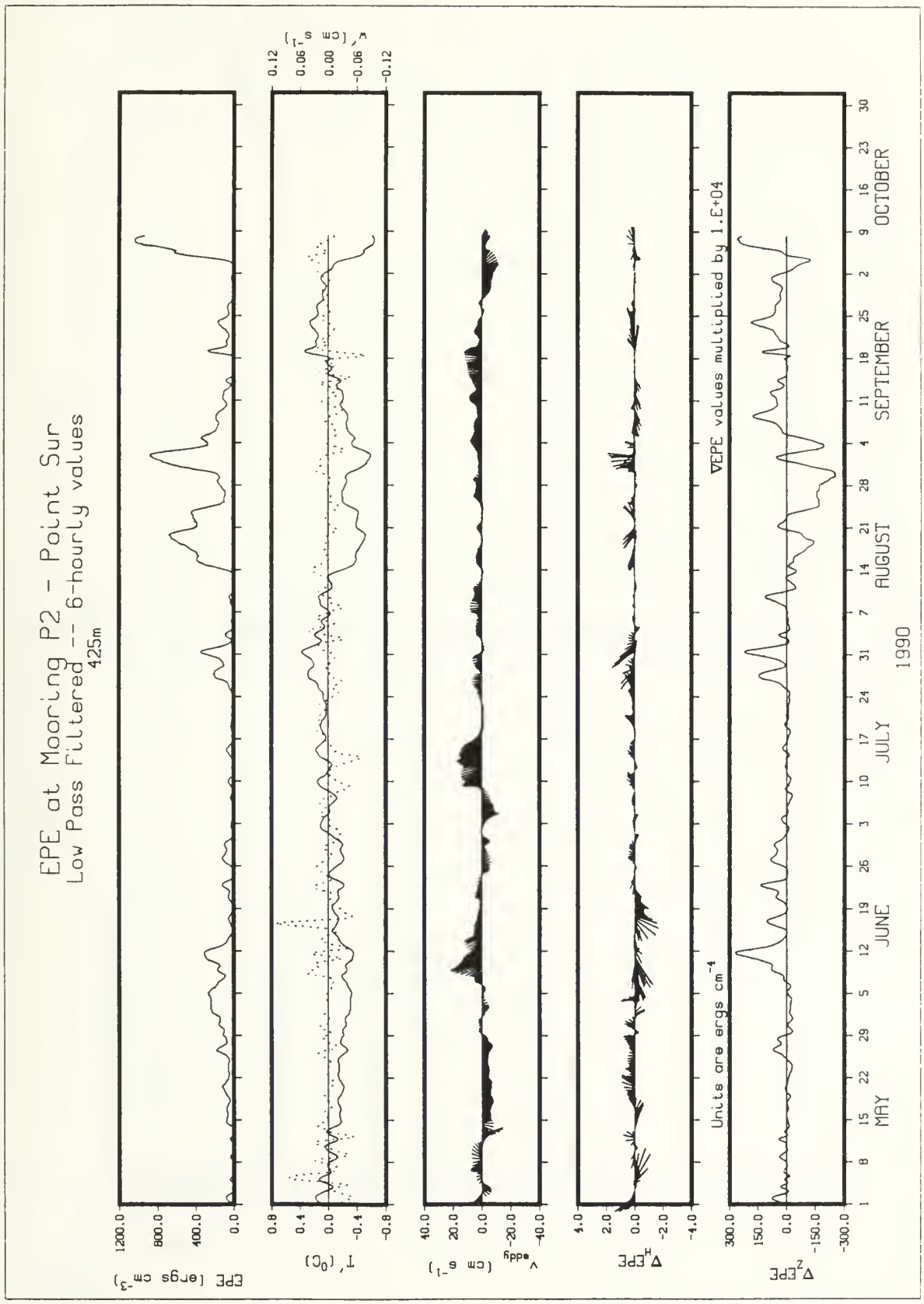
EPE at Mooring P2 - Point Sur
Low Pass Filtered -- 6-hourly values
425m
EPE (ergs cm-3)
T' (°C)
v'eddy (cm s-1)
∇HEPE
∇ZEPE
Units are ergs cm-4
∇EPE values multiplied by 1.E+04
MAY
JUNE
JULY
AUGUST
SEPTEMBER
OCTOBER
1990

EDDY POTENTIAL ENERGY AT MOORING P3 - 225 M

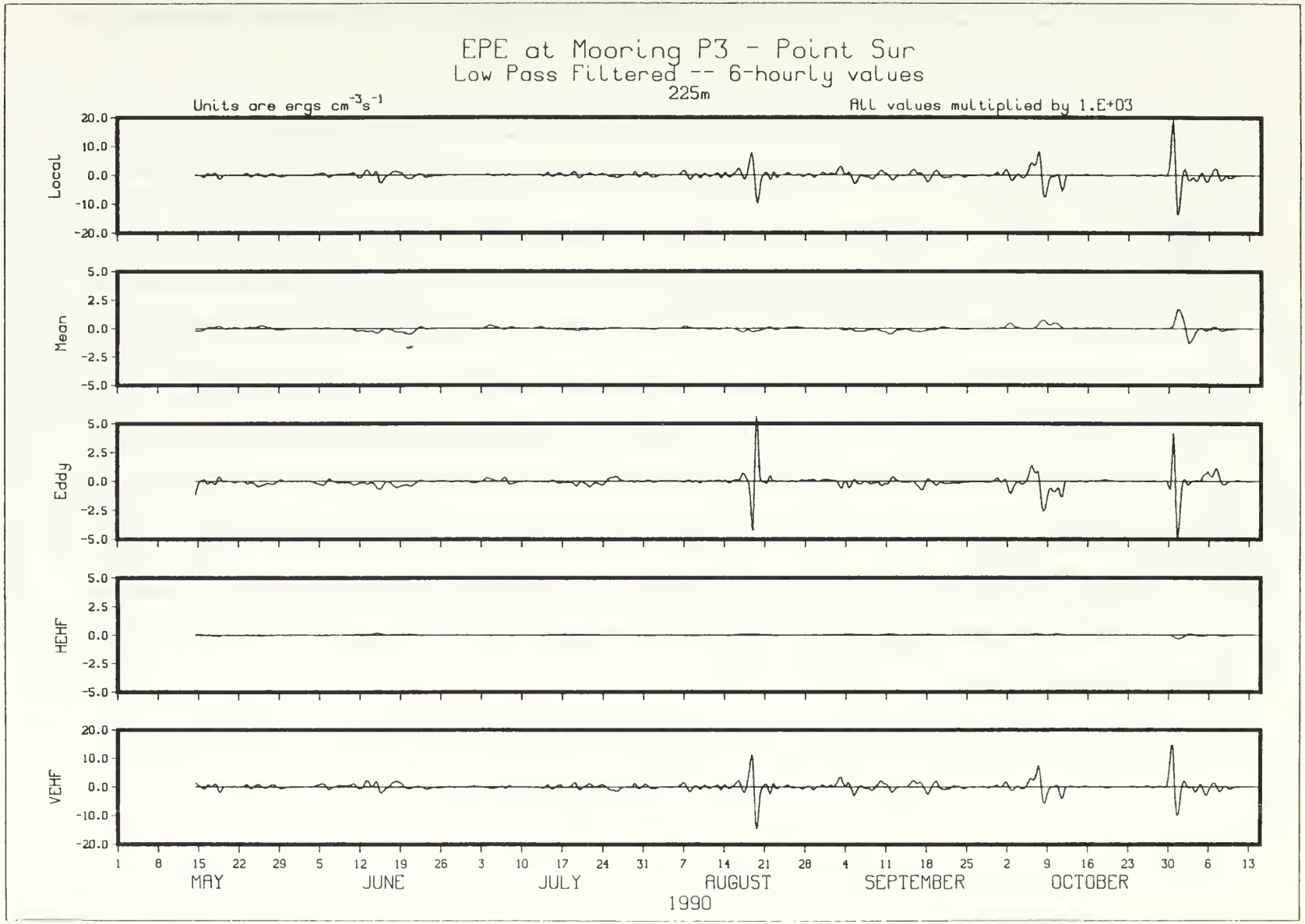
EPE at Mooring P3 - Point Sur
Low Pass Filtered -- 6-hourly values
225m
Units are ergs cm^{-3}s^{-1}
All values multiplied by 1.E+03
Local
Mean
Eddy
HEHF
VEHF
20.0
10.0
0.0
-10.0
-20.0
5.0
2.5
0.0
-2.5
-5.0
1 8 15 22 29 5 12 19 26 3 10 17 24 31 7 14 21 28 4 11 18 25 2 9 16 23 30 6 13
MAY
JUNE
JULY
AUGUST
SEPTEMBER
OCTOBER
1990

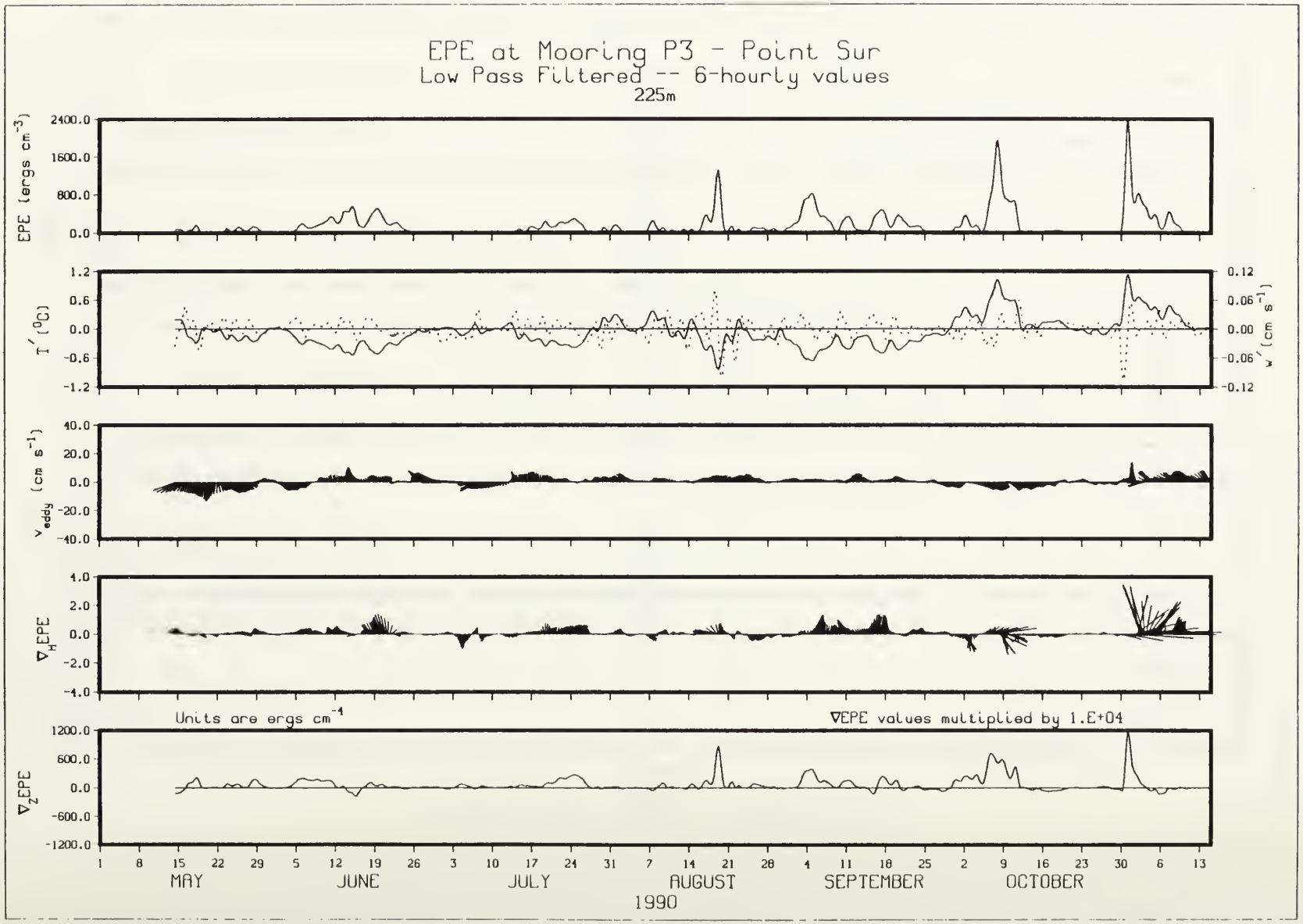
EPE at Mooring P3 - Point Sur
Low Pass Filtered -- 6-hourly values
225m
EPE (ergs cm-3)
2400.0
1600.0
800.0
0.0
T' (°C)
1.2
0.6
0.0
-0.6
-1.2
w' (cm s-1)
0.12
0.06
0.00
-0.06
-0.12
veddy (cm s-1)
40.0
20.0
0.0
-20.0
-40.0
∇HEPE
4.0
2.0
0.0
-2.0
-4.0
Units are ergs cm-4
∇EPE values multiplied by 1.E+04
∇2EPE
1200.0
600.0
0.0
-600.0
-1200.0
1 8 15 22 29 5 12 19 26 3 10 17 24 31 7 14 21 28 4 11 18 25 2 9 16 23 30 6 13
MAY
JUNE
JULY
AUGUST
SEPTEMBER
OCTOBER
1990

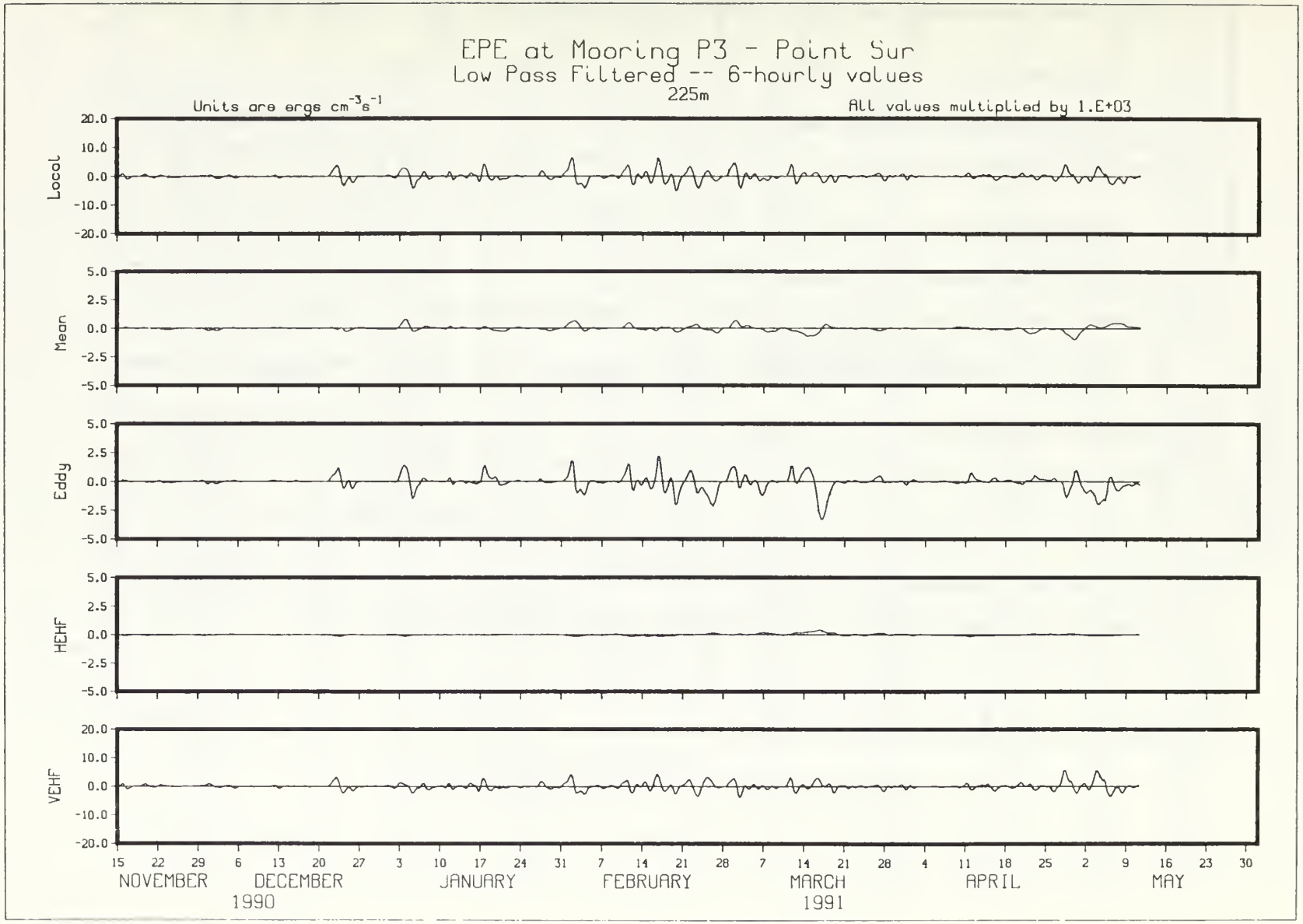
EPE at Mooring P3 - Point Sur
Low Pass Filtered -- 6-hourly values
225m
Units are ergs cm-3s-1
All values multiplied by 1.E+03
Local
Mean
Eddy
HEHF
VEHF
20.0
10.0
0.0
-10.0
-20.0
5.0
2.5
0.0
-2.5
-5.0
15 22 29 6 13 20 27 3 10 17 24 31 7 14 21 28 7 14 21 28 4 11 18 25 2 9 16 23 30
NOVEMBER DECEMBER JANUARY FEBRUARY MARCH APRIL MAY
1990
1991

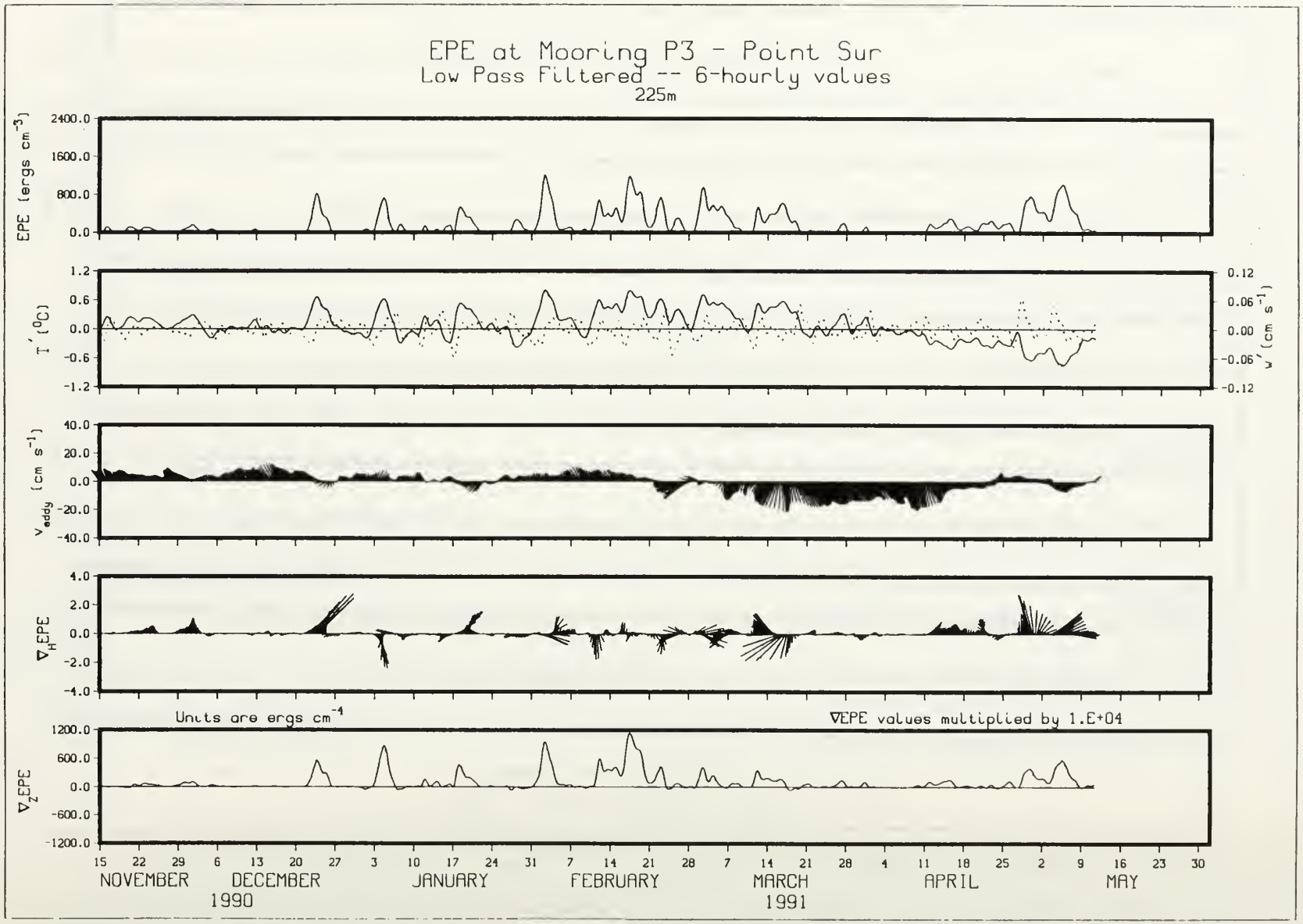
EPE at Mooring P3 - Point Sur
Low Pass Filtered -- 6-hourly values
225m
EPE (ergs cm^{-3})
2400.0
1600.0
800.0
0.0
T' (°C)
1.2
0.6
0.0
-0.6
-1.2
w' (cm s^{-1})
0.12
0.06
0.00
-0.06
-0.12
v$_{eddy}$ (cm s^{-1})
40.0
20.0
0.0
-20.0
-40.0
∇$_H$EPE
4.0
2.0
0.0
-2.0
-4.0
Units are ergs cm^{-4}
∇EPE values multiplied by 1.E+04
∇$_z$EPE
1200.0
600.0
0.0
-600.0
-1200.0
15 22 29 6 13 20 27 3 10 17 24 31 7 14 21 28 7 14 21 28 4 11 18 25 2 9 16 23 30
NOVEMBER DECEMBER JANUARY FEBRUARY MARCH APRIL MAY
1990
1991

REFERENCES

Aanderaa Instruments Technical Description No. 159, 1990: *Operating Manual RCM 7 & 8*, Aanderaa Instruments, Bergen, Norway, 74 pp.

Allen, J.S., 1980: Models of wind-driven currents on the continental shelf, *Ann. Rev. Fluid Mech.*, **12**, 389-433.

Auad, G., A. Parés-Sierra, and G.K. Vallis 1991: Circulation and energetics of a model of the California Current System, *J. Phys. Oceanogr.*, **21**, 1534-1552.

Batteen, M.L., R,L. Haney, T.A. Tielking and P.G. Renaud, 1989: A numerical study of wind forcing of eddies and jets in the California Current System, *J. Mar. Res.*, **47**, 493-523.

Beardsley, R.C., and S.J. Lentz, 1987: The Coastal Ocean Dynamics Experiment Collection: An Introduction, *J. Geophys. Res.*, **92**, 1455-1463.

Bendat, J.S., and A.G. Piersol, 1986: *Random Data, Analysis and Measurement Procedures,* 2nd Ed., John Wiley and Sons, Inc., NY, 586 pp.

Bernstein, R.L., L. Breaker, and R, Whritner, 1977: California Current eddy formation: Ship, air, and satellite results, *Science*, **195**, 353-359.

Breaker, L.C., and R.P. Gilliland, 1981: A satellite sequence on upwelling along the California coast, in *Coastal Upwelling, Coastal Estuarine Sci. Ser.*, Vol. 1, edited by F.A. Richards, pp. 87-94, AGU, Washington, D.C.

Breaker, L.C., and W.W. Broenkow, 1989: The circulation of Monterey Bay and related processes, Moss Landing Marine Laboratories, Moss Landing Calif., *Technical Publication*, 89-1, 99 pp.

Brink, K.H., and T.J. Cowles, 1991: The Coastal Transition Zone Program, *J. Geophys. Res.*, **96**, 14,637-14,647.

Brink, K.H., R.C. Beardsley, P.P. Niiler, M Abbott, A.Huyer, S. Ramp, T. Stanton, and D. Stuart, 1991: Statistical properties of near-surface flow in the California Coastal Transition Zone, *J. Geophys. Res.*, **96**, 14,693-14,706.

Brooks, I.H., and P.P. Niiler, 1977: Energetics of the Florida Current, *J. Mar. Res.*, **35**, 163-191.

Box, G.E.P, and G.M. Jenkins, 1976: *Time Series Analysis: forecasting and control*, Holden-Day, Inc., Oakland, California, 596 pp.

Cannon, G.A., N.P. Laird, and T.V. Ryan, 1975: Flow along the continental slope off Washington, Autumn 1971, *J. Mar. Res.*, **33**, Suppl., 97-105.

Chapman, D.C., 1987: Application of wind-forced, long, coastal-trapped wave theory along the California coast, *J. Geophys. Res.*, **92**, 1798-1816

Chelton, D.B., 1984: Seasonal variability of alongshore geostrophic velocity off central California, *J. Geophys. Res.*, **89**, 3473-3486.

Chelton, D.B., A.W. Braktovich, R.L. Bernstein, and P.M. Kosro, 1988: Poleward flow off central California during the spring and summer of 1981 and 1984, *J. Geophys. Res.*, **93**, 10,604-10,620.

Crepon, M., C. Richez, and M. Chartier, 1984: The effect of coastline geometry on upwellings, *J. Phys. Oceanogr.*, **14**, 1365-1382.

Davis, R.E., and P.S. Bogden, 1989: Variability on the California shelf forced by local and remote winds during the Coastal Ocean Dynamics Experiment, *J. Geophys. Res.*, **94**, 4763-4784.

Denbo, D.W., K. Lolain, J.S. Allen, A, Huyer, and R.L. Smith, 1984: Current meter observations over the continental shelf off Oregon and California February 1981 - January 1984, Data Report 112, Ref. 84-12, College of Oceanography, Oregon State University, Corvallis, Oregon.

Dewar, W.K., and J.M. Bane, Jr., 1985: The subsurface energetics of the Gulf Stream near the Charleston Bump, *J. Phys. Oceanogr.*, **15**, 1771-1789.

Dewar, W.K., and J.M. Bane, Jr., 1989a: Gulf Stream dynamics. Part I: Mean flow dynamics at 73° W, *J. Phys. Oceanogr.*, **19**, 1558-1573.

Dewar, W.K., and J.M. Bane, Jr., 1989b: Gulf Stream dynamics. Part II: Eddy energetics at 73° W, *J. Phys. Oceanogr.*, **19**, 1574-1587.

EG&G, 1988: The Northern California Coastal Circulation Study Data Report No. 1: Pilot measurement program, March-August 1987. Prepared for Department of Interior, Minerals Management Service, EG&G WASC Oceanographic Services Report No. NCCCS-88-9, Waltham, Massachusetts, 268 pp.

Gerald, C.F., and P.O. Wheatley, 1989: *Applied Numerical Analysis*, Addison-Wesley Publishing Co., New York, 679 pp.

Gill, A.E., J.S. A. Green,and A.J. Simmons, 1974: Energy partition in the large-scale ocean circulation and the production of mid-ocean eddies, *Deep Sea Res.*, **21**, 499-528.

Hall, M.M., 1986a: Assessing the energetics and dynamics of the Gulf Stream at 68° W from moored current meter observations, *J. Mar. Res.*, **44**(3), 423-443.

Hall, M.M., 1986b: Horizontal and vertical structure of the Gulf Stream velocity field at 68° W, *J. Phys. Oceanogr.*, **16**, 1814-1828.

Hall, M.M., 1989a: Velocity and transport structure of the Kuroshio Extension at 35° N, 152° E, *J. Geophys. Res.*, **94**, 14,445-14,459.

Hall, M.M., 1989b: Temperature and velocity corrections for vertical motion of a mooring at 35°N, 152°E in the Kuroshio Extension, *Deep Sea Res.*, **36**(1), 55-69.

Hall, M.M., 1991: Energetics of the Kuroshio Extension at 35°N, 152°E, *J. Phys. Oceanogr.*, **21**, 958-975.

Hall, M.M., and H.L. Bryden, 1985: Profiling the Gulf Stream with a current meter mooring, *Geophys. Res. Lett.*, **12**, 203-206.

Halpern, D., R.L. Smith, and R.K. Reed, 1978: On the California Undercurrent over the continental slope off Oregon, *J. Geophys. Res.*, **83**, 1366-1372, 1978.

Harvey, A.C., 1981: *Time Series Models*, Philip Allan, a division of Simon & Schuster International Group, 239 pp.

Harvey, A.C., 1989: *Forecasting, structural time series models and the Kalman filter*, Cambridge University Press, New York, 570 pp.

Hicks, M.R., 1992: Alongshore sub-surface current variability in the central California Current System, Master's Thesis, Naval Postgraduate School, Monterey, California, 60 pp.

Hickey, B.M., 1979: The California Current System - hypotheses and facts, *Prog. Oceanog.*, **8**, pp. 191-279.

Hogg, N.G., 1986: On the correction of temperature and velocity time series for mooring motion, J. Atmos. Oceanic Technol., 3(1), 204-214.

Holland, W.R., and P.B. Rhines, 1980: An example of eddy-induced ocen circulation, *J. Phys. Oceanogr.*, **10**, 1010-1031.

Holland, W.R., and W.J. Schmitz, Jr., 1985: Zonal penetration scale of model midlatitude jets, *J. Phys. Oceanogr.*, **15**, 1859-1875.

Holland, W.R., and G.K. Vallis, 1990: An eddy resolving model of the California Current nested in a model of the North Pacific, *J. Phys. Oceanogr.*, submitted.

Holton, J.R., 1979: *An Introduction to Dynamic Meteorology*, Academic Press Inc., 403 pp.

Huyer, A., 1983: Coastal upwelling in the California Current System, *Prog. Oceanogr.*, **12**, pp. 259-284.

Huyer, A., and P.M. Kosro, 1987: Mesoscale surveys over the shelf and slope in the upwelling region near Point Arena, California, *J. Geophys. Res.*, **92**, 1655-1681.

Huyer, A., P.M. Kosro, S.J. Lentz, and R.C. Beardsley, 1989: Poleward flow in the California Current System, in *Poleward Flows along Eastern Oceanic Boundaries*, Coastal and Estuarine Studies No. 34, pp.142-156, Springer-Verlag New York Inc.

Huyer, A., P.M. Kosro, J. Fleischbein, S.R. Ramp, T. Stanton, L. Washburn, F.P. Chavez, T.J. Cowles, S.D. Pierce, and R.L. Smith, 1991: Currents and water masses of the Coastal Transition Zone off northern California, June to August 1988, *J. Geophys. Res.*, **96**, 14,809-14,831.

Ikeda, M. and W.J. Emery, 1984: Satellite observations and modelling of meanders in the California Current System off Oregon and northern California, *J. Phys. Oceanogr.*, **14**, 1434-1450.

Ikeda, M, L.A. Mysak, and W.J. Emery, 1984: Observation and modelling of satellite-sensed meanders and eddies off Vancouver Island, *J. Phys. Oceanogr.*, **14**, 3-21.

Jenkins, G.M., and D.G. Watts, 1968: *Spectral Analysis and its Applications*, Holden-Day, Inc., Oakland, California, 543 pp.

Jones, R.H., 1971: Spectrum estimation with missing observation, *Annuls of. Inst. Stat. Math.*, **23**, 387-398.

Kamenkovich, V.M., M.N. Koshlyakov, and A.S. Monin, 1986: *Synoptic Eddies in the Ocean*, D. Reidel Publishing Company, Dordrecht, Holland, 443 pp.

Knauss, J.A., 1978: *Introduction to Physical Oceanography*, Prentice-Hall, Inc., Englewood Cliffs, NJ, 350 pp.

Koehler, K.A., 1990: Observations and modeling of currents within the Monterey Bay during May 1988, Master's Thesis, Naval Postgraduate School, Monterey, California, 121 pp.

Lynn, R.J., and J.J. Simpson, 1987: The California Current System: The seasonal variability of its physical characteristics, *J. Geophys. Res.*, **92**, 12,947-12,966.

Magnell, B.A., 1991: Subtidal currents on the northern California continental shelf, abstract in *Trans. Amer. Geophys. Un.*, **72**(44), 255.

McCreary, J.P., 1981: A linear stratified ocean model of the coastal undercurrent, *Ph. Trans. Roy. Soc. Lon.*, **A302**, 385-413.

McCreary, J.P., P.K. Kundu, and S.-Y Chao, 1987: On the dynamics of the California Current System, *J. Mar. Res.*, **45**, 1-32.

Mooers, C.N.K., 1989: Workshop summary: Poleward flow-Observational and theoretical issues, in *Poleward Flows along Eastern Oceanic Boundaries*, Coastal and Estuarine Studies No. 34, pp.2-16, Springer-Verlag New York Inc.

Nelson, C.S., 1977: Wind stress and wind stress curl over the California Current, *Tech. Rep. NMFS-SSRF-714*, Nat. Oceanic and Atmos. Admin., Wash. D.C.

Niiler, P.P., and M.M. Hall, 1988: Low-frequency eddy variability at 28°N, 152°W in the eastern North Pacific subtropical gyre, *J. Phys. Oceanogr.*, **18**, 1670-1685.

Nishida, H., and W.B. White, 1982: Horizontal eddy fluxes of momentum and kinetic energy in the near surface of the Kuroshio Extension, *J. Phys. Oceanogr.*, **12**, 160-170.

Noble, M., R.C. Beardsley, J.V. Gardner, and R.L. Smith, 1987: Observations of subtidal currents over the northern California continental slope and adjacent basin: Some evidence for local wind forcing, *J. Geophys. Res.*, **92**, 1709-1720.

Parres-Sierra, A. W.B. White, and C.-K,. Tai, 1990: On the mesoscale variability in the California Current region: A model-satellite intercomparison, *J. Phys. Oceanogr.*, submitted.

Peffley, M.B., and J.J. O'Brien, 1976: A three-dimensional simulation of coastal upwelling off Oregon, *J. Phys. Oceanogr.*, **6**, 164-180.

Philander, S.G.H. and J.-H. Yoon, 1982: Eastern boundary currents and coastal upwelling, *J. Phys. Oceanogr.*, **12**, 862-879.

Pickard, G.L., and W.J. Emery, 1982: *Descriptive Physical Oceanography an Introduction*, 4th Ed., 263 pp., Pergamon Press Inc., Elmsford, NY.

Pierce, S.D., J.S. Allen, and L.J. Walstad, 1991: Dynamics of the Coastal Transition Zone Jet 1. Linear Stability Analysis, *J. Geophys. Res.*, **96**, 14,979-14,993.

Preller, R., and J.J. O'Brien, 1980: The influence of bottom topography on upwelling off Peru, *J. Phys. Oceanogr.*, **10**, 1377-1398.

Ramp, S.R., 1989: Moored observations of current and temperature on the shelf and upper slope near Ring 82B, *J. Geophys. Res.*, **94**, 18,071-18,087.

Ramp, S.R., P.F. Jessen, K.H. Brink, P.P. Niiler, F.L. Daggett, and J.S. Best, 1991a: The physical structure of cold filaments near Point Arena, California, during June 1987, *J. Geophys. Res.*, **96**, 14,859-14,883.

Ramp, S.R., T.D. Tisch, and T. Anderson, 1991b: Two-year time series of current, temperature, and conductivity on the continental slope off Point Sur, California, and their relation to local and remote forcing, abstract in *Trans. Amer. Geophys. Un.*, **72**(44), 254.

Reed, R.K., and D. Halpern, 1976: Observations of the California Undercurrent off Washington and Vancouver Island, *Limnol. Oceanogr.*, **21**, 389-398.

Reid, J.L., and R.A. Schwartzlose, 1962: Direct measurements of the Davidson Current off central California, *J. Geophys. Res.*, **67**, 2491-2497.

Reinecker, M.M., and L.L. Ehret, 1988: Wind stress curl variability over the North Pacific from the Comprehensive Ocean-Atmosphere Data Set, *J. Geophys. Res.*, **93**, 5069-5077.

Reinecker, M.M., and C.N.K. Mooers, 1989: Mesoscale eddies, jets, and fronts off Point Arena, California, July 1986, *J. Geophys. Res.*, **94**, 12,555-12,570.

Reinecker, M.M., C.N.K. Mooers, and R.L. Smith, 1988: Mesoscale variability in current meter measurements in the California Current System off northern California, *J. Geophys. Res.*, **93**, 6711-6734.

Rossby, T., 1987: On the energetics of the Gulf Stream at 73° W, *J. Mar. Res.*, **45**,59-82.

Send, U., R.C. Beardsley, and C.D. Winant, 1987: Relaxation from upwelling in the Coastal Ocean Dynamics Experiment, *J. Geophys. Res.*, **92**, 1683-1698.

Sielbeck, S.L., 1991: Bottom trapped waves at tidal frequencies off Point Sur, California, Master's Thesis, Naval Postgraduate School, Monterey, California, 71 pp.

Simpson, J.J., C.J. Koblinsky, J. Peláez, L.R. Haury, and D. Wiesenhahn, 1986: Temperature-Plant Pigment-Optical relations in a recurrent offshore mesoscale eddy near Point Conception, California, *J. Geophys. Res.*, **91**, 12,919-12,396.

Schmitz, W.J., Jr., 1984: Observations of the vertical structure of the eddy field in the Kuroshio Extension, *J. Geophys. Res.*, **89**, 6355-6364.

Schmitz, W.J., Jr., and W.R. Holland, 1982: A preliminary comparison of selected numerical eddy-resolving general circulation experiments with observations, *J. Mar. Res.*, **40**(1), 75-117.

Schmitz, W.J., Jr., and W.R. Holland, 1986: Observed and modeled mesoscale variability near the Gulf Stream and Kuroshio Extension, *J. Geophys. Res.*, **91**, 9624-9638.

Schmitz, W.J., Jr., and P.P. Niiler, 1969: A note on the kinetic energy exchange between fluctuations and mean flow in the surface layer of the Florida Current, *Tellus*, **21**, 814-819.

Shumway, R.H., 1988: *Applied Statistical Time Series Analysis,* Prentice Hall, Englewood Cliffs, New Jersey, 394 pp.

Strub, P.T., J.S. Allen, A. Huyer, R.L. Smith, and R.C. Beardsley, 1987: Seasonal cycles of currents, temperatures, and sea level over the Northeast Pacific continental shelf: 35° N to 48°N, *J. Geophys. Res.*, **92**, 1507-1526.

Sturges, W., 1991: Recovering a continuous spectrum from gappy data, abstract in *Trans. Amer. Geophys. Un.*, **72**(44), 261.

Stull, R.B., 1988: *An Introduction to Boundary Layer Meteorology*, Kluwer Academic Publishers, 679 pp.

Thomson, R.E., 1984: A cyclonic eddy over the continental margin of Vancouver Island: Evidence for dynamical instability, *J. Phys. Oceanogr.*, **14**, 1326-1348.

Tisch, T.D., 1990: Seasonal variability of the geostrophic velocity and water mass structure off Point Sur, California, Master's Thesis, Naval Postgraduate School, Monterey, California, 163 pp.

Tisch, T.D., S.R. Ramp, and C.A. Collins, 1992: Observations of the geostrophic velocity and water mass characteristics off Point Sur, California from May 1988 through November 1989, *J. Geophys. Res.*, **97**,12,535-12,555.

Tracy, D.E., 1990: Surface circulation of Monterey Bay using AVHRR Satellite Imagery, Master's Thesis, Naval Postgraduate School, Monterey, California, 135 pp.

UNESCO, 1987: International Oceanographic Tables, *UNESCO Tech. Pap. in Mar. Sci.*, Vol 4., No. 40.

Walstad, L.J., J.S. Allen, P.M. Kosro, and A. Huyer, 1991: Dynamics of the Coastal Transition Zone through data assimilation studies, *J. Geophys. Res.*, **96**, 14,959-14,977.,

Watts, D.R., and W.E. Johns, 1982: Gulf Stream meanders: Observations on propagation and growth, *J. Geophys. Res.*, **87**, 9467-9476.

Webster, F., 1961: The effect of meanders on the kinetic energy balance of the Gulf Stream, *Tellus*, **13**, 392-401.

Webster, F., 1965: Measurements of eddy fluxes of momentum in the surface layer of the Gulf Stream, *Tellus*, **17**, 239-245.

Wickham, J.B., A.A. Bird, and C.N.K. Mooers, 1987: Mean and variable flow over the central California continental margin, 1978-1980, *Continental Shelf Res.*, **7**(8), 827-849.

Winant, C.D., R.C. Beardsley, and R.E. Davis, 1987: Moored wind, temperature, and current observations made during Coastal Ocean Dynamics Experiments 1 and 2 over the northern California continental shelf and upper slope, *J. Geophys. Res.*, **92**, 1569-1604.

Wooster, W.S., and J.H. Jones, 1970: California undercurrent off northern Baja California, *J. Mar. Res.*, **28**, 253-260.

INITIAL DISTRIBUTION LIST

		No. Copies
1.	Defense Technical Information Center Cameron Station Alexandria, VA 22314	2
2.	Library, Code 52 Naval Postgraduate School Monterey, CA 93943-5000	2
3.	Chairman (Code OC/Co) Department of Oceanography Naval Postgraduate School Monterey, CA 93943-5000	1
4.	Chairman (Code MR/Hy) Department of Meteorology Naval Postgraduate School Monterey, CA 93943-5000	1
5.	Professor C.A. Collins (OC/Co) Department of Oceanography Naval Postgraduate School Monterey, CA 93943-5000	1
6.	Professor R.L. Haney (MR/Hy) Department of Meteorology Naval Postgraduate School Monterey, CA 93943-5000	1
7.	Professor Steven. R. Ramp (OC/Ra) Department of Oceanography Naval Postgraduate School Monterey, CA 93943-5000	1
8.	Professor M.L. Batteen (OC/Ba) Department of Oceanography Naval Postgraduate School Monterey, CA 93943-5000	1

9. Professor W. Gragg (MA/Gg) 1
Department of Mathematics
Naval Postgraduate School
Monterey, CA 93943-5000

10. LT Timothy D. Tisch 1
Department of Oceanography
Naval Postgraduate School
Monterey, CA 93943-5000

11. Director, Office of Ocean and Earth Sciences 1
National Atmospheric and Oceanic
Administration
6010 Executive Blvd.
Rockville, MD 20852

12. Chief, Career Development Division (CPC2) 1
Commisioned Personnel Center
National Atmospheric and Oceanic
Administration
Rockville, MD 20852

13. NOAA Library 1
7600 Sand Point Way NE
Building 3
Seattle, WA 98115

Thesis
T5453
c.1

Tisch
Assessing the energetic interactions of subtidal flow on the continental slope in an Eastern boundary region.